

**A Study of the Biological Activity of Bee Venom and its Fractions
With Regard to Cosmetic Science and Immunology**

A Thesis Submitted in Fulfilment of the Requirements for the Degree of
Doctor of Philosophy in the Strathclyde Institute of Pharmacy and
Biomedical Sciences at the University of Strathclyde

by

Jonans Tusiimire

2016

Declaration

‘I declare that, except where specifically indicated, all the work presented in this report is my own and I am the sole author of all parts.’

‘The copyright of this thesis belongs to the author under the terms of the United Kingdom Copyright Acts as qualified by University of Strathclyde Regulation 3.50. Due acknowledgement must always be made of the use of any material contained in, or derived from, this thesis.’

Signed: _____

Date: _____

Acknowledgement

I would like to extend my heartfelt appreciation to my supervisors Dr David Watson and Dr Mark Dufton for offering me this rare opportunity to study PhD on their funded project. I owe much of my understanding of this research to their dedicated teaching and guidance. I would like also to express my gratitude to my academic assessor, Professor Clive Wilson who periodically reviewed my research progress through mini-vivas. He always asked intriguing questions which led to clarification of my thoughts about this work. In addition, my academic adviser Professor Alexander Gray provided an intellectually rich and relaxed atmosphere whenever we met.

Additionally, I am thankful for the wonderful support the entire project team has accorded me. Jennifer Wallace and John Parkinson were of great help with NMR studies; Louise Young, Grainne Abbott and Nicola Woods trained me in bioassays; while Carol Clements helped to run some microbiological assays. I am also grateful to Dr Darren Edwards, Wilma Wilson and Lorraine Allan for the essential lab skills they have taught me as a demonstrator on the MSc. Pharmaceutical Analysis program.

I would also like to express my gratitude to the entire research team in Dave's lab consisting of Alex, Sami, Khaled S, Naif, Sanad, Ibrahim, Adel, Adnan, Mohammed, Mohammad, Khaled O, Ahmed, Ali, Adel, Ruwida, Weam, Samyah and Aliyah. It was such a rewarding experience working with such a wonderful group of people.

This work would not have been possible without the infinite love and support from my wife Elizabeth and our children Martha, Annalisa and Albert. I am also grateful for the love and support from my Dad, my brothers Moderns, Eliots, Barham, Ahwera, and my sisters Ritah, Ruth and Racheal. Thank you all for being there for me.

Finally, this project was funded by the University of Strathclyde in collaboration with Beesen Co. Ltd., Korea, through the University's KIAT scheme. My employer, Mbarara University of Science and Technology, offered me official leave to undertake this research.

Dedication

This work is dedicated, first and foremost, to the memory of my mother who lived a rich life filled with love and purpose. Her departure at the very start of this PhD meant that it was going to be such a tough time for me. Her memory kept me fully focussed and inspired me to wake up each morning to go to the lab.

During the past three years, Annalisa and Albert were born, while Martha swiftly completed her pre-school year and is now in primary three. My constant awareness of their existence gave me hope, especially when the situation was so difficult, and the mere thought of going home to see them was a source of much motivation. I knew that I had to complete this work in order to justify my long years of absence. Hence, this achievement is for them—to inspire them to always aim for more.

Finally, for all her love, unwavering support, and patience during the past four years of my absence, first during the MSc. and later, PhD, I will forever be indebted to my wife. She has not only looked after our lovely children and kept the family afloat during this time but has also successfully overseen a number of our joint projects, while also undertaking her full-time job and a part-time Master of Arts course. I would have had absolutely no explanation whatsoever had this thesis not materialised. Because of this, she has as much claim to the PhD as I do, and I dedicate this work to her valour.

Jonans Tusiimire
University of Strathclyde

TABLE OF CONTENTS

Declaration	i
Acknowledgement	ii
Dedication	iii
List of Tables	xii
List of Figures	xiv
Abbreviations and Acronyms	xix
Published Work	xxi
Abstract	xxii
1 The Skin and its Ageing Process	2
1.1 Skin physiology	3
1.1.1 The epidermis.....	3
1.1.2 The dermis.....	6
1.1.3 The hypodermis.....	7
1.2 Mechanisms of skin ageing	8
1.2.1 Intrinsic ageing.....	9
1.2.2 Extrinsic ageing.....	12
1.2.3 Role of glucocorticoids	15
1.2.4 Role of oestrogens.....	16
1.3 Clinical and physical facial ageing.....	17
1.4 Anti-ageing approaches	18
1.4.1 General approaches	18
1.4.2 Use of botox injections.....	21
1.4.3 The role of peptides and proteins	22
2 The Venom of <i>Apis mellifera</i>, its Applications and Analysis	28

2.1	Introduction to honey bee venom (HBV).....	28
2.2	Chemical constituents and biological actions.....	30
2.2.1	Melittin.....	31
2.2.2	Phospholipase.....	33
2.2.3	Hyaluronidase	36
2.2.4	Apamin.....	37
2.2.5	Secapin	38
2.2.6	Mast cell degranulating peptide	39
2.2.7	Adolapin.....	40
2.2.8	Other components of HBV.....	45
2.3	Applications and uses of BV	45
2.4	Analysis of BV	47
2.4.1	High performance liquid chromatography (HPLC).....	48
2.4.2	Mass spectrometry	50
2.4.3	Edman degradation.....	53
2.4.4	SDS-PAGE and immunoblotting	54
2.4.5	Capillary zone electrophoresis	54
2.4.6	Circular dichroism spectroscopy.....	55
2.4.7	Nuclear magnetic resonance spectroscopy.....	56
2.4.8	Biological and functional assays	56
2.4.9	Other techniques for BV analysis	56
2.5	Bee venom as an active ingredient in cosmetics	57
2.6	Principles of chromatographic analysis.....	59
2.6.1	Theory of chromatography.....	59
2.6.2	Modes of chromatography	59
2.6.3	Chromatographic resolution and performance.....	62

2.6.4	Chromatographic elution profiles	65
2.6.5	Medium pressure liquid chromatography	67
2.6.6	Principle of detection by ELSD	69
2.6.7	Mode of operation of HPLC	69
2.7	Principles of mass spectrometry	71
2.7.1	The ESI technique	73
2.7.2	The LTQ-Orbitrap MS	75
2.7.3	The quadrupole mass analyser	79
2.7.4	Electron impact (EI) ionisation	81
2.8	Research hypothesis	82
2.8.1	Hypothesis one	82
2.8.2	Hypothesis two.....	82
2.9	Aims & objectives	83
2.9.1	Preliminary profiling studies.....	83
2.9.2	Antimicrobial effects and selective toxicity.....	83
2.9.3	Assay of BV-containing cosmetics formulations.....	84
2.9.4	Stability and mechanisms for melittin degradation.....	84
2.9.5	Pro-inflammatory and potential immuno-adjuvant effects	85
3	Materials and Methods for Flash Chromatography, LC-MS and GC-MS.	87
3.1	Study samples.....	87
3.2	Instrumental systems and techniques	87
3.2.1	MPLC system.....	87
3.2.2	HPLC-ESI-MS systems	87
3.2.3	The GC-EI-MS system.....	88
3.3	Other apparatus.....	89
3.4	Solvents and chemicals	89

3.5	General sample preparation procedures	90
3.5.1	Preparation of filtered whole BV	90
3.5.2	Fractionation and lyophilisation of BV	90
3.5.3	Melittin purification	91
3.6	LC-MS analysis	91
3.6.1	LTQ-Orbitrap MS conditions.....	91
3.6.2	Reversed phase (C18) conditions.....	91
3.6.3	Reversed phase (PS-DVB) conditions	92
3.6.4	HILIC (Sequant® ZIC®-cHILIC) conditions.....	92
3.7	GC-MS conditions.....	92
4	Fractionation, Purification and Profiling of the Main Components of Honey	
	Bee Venom	94
4.1	Introduction	94
4.2	Methods	95
4.2.1	LC-MS analysis of BV and fractions	95
4.2.2	GC-MS of BV and fraction F-4	95
4.2.3	LoD and LoQ determination	95
4.2.4	SDS-PAGE assay	96
4.2.5	Western blot analysis	96
4.3	Results	97
4.3.1	Whole venom assay by LC-MS	97
4.3.2	GC-MS of whole BV	99
4.3.3	Fractionation	100
4.3.4	Detection of phospholipase and hyaluronidase in BV	116
4.3.5	Determination of LoD and LoQ for melittin.....	117
4.4	Discussion	118

5	Antimicrobial and Cell Viability Assays.....	121
5.1	Introduction	121
5.2	Materials and methods.....	122
5.2.1	Test organisms and cells used in the assays.....	122
5.2.2	Test sample fractions and their preparation	122
5.2.3	Assay for anti-trypanosomal activity	122
5.2.4	α -Glucosidase inhibition assay.....	124
5.2.5	Cell viability assays	126
5.2.6	Assay for TNF- α -induced NF- κ B inhibition.....	127
5.3	Results	128
5.3.1	Antibacterial assays.....	128
5.3.2	Activity against <i>T. brucei</i>	128
5.3.3	α -Glucosidase activity.....	131
5.3.4	Effect BV fractions on cell viability	132
5.3.5	TNF- α -induced NF- κ B inhibition assay.....	139
5.4	Discussion	140
6	Investigation of Stability and Biochemical Activity of Bee Venom.....	145
6.1	Introduction	145
6.2	Materials and methods.....	145
6.2.1	Protease enzymes	145
6.2.2	Protease inhibitors.....	146
6.2.3	Melittin auto-degradation in BV	146
6.2.4	Enzymatic degradation of melittin.....	146
6.3	Results	147
6.3.1	Spontaneous degradation of melittin in BV solution.....	147
6.3.2	Effect of storage temperature	154

6.3.3	Effect of added proteolytic enzymes.....	156
6.3.4	Effect of added enzyme inhibitors	158
6.4	Discussion	159
7	An LC-MS Method for the Assay of Melittin in Cosmetic Formulations Containing Bee Venom	162
7.1	Introduction	164
7.2	Materials and methods.....	167
7.2.1	Study samples	167
7.2.2	Solvents and chemicals	167
7.2.3	Instrumentation and Consumables	168
7.2.4	LC-MS method conditions.....	168
7.2.5	Melittin isolation from bee venom.....	169
7.2.6	Melittin purity measurement by NMR.....	169
7.2.7	Assay method for the creams	170
7.2.8	Calibration with standard additions	170
7.3	Results	171
7.3.1	Melittin purity determination.....	171
7.3.2	Mean melittin content in creams	173
7.3.3	Assay precision	174
7.3.4	Recovery, specificity and linearity.....	177
7.4	Discussion	178
7.5	Conclusion.....	182
8	Effect of Bee Venom and its Fractions on the Release of Pro-Inflammatory Cytokines in PMA-Differentiated U937 Cells Co-Stimulated with LPS.....	184
8.1	Introduction	186
8.2	Materials and methods.....	189

8.2.1	Cell culture	189
8.2.2	Test sample isolation, preparation and analysis	189
8.2.3	Cell viability assay	190
8.2.4	Induction of cell differentiation	190
8.2.5	Stimulation of cytokine release by PMA	191
8.2.6	Assessment of cytokine release.....	191
8.2.7	Data analysis	192
8.2.8	NMR spectroscopy.....	193
8.3	Results	195
8.3.1	Viability of U937 cells incubated with BV fractions.....	195
8.3.2	Selection of BV and fraction concentrations for assay	198
8.3.3	Observed effects of PMA on U937 cells	198
8.3.4	Effect on TNF- α production.....	199
8.3.5	Effect on IL-1 β production	200
8.3.6	Effect on IL-6 production.....	201
8.3.7	Identification of active compound in BV fraction F-4.....	202
8.3.8	Identification of minor impurity in F-4.....	210
8.4	Discussion	211
8.4.1	Cytotoxicity.....	211
8.4.2	Effect on cytokine release	212
8.4.3	Conclusion	214
	General Discussion and Conclusion	217
	References	221
	Appendices and Supplementary Information	253
	Appendix I: Supplementary data for Chapter 7.....	253
	Standard Addition Calibration curves for sample A (PBV)	253

Calibration curves for sample B (BVE).....	254
Calibration curves for sample C (MDR1).....	256
Calibration curves for sample D (NBC)	257
Calibration curves for sample E (MDM).....	259
Calibration curves for sample F (MDR2)	260
Appendix II: Supplementary data for Chapter 8	262
Supplementary Figures	262
Supplementary Tables.....	274

List of Tables

Table 1.1: The layers of the human skin epidermis as summarised from (Arda <i>et al.</i> , 2014, Bárány <i>et al.</i> , 2000, Lodén, 2003).....	5
Table 1.2: Changes associated with intrinsically aged skin (Sadick <i>et al.</i> , 2009, Mizukoshi <i>et al.</i> , 2014, Zouboulis and Makrantonaki, 2011).....	9
Table 1.3: Changes associated with extrinsically aged skin (Sadick <i>et al.</i> , 2009, Mizukoshi <i>et al.</i> , 2014, Zouboulis and Makrantonaki, 2011).....	14
Table 1.4: Structural features of aged skin	17
Table 1.5: Categories of common cosmetic ingredients	18
Table 2.1: Main peptide components of honey bee venom.	41
Table 2.2: Main allergenic proteins of <i>Apis mellifera</i> . Note that Api m1-4, 6, 7 are major components of honey bee venom ((WHO/IUIS, 2014)).	43
Table 4.1: Summary of the main components identified in F-1, the polar fraction of bee venom.....	102
Table 4.2: The main peptides identified in F-2 and their diagnostic ions in the mass spectra.	106
Table 4.3: The two polypeptides present in sample F-2 showing their diagnostic ions and approximate molecular weights.	108
Table 5.1: Microwell plate set up for MIC determination	125
Table 5.2: Biological activity of bee venom fractions on <i>M. marinum</i> , <i>N. farcinia</i> and <i>T. brucei</i> (sample stock solution prepared in water)	129
Table 5.3: Biological activity of bee venom fractions on <i>M. marinum</i> , <i>N. farcinia</i> and <i>T. brucei</i>	130
Table 5.4: Micrographs of wells containing PNT2A (normal epithelial) cells incubated with 30 µg/mL concentration of melittin-containing bee venom fractions LG ₁ T ₁₃ and LG ₂ T ₅₀ taken at 24 and 48 h.	134
Table 6.1: Investigation of melittin-degrading enzyme activity in bee venom.....	147
Table 6.2: Summary of interpretation of the degradation of melittin.	154
Table 7.1: Values used in the calculation of melittin purity	173

Table 7.2: Triplicate assays of commercial facial creams claimed to contain unstated amounts of bee venom.	174
Table 7.3: Intra-assay precision estimates at 95% confidence level ($p=0.05$, $df=5$).....	175
Table 7.4: Summary of the equations of calibration curves (in the form of $y = mx + c$) obtained during the assay of the 6 creams (A-F).	176
Table 7.5: Recovery data obtained using a blank cream fortified at three different levels of 5, 10 and 15 μg per mL of extract containing 100mg cream.	177
Table 7.6: Peak areas of standard melittin assayed at 10 $\mu\text{g}/\text{mL}$ concentration	177
Table 8.1: Volumes of LPS, fractions and media used to stimulate cytokine production in PMA-differentiated U937 cells.	191
Table 8.2: The constant values of the 4-PL regression curve fitted to the data of TNF- α , IL-1 β and IL-6 standards respectively ($n=3$).	193
Table 8.3: Concentrations of the fractions used in the assay of immunomodulatory effects on PMA-differentiated U937 cells.	198
Table 8.4: Data arising from the 1D ^1H NMR spectrum of the lipid component.	204
Table 8.5: Summary of ^{13}C NMR data for the lipid molecule as revealed by 1D $^{13}\text{C}\{-^1\text{H}\}$ and 2D [^1H , ^{13}C] HSQC NMR data.	206
Table 8.6: Coupling partners revealed through 2D [^1H , ^1H] COSY (C) and TOCSY (T) NMR data.....	208
Table 8.7: Coupling partners revealed by analysis of 2D [^1H , ^{13}C] HSQC (HS) and HMBC (HM) NMR data for the lipid component.	208

List of Figures

Figure 1.1: Structure of the human skin showing cell populations (Kendall and Nicolaou, 2013).	4
Figure 1.2: Structure of the epidermis of the human skin.....	5
Figure 1.3: Features characteristic of young, intrinsically aged and photo-aged skin, picture courtesy of (Wlaschek <i>et al.</i> , 2001).	12
Figure 1.4: A section of the sun’s electromagnetic radiation showing the wavelength range of UV (A) and their transmittance through the skin (B).	13
Figure 1.5: Structures of retinol and tretinoin.....	20
Figure 1.6: Structure of Argireline®.....	24
Figure 2.1: Structure of melittin, the main component in BV	29
Figure 2.2: The amino acid sequence of prepromelittin.	31
Figure 2.3: Amino acid composition of the “pre” and “pro” fragments of prepromelittin. ...	32
Figure 2.4: The structure of melittin	33
Figure 2.5: Structure of phospholipase A ₂	35
Figure 2.6: Crystal structures of BV hyaluronidase.....	37
Figure 2.7: Structure of the BV peptides apamin and mast cell degranulating peptide showing their amino acid compositions.....	38
Figure 2.8: Comparison of the amino acid composition of secapin (Vlasak and Kreil, 1984) and other identified secapin-related peptides secapin-1 (Meng <i>et al.</i> , 2012) and secapin-2 (Mourelle <i>et al.</i> , 2014).	39
Figure 2.9: The Reveleris® flash chromatography system (Grace®) showing the main components (A) and a schematic diagram to show the flow of solvent through the main parts on the system (B).	68
Figure 2.10: Schematic diagram of a modern HPLC system.....	70
Figure 2.11: The main components of a mass spectrometer.....	73
Figure 2.12: Mechanism of ESI as modified from (Banerjee and Mazumdar, 2012).....	74
Figure 2.13: A schematic layout of the Orbitrap mass spectrometer.....	76

Figure 2.14: A section through the Orbitrap mass analyser.....	78
Figure 2.15: A schematic diagram for the structure of the DSQII mass spectrometer.	79
Figure 2.16: Action of the quadrupole mass analyser.....	79
Figure 2.17: Ionisation and fragmentation processes during electron impact ionisation.....	82
Figure 4.1: Some of the components identified in whole BV.....	98
Figure 4.2: Qualitative differences between the two batches of BV (NWBV and OWBV) tested based on PCA-X modelling with Simca version 14.	98
Figure 4.3: Full gas chromatogram of the ethyl acetate extract of whole BV sample batch A and B.....	99
Figure 4.4: Chromatogram obtained in the MPLC separation of BV components using the Grace® system.....	100
Figure 4.5: Some of the identified main components in fraction F-1 samples.	101
Figure 4.6: Some of the unidentified components in fraction F-1 samples.	102
Figure 4.7: Chromatogram of sample fraction obtained from fraction F-1 of the MPLC showing early eluting small polar compounds in BV.....	104
Figure 4.8: Some of the polar compounds identified with the HILIC method (section 3.6.4) in sample F-1.....	105
Figure 4.9: Chromatograms showing the full scan (a) and extracted ion chromatograms (b-e) of the components of Fraction-2.	106
Figure 4.10: Mass spectrum of apamin showing a minor co-eluting peptide (red arrow) with a triply charged base ion of m/z 709.2963 (MW 2124.89 Da).	107
Figure 4.11: Mass spectrum of MCD peptide revealing 2 minor peptides (MW 2684.3960, Blue Arrow; and MW 2748.4825, Red Arrow) each with a quintuply-charged base ion with m/z 537.8792 and 550.6965 respectively.....	108
Figure 4.12: Mass spectrum of the two polypeptides showing the diagnostic m/z of the ions for polypeptide-1 (red) and polypeptide-2 (blue).....	109
Figure 4.13: Chromatogram of sample from F-3 showing the melittin peak in a relatively pure form (A).	110
Figure 4.14: Chromatogram obtained in the MPLC separation of BV components using the Grace® system.....	111

Figure 4.15: Gas chromatogram for the sample obtained from F-4 showing a single peak at 14.45 min (A).....	112
Figure 4.16: LC-MS assay of F-4 showing a single peak at 8.53 min with a singly charged ion of m/z 793.4656.	113
Figure 4.17: MS ¹ and MS ² of the unknown compound present in fraction 4 of BV.	115
Figure 4.18: SDS-PAGE analysis of BV to detect the main allergens.	116
Figure 4.19: Determination of LoD and LoQ of melittin.....	118
Figure 5.1: Inhibitory effect of aqueous BV fractions on α -glucosidase enzyme at 30 μ g/mL concentration.....	131
Figure 5.2: Action of melittin on α -glucosidase.	132
Figure 5.3: Effect of BV fractions on PNT2A normal epithelial cells at 30 and 100 μ g/mL concentrations.	133
Figure 5.4: Action of melittin on PNT2A cells.....	134
Figure 5.5: Micrographs showing the effect of Melittin-1 on PNT2A cells confirming the results obtained with the Alamar Blue® viability probe.....	135
Figure 5.6: Micrographs showing the effect of Melittin-2 on PNT2A cells confirming the results obtained with the Alamar Blue® viability probe.....	136
Figure 5.7: Effect of samples of BV fractions at 1, 3, 10 and 30 μ g/mL on normal human keratinocytes.	137
Figure 5.8: Graphs of viability of HS27 cells against log of concentration in g/mL.	138
Figure 5.9: Micrographs of the HS27 cells after 24 h showing the effects of fractions F-3 and F-4 at different concentrations.	139
Figure 5.10: Inhibitory effect of aqueous BV on TNF- α -induced NF- κ B in NCTC2544 cells at 10 and 30 μ g/mL concentrations.....	140
Figure 6.1: Time-dependent degradation of melittin in a solution of BV.....	148
Figure 6.2: Plot of lnA versus time (in hrs) to estimate the rate of melittin degradation in solution at ambient temperatures.	149
Figure 6.3: Chromatogram of BV showing the peaks of the main fragments of melittin after 40 days of storage at room temperature (25°C).	150
Figure 6.4: Possible site of degradation of melittin to yield <i>pl</i>	151

Figure 6.5: Possible site of degradation of melittin to yield <i>p2</i>	152
Figure 6.6: Possible sites of degradation of melittin to yield <i>p3</i> and <i>p4</i>	153
Figure 6.7: Effect of storage conditions on melittin stability.	155
Figure 6.8: Effect of storage on melittin degradation.	156
Figure 6.9: Chromatogram for melittin spiked with different proteolytic enzymes.	157
Figure 6.10: Chromatogram for BV with inhibitors after 24 h of incubation.	158
Figure 6.11: Chromatogram obtained 14 days following incubation.	159
Figure 7.1: NMR spectra of melittin with and without methanol spike.	171
Figure 7.2: NMR spectra of melittin (A) and melittin + methanol (B).	172
Figure 7.3: The mass spectrum of melittin.	178
Figure 7.4: Calibration plot of peak area versus amount of melittin spiked into the extract of cream E replicate 1.	180
Figure 8.1: Cytotoxicity of the BV sample fractions F-1 to F-4 against U937 cells.	196
Figure 8.2: Cytotoxic effects of BV fractions on U937 cells.	197
Figure 8.3: Effect of PMA on U937 cells.	199
Figure 8.4: Effect of BV and its fractions of TNF- α production in PMA-differentiated U937 cells.	200
Figure 8.5: Effect of BV and its fractions of IL-1 β production in PMA-differentiated U937 cells.	201
Figure 8.6: Effect of BV and its fractions with and without LPS on IL-6 production in PMA-differentiated U937 cells.	202
Figure 8.7: 600 MHz 1D ^1H NMR spectrum of the lipid component from fraction F-4 showing signal integrals.	203
Figure 8.8: ^{13}C - $\{^1\text{H}\}$ NMR spectrum of the lipid component from fraction F-4 with expansions shown to reveal details of crowded region.	205
Figure 8.9: 600 MHz 2D [^1H , ^{13}C] HSQC NMR data for the lipid component of fraction F-4.	206

Figure 8.10: Basic lipid structure from an analysis of the NMR data showing the signal assignments associated with protons (upper case labels) and carbons (lower case labels) at each position.	209
Figure 8.11: Simulations and experimental data for two possible configurations of the lipid molecule for ¹ H resonances A (left) and E (right).	209
Figure 8.12: (Z)-eicos-9-en-1-ol	210
Figure 8.13: Chromatogram of the impurity in F-4 with [M-H] ⁻ of 793.4651 and elemental composition C ₄₃ H ₇₀ O ₁₁ P.	211

Abbreviations and Acronyms

AHAs	Alpha Hydroxy Acids
AP	Alkaline Phosphatase
BCIP	5-Bromo-4-Chloro-3-Indolyl Phosphate
BV	Bee Venom
BVT	Bee Venom Therapy
CD	Circular Dichroism
CZE	Capillary Zone Electrophoresis
Da	Daltons
DAD	Diode Array Detector
ELISA	Enzyme Linked Immunosorbent Assay
ELSD	Evaporative Light Scattering Detection
ESI	Electrospray Ionisation
FT	Fourier Transformation
FTIR	Fourier Transformation Infrared
FWHM	Full Width at Half Maximum
HDX	Hydrogen Deuterium Exchange
HILIC	Hydrophilic Interaction Liquid Chromatography
HPLC/E	High Performance Liquid Chromatography/Electrophoresis
HPLC-ESI-MS	High Performance Liquid Chromatography-Electrospray Ionisation-Mass Spectrometry
HRMS	High Resolution Mass Spectrometry
IR	Infrared
IUIS	International Union of Immunological Societies
LC	Liquid Chromatography
LC-MS	Liquid Chromatography-Mass Spectrometry
LoD/Q	Limit of Detection/Quantification
LPS	Lipopolysaccharide
LTQ	Linear Trap Quadrupole
MALDI	Matrix Assisted Laser Desorption/Ionisation
MCDP	Mast Cell Degranulating Peptide

MPLC	Medium Pressure Liquid Chromatography
MRM	Multiple Reaction Monitoring
MS	Mass Spectrometry
MS/MS	Tandem Mass Spectrometry
MSI	Mass Spectrometry Imaging
NBT	p-Nitroblue Tetrazolium Chloride
NHDFs	Normal Human Dermal Fibroblasts
NMR	Nuclear Magnetic Resonance
NSF	N-Ethylmaleimide-Sensitive Factor
SDS/PAGE	Sodium Dodecyl Sulphate/Polyacrylamide Gel Electrophoresis
PBMC	Peripheral Blood Mononuclear Cell
PCR	Polymerase Chain Reaction
PDA	Photodiode Array detector
PMA	Phorbol-12-Myristate-13-Acetate
PMSF	Phenylmethylsulfonylfluoride
PS-DVB	Polystyrene Divinyl Benzene
QqToF	Tandem-Time of Flight
QToF	Quadrupole-Time of Flight
RP	Reversed phase
RT	Room Temperature
SIDR	Strathclyde Innovations in Drug Research
SNAP	Soluble NSF Attachment Protein
SNARE	SNAP Receptor
STP	Standard Temperature and Pressure
TFA	Tetra Fluoroacetic Acid
TFE	Tetrafluoro Ethylene
TNF- α	Tumour Necrosis Factor Alpha
ToF	Time of Flight
UV/Vis	Ultraviolet/Visible
VCD	Vibrational Circular Dichroism
YGG	Tyrosine-Glycine-Glycine
α -CHCA	Alpha Cyano-4-hydroxycinnamic acid

Published Work

The following sections of this thesis have been published or have been submitted for publication.

Chapter 7

Tusiimire, J., Wallace, J., Dufton, M., Parkinson, J., Clements, C. J., Young, L., Park, J. K., Jeon, J. W. & Watson, D. G. 2015. An LC-MS method for the assay of melittin in cosmetic formulations containing bee venom. *Analytical and Bioanalytical Chemistry*, **407**, 3627-3635.

Chapter 8

Tusiimire, J., Wallace, J., Woods, N., Dufton, J. M., Parkinson, J. A., Abbott, G., Clements, C. J., Young, L., Park, J. K., Jeon, J. W., Ferro, A. V. & Watson, D. G. (2016). Effect of Bee Venom and its Fractions on the Release of Pro-Inflammatory Cytokines in PMA-Differentiated U937 Cells Co-Stimulated with LPS. *Vaccines*, **4**(2): 11.

Abstract

Apis mellifera venom has been used since antiquity to treat various ailments but scientific evidence to justify its therapeutic claims is incomplete. The venom has recently entered cosmetic usage as a mimetic ingredient to alleviate signs of facial aging. This study investigated the potential of bee venom (BV) as a source of cosmetic and immunomodulatory agents for use in skin anti-ageing applications and as a vaccine adjuvant, respectively. BV fractions were obtained by reversed phase preparative chromatography and characterised by LC-MS and NMR techniques. The fractions were assayed for antimicrobial and cytotoxic activities against a range of microbes (*Mycobacterium marinum*, *Nocardia farcinia* and *Trypanosoma brucei brucei*) and human cell lines [NCTC2544 (normal keratinocytes), PNT2A (normal epithelial cells), and HS27 (normal fibroblasts)] respectively. Immunomodulatory effects were investigated in PMA-differentiated U937 cells with and without LPS co-stimulation. The aqueous stability of the venom and its susceptibility to protease action were assessed by LC-MS assays. An LC-MS method was also developed and validated for the assay of BV in commercial creams using the melittin signal as an indicator of BV content. Of the 4 BV fractions (F-1 to F-4), the largest, containing melittin, showed the most activity against *N. farcinia* (25-50 μ g/mL) and *T. b. brucei* (0.78-1.56 μ g/mL), but was not very active against *M. marinum* (>100 μ g/mL). The melittin fraction (96% pure) was the most cytotoxic against keratinocytes, fibroblasts and epithelial cells, with $IC_{50} \geq 2.5-4.0\mu$ g/mL. All fractions significantly enhanced IL-1 β release, while only F-4, a lipophilic fraction, enhanced TNF- α release. F-4, which was revealed through NMR elucidation to contain (Z)-9-eicosen-1-ol, produced significant inhibition of IL-6 release. Melittin in aqueous solutions of BV, but not of the melittin fraction alone, underwent a temperature-dependent spontaneous degradation within the ²¹Lys-²²Arg-²³Lys-²⁴Arg sequence due to a serine carboxypeptidase-like activity attributed to the BV allergen, Api m9. Taken together, these results suggest that a formulation matching the 3.2–37.2ppm content of melittin assayed in commercial creams would be safe for skin application based on IC_{50} values in human cells. The immunomodulatory effects observed in U937 cells highlight the potential of BV as a possible source of vaccine adjuvants.

Chapter One

The Skin and its Ageing Process

1 The Skin and its Ageing Process

Ageing of the human body is a natural process features of which first become apparent on the skin, especially on the face (Sadick *et al.*, 2009; Ramos-e-Silva and Carneiro, 2001). Facial ageing signs begin to appear as early as the third decade of one's life—about 3 to 4 decades earlier than they do on unexposed areas such as the abdomen. Cutaneous ageing results from a systematic reduction in the number and size of cells in the layers that make up the skin, as well as from the slowing down of many of the skin's organic functions. Biological functions that slow down with ageing include the ability of the skin to replace lost cells, response to injury, barrier function, clearance of chemicals, perception of sensations, immune and vascular response, sweat production, thermoregulation, and production of vitamin D and sebum (Ramos-e-Silva and Carneiro, 2001). These biological events bring about changes in the aesthetic appearance of the skin, skeletal support structures, and soft tissues (Sadick *et al.*, 2009). These features are also accompanied by increase in the size and distribution of pores (Mizukoshi and Takahashi, 2014).

The process of skin ageing is a complex one which is both inevitable and irreversible, but the appearance of its symptoms can be slowed down or masked. These symptoms include wrinkles, a leathery texture, mottled pigmentation, laxity and sallow discoloration (Fisher *et al.*, 1999). Others include irregular pigmentation, telangiectasia—defined as “small clusters of widened blood vessels on the skin, often spidery in appearance”—and a variety of neoplasms of varying degrees of malignancies (El-Domyati *et al.*, 2002a). Since early on-set skin ageing is due to exposure to the sun, cosmetic anti-ageing interventions must therefore aim at blocking the skin's uptake of UV rays while at the same time revamping the biochemical processes that lead to restoration of the skin's histological integrity leading to a more youthful appearance.

1.1 Skin physiology

Being the outermost part of the body that encloses internal organs, the skin acts as a medium through which the body learns about the external environment. It is a barrier against passage of certain materials in or out of the body, depending on the body's homeostatic or defensive requirements (Staff, 1978). The skin guards against invasion of the body by disease-causing organisms (e.g. bacteria) and harmful substances (e.g. chemical irritants), thus forming part of the innate immune system and a first line of defence for the body. It also takes part in thermoregulation by controlling the production and loss of water as sweat during homeostasis. Through melanin production, the skin ensures that just the right amount of light needed for vitamin D production—which itself is required for bone tissue—penetrates to the deeper layers without causing damage to the underlying tissues (Staff, 1978).

The skin consists of three main layers: (i) the epidermis which is the outermost layer, (ii) the dermis which is referred to as the “true skin”, and (iii) the hypodermis which is largely made up of subcutaneous fatty material (**Figure 1.1**) (Arda *et al.*, 2014).

1.1.1 The epidermis

The epidermis contains pigment-producing melanocytes which produce melanin thus determining the shade or colour of the skin. It is divided into five different functional sublayers (strata) which are (from outermost to innermost): stratum corneum, stratum lucidum, stratum granulosum, stratum spinosum, and stratum basale (**Figure 1.2**). The innermost layers contain young, actively dividing and growing keratinocytes which gradually flatten as they get pushed to the outer layers by newer cells underneath them. This flattening occurs concomitantly with exocytotic extrusion of lipids and complete cornification to become corneocytes, so that the outermost layer (stratum corneum) consists exclusively of dead keratinized cells in an amorphous matrix containing proteins and fats (Lodén, 2003; Staff, 1978).

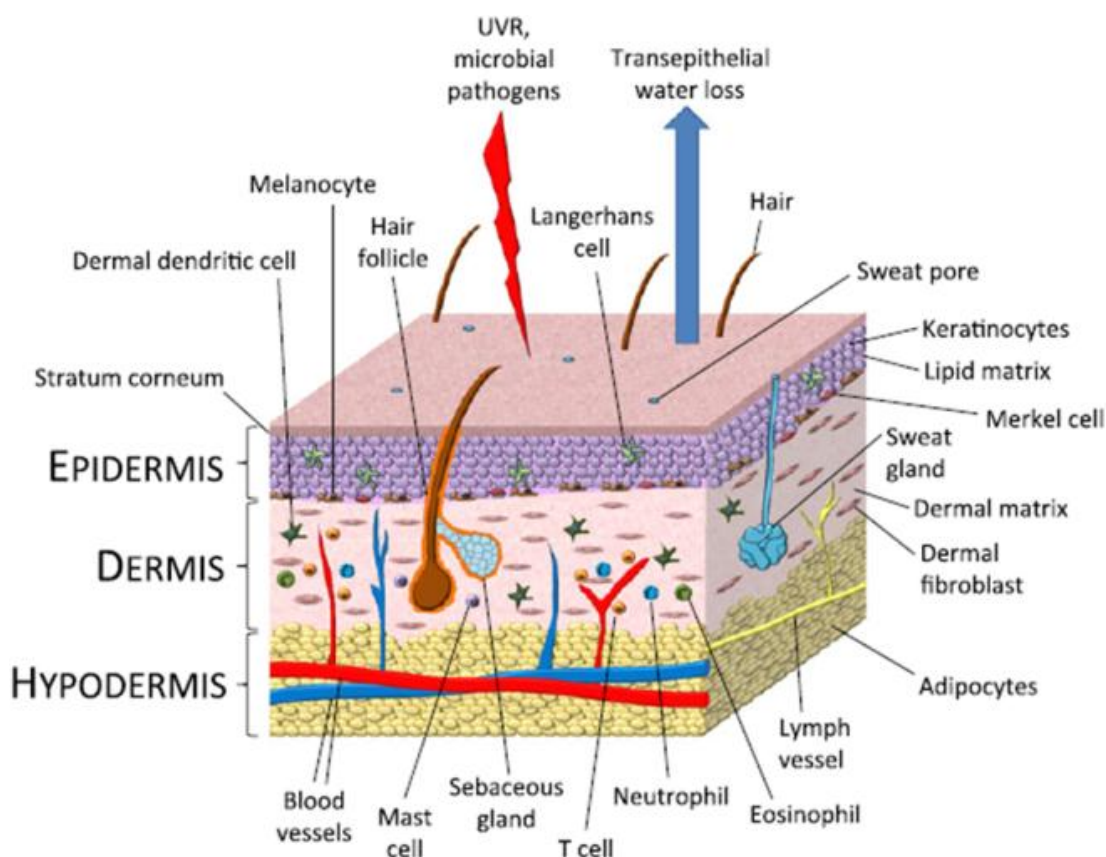


Figure 1.1: Structure of the human skin showing cell populations. The three main layers—the epidermis, dermis and hypodermis—are also shown (Kendall and Nicolaou, 2013). This figure has been reproduced with permission from publisher¹.

Cells on the surface of the stratum corneum continually get sloughed off (Rawlings, 2014); sloughed off cells are replaced by smoother, newly cornified cells beneath them to maintain a state of balance in the epidermis. However, this balance can be disrupted due to impaired physiological function of the skin (e.g. atopic dermatitis) (Lodén, 2003), and naturally slows down with skin ageing. In the normal skin, complete epidermal renewal takes approximately 28 days (Stiefel and Schwack, 2014). Exfoliating and keratolytic agents such as glycolic and salicylic acids, which are respectively alpha and beta hydroxy acids, act by reducing the adhesion of corneocytes in the stratum corneum thus accelerating the sloughing off of dead cells (Flynn *et al.*, 2001; Ramos-e-Silva and Carneiro, 2001). This exfoliating property, leading to

¹ The figure has been reproduced in this thesis from Progress in Lipid Research, Volume 52, Issue 1, Alexandra C. Kendall and Anna Nicolaou, Bioactive Lipid Mediators in Skin Inflammation and Immunity, 141–164, 2013, with permission from Elsevier.

smoother and softer sensation of aged skin, is a key marketing claim for a variety of cosmetic formulations (Draelos, 2008).

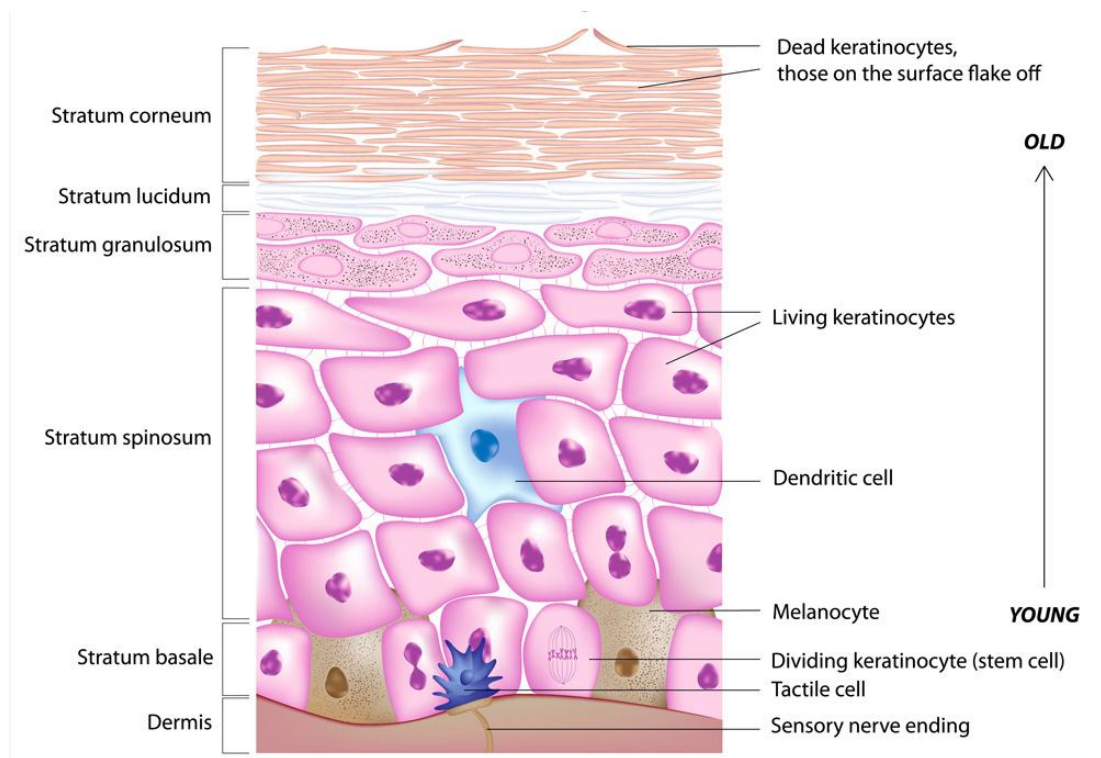


Figure 1.2: Structure of the epidermis of the human skin.

The table below (**Table 1.1**) summarises the features and functions of the 5 sub-layers constituting the epidermis.

Table 1.1: The layers of the human skin epidermis as summarised from (Arda *et al.*, 2014; Bárány *et al.*, 2000; Lodén, 2003).

<i>Layer</i>	<i>Features and functions</i>
Stratum basale	Highest mitotic activity of the skin layers. Composed mainly of keratinocytes, both proliferating (stem cells) and non-proliferating. Continuous cell division of proliferating keratinocytes results in corneocytes that are exfoliated at the skin surface. Base cells have large nuclei, numerous free ribosomes, few mitochondria, small golgi apparatus, and a rough endoplasmic reticulum. Several Merkel cells (tactile cells or touch receptors) and melanocytes are located in this layer.

Stratum spinosum	Thickest layer of skin. It consists of multilayered cells formed from gradual transformation of keratinocytes to become larger, polygonal and flattened in the outward part of the layer. Cells in this layer synthesize cytokeratins (intermediate filaments), which are grouped into bundles known as tonofilaments. Keratinocytes are linked to each other by multiple, prickle-shaped intercellular bridges (desmosomes) where the tonofilaments are anchored to the cell membrane. The resulting reticulate structure accounts for the typical name. Langerhans cells which play a role in the immune system are located in this layer.
Stratum granulosum	There is increased synthesis of keratohyalin in keratinocytes in this layer which initiates the process of their cornification/keratinization. In addition, loss of cell organelles such as nuclei occurs. Lipids in the lamellar bodies are released to form the skin lipid barrier.
Stratum lucidum	Present only in the skin of the palms and soles of feet, the stratum lucidum forms a clear and thin layer of dead cells covering the stratum granulosum.
Stratum corneum	This cornified/horny layer consists of 10-30 layers of enucleated polyhedral corneocytes. These are embedded in a matrix of cornified proteins, including loricrin, involucrin and filaggrins, which are filled with keratin that gives them their water-retaining properties. Corneocytes are “glued” to each other through corneodesmosomes and the surrounding hydrophobic lipids. The stratum corneum accounts for most of the barrier functions of the epidermis by preventing water loss from the body and acting as an impermeable layer for excluding foreign substances.

1.1.2 The dermis

The dermal layer of the skin is separated from the stratum basale of the epidermis by a basement membrane. Fibroblasts are the principal cells found in this layer. Their

role is to secrete extracellular matrix (ECM), and they also produce collagen and elastin, the principal fibrillous connective tissue of the skin responsible for maintaining its mechanical stability and resilience (Teti, 1992). Collagen is the most abundant structural protein in connective tissue (Min *et al.*, 2004), and although there are several forms of the protein in the skin, type 1 is the most abundant, comprising approximately 90% of its dry weight (Takasao *et al.*, 2012).

The dermis also contains sebaceous glands, hair follicles, sweat glands and apocrine glands all of which provide homeostatic functions to the skin and body (Stiefel and Schwack, 2014; Kendall and Nicolaou, 2013). Numerous blood and lymphatic vessels are present which supply nourishment to dermal and epidermal cells and carry away toxic wastes for removal via an excretion process. In addition to the fibroblasts, immune cells are also present. The immune cells found in the dermis include dendritic cells, monocytes/macrophages, lymphocytes, neutrophils, T cells, B cells, eosinophils, and mast cells (**Figure 1.1**). These provide routine surveillance to the blood vessels in the dermis and will infiltrate cutaneous tissues during inflammation, after stimulation by inflammatory mediators such as cytokines (e.g. TNF- α and interleukins IL-1, IL-6) and bioactive lipids, leading to a cutaneous immune cell population (Kendall and Nicolaou, 2013). The dermis consists of both the papillary layer (stratum papillare) and the reticular layer (stratum reticulare) (Stiefel and Schwack, 2014).

1.1.3 The hypodermis

The hypodermis or subcutaneous tissue is the innermost layer of the skin containing mainly adipocytes, larger blood vessels and nerves. It acts as the layer that attaches the skin to underlying tissues such as bone and muscle. The main cells present in the subcutaneous tissue are fibroblasts, adipocytes and macrophages. The adipose tissue acts as a store for energy and free fatty acids. At the same time a range of bioactive mediators for cutaneous cell functions are produced here. For example, fibroblast function in the dermis of the skin is impaired by free fatty acids (FFAs), such as palmitic acid, released by abnormally enlarged adipocytes resulting in impairment of

fibroblast proliferation which consequently affects collagen and elastin production. The negative influence of palmitic acid on fibroblast proliferation was shown to be counteracted by supplementation with eicosapentaenoic acid (EPA), an inhibitor of Toll-like receptors (TLRs), which suggested that enlarged adipocytes possibly decreased the function of dermal fibroblasts through activation of TLRs by secreted FFAs (Ezure and Amano, 2011). Adipocytes are also a source of peptide hormones known as adipokines which regulate various local and systemic effects such as inflammation, insulin sensitivity, fat storage, and appetite regulation (Falcao-Pires *et al.*, 2012). In addition, the adipose tissue has recently been identified as a key source of stem cells with potential to accelerate keratinocyte proliferation and migration, as well as dermal fibroblast proliferation and contraction (Moon *et al.*, 2012; Lee *et al.*, 2012)—processes which can augment wound healing and reverse the effects of an ageing skin.

1.2 Mechanisms of skin ageing

It is generally known that skin ageing is caused by both genetically determined (intrinsic) factors that are mediated via hormones and other biochemical processes, as well as environmentally determined (extrinsic) factors that largely result from exposure to UV radiation, leading to skin damage and loss of its integrity (Sadick *et al.*, 2009).

While intrinsic and extrinsic ageing result in distinct histological features, the main functional changes are similar (Sadick *et al.*, 2009). For instance, intrinsic ageing leads to loss of elastic tissue and reduction in number and size of cells (Gunin *et al.*, 2011; Gunin *et al.*, 2014a; Gunin *et al.*, 2014b) but extrinsically damaged skin features elastosis and increased numbers of mast cells, fibroblasts and histiocytes (Sadick *et al.*, 2009). Thus intrinsic ageing generally demonstrates overall loss of extracellular matrix while photoageing demonstrates selective increases, especially of elastin. However, both types of skin ageing share functional features which include reduced melanocyte and collagen content and impaired wound healing, although these features may be more marked in photo-damaged skin.

1.2.1 Intrinsic ageing

Intrinsic or innate skin ageing has been called the “biologic clock”-type of ageing (El-Domyati *et al.*, 2002a) which affects the skin in a similar way that it affects internal organs—that is, in a slow, irreversible manner. The ageing is associated with gradual loss of homeostatic, structural and functional processes modulated through gene expression of which Sirtuin 6 (SIRT6) is a recently identified regulator (Sharma *et al.*, 2013). Whereas photo-ageing affects mainly areas exposed to the sun such as the face, intrinsic ageing takes place even in sun-protected areas leading to a progressive decrease in the amount of elastic and collagen tissues (El-Domyati *et al.*, 2002b). Histopathological features (**Table 1.2**) are particularly demonstrable during the 8th and 9th decades of human life, implying that features of intrinsic ageing are much more gradual compared to those of photo-ageing which begin to appear around the 3rd decade.

Table 1.2: Changes associated with intrinsically aged skin (Sadick *et al.*, 2009; Mizukoshi *et al.*, 2014; Zouboulis and Makrantonaki, 2011).

<i>Intrinsic features of ageing</i>	<i>Consequences</i>
Flattening of the epidermal-dermal interface	Decreased surface contact area and higher risk of layers being separated by shearing forces
Abnormality or loss of dermal papilla structures	Decreased surface contact area and higher risk of layers being separated by shearing forces
Dermal atrophy resulting in loss of thickness	Reduced strength and resiliency
Loss of elastic tissue in the fine subepidermal elastin network	Sensitization to deformational forces, fine wrinkle formation
Irregular thickening, fragmentation and disorganization of elastic tissue network in the reticular dermis	Dermal deformation and loss of skin firmness leading to wrinkles
Increase in heterogeneously sized basal cells	Increased vulnerability and fragility

Atrophy of the stratum spinosum	Increased vulnerability and fragility
Thinning of the epidermis by 10-50%	Increased vulnerability and fragility
Reduction of fibroblasts	Reduced strength and resiliency
Decreased in the number of Langerhans cells	Reduced immune functions in cutaneous tissue
Reduced melanocyte activity due to decrease in number and increase in their heterogeneity	Greying of hair, guttate amelanosis and lentigines
Atrophy of the extracellular matrix	Reduced strength and resiliency
Reduced production of type I and type III collagens	Fine wrinkle formation
Reduction and disintegration of collagen and elastic fibres, deposition of exogenous substances (e.g. amyloid P)	Sensitization to deformational forces, fine wrinkle formation
Decreased mitotic activity, increased duration of cell cycle and migration time; lower epidermal turnover rate	Decreased desquamation and delayed wound healing
Decreased hyaluronidase protein expression and thus impaired cleavage of hyaluronan (Reed <i>et al.</i> , 2013).	Decreased wound healing ability, perhaps due to decreased cleavage of hyaluronic acid from decreased (Reed <i>et al.</i> , 2013)
Slow replacement of lipids	Disturbed barrier function
Reduced cutaneous microvasculature	Low cutaneous vascular responsiveness, disturbed thermoregulation and reduced nutrient supply of skin
Decrease in size/number and function of skin appendages such as sebaceous glands, sweat glands, apocrine glands	Decreased lipid and sweat production, disturbed reepithelization of deep cutaneous wounds
Thinning of subcutaneous fat	Reduced insulation and energy production
Reduction of nerve endings	Disturbed sensory function

Intrinsic features of ageing (**Table 1.2**) may be attributed to increase in catabolic processes coupled with decreased anabolism in relation to dermal collagen and elastin fibres produced by fibroblasts in the reticular dermis of the skin. It has also been suggested that the growth capacity of fibroblasts decreases with age even in sun-protected skin. At the same time the rate of expression of elastin gene in fibroblasts markedly reduces around the 4th or 5th decade of life. Both these factors reduce the capacity for collagen and elastin synthesis by fibroblasts. This occurs hand in hand with an increasingly abnormal expression of matrix metalloproteinases which lead to increased degradation of the collagen fibres. Altogether these processes lead to dermal atrophy and appearance of fine lines that portray intrinsically aged skin. In addition, the matricellular protein, periostin, which is produced by fibroblasts and non-follicular skin derived precursors, has been shown to play a role in the homeostasis and proper assembly of collagen. When this protein is down-regulated as occurs in ageing skin, it leads to increased susceptibility of collagen towards proteases which contributes to the observed features (Egbert *et al.*, 2014).

The main structural differences between young skin and skin that has undergone intrinsic and photo-ageing are summarised in **Figure 1.3** Young skin shows balanced distribution of keratinocytes in the multi-layered epidermis (E) and in the dermis (D), and the ECM components are quite distinct. Skin that has aged intrinsically shows both epidermal and dermal atrophy. Collagen and elastin in the extracellular matrix are reduced, while the amount of cross linkages in collagen fibres rises. The net number of fibroblast cells reduces; the few remaining ones reveal a more senescent morphological and functional phenotype, with elevated release of matrix-degrading metalloproteinases (MMPs). On the other hand, photoaged skin is hyperplastic with an increased thickness of the stratum corneum (H), epidermis (E) and the dermis layer (D). The epidermis presents with significant roughness and dryness. Melanocyte distribution becomes increasingly inhomogeneous resulting in pigmentary changes. There is a reduction in the number of anchoring fibrils that link the epidermis to the dermis. Interstitial collagen is severely damaged and reduced as well. Elastosis and an increase in microfibrillar components lead to a severely disorganized supramolecular structure that is almost dysfunctional. In the long term continued sun exposure

leads to heliodermatitis, an inflammatory state associated with increased numbers of mast cells and mononucleocytes (Wlaschek *et al.*, 2001).

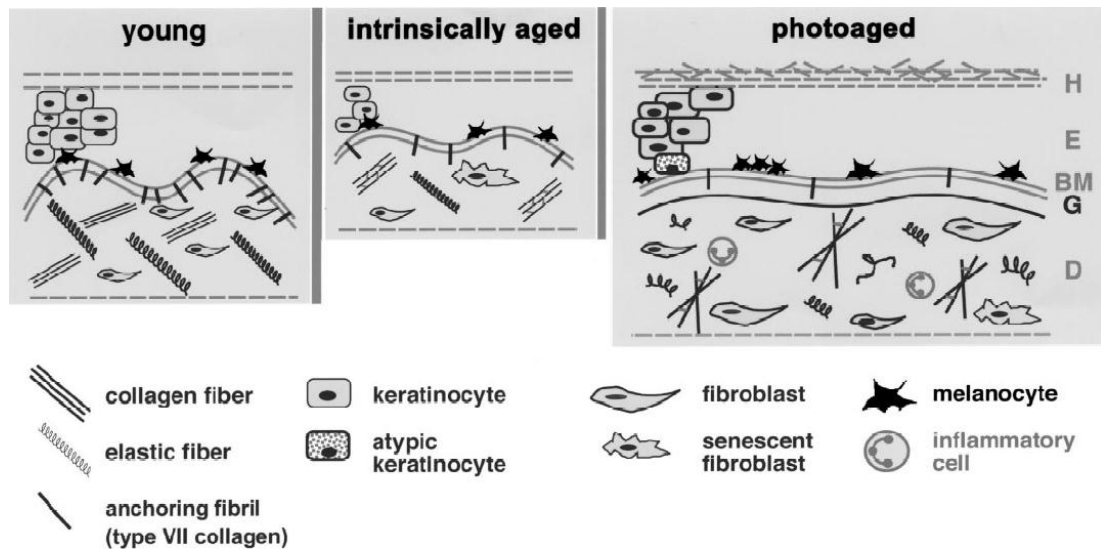


Figure 1.3: Features characteristic of young, intrinsically aged and photo-aged skin. The figure was reproduced with modifications from a previous paper (Wlaschek *et al.*, 2001).

1.2.2 Extrinsic ageing

The ultra violet radiation from the sun can be subdivided into four different wavelengths ranges: UVC, which is less than 290nm wavelength (λ), UVB ($\lambda=290-320\text{nm}$), UVA₂ ($\lambda=320-340\text{nm}$), and UVA₁ ($\lambda=340-400\text{nm}$) (**Figure 1.4**). All of UVC and majority of UVB are absorbed by the ozone layer which is present in the earth's stratosphere. The most damaging biological effects of ultraviolet radiation are due to residual UVB that fails to get absorbed in the earth's stratosphere, although UVA₂ penetrates the skin more deeply and also contributes to photo-ageing (Fisher *et al.*, 1998). Other extrinsic factors for skin ageing include tobacco smoking (Bernhard *et al.*, 2007; Lotfi *et al.*, 2014) and climatic factors such as wind, humidity, pollution, and high temperatures (Singh and Maibach, 2013).

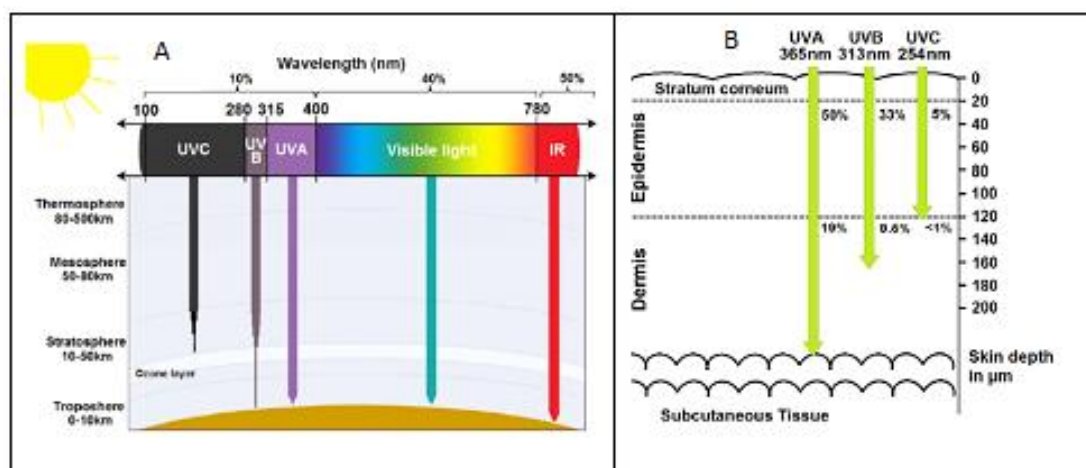


Figure 1.4: A section of the sun's electromagnetic radiation showing the wavelength range of UV (A) and their transmittance through the skin (B). The figures were reproduced with modifications from a previous paper (Stiefel and Schwack, 2014).

It has been suggested that the main mechanism by which exposure to UV radiation induces premature skin ageing is via upregulation of the transcription factor activator protein (AP)-1, and the induction of AP-1-regulated matrix metalloproteinases (MMPs), including collagenase, stromelysin and 92-kD gelatinase, that significantly degrade skin collagen (Fisher *et al.*, 1998; Fisher *et al.*, 1999). At the same time, inhibition of procollagens type I and type III, at least partly due to induction of c-Jun, interferes with the process of transcription of procollagen (Fisher *et al.*, 2000). Both these mechanisms i.e. induction of collagen degradation and inhibition of synthesis of its precursor, procollagen, can be overcome through *in vivo* pre-treatment of skin with *all-trans* retinoic acid (Fisher *et al.*, 2000; Fisher *et al.*, 1998; Fisher *et al.*, 1999), at least 16h prior to exposure to the sun, thereby retarding the process of premature ageing.

Production of oxidant free radicals in form of reactive nitrogen or oxygen species in the skin is an inevitable consequence of physiological metabolism. The most common reactive species in the body are superoxide ions (O_2^-), nitrogen monoxide free radicals ($NO\cdot$) and hydroxyl radicals ($OH\cdot$). Other species of biological importance are hydrogen peroxide (H_2O_2), hypochlorous acid ($HOCl$), singlet oxygen, and peroxynitrite (Wolfe *et al.*, 2014). The harmful effects of reactive molecule species are mediated through impairment of DNA structure and function, leading to damage of

enzymes and cellular structures, and interference with specific signalling pathways in cell metabolism. The body's physiological protection mechanisms include enzymatic and non-enzymatic antioxidant defence systems such as catalase, glutathione, ascorbic acid, and α -tocopherol (Rhie *et al.*, 2001) which are able to keep these harmful substances largely neutralized in a normal body state. However, exposure of the skin to pollutants and UV irradiation produces additional oxidants which eventually overwhelm endogenous protection mechanisms and cause early skin ageing in addition to other skin problems such as immune impairment and cancer. The morphological features of photo-aged skin are shown in **Table 1.3**. It should be noted however that reactive molecular species also trigger metabolic processes that lead to cellular homeostasis, growth and development, immune defence, cell and tissue repair, and apoptosis. The use of antioxidants in cosmeceutical formulations can augment the body's mechanisms to restore the balance between oxidative and anti-oxidative mechanisms in the skin (Wolfe *et al.*, 2014).

Table 1.3: Changes associated with extrinsically aged skin (Sadick *et al.*, 2009; Mizukoshi *et al.*, 2014; Zouboulis and Makrantonaki, 2011).

<i>Morphological features of photo-aged skin</i>
<ul style="list-style-type: none"> • Thickened basement membrane • Generally inflamed with dilated, tortuous blood vessels • Increased populations of mast cells, histiocytes and fibroblasts • Impaired proliferation, differentiation, desquamation and apoptosis of keratinocytes • Epidermis shows an acanthosis and mild hyperkeratosis, which clinically presents as roughness and dryness. • Dermal elastosis (overgrowth of abnormal elastic fibres) due to UV-mediated damage to dermal fibroblasts • Abnormal elastin production • Prolonged breakdown of extracellular matrix by proteases elicited by inflammatory mediators. • Increased levels of dysfunctional glycosaminoglycans and proteoglycans • Hyper-plasticity with an increase in the thickness of the horny layer (H), the

epidermis (E) and the dermal compartment

- Degeneration of collagenous meshwork, increased collagen degradation
 - Stellate phenotype of fibroblasts and increased biosynthetic activity
 - Impairment of wound healing
 - Reduction of melanocyte activity
 - Distribution of the melanocytes becomes inhomogeneous resulting in pigmentary changes ranging from pigmented maculae (solar lentigines) to areas of hypopigmentation (guttate hypomelanosis)
 - Anchoring fibrils which connect the epidermis with the dermis are reduced in number, and also interstitial collagen is reduced and severely damaged.
 - There is an increase in elastic fibres and the microfibrillar components resulting in a non-functional severely disturbed supramolecular structure.
 - State of inflammation (heliodermatitis) with an increase in mononuclear cells and mast cells.
 - Flattening of the dermo-epithelial junction, reduction of anchoring fibrils
-

1.2.3 Role of glucocorticoids

Glucocorticoids (GCs) are potent inhibitors of inflammation whose actions are mediated either through direct binding of the GC/GC-receptor complex to GC-responsive elements in the promoter region of genes, or indirectly through binding of the complex to other transcription factors such as activating protein-1 (AP-1) and nuclear factor-kappaB (NF- κ B). GCs inhibit many pro-inflammatory mediators such as cytokines, chemokines, metabolites of arachidonic acid, and adhesion molecules while at the same time up-regulating anti-inflammatory mediators (Van der Velden, 1998). Current evidence suggests that changes in tissue-specific pre-receptor regulation of local glucocorticoid (GC) availability by 11 β -hydroxysteroid dehydrogenase type 1 (11 β -HSD1) may explain the phenotypic link between GC excess (such as occurs in Cushing's disease) and ageing skin. The role of 11 β -HSD1 in intact cells is exclusively limited to NADPH-dependent oxo-reduction of cortisone to form the active form cortisol (Tiganescu *et al.*, 2011). Expression of 11 β -HSD1 has been characterized in both human and rodent skins, where increased expression of 11 β -HSD1 was

found in primary human dermal fibroblasts (HDFs) donated from older skins, and in donor-matched photo-exposed skin compared to photo-protected ones. This observation has led to suggestions that increased capacity for local GC activation may represent a novel mediator of age-related changes in the physiology, function and appearance observed in both intrinsically and extrinsically aged skin phenotypes (Tiganescu *et al.*, 2013; Tiganescu *et al.*, 2011). Inhibition of the 11β -HSD1 enzyme in mice was demonstrated to prevent age-associated dermal atrophy leading to improved collagen density and restoration of its structural organization, suggesting a novel application of these inhibitors in the treatment of age-related dermal malfunction and enhancement of wound healing (Tiganescu *et al.*, 2013).

1.2.4 Role of oestrogens

Recent studies suggest that the observed deterioration of skin in perimenopausal women may be partly due to declining oestrogen levels. The decline in oestrogen level is thought to lead to decreased rates of collagen production due to effects of oxidative stress caused by reactive oxygen species (ROS) (Bottai *et al.*, 2013). Oestrogens have been reported to exert anti-oxidant and vaso-protective effects in vascular smooth muscle cells through diminished free-radical production mediated via upregulation of superoxide dismutase (SOD) expression and enzyme activity (Strehlow *et al.*, 2003). The SOD enzyme catalyses the dismutation of the cell damaging superoxide (O_2^-) radicals into a less damaging hydrogen peroxide (H_2O_2) or molecular oxygen (O_2), thus protecting the cells from oxidative stress induced by these radicals. This oxidative stress results in damage to cellular membranes and the structure of nucleic acids, resulting in loss of cell viability (Wofle *et al.*, 2014). Another study with 17β -estradiol demonstrated restoration of collagen production in fibroblasts and improved viability of HaCaT cells (keratinocytes) by blocking the effects of H_2O_2 -mediated oxidative cell damage. This demonstrated the effectiveness of oestrogen in restoring dermal integrity and improving skin appearance (Bottai *et al.*, 2013).

1.3 Clinical and physical facial ageing

A combination of both histological and functional changes in the skin gives rise to structural changes that slowly begin to appear on the skin as early as one's third decade of life when soft tissue facial structures begin to weaken (**Table 1.4**).

Table 1.4: Structural features of aged skin (Sadick *et al.*, 2009; Mizukoshi *et al.*, 2014; Zouboulis and Makrantonaki, 2011).

<i>Facial area</i>	<i>Structural and functional features</i>
Upper third	<p>Drooping of eyebrows due to reduced skin elasticity, action of force of gravity, and repeated periorbital muscular contraction</p> <p>Excess lid folds leading to an aged and tired facial appearance <i>due to loss of elasticity in the skin of the upper eyelid.</i></p> <p>Fine deep horizontal lines on the forehead and vertical rhytides on the glabella due to <i>repeated contraction of the frontalis, procerus and corrugators supercilii muscles</i></p> <p>Exposed bony orbital rims due to recession of the soft-tissue prominences near the cheeks</p>
Middle third	<p>Appearance of excess fat in the lower eyelid due to loss of soft tissue over the orbital rims</p> <p>Development of a palpebronasal groove and thinning of subcutaneous fat <i>due to the ageing process</i></p> <p>Prominent nasal fold due to weakening of the malar and orbital ligaments resulting in descent of the malar fat pad and its overlap with the more firmly attached ligaments of the cheek-lip groove.</p>
Lower third	<p>Development of vertical rhytides above the vermilion border <i>due to thinning of the skin in the area</i></p> <p>Elongation of lips and their loss of fullness</p> <p>Accumulation of excess skin and soft tissue near the jaws and chin obscures the well-defined jawline of youth and gives rise to jowls. <i>This results from volume loss and laxity of ligaments and skin in the malar and perioral areas</i></p>

1.4 Anti-ageing approaches

1.4.1 General approaches

Because skin wrinkling is mainly due to volume loss in the cutaneous tissues, any cosmetic application that improves skin hydration will have at least some minimal effect on improving skin appearance. Cutaneous hydration can be improved by reducing trans-epidermal water loss (TEWL) through the use of occlusive agents (e.g. petrolatum or lanolin) or by using agents with water adsorbing properties such as humectants (e.g. glycerin or honey) and hydrophilic matrix agents (e.g. proteins) (**Table 1.5**) (Rudikoff, 1998; Flynn *et al.*, 2001). Incorporation of ceramides into cosmetic formulations aids in improving the skin barrier function and replenishing skin ceramides (Meckfessel and Brandt, 2014) which, along with free fatty acids and cholesterol, play the “mortar” role to the corneocytes’ “brick” in the “brick and mortar” theory of the stratum corneum (Rawlings, 2014).

By forming a film over the surface of the skin, hydrophilic matrices (e.g. proteins) in cosmetic formulations impede trans-epidermal water loss and increase the smoothness of the skin surface. Thus products which incorporate occlusive agents and moisturizing agents will sometimes claim immediate reduction of wrinkled appearance through a combination of better moisturisation and evenness of skin surface which is an anti-ageing claim (Draelos, 2008).

Table 1.5: Categories of common cosmetic ingredients (Draelos, 2008).

<i>Activity</i>	<i>Ingredient</i>	<i>Actions</i>
Occlusive agents	<ul style="list-style-type: none">• Petrolatum• Dimethicone• Mineral oil• Vegetable oils• Waxes• Lanolin	Oily substances that act as barrier on the skin to water loss. Petrolatum blocks up to 99% of water loss from the surface of the skin; it is the gold standard for skin moisturisation. It smells bad, feels sticky and can stain clothes. Prevention of TEWL leads to improvement of fine line of dehydration especially apparent around the eyes.

Humectants	<ul style="list-style-type: none"> • Glycerin • Honey • Sodium lactate • Urea • Propylene glycol • Sorbitol • Pyrrolidone carboxylic acid • Gelatin • Hyaluronic acid • Vitamins • Some proteins 	<p>Rehydrates stratum corneum leading to reduction in fine wrinkling. Once applied onto the surface of the skin, humectants attract water and hold it in a sponge-like manner. They act most effectively when in combination with occlusive to reduce appearance of fine wrinkles on the face, thus helping to substantiate anti-ageing claims.</p>
Hydrophilic matrices	<ul style="list-style-type: none"> • Proteins • Oatmeal bath • Hyaluronic acid 	<p>These large MW film-forming agents cause wrinkle reduction by reducing water escape from the skin through the thin film covering they form on application.</p>

The use of sunscreens is the most obvious approach for counteracting signs of skin ageing. By trapping dangerous UVA and UVB radiations from the sun, sunscreens minimize exposure of the dermis and deeper layers of the epidermis to photo-damage. The incorporation of sunscreens into some cosmetic formulations provides justification for manufacturers to claim enhanced anti-ageing benefits to the skin. This arises from the fact that whereas the moisturizing benefits of the formulation are realized within a matter of hours owing to the softer feel and shinier look of the skin upon application, the photo-protection-related anti-ageing effects may take weeks or months to manifest. Given that UVA radiation is one of the greatest contributors to photo-ageing, broad spectrum photo-protection in the UVA range of wavelengths affords the most anti-ageing benefits. UVA absorbing ingredients used in sunscreens include benzophenone and its complexes, avobenzone and ecamsule (Draelos, 2008).

Products containing *all-trans* retinoic acid and its derivatives, including tazarotene, a second-generation retinoid, offer significant improvements in the appearance of fine

wrinkles and clear away localized cutaneous spots of hyper- and hypo-pigmentation on the skin (Sadick *et al.*, 2009). Retinoid therapy is the mainstay for treatment of photo-ageing; retinoid creams act both by antagonizing the c-Jun mediated inhibition of transcription of procollagen, and inhibiting the breakdown of procollagen types I and III by matrix metalloproteinases, including collagenase, processes that are both induced by UV exposure (Fisher *et al.*, 2000; Fisher *et al.*, 1998; Fisher *et al.*, 1999). Retinoic acid is the active form and therefore must be derived from its various precursors (e.g. retinol, **Figure 1.5**) and derivatives (e.g. retinyl esters with fatty acids, such as palmitic acid) that comprise most retinoid formulations (Draelos, 2008). It should be noted that the body's conversion of some retinoids into retinoic acid is quite low, thus affecting their efficacy, and that retinoic acid itself is irritating (Draelos, 2008). In addition, intact retinyl palmitate is a humectant with potent anti-oxidant properties; this multi-functionality makes retinoids quite popular among cosmetic formulators, particularly those targeting anti-ageing claims (Draelos, 2008). The overall effect of retinoids in cosmetic formulations is improved skin strength and resiliency, as well as an increased water retention in the epidermal layer (Sadick *et al.*, 2009).

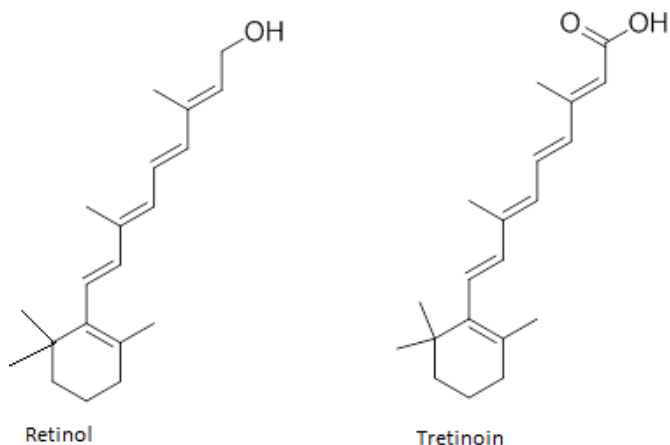


Figure 1.5: Structures of retinol and tretinoin. Tretinoin® is the synthetic form of retinoic acid which has demonstrated potent effects on aged skin (Orfanos *et al.*, 1997) leading to increased collagen synthesis by fibroblasts.

Anti-oxidants represent another avenue for delaying skin ageing. Topical antioxidants act as reducing agents for UV-induced oxygen free radicals produced during metabolism in the body, including in the skin, so as to render them unreactive. Some of these antioxidants include L-ascorbic acid (vitamin C), ferulic acid, alpha-lipoic acid, kinetin, coffee berry, idebenone, coenzyme Q10 (Bentinger *et al.*, 2010) and green tea (Sadick *et al.*, 2009). Because free-radical production in the skin is exacerbated by exposure to UV radiation, antioxidants and retinoids may produce synergistic effects; thus their co-formulation into sunscreens should, in theory, lead to remarkable reduction in skin wrinkles.

It has also been suggested that the long term use of α -hydroxy acids (AHAs) in topical applications can improve skin wrinkling, reduce roughness and correct discoloration in photo-damaged skin. AHAs constitute a small group of low molecular weight organic acids including glycolic acid, citric acid, malic acid and ascorbic acid. While these agents are known for their exfoliating and degranulating properties, they may also lead to increased thickness of the epidermis, induce dermal collagen production, increase dermal perfusion, and improve moisture content of the epidermis. These processes eventually lead to improved skin elasticity and appearance. Because the efficacy of these agents relies on their use at high concentrations at low pH (<3.5), they are not currently available over the counter but only to by prescription from cosmetic dermatologists (Sadick *et al.*, 2009). This limits their use in the general population as easily accessible alternative anti-ageing cosmetic ingredients.

1.4.2 Use of botox injections

Botulinum toxin (botox) is the toxin produced by the bacterium *Clostridium botulinum*. It is a neurotoxin which upon local injection causes temporary muscle paralysis (denervation) by preventing transmission of impulses at the neuromuscular junctions (NMJ) of peripheral cholinergic neurons, thus resulting in relaxation (Benedetto, 1999; Monheit *et al.*, 2007; Huilgol *et al.*, 1999). Botox has no intrinsic effects on the skin's metabolic state that would fit the description of an anti-ageing effect. However, when injected into facial muscles, botox smooths the skin overlying them,

thus providing some relief of the wrinkled appearance of aged skin. Botulinum toxin A (Botox Cosmetic, Allergan Inc., USA) is licensed by US-FDA for managing moderate to severe glabellar lines in individuals who are 65 years or younger, although it also improves other facial lines especially dynamic lines and wrinkles in the upper third of the face (Sadick *et al.*, 2009). The injection is made into the muscles underlying the skin causing specific groups of them to become temporarily denervated (Monheit *et al.*, 2007).

1.4.3 The role of peptides and proteins

Whereas the above approaches mainly aim at offsetting physical and catabolic processes that exacerbate signs of skin ageing, perhaps the most pragmatic approach to anti-ageing is to modulate cell function such as inducing collagen production by dermal fibroblasts. Gradual loss of collagen production and slackening of elastin is one of the key features of ageing in mature skin. Through loss of collagen, the skin loses the very vital foundation and building blocks that confer upon it its youthful appearance of fullness, leading to skin thinning, unevenness, and a wrinkled appearance (Draelos, 2008). Therefore, restoration of collagen production is one of the novel ways in which anti-ageing effects may be attained.

The structural protein, collagen, consists of long chains of amino acids strung together to form a triple helix. Its breakdown by the action of collagenase, an enzyme that naturally degrades collagen, leads to formation of shorter peptide segments composed of 3-5 (or even more) amino acids. It has been suggested that some of these peptide fragments of collagen breakdown may act as signalling messengers arousing the skin to produce more collagen; their presence in the skin acts as an indicator that too much collagen has been broken down which triggers internal repair mechanisms (Draelos, 2008). Thus a positive collagen balance can be achieved, in one part, from down-regulation of collagenase, leading to decreased collagen destruction and, and in the other, from enhancement of collagen synthesis.

One of the earliest and best-known signalling peptides in cosmetic use today is palmitoyl pentapeptide-3 (Matrixyl, Sederma, France). Matrixyl is composed of Lys (K), Thr (T), Thr (T), Lys (K) and Ser (S), thus the term KTTKS that is sometimes used to refer to the peptide (Draelos, 2008). KTTKS's linkage, through chemical bonding, to the free fatty acid palmitic acid (thus the name Pal-KTTKS), is aimed at improving its ability to penetrate the skin (Draelos, 2008; Bissett, 2009), by conferring upon the peptide a hydrophobic property. Matrixyl contains approximately 800 ppm of Pal-KTTKS and in moisturising cosmeceutical formulations it is applied in concentrations of 1 to 4 ppm. Variations of this peptide have been produced by Croda (www.croda.com). The other signalling peptide is dipeptide-2 (Eyeliss, also made by Croda) which is used in cosmetic applications for reducing "eye bags".

Aside from inducing collagen production, other peptides exert their anti-ageing effects through different mechanisms (Gorouhi and Maibach, 2009). Argireline® (**Figure 1.6**) is a synthetic neuropeptide (acetyl hexapeptide-3, distributed by Centerchem) which has been reported to demonstrate *in vitro* blockade of neurotransmitter release from nerves in a botulinum toxin-like fashion (Blanes-Mira *et al.*, 2002; Choi and Berson, 2006; Gorouhi and Maibach, 2009; Lupo, 2005), although it is significantly weaker in strength. Argireline®'s botulinum toxin-like activity is based on blockade of the SNARE (soluble N-ethylmaleimide-sensitive factor attachment receptor) protein complex formation, an important step in the Ca²⁺-dependent synaptic vesicle fusion prior to neurotransmitter release across the synapse (Blanes-Mira *et al.*, 2002). This leads to inhibition of muscular contraction as seen with botulinum toxin; and although it is somewhat less efficacious, Argireline® is also less toxic and non-irritating in comparison to botulinum toxin A.

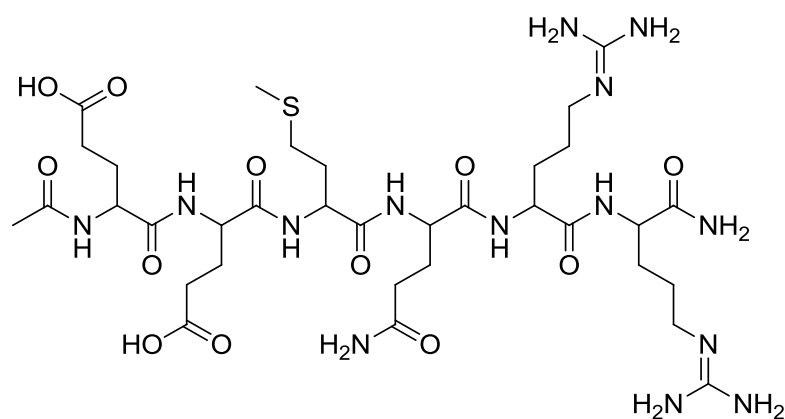


Figure 1.6: Structure of Argireline®.

Other peptides have various applications in, and are linked to, the induction of dermal cell activity to improve the health of the skin. Serilesine®, for example, is hexapeptide-10 which restores normal activity at the dermal-epithelial junction (DEJ). Its manufacturers (Lipotec, Spain) claim that it improves cell adhesion by enhancing synthesis of laminin-5, leading to improved contact between skin cells, which results in firmness of the skin. It's also claimed to induce significant increases in the density of the dermis leading to improved skin compactness (Lipotec, 2008). Eyeseryl® is acetyl tetrapeptide-5 which reduces puffy eyes and minimises ring formation under the eyes. It is also reported to inhibit glycation of collagen, thus preventing loss of elasticity and eye bag formation (Lipotec, 2014a). Liporeductyl® is tripeptide-1 which possesses anti-cellulite activity. This effect is achieved via the peptide's lipolytic action acting through inhibition of adipocyte maturation, and its *venotonic* effect which leads to improved microcirculation (Lipotec, 2014b). Both these products are also being distributed on the market by Lipotec (www.lipotec.com). It is important to note that, as with most cosmetic products, scientific evidence to support these marketing claims is not readily available in public literature.

The Serilesine® hexapeptide is synthesized from the alpha chain of a laminin isoform, laminin-1, a 850kDa glycoprotein found in the basal lamina of the DEJ (Lipotec, 2008; Yoon *et al.*, 2012). Various laminin isoforms exist in various tissues (Ramadhani *et al.*, 2012; Kumagai *et al.*, 2000; Ogawa *et al.*, 2007), of which laminin-1 and laminin-5 are crucial to maintaining the structural integrity of the DEJ, thereby playing key roles in cell proliferation, migration and adhesion (Lipotec,

2008). Laminin-5 has been found to decrease with age but use of Serilesine® helps to restore many of the functions including improvement of cell adhesion through stimulation of α 6-integrins, improved firmness of skin, increase in dermal density to improve compactness of skin, and stimulation of formation of hemidesmosomes—cell structures formed by proteins, α 6-integrins and laminin-332 (Hopkinson *et al.*, 2014)—which improves cohesion between the dermal and epidermal layers of the skin. These processes help to maintain the structural balance of the skin and are also essential to wound healing (Lipotec, 2008).

Another laminin pentapeptide, YIGSR (tyrosine-isoleucine-glycine-serine-arginine), was identified as a strong enhancer of collagen type-1 synthesis in human dermal fibroblasts (HS27 cells) (Yoon *et al.*, 2012). This effect was shown to occur without any changes in cell proliferation or cellular MMP-1 level, and was mediated via phosphorylation of focal adhesion kinase (FAK) and mitogen/extracellular signal-regulated kinase (MEK), since inhibition of these kinases prevented YIGSR-induced collagen-1 synthesis. This suggests that the YIGSR peptide, which corresponds to the 929–933 sequence of the laminin b₁ chain (Yoon *et al.*, 2012), may have potential as an active ingredient in anti-ageing cosmetic applications.

A number of related peptides are also being used in the cosmetic industry for unique and varied functions on the human skin. The company Unipex (Quebec, Canada) produces caprooyl tetrapeptide-3 (marketed by LucasMeyer Cosmetics as ChroNO-line™) which claims anti-ageing properties (LucasMeyerCosmetics, 2014a). The peptide is described as a biomimetic lipopeptide derived from a signal peptide that stimulates the production of laminin-5, collagen VII, and fibronectin—key components at the dermo-epithelial junction. The company also markets Melanostatin®-5 which contains nonapeptide-1, a biomimetic skin-whitening peptide that antagonises α -MSH (alpha-melanocyte-stimulating hormone) receptors involved in melanin production (LucasMeyerCosmetics, 2014d). The α -MSH peptide also exerts anti-inflammatory properties by inhibiting the gene expression of IL-1 β and IL-8 pro-inflammatory cytokines (Capsoni *et al.*, 2015), possibly via inhibition of nuclear factor-kappa B (NF- κ B) transcriptional activity (Yang *et al.*, 2015). On the other hand,

Kollaren® contains tripeptide-1 which is described as a biomimetic signal peptide, derived from natural growth factor, and is reported to stimulate the production of ECM components (including collagen types I&III, elastin, laminin, and fibronectin), thereby increasing skin firmness and improving healing and tissue renewal (LucasMeyerCosmetics, 2014c). Tripeptide-2 (ECM-Protect®) is claimed to provide firmness and improve elasticity of the skin (LucasMeyerCosmetics, 2014b). Cyclopeptide-5 (RonaCare®) from Merck is claimed to reactivate the repair process of aged skin thus stimulating its natural regeneration. Unlike other peptides, cyclopeptide-5 possesses unique stability owing to its cyclic structure and has demonstrated optimal cutaneous efficacy. Finally, a number of patents from Helix BioMedix Inc. claim various bioactivities attributed to peptides of 4 to 6 amino acid residues, including cellular modulation, antimicrobial action, and immunomodulation (Falla *et al.*, 2008; Harris *et al.*, 2011; Harris *et al.*, 2010; Owen, 2002; Owen, 2008; Zhang *et al.*, 2008).

Although peptides have been around in the medical field for the past half century and more, they have only recently been brought into cosmetic usage. Peptides have high biological potencies and are of key value as therapeutic agents in spite of their relatively low stability. Anti-ageing peptides are categorised as signal peptides, enzyme-inhibitor peptides, neurotransmitter-inhibitor peptides, and carrier peptides (Gorouhi and Maibach, 2009). Because of their potential as skin modulating agents, peptides have rapidly emerged on the recent cosmetic scene. They are frequently in formulations accompanied by other active ingredients such as antioxidants, retinoids, and sunscreens. This allows for multiple claims to be made by cosmetic manufacturers with their high cost of production subsequently being transmitted to the consumer in the form of high prices. Peptides may be used to promote cellular growth, immunomodulation or healing of wounds; as synergists or adjuvants to, or in the manufacture of, antimicrobial and anticancer agents.

Chapter Two

The Venom of *Apis mellifera* L. (Honey Bee): Its Applications, Analysis and Theory of Main Techniques Employed

2 The Venom of *Apis mellifera*, its Applications and Analysis

The term “venom” broadly refers to “a secretion, produced within a specialised gland in an animal and delivered to a target animal through the infliction of a wound, of any size, and which contains molecules that disrupt normal physiological or biochemical processes in order to facilitate feeding or defence by the producing animal” (Casewell *et al.*, 2013). Animal venoms generally evolved as a natural innovation to facilitate acquisition of prey or for defence against predatory intrusion (Abdel-Rahman *et al.*, 2011; Newton *et al.*, 2007). Throughout human history, the danger associated with venomous animals and the apparent incongruity between the vulnerable appearance of some venom-producing species and the devastating damage they inflict, paved the way for public fascination with these creatures. Although there are plenty of venomous species in the animal kingdom across several phyla, snakes and bees are the most frequently encountered by humans (Casewell *et al.*, 2013). It has been suggested that snake venoms may have acted as a key selection pressure in the evolution of the primate brain and sensory systems in order to escape predation (Isbell, 2006). On the other hand, the use of weapons as a means of defence is suggested to have favoured evolution of eusociality in insects, particularly bees (Baracchi *et al.*, 2011). Whether for trophic or defence functions, venoms are still a significant subject of research interest among many scientists (Pedarzani *et al.*, 2002). Although most animal venoms remain largely unstudied, they can provide useful models for investigating molecular evolution, functional convergence and prey-predator interactions (Casewell *et al.*, 2013). Their complex chemical composition and the range of bioactivities that they can elicit in biological systems make venoms key targets for novel drug discovery (Harrison *et al.*, 2014; Abdel-Rahman *et al.*, 2013).

2.1 Introduction to honey bee venom (HBV)

The venom of the honeybee (*Apis mellifera* L., Family: Apidae), like that of most other insects belonging to the order Hymenoptera, is mainly used for defence of the colony in order to bolster their eusocial behaviour. Its principal purpose is to inflict

pain on any intruder although it can also be lethal to some arthropods (Moreau, 2013). Also known as apitoxin, bee venom (BV) is essentially a complex mixture, comprising of toxic proteins, peptides and several other bioactive components (Baracchi *et al.*, 2011; Ferreira Junior *et al.*, 2010a; Sciani *et al.*, 2010; Van Vaerenbergh *et al.*, 2013; Zhou *et al.*, 2010). Although HBV is among the most complex of all bee-related materials, only propolis is more complex, but the former has not attracted as much scientific interest as the other bee-resources such as bees-wax, propolis and royal jelly until only just a decade ago (Jones *et al.*, 2011). This is despite the fact that BV has been in use since ancient times for the treatment of various pain-related disorders of the skin and musculoskeletal disorders.

Biological actions of BV are due to its various chemical constituents, the main one of which is the 26 amino acid haemolytic peptide melittin (**Figure 2.1**). The other components are the enzymes: phospholipase A₂ and hyaluronidase; peptides: promelittin, apamine, mast cell degranulating peptide (MCDP), secapin, adolapin and apidaecin; and the amines: histamine, dopamine, and norepinephrine. The venom also contains variable amounts of serotonin, sinkaline, glycerol, phospholipids, sugars, minerals, volatiles and amino acids (Matysiak *et al.*, 2011; Sciani *et al.*, 2010).

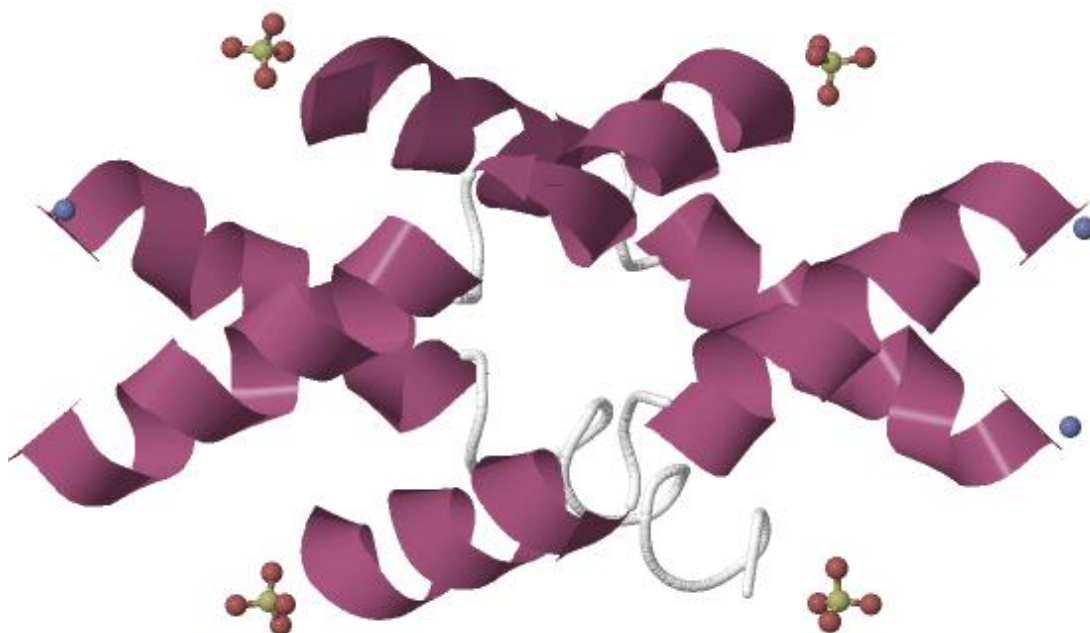


Figure 2.1: Structure of melittin, the main component in BV, as a tetramer, as obtained from the Protein Data Bank (<http://www.rcsb.org/pdb/explore/explore.do?structureId=2MLT>).

The use of BV as an alternative and complementary medicine is deeply rooted in folklore. For thousands of years, the venom was used traditionally to treat both rheumatic and osteoarthritis, tendonitis, musculoskeletal pain, angiocardopathy, multiple sclerosis, wounds, gout, infections and burns among others (Chen and Lariviere, 2010; Rho *et al.*, 2009; Zhou *et al.*, 2010). It is reported to have played notable roles in ancient Chinese, Greek, and Egyptian traditional medicine, although documented evidence linking BV therapy (BVT) to rheumatism did not appear in the literature until late in the 1880's (Chen and Lariviere, 2010). However, bee stings are ordinarily associated with being a source of pain rather than the cure of it; this painful effect is due to the toxic components contained in the venom which induce intense pain in the body by neutralising the analgesic effects of endogenous ligands for the opioid receptor system, such as enkephalins, located in the brain and spinal cord. Other components can cause allergic reactions in sensitive individuals, some of them life threatening. This has made bee stinging, especially that of the more aggressive Africanized variants, a public health concern (Ferreira Junior *et al.*, 2010; Sciani *et al.*, 2010).

2.2 Chemical constituents and biological actions

The honey bee is one of the most widely studied insects (Sciani *et al.*, 2010), and its venom, among the most well characterised of all Hymenopteran secretions (Baracchi *et al.*, 2011; Sciani *et al.*, 2010). Complete characterisation of the venom is far from complete although profiling research has been ongoing for over 2 decades. In fact recent studies have reported newly discovered components, and there is a suggestion that the composition of the venom may vary according to season and geographical location (Matysiak *et al.*, 2011; Meng *et al.*, 2012). However, it is well known that proteins and peptides are the most predominant components (Van Vaerenbergh *et al.*, 2013; Matysiak *et al.*, 2011; Orsolich, 2012) and are responsible for most of the venom's observed biological effects.

2.2.1 Melittin

The main peptide, melittin, constitutes between 40-60% by dry weight of the crude venom (Chen and Lariviere, 2010). Francese *et al.* (2009) reported that melittin is classified as a minor allergen (Api m 4) according to the World Health Organisation (WHO) and International Union of Immunological Societies (IUIS) (Francese *et al.*, 2009). Its main biological effect being haemolytic (Zhou *et al.*, 2010; Sciani *et al.*, 2010), due to its strong surface interaction with the phospholipid bilayer of cell membranes as a result of its amphiphilic nature (Florance *et al.*, 2011; Baracchi *et al.*, 2011). This membrane permeating ability of melittin may be the basis for its cell cytotoxic and anticancer effects.

The biosynthesis of melittin in the venom glands of the honey bee was first studied by Vlasak *et al.* (1983) using mRNA isolated from young queens. The mRNA in these glands almost exclusively codes for prepromelittin, since melittin mRNA accounts for 80% of the total mRNA in the glands. Vlasak *et al.* cloned cDNA transcripts of the total mRNA into a plasmid vector pBR322 followed by transfection to *E. coli*. Two clones with inserts for melittin were found; the longer of the two had a total coding capacity for a 70 amino acid peptide prepromelittin (Vlasak *et al.*, 1983) (Figure 2.2).

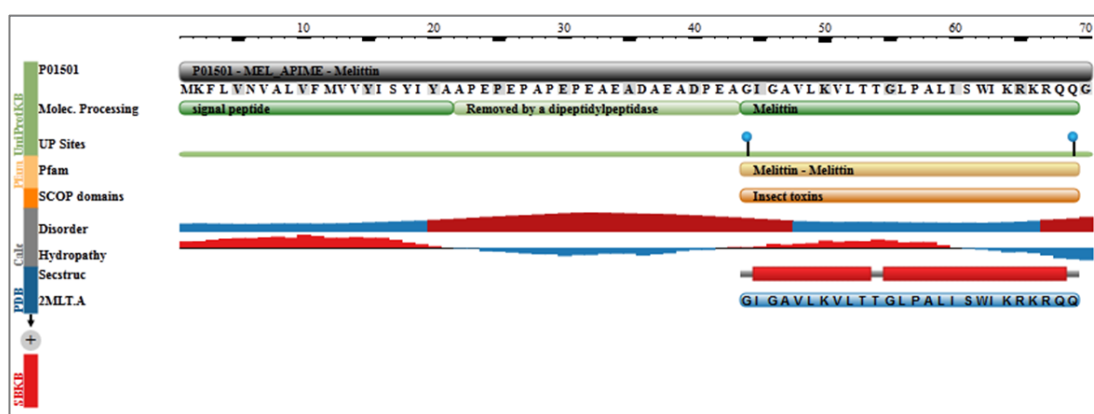


Figure 2.2: The amino acid sequence of prepromelittin. Processing of this protein leads to formation of the mature peptide melittin with 26 amino acid residues: GIGAVLKVLTTGLPALISWIKRKRQQ. The carboxyl terminal glycine forms an amide group in the mature peptide. The figure was obtained from the Protein Data Bank (Eisenberg *et al.*, 1990).

The prepromelittin precursor contains, on its amino-terminal end, a 21-amino acid signal peptide (“pre” region), followed by a 22-amino acid intermediate pro-region. The pre-region is strongly hydrophobic and plays a crucial role in the attachment of the growing polypeptide chain to the membrane of the endoplasmic reticulum and its subsequent discharge into the lumen (Suchanek *et al.*, 1978). The signal peptide is removed by a signal peptidase through cleavage of the peptide bond between amino acid residues 21 and 22, both of which are alanine (**Figure 2.2**). This specific endo-protease activity was demonstrated using a proteolytic extract from rat liver microsomes on honey bee prepromelittin leading to formation of promelittin (Mollay *et al.*, 1982). On the other hand, the “pro” fragment is removed during processing by a di-peptidylpeptidase-like enzymatic action (Kreil *et al.*, 1980).

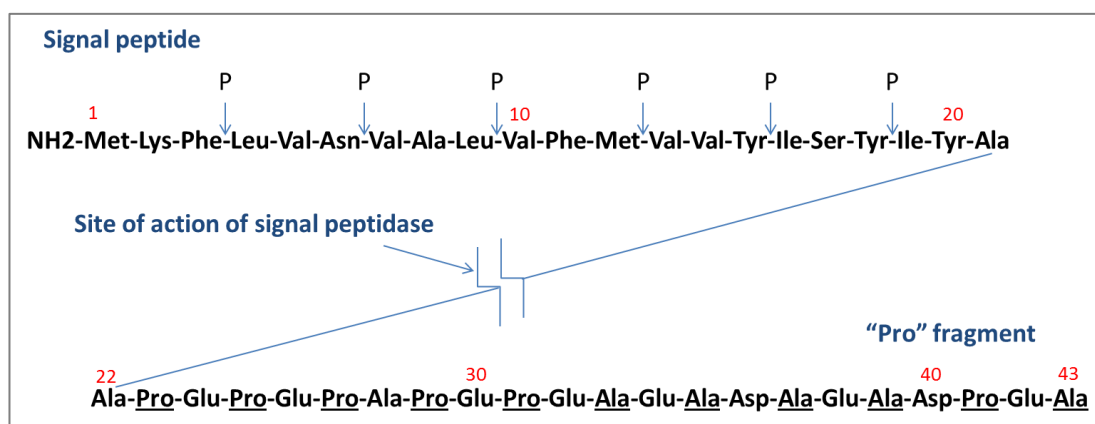


Figure 2.3: Amino acid composition of the “pre” and “pro” fragments of prepromelittin. P denotes sites of peptidase attack. The enzyme signal peptidase cleaves the 21-amino acid signal peptide (“pre” fragment) to form promelittin. The 22-amino acid “pro” fragment contains only four distinct amino acid residues with Ala or Pro at every second position. Figure adapted from (Mollay *et al.*, 1982; Kreil *et al.*, 1980; Suchanek *et al.*, 1978).

The “pro” region of promelittin is peculiar in that its 22-amino acid fragment contains only four distinct amino acids: alanine, proline, glutamate, and aspartate, and every second amino acid in the sequence is either proline or alanine (Mollay *et al.*, 1982) (**Figure 2.3**).

On the carboxyl-terminal end of prepromelittin is a glycine residue which in the mature melittin peptide forms the carboxyl-terminal amide group via a transamidase-like reaction (Suchanek and Kreil, 1977). Thus the melittin peptide occupies the re-

gion between the amino acid 44 (glycine) up to amino acid 69 (amidated glutamine) of prepromelittin—a total of 26 amino acid residues (**Figure 2.4**). Its molecular weight is 2845.6 (Tusiimire *et al.*, 2015). An isoform of melittin, known as melittin-S, was isolated from the venom of Africanised *A. mellifera* which contained a Ser residue instead of Thr at position 10. This peptide was demonstrated to be less haemolytic than melittin, and was found to adopt a less organised secondary structure following studies involving circular dichroism spectroscopy (Sciani *et al.*, 2010).

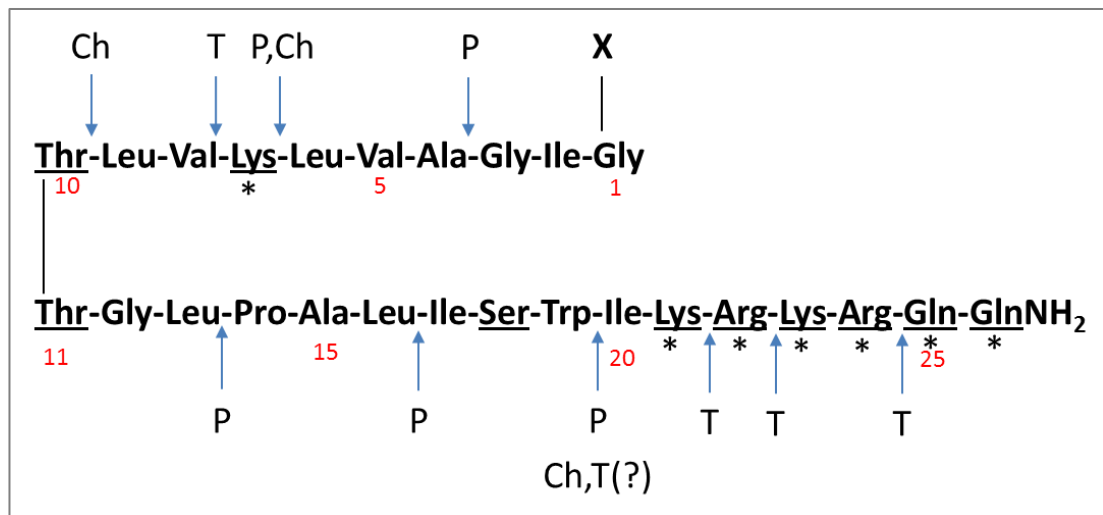


Figure 2.4: The structure of melittin. The underlined amino acids are hydrophilic while those with an asterisk are positively charged. The left side of the structure is thus predominantly hydrophobic and the right side hydrophilic. **X** is mainly hydrogen but in formyl melittin it is a formyl group. The sites for enzymatic attacks by pepsin (**P**), chymotrypsin (**Ch**), and trypsin (**T**) are shown. The melittin isoform, melittin-S, contains a Ser instead of Thr at position 10. Figure adapted from (Habermann, 1972).

2.2.2 Phospholipase

There are two forms of phospholipase, A and B, in Hymenoptera venoms. Phospholipase A (PLA) hydrolyses the 2-ester bond of L-glycerophospholipids (Scott *et al.*, 1990)—which are natural phospholipids including phosphatidyl cholines, phosphatidyl serines and phosphatidyl ethanolamines. Bee venom PLA is of the type PLA₂ which was demonstrated using 1-oleoyl-2-isolauroylphosphatidyl ethanolamine (Habermann, 1972). Bee venom PLA, just like that of snake venoms, acts on structural phospholipids which are integral components of cell membranes and mitochon-

dria; their loss results in failure of cellular processes in the affected region. The effect of PLA on phospholipids is enhanced by formation of lysophospholipids as one of the breakdown products. The latter are surfactants due to their aliphatic acyl and hydrophilic phosphorylated groups; their surfactant properties lead to reduced surface tension of water, micelle formation and solubilisation of cholesterol and lecithin. Lysolecithin has surface active properties similar to those of melittin. It has been suggested that some of the effects produced by PLA₂ may be due to the fatty acids released from the β -position of the phospholipid following enzymatic hydrolysis.

PLA₂ is highly active on lipoproteins. However, unlike melittin, PLA₂ does not directly act on the phospholipids present in intact red blood cell membranes to cause haemolysis. This has been explained to result from the fact that, in the lipid bilayers which constitute membranes, the PLA₂-susceptible 2-ester bond is hidden interiorly, thus inaccessible to the enzyme. This distinguishes PLA₂ from phospholipase C produced by *Clostridium perfringens* which can hydrolyse intact lipid bilayers. The susceptibility of the intact membrane to phospholipase C is due to the fact that this enzyme attacks glycerophosphoryl bonds, which are exterior to the membrane (Habermann, 1972). In the presence of serum lipoproteins or other accessible substrate such as egg yolk, PLA₂ can induce the haemolysis indirectly via formation of lyso-lecithin (Drainas and Lawrence, 1980). A combination of melittin and PLA₂ acts synergistically in that as melittin exerts its direct haemolytic action, it releases material that then becomes accessible to PLA₂ action leading to formation of yet more lytic compounds that are themselves directly acting (Habermann, 1972).

Whether from arachnid, insect, snake or mammalian sources, the PLA₂ enzymes are functionally similar but they differ in their structural complexity (Burke and Dennis, 2009). Structurally, PLA₂ is composed of 129 amino acid residues (**Figure 2.5**). The calculated molecular weight based on the primary amino acid sequence is 14,629 Da although estimates based on ultracentrifugation measurements give a value of 20,000 Da due to extensive glycosylation (Shipolini *et al.*, 1971; Peiren *et al.*, 2008). Fourteen glycoforms of BV PLA₂ have been reported (Lai and Her, 2000). N-glycans are formed by linkage to asparagine 13 (Asn-13) (Hoffman, 2006), and those containing

mannose, glucosamine, fructose and galactose have been identified, although the enzyme can also exist in an unglycosylated form. The presence of sugars leads to overestimation of the actual MW of the glycosylated protein by ultracentrifugation as they lower its partial specific volume (Shipolini *et al.*, 1971). Thus more accurate measurements of molecular weight such as with electrospray ionisation (ESI) mass spectrometry give values between 15.7 and 16.1 kDa (Lai and Her, 2000; Ferreira Junior *et al.*, 2010).

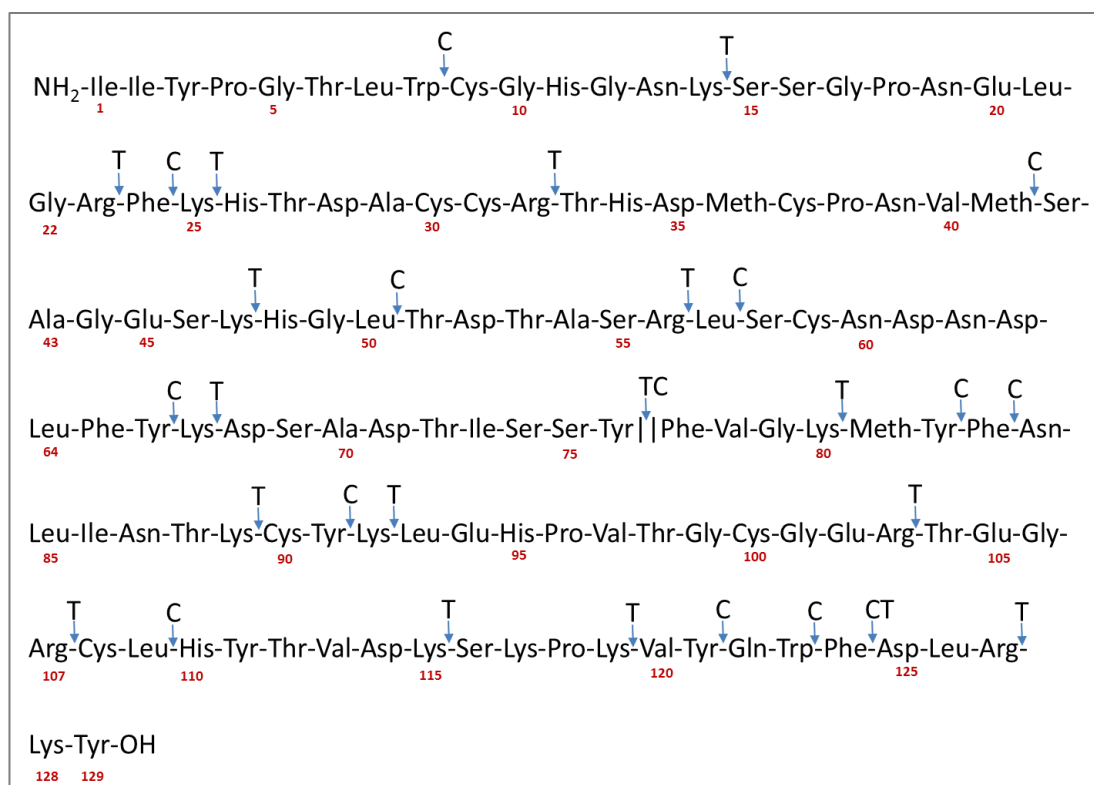


Figure 2.5: Structure of phospholipase A₂. The protein is composed on 129 amino acid residues. Arrows show the sites for protease action by trypsin (T) or chymotrypsin (C). Figure adapted from (Shipolini *et al.*, 1971).

Phospholipase A₂ is one of the main allergens (Api m1) present in BV at levels between 10-20% by dry weight (**Table 2.2**). It can induce IgE-mediated hypersensitivity in allergic persons sensitised to the venom which may be fatal. PLA₂ activity is calcium-dependent and its binding to IgE is greatly affected by its conformation and is significantly reduced by reduction and alkylation reactions (Hoffman, 2006).

2.2.3 Hyaluronidase

Hyaluronidase is present in BV at levels of 2-3% by dry weight and is more active than commercial mammalian testicular hyaluronidase (Habermann, 1972), although their biological actions are similar. The enzyme acts as a spreading factor through its β -1,4-glycosidase action on tissue hyaluronic acid, a linear polymer of repeated disaccharide units consisting of D-glucuronic acid (GlcA) and N-acetyl-glucosamine (GlcNAc), thus aiding the distribution of other venom components (Markovic-Housley *et al.*, 2000). The enzyme is an endo-N-acetyl-D-hexosaminidase, just like bovine testicular hyaluronidase, whose end product of exhaustive hydrolysis is the tetrasaccharide GlcA–GlcNAc–GlcA–GlcNAc (Takagaki *et al.*, 1994; Cramer *et al.*, 1994). Isolation of hyaluronidase mRNA in drone testes and its structural homology to a membrane protein (PH-20) of guinea pig sperm suggested that this protein is also involved in fertilisation (Gmachl and Kreil, 1993).

Structurally, the protein is composed of 350 amino acid residues with 4 cysteine residues (2 disulphide bridges) and 4 possible sites for N-glycosylation (Asn—X—Thr, where X is any amino acid), although only two of those (Asn115 and Asn 263) are glycosylated (Markovic-Housley *et al.*, 2000) (**Figure 2.6**). The carbohydrate content is approximately 7% (Kemeny *et al.*, 1984) and its molecular weight is about 41 kDa (Padavattan *et al.*, 2007), although values of between 35-50 kDa have been reported depending on the method of analysis (Kemeny *et al.*, 1984). Alongside PLA₂, hyaluronidase is one of the principal allergens in BV which can induce life-threatening IgE-mediated allergic reactions among humans (Padavattan *et al.*, 2007) (**Table 2.2**).

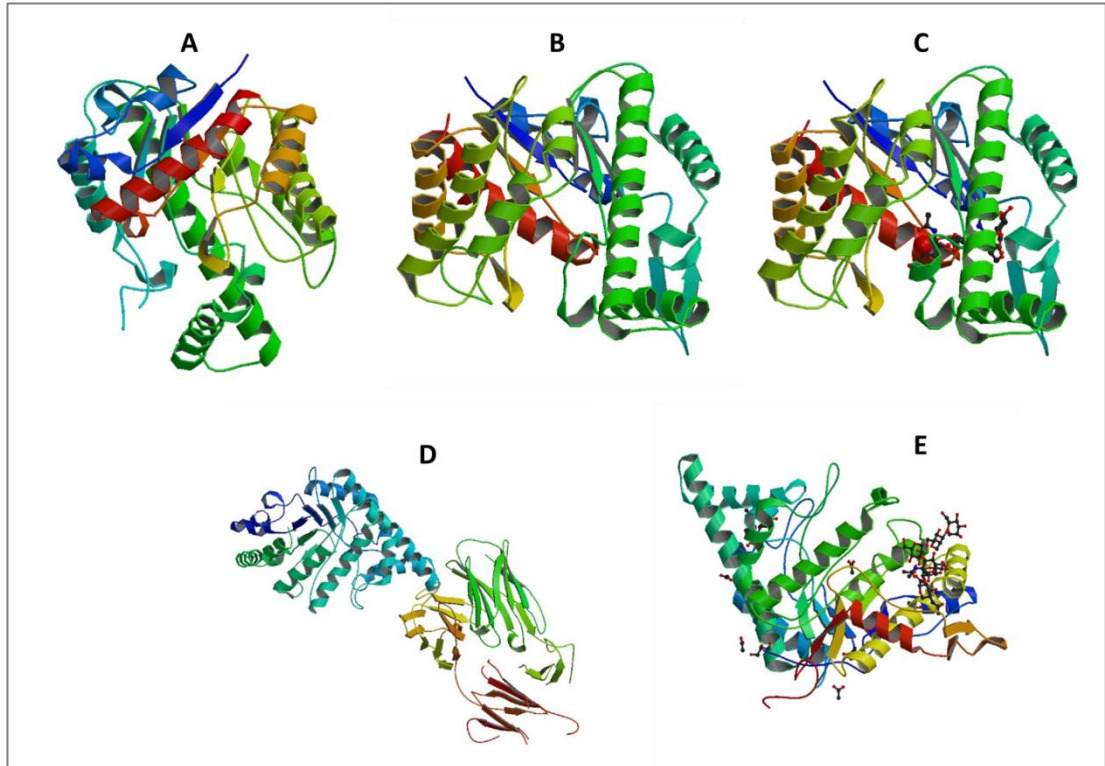


Figure 2.6: Crystal structures of BV hyaluronidase. Structures **A**: monoclinic, **B**: trigonal, **C**: complex with hyaluronic acid tetramer (Markovic-Housley *et al.*, 2000) and **D**: complex with monoclonal IgG Fab fragment (Padavattan *et al.*, 2007). Human hyaluronidase-1 shown in **E** (Chao *et al.*, 2007). Protein chains are coloured from the N-terminal to the C-terminal using a rainbow (spectral) colour gradient.

2.2.4 Apamin

The other major peptide present in HBV is apamin which is an 18 amino acid molecule with a molecular weight of about 2038Da (Chen and Lariviere, 2010; Habermann, 1972). Constituting 2-3 % of BV, apamin is a Ca^{2+} -activated K^+ channel blocker which thus acts as a neurotoxin—the smallest one currently known (Zhou *et al.*, 2010). This peptide was shown to induce uncoordinated, uninterrupted movements in mice which culminated into generalised convulsions following parenteral (intramuscular) administration at doses of 1 mg/kg body weight (Habermann, 1972).



Figure 2.7: Structure of the BV peptides apamin and mast cell degranulating peptide showing their amino acid compositions. The locations of their disulphide chains linking the cysteine residues are shown. Structures adapted from (Gauldie *et al.*, 1978; Habermann, 1972).

2.2.5 Secapin

Secapin (MW 2.87 kDa) is the other main BV peptide and it is made up of 25 amino acid residues with a sequence of YIIDVPPRCPPGSKFIKNRCRVIVP-NH₂ (Vlasak and Kreil, 1984) (**Figure 2.7**). It has been reported that secapin, which constitutes about 1% in dried crude BV, was first isolated in 1976 and that its injection at doses of 40 mg/kg and 80 mg/kg could cause obvious signs of marked hypothermia and sedation. A recently isolated peptide, secapin-1, of molecular weight 2.8 kDa from *A. mellifera* in China which ‘closely resembles’ secapin, and has been reported to be present in the venom at about 0.15% by dry weight (Meng *et al.*, 2012). Secapin-1 (YIINVPPRCPPGSKFVKNKCRVIVP-NH₂) differed in the amino acid sequence from secapin at Gln⁴, Val¹⁶ and Lys¹⁹ (Meng *et al.*, 2012) (Figure 2.8). Another secapin-related peptide was later isolated from the venom of Africanized honey bees with a sequence (YIIDVPPRCPPGSKFVHKRCRVIVP-NH₂) which only differed at Val¹⁸, His¹⁷ and Lys¹⁸ (Mourelle *et al.*, 2014). Biological assays of this peptide showed no induction of haemolysis, mast cell degranulation or chemotaxis but it led to potent dose-related hyperalgesia and edematogenic responses in experimental animals which were mediated via the lipoxygenase pathway (Mourelle *et al.*, 2014). All of these different forms of Secapin shared a disulfide bridge between the Cys 9 and Cys 20 residues (**Figure 2.8**).

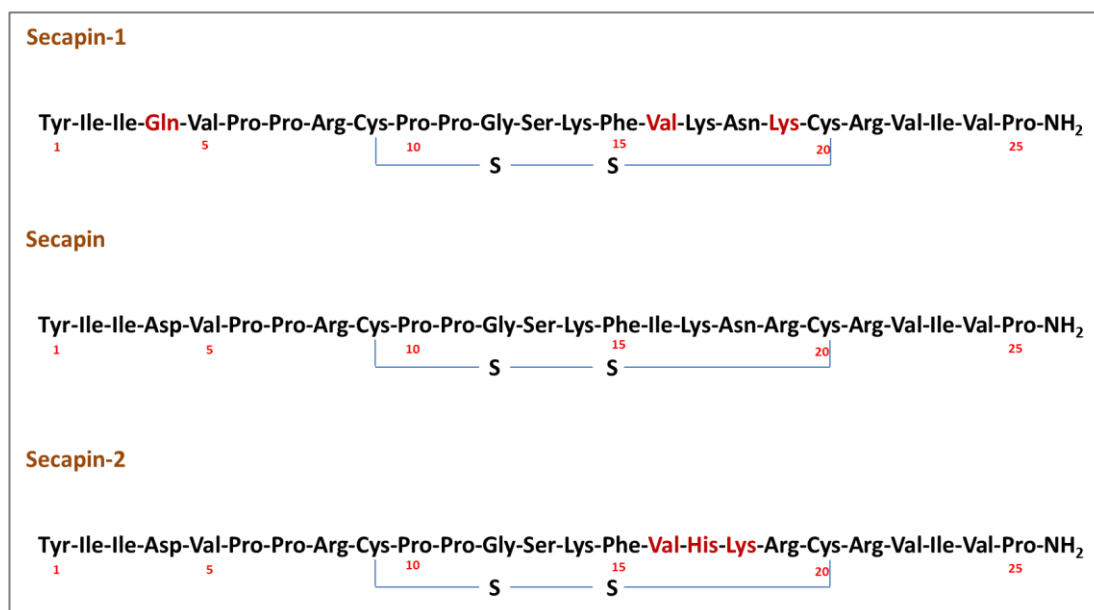


Figure 2.8: Comparison of the amino acid composition of secapin (Vlasak and Kreil, 1984) and other identified secapin-related peptides secapin-1 (Meng *et al.*, 2012) and secapin-2 (Mourelle *et al.*, 2014).

2.2.6 Mast cell degranulating peptide

Mast cell degranulating peptide (MCDP) is another peptide constituting about 2 % by dry weight of HBV. With a molecular weight of about 2.59 kDa, MCDP consists of 22 amino acid residues, with two disulphide bridges (Francese *et al.*, 2009; Habermann, 1972) (**Figure 2.7**). As the name suggests, MCDP acts at low concentrations to cause degranulation of mast cells; their breakdown subsequently releases massive quantities of histamine during an allergic reaction (Baracchi *et al.*, 2011; Baracchi and Turillazzi, 2010). At high concentrations, MCDP demonstrates anti-inflammatory activity. It has been suggested that because of these unique immunologic properties, MCD peptide may serve as a useful tool for studying secretory mechanisms of inflammatory cells such as leukocytes, basophils, and mast cells which might result in the design therapeutic compounds (Buku, 1999).

2.2.7 Adolapin

Adolapin is a basic polypeptide (MW 11,500 Da) which has been reported to possess anti-inflammatory and analgesic activity in carrageenan-, prostaglandin- and adjuvant-induced rat edemas and adjuvant polyarthritis (Shkenderov and Koburova, 1982). These effects were attributed to inhibition of prostaglandin synthesis, via cyclooxygenase inhibition, as well as through central mechanisms (Shkenderov and Koburova, 1982). The polypeptide was also shown to inhibit the activity of both BV phospholipase A₂ and human lipoxygenase from platelets, and it possessed antipyretic as well as analgesic effects (Koburova *et al.*, 1985).

Table 2.1 and **Table 2.2**, respectively, summarise the major peptide and protein constituents of *Apis mellifera* venom, their approximate proportions in the crude venom, and their main effects.

Table 2.1: Main peptide components of honey BV.

<i>Component (% of venom)</i>	<i>MW (Da)</i>	<i>Description</i>
Melittin (40-60)	2846.5	A 26 amino acid peptide. Classified as a cytolytic toxin and minor allergen (Api m4). Main active component of honey BV. Amino acid sequence: GIGAVLKVLTTGLPALISWIKRKRQQ (Zhou <i>et al.</i> , 2010; Sciani <i>et al.</i> , 2010). It is a minor allergen according to the IUIS (Kettner <i>et al.</i> , 2001).
Apamin (~2-3)	2029.9	An 18 amino acid peptide. Smallest known neurotoxin. Amino acid sequence: CNCKAPETALCARRCQQH with two disulfide bonds [Cys ¹ -Cys ¹¹ and Cys ³ -Cys ¹⁵] (Zhou <i>et al.</i> , 2010).
41 Secapin (~1-2)	2866.5	A 25 amino acid peptide. Reported to cause obvious signs of marked hyperthermia and sedation when injected at 40 mg/kg and 80 mg/kg in laboratory animals. Amino acid sequence: YIIDVPPRCPPGSKFIKNRCRVIVP (Meng <i>et al.</i> , 2012; Matysiak <i>et al.</i> , 2011).
Mast Cell Degranulating (MCD) peptide (~2)	2589.4	A 22 amino acid peptide. It causes a massive breakdown of mast cells to cause release of histamine during an allergic reaction. The amino acid sequence of the MCDP precursor is: IKCNCKRHVIKPHICRKICGKN+Amidated (C-term) (Matysiak <i>et al.</i> , 2011).
Secapin – 1 (0.15)	2821.6	A 25 amino acid, newly discovered peptide, with close resemblance to secapin. But differs from secapin at only 3 positions. Amino acid sequence: YIINVP-

Melittin-S (1-2 %) but may rise to 10% during the southern winter months (Sciani <i>et al.</i> , 2010).	2832.4	PRCPPGSKFVKNKCRVIVP with a disulfide bond between Cys ⁹ and Cys ²⁰ . Differs from secapin at the Gln ⁴ , Val ¹⁶ and Lys ¹⁹ residues (Meng <i>et al.</i> , 2012). A less haemolytic isoform of melittin containing a Ser residue at the 10 th position instead of a Thr in melittin. Tends to adopt a less organized secondary structure compared to melittin. Amino acid sequence: GIGAVLKVLSTGLPALISWIKRKRQQ (Sciani <i>et al.</i> , 2010).
New peptide [HTGAVLAGV] with an amidated C-term.	822.53	Reported for the very first time by (Matysiak <i>et al.</i> , 2011).
Tertiapine (<1%)	Unspecified	Has a high-affinity binding sites in rat brain; inhibits the enzyme-activating ability of calmodulin; inhibits activity of soluble phosphodiesterases (Chen and Lariviere, 2010).
Cardiopep (0.7%)	Unspecified	Possesses β -Adrenergic and anti-arrhythmic effects (Chen and Lariviere, 2010).
Promelittin (un specified)	Varied	A range of peptides having molecular weights from ~3.0 kDa to 4.9 kDa (Matysiak <i>et al.</i> , 2011).
Protease inhibitor (unspecified)	Unspecified	Unspecified

Table 2.2: Main allergenic proteins of *Apis mellifera*. Note that Api m1-4, 6, 7 are major components of honey BV (WHO/IUIS, 2014).

<i>Protein Allergen (% composition)</i>	<i>MW (kDa)</i>	<i>Description/Notes</i>
Phospholipase A ₂ (10-20)	16	A protein allergen (Api m1). Acts in synergy with melittin to cause cell cytotoxicity. Occurs mainly as glycosylated forms thus giving it higher molecular weights ranging between 15.2 and 16.7 kDa depending on the number of sugar residues present (ranging from 1 to 9).
Hyaluronidase (1-2)	39	Large protein allergen (Api m2). Molecular weight dependent on N-linked carbohydrate present. This protein is called the “spreading factor” because it disrupts hyaluronic acid intracellular matrix.
Acid Phosphatase (1-2)	43	Protein allergen (Api m3). The molecular weight of 43.9 kDa is from processed amino acid sequence. Thus actual molecular weight might vary and can increase due to glycosylation. It’s thought to act like other high molecular weight phosphatases by hydrolysing phosphoesters in a 2-step process.
Melittin (40-60)	3	See Table 2.1above.
Dipeptidylpeptidase IV	100	Api m5.
Newly Discovered Small Protein (1-2)	8	This small protein allergen (Api m6) consists of four isoforms in equimolar amounts and with same allergenicity. Api m6.01 and Api m6.03 have five disulfide bonds with MWs 7179.6 and 7588.1 resp. Api m6.02 and Api m6.04 have extra two amino acids at C-terminus (Leu and Pro) and have MWs 7389.9 and 7798.3 resp. Api m6 was recognised by IgE antibodies more than 40% of HBV-hypersensitive patients (Kettner <i>et</i>

		<i>al.</i> , 2001).	
	CUB ² Serine Protease	39	Api m7. This allergen contains a typical tryptic protease domain with a serine protease catalytic triad. Structural organization suggests that the CUB domain is involved in interactions with natural substrates while the Serine Protease-like domain probably activates zymogens. It also shows structural and functional similarity to the members of the PPAF-II family (Georgieva <i>et al.</i> , 2011; Georgieva <i>et al.</i> , 2010).
	Carboxylesterase	70	Api m8.
	Serine carboxypeptidase	60	Api m9.
	Icarapin variant 2, carbohydrate-rich protein	50-55	Api m10.
44	Major royal jelly protein (Royalactin)	50 (deglycosylated form)	Api m11. Kamakura (2011) showed that a 57-kDa protein in royal jelly, previously designated as royalactin, induced the differentiation of honeybee larvae into queens (Kamakura, 2011).
	Vitellogenin	200	Api m12. It's a precursor of the egg-yolk proteins that are sources of nutrients during embryonic development. Involved in the differentiation of honeybee larvae into queens.

²CUB is named for a class of compounds including Complement subcomponents C1r/C1s, Uegf, and Bone morphogenic protein-1 (LEVINE, M. Z., HARRISON, P. J., WALTHALL, W. W., TAI, P. C. & DERBY, C. D. 2001. A CUB-serine protease in the olfactory organ of the spiny lobster *Panulirus argus*. *J Neurobiol*, 49, 277-302).

2.2.8 Other components of HBV

Apart from peptides and proteins, which are the main components, HBV also contains variable amounts of carbohydrates (2%) (mainly monosaccharides e.g. fructose and disaccharides e.g. sucrose), catecholamines (e.g. dopamine and noradrenaline) (Owen and Bridges, 1982), as well as lipids (5%). The other components include: acetylcholine, adolapin (1%), amino acids, esterase, histamine (1.5%), and lipids (5%) (Chen and Lariviere, 2010). In addition to these there are also variable amounts of volatile constituents probably derived from plants such as essential oils.

2.3 Applications and uses of BV

The earliest and most popular use of BV since antiquity is that of pain relief. It was a key component of ancient Greek, Chinese and Egyptian traditional and complementary medicine to treat arthritic or rheumatic pain, although it remained largely unrecognised in general medical circles (Chen and Lariviere, 2010). It was only around the beginning of the past century that there was increased awareness of the pain-relieving effects of HBV. Soon it was being used in treatment of various disorders including autoimmune diseases, with the global standard for the dried purified sample being established by the US FDA. But even then HBV remained largely at the periphery of conventional therapy, due perhaps to its questionable efficacy, but certainly because its safety could not be guaranteed because of the multiple allergens present, some of which have only just recently been characterised (Chen and Lariviere, 2010; Kettner *et al.*, 2001).

However BV therapy has continued to make important inroads towards general acceptance. It is currently used for management of several kinds of neurological pain (Chen and Lariviere, 2010) and some immune-related disorders (Orsolich, 2012) in a field of therapy now known as apitherapy. Recently, the scope of apitherapy has expanded to include treatment of tumours such as those of renal, lung, liver, prostate, bladder, and mammary type as well as leukemia cancer cells. It has been reported that melittin, phospholipase A₂, and probably apamin are the primary components

with anticancer activity through their cell cytotoxic effects, and that melittin activates PLA₂ thus potentiating its cell lytic effects. These venom components have also been shown to act on cancer cells through various other mechanisms involving different cellular pathways such as activation of caspase and matrix metalloproteinases resulting in cell apoptosis (Orsolich, 2012).

Recent evidence also suggests that BV may have a role in attenuating inflammatory changes in Parkinsonism by decreasing the expression of inducible nitric oxide synthase and macrophage antigen complex-1. The same authors also suggest that melittin restores proteasome functionality in animal models of amyotrophic lateral sclerosis and multiple sclerosis (Kapoor, 2012).

The use of BV in pharmacopuncture has also been shown to be effective in alleviating symptoms of peripheral neuropathies secondary to chemotherapy and similar etiologies. At the same time, due to its inhibitory effect on *Borrelia burgdorferi*, it has been suggested that melittin may play a role in treating the neurological stage of Lyme disease (Kapoor, 2012).

But perhaps the most significant field for our interest in BV research is its use in the cosmetic industry. There are a number of registered pharmaceutical honey BV products on the European and global markets including Forapin in Germany, Virapin in Slovakia, Apiven in France, Melivenon in Bulgaria and Apifor in Russia (Matysiak *et al.*, 2011). But all these products, which are mainly skin ointments, are largely still formulated with the crude BV. Also BV is stated to be an ingredient in a number of the “Bee Venom Purified” Manuka brand skin care collection of products available on the UK and other European markets. Given the high allergenic content of BVs, the safety of these products may not be guaranteed especially in sensitive individuals. A means of separating all of possible allergens is thus sought before the venom can be formulated into safe commercial products.

2.4 Analysis of BV

Due to the complexity of the BV sample, any successful method of differential analysis should ideally attempt to separate the main components. Thus separation techniques based on liquid chromatography (e.g. HPLC), size exclusion gel electrophoresis (Kettner *et al.*, 2001) and capillary zone electrophoresis (Lai and Her, 2000; Kokot *et al.*, 2011a; Wojcik *et al.*, 2012) have been at the forefront of most BV profiling studies in the recent past.

The detector systems used have included the diode array detector (DAD) (Zhou *et al.*, 2010; Kokot *et al.*, 2009; Kokot *et al.*, 2011a), although the commonest one has been a mass spectrometer hyphenated to a separation technique, mainly the HPLC, by way of an ESI interface as the ion source (Baracchi *et al.*, 2011; Francese *et al.*, 2009; Matysiak *et al.*, 2011; Sciani *et al.*, 2010; Stoecklin *et al.*, 2010; Ferreira Junior *et al.*, 2010). A number of studies have also been undertaken using the matrix assisted laser desorption/ionisation–time of flight (MALDI-TOF) technique (Baracchi *et al.*, 2011; Matysiak *et al.*, 2011), including mass spectrometry imaging (MSI) (Seppala *et al.*, 2012; Francese *et al.*, 2009). The other mass analysers which have been used in HBV or related peptide analysis are tandem mass spectrometry (MS/MS) (Zhou *et al.*, 2010; Stoecklin *et al.*, 2010) and high resolution mass spectrometry (Baracchi *et al.*, 2011; Francese *et al.*, 2009).

There has been an increased tendency in the recent past few years to move towards the use of high resolution mass spectrometry (HRMS), employing Fourier Transform (FT) technology (Scigelova *et al.*, 2011), in the analysis of proteins (Michalski *et al.*, 2011; Zhang *et al.*, 2010; Olsen *et al.*, 2009). This is because of its high resolving power and superior mass accuracy in comparison to MALDI-TOFs and other non FT instruments (Hu *et al.*, 2005; Denisov *et al.*, 2012; Makarov and Denisov, 2009; Makarov *et al.*, 2009; Scigelova *et al.*, 2011; Scigelova and Makarov, 2006). However it is not clear from the past HBV studies why these techniques have not been more widely applied although the techniques have only been widely available for around six years.

While the above techniques have been useful for the assay of whole BV components, the elucidation of molecular structures, amino acid sequences, and molecular structural configurations have been mainly based on some more elaborate systems. For example the amino acid sequencing of the peptides melittin (Sciani *et al.*, 2010; Ferreira Junior *et al.*, 2010) and secapin-1 (Meng *et al.*, 2012), and of the allergen Api m 6 (Kettner *et al.*, 2001) have been determined by Edman degradation. The latter authors carried out tryptic digests of the approximately 7.2-7.8 kDa isoforms of Api m6 prior to the Edman N-terminal sequencing of the protein and proteolytic fragments from the allergens. On the other hand C-terminal sequencing required the use of a MALDI-TOF to analyse V8 proteinase digests (Kettner *et al.*, 2001).

There are a number of other techniques which have been recently used in HBV analysis to study melittin structural configurations. These include: ion mobility MS, molecular dynamics and hydrogen-deuterium exchange in the gas phase (Florance *et al.*, 2011), x-ray crystallography (Anderson *et al.*, 1980; Terwilliger and Eisenberg, 1982; Terwilliger *et al.*, 1982), circular dichroism (Sciani *et al.*, 2010; Wang and Polavarapu, 2003), and NMR (Miura, 2011).

2.4.1 High performance liquid chromatography (HPLC)

The most commonly used assay technique for BV is the reversed phase HPLC method. Peptides have varying proportions of amino acids possessing basic, acidic, neutral, and hydrophobic side chains. Therefore, their degrees of ionisation and, mainly, interaction with the stationary and mobile phases during liquid chromatography differ which leads to their separation, as described in section 2.6. As with most complex mixtures, BV profiling by HPLC requires the use of gradient elution profiles (Dolan, 2013a; Dolan, 2013b). This ensures optimal resolution (and high chromatographic efficiency) of most components within reasonable analysis times. Isocratic profiles would ideally take longer times but perhaps their main disadvantage comes from poorly resolved peaks on the chromatogram, resulting from band broadening due to longitudinal analyte diffusion among other processes (Watson, 2012).

2.4.1.1 Sample preparation

The main components of BV are quite polar, thus sample preparation prior to LC involves extraction in pure water (Zhou *et al.*, 2010; Kokot *et al.*, 2011a; Meng *et al.*, 2012) or in an acidic solution of 0.1% trifluoroacetic acid (TFA) (Ferreira Junior *et al.*, 2010; Sciani *et al.*, 2010) or 0.2% formic acid in acetonitrile:water mixtures for LC-MS. Typical concentrations used are in the nominal range of 0.02 mg/mL for LC-DAD-MS/MS (Zhou *et al.*, 2010), to 0.3 mg/mL for LC-DAD (Kokot and Matysiak, 2009; Kokot *et al.*, 2011b), to 1 mg/mL for LC-PDA (Sciani *et al.*, 2010; Ferreira Junior *et al.*, 2010), and 10 mg/mL for peptidomic analysis (Van Vaerenbergh *et al.*, 2013) using UV/Vis detector.

2.4.1.2 Columns

Both C8 (Kokot *et al.*, 2009; Ferreira Junior *et al.*, 2010; Sciani *et al.*, 2010) and C18 (Zhou *et al.*, 2010; Meng *et al.*, 2012; Van Vaerenbergh *et al.*, 2013) reversed phase columns have been used for BV analysis. In addition, successful use of a PepSwift monolithic polystyrene divinylbenzene (PS-DVB) column in the profiling of BV has also been reported (Baracchi *et al.*, 2011; Baracchi and Turillazzi, 2010). The PS-DVB microparticle is based on the aromatic ring chemistry, of a polystyrene divinylbenzene copolymer, leading to similar but distinct separation properties when compared to conventional C8 and C18-type resins.

2.4.1.3 Mobile phases

The commonly used mobile phases are 0.1% (w/w) solution of TFA in water as solvent A and 0.1% (w/w) solution of TFA in acetonitrile as solvent B. Formic acid, instead of TFA, has also been used in some studies especially those meant for LC-MS analysis since TFA produces a high background signal in mass spectrometry.

2.4.1.4 Detection systems

The most commonly used detector for BV in HPLC profiling studies has been a mass spectrometer to which the LC is coupled. The other detectors have included: the

DAD (Kokot *et al.*, 2009; Kokot *et al.*, 2011a), UV/Vis (Van Vaerenbergh *et al.*, 2013), and the PDA (Ferreira Junior *et al.*, 2010; Sciani *et al.*, 2010).

2.4.1.5 Elution processes

The elution profiles for the analysis of BV are mainly gradient-based as the venom is a complex mixture. This is because using an isocratic profile of elution would lead to prolonged analysis times before all components could be eluted. At the same time, this permits an increased longitudinal diffusion which leads to peak tailing and a loss of resolution and chromatographic efficiency. Given that most of the LC assays for BV are of the reversed phase type, gradient profiles start with high aqueous (low strength solvent) and gradually change to high organic (high strength solvent). In the past HBV profiling studies both linear (Kokot *et al.*, 2009; Kokot *et al.*, 2011a; Zhou *et al.*, 2010) and step-wise or multi-linear gradients (Ferreira Junior *et al.*, 2010; Sciani *et al.*, 2010; Baracchi *et al.*, 2011; Baracchi and Turillazzi, 2010) have been used. Typical flow rates used have ranged from 200 $\mu\text{l}/\text{mL}$ (Ferreira Junior *et al.*, 2010; Sciani *et al.*, 2010); 300 $\mu\text{l}/\text{mL}$ (Baracchi *et al.*, 2011; Baracchi and Turillazzi, 2010; Zhou *et al.*, 2010); 700 $\mu\text{l}/\text{mL}$ (Van Vaerenbergh *et al.*, 2013), and 1 mL/min (Kokot *et al.*, 2009).

2.4.2 Mass spectrometry

There are various mass spectrometric techniques currently in use in pharmaceutical analysis studies. However latest studies on BV have utilised mainly the MALDI-ToFs (Francese *et al.*, 2009; Baracchi *et al.*, 2011), triple quadrupoles (Zhou *et al.*, 2010; Stoecklin *et al.*, 2010), QqToFs (Matysiak *et al.*, 2011) and high resolution mass spectrometry (HRMS) (Baracchi *et al.*, 2011). The latter are some of the latest high resolution and accurate mass measurement MS systems, based on the FT mathematical operation, which have gained prominence in protein and peptide studies in proteomics (Denisov *et al.*, 2012; Makarov and Denisov, 2009; Scigelova and Makarov, 2006).

The use of mass spectrometry in protein and peptide analysis was made possible by the development of two soft ionisation techniques – matrix assisted laser desorption ionisation (MALDI) and electro-spray ionisation (ESI) (Matysiak *et al.*, 2011). While the latter provides an interface for hyphenation of the mass spectrometer to a liquid chromatographic separation technique (e.g. HPLC), the former provides the advantages of direct analysis including robustness, speed, and sensitivity although it is not suitable for absolute quantification studies (Matysiak *et al.*, 2011). Both ESI and MALDI ionisation techniques are capable of operating in negative or positive ionisation modes, or both.

2.4.2.1 MALDI-TOF mass spectrometry

In MALDI-TOF mass spectrometry the BV sample solution is mixed with an appropriate matrix solution and the mixture loaded on a sample plate which is then dried. The common matrices used for HBV include α -cyano-4-hydroxycinnamic acid (α -CHCA) (Matysiak *et al.*, 2011; Baracchi *et al.*, 2011; Baracchi and Turillazzi, 2010; Ferreira Junior *et al.*, 2010a; Francese *et al.*, 2009) and sinapinic acid (Matysiak *et al.*, 2011; Francese *et al.*, 2009). Solvents used for dissolving the matrices are 50/50 (Matysiak *et al.*, 2011) or 70/30 (Baracchi *et al.*, 2011; Francese *et al.*, 2009) mixtures of acetonitrile/0.1 % TFA to make solutions of approximately 10-20 mg/mL. The venom and matrix solutions are then mixed in ratios dependent on the concentration of the BV sample. One author (Matysiak *et al.*, 2011) has reported using approximately a BV/matrix ratio of 1:20 (w/w) for α -CHCA and 1:40 (w/w) for sinapinic acid. The mixed sample can then be loaded on the sample plate as 1 μ l drops before the plate is dried in a stream of air at low temperature (e.g. 35°C) ready for analysis (Matysiak *et al.*, 2011).

The authors of the above comprehensive venom profiling study further noted that although sinapinic acid enabled the detection of more peptides than α -CHCA, the latter was a prerequisite for the detection of apamin and MCD peptide, the less characterised peptides of those studied (Matysiak *et al.*, 2011). The TOF can be operated in either positive or negative reflectron modes with scan ranges of m/z 100 – 4000 for peptides and m/z 6000 – 50,000 for proteins (Francese *et al.*, 2009). Calibrations

for each of these ranges are also carried out accordingly, for example using the Bruker peptide (m/z 1000 – 3500) or protein (m/z 18,000 – 66,000) calibrants, respectively, as reported by (Francese *et al.*, 2009). The instrument run conditions are optimised for the peptides and proteins according to manufacturer's guidelines and the results obtained can be analysed using relevant software.

A similar technique has been shown to work for in-situ imaging of honey BV components in $Al(OH)_3$ adsorbed BV immunotherapy preparations (Seppala *et al.*, 2012) and other envenomed tissues (Francese *et al.*, 2009) in a process known as mass spectrometry imaging (MSI). In this case the matrix is sprayed on marked points or sections on the surface of the tissue and laser fired at each of these points to obtain a mass spectrum. Combining these spectra yields the ion image of the tissue surface (Francese *et al.*, 2009; Seppala *et al.*, 2012).

2.4.2.2 Tandem mass spectrometry

The tandem mass spectrometer uses triple quadrupoles (Q_1 , Q_2 , and Q_3) as its mass analyser. Its ability to form, and then select, ions in Q_1 , perform collision induced dissociation (CID) with gas (e.g. argon or nitrogen) molecules in Q_2 , and scan specific selected mass ranges in Q_3 , makes it an instrumental tool in structure elucidation and reaction monitoring studies (Edmond, 1996).

The tandem mass spectrometer has been used recently to quantify peptides melittin and apamin in lyophilised HBV samples (Zhou *et al.*, 2010). The authors used multiple reaction monitoring (MRM) scan transitions of m/z 570.2 – 85.9 for melittin and m/z 507.7 – 110.0 for apamin. The precursor ions used (m/z 570.2 for melittin and 507.7 for apamin) corresponded to the most abundant ions in the respective full scan spectra. The daughter ions (m/z 85.9 and 110.0) were also some the most abundant in product ion scan MS^2 spectra of daughter ions produced by CID of the respective precursor ions using high purity nitrogen.

The melittin m/z 85.9 daughter ion is the N-terminal b35+ due to the loss of y^{23} (GIGAVLKVLTTGLPALISWIKRK) amino acid residues from the C-terminal side,

while the apamin m/z 110.0 daughter ion is y^{33+} due to loss of b^{15} (KAPETAL-CARRCQQH) amino acid residues accompanying two disulfide bond cleavages (Cys¹–Cys¹¹ and Cys³–Cys¹⁵). Because of the specificity of this technique, there was no need for complete resolution of apamin from melittin in the hyphenated LC technique; thus the two components could be distinguished even though they closely eluted at 3.5 min and 3.6 min respectively. This is one of the key advantages of tandem MS.

2.4.2.3 Fourier transform (FT) mass spectrometry

FT mass spectrometers have been used in some recent BV profiling studies despite having quite a slow start since these instruments became commercially available. The Orbitrap has been employed to determine components of *A. mellifera* venom and cuticular peptides (Baracchi *et al.*, 2011) and to detect HBV in envenomed tissue extracts (Francese *et al.*, 2009). On the other hand, Meng *et al.* (2012) reported employing an FTICR to determine the molecular weight of a new peptide, secapin-1, and its homogeneity to a relatively known peptide, secapin (Meng *et al.*, 2012).

There has been an upward trend in the use of the Orbitrap mass spectrometer in the analysis of peptides and proteins in general, as well as general proteomic and proteolytic studies, since it was first commercialised in 2005 (Hu *et al.*, 2005). This is mainly because of its high mass resolution of up to 150 000, high space charge capacity, high mass accuracy (<2 ppm), a mass/charge range of at least 6000, and dynamic range greater than 10000. Besides these advantages, the Orbitrap also offers a lower cost, more modest power requirements, and smaller size compared to the FTICR (Hu *et al.*, 2005).

2.4.3 Edman degradation

Automatic Edman degradation sequencing of BV peptides and N-terminal analysis of proteins has been reported for secapin-1 (Meng *et al.*, 2012), the allergen Api m6 (Kettner *et al.*, 2001), melittin isoforms, and phospholipase A₂ (Ferreira Junior *et al.*, 2010a; Sciani *et al.*, 2010), as well as in the profiling of some other Hymenoptera venoms (Monincova *et al.*, 2010; Stoecklin *et al.*, 2010; Čerovský *et al.*, 2008). Ed-

man sequencing employs phenyl isothiocyanate and a general acid such as HF to sequentially cleave one amino acid at a time from the N-terminus of the peptide or protein, leading to the formation of a 5-membered thiazoline ring (phenyl thiohydantoin) which can then be separated chromatographically using LC or electrophoresis.

2.4.4 SDS-PAGE and immunoblotting

Following separation by gel electrophoresis, typically SDS-PAGE under reducing conditions, proteins are blotted onto a PVDF membrane in an appropriate buffered medium. The membrane is then blocked typically with proteins and then incubated with patient sera containing antibodies that bind to the venom proteins. The resulting specific binding by the applied primary antibody can then be detected by using a biotinylated monoclonal detection anti-body that binds the primary antibody, followed by incubation with streptavidin-conjugated horseradish peroxidase. The peroxidase reactivity is then visualized by means of enhanced chemiluminescence arising from the enzymatic action on a suitable chromogenic substrate such as 3,3',5,5'-tetramethylbenzidine (TMB). A detailed procedure has been described for the study of Api m6, a new BV allergen (Kettner *et al.*, 2001) and in the study of recombinant honey bee Ag₅-like protein (Van Vaerenbergh *et al.*, 2013).

2.4.5 Capillary zone electrophoresis

A capillary zone electrophoresis (CZE) method developed for the analysis and standardisation of honey BV has been reported. The developed method was validated for simultaneous determination of melittin, apamin, MCDP, and phospholipase A₂, and was deemed simple enough to be used for routine analysis of honey BV samples (Kokot *et al.*, 2011b). Moreover the developed method showed no significant difference from an established HPLC technique. In this method, an internal standard, cytochrome C, at a concentration of 25 µg/mL, was used and sample solutions were prepared at a concentration of 0.3 mg/mL using the internal standard solution. The detection was by means of UV-DAD system (Kokot *et al.*, 2011b).

2.4.6 Circular dichroism spectroscopy

Vibrational circular dichroism (VCD) studies are used in investigations of the secondary structure of proteins; to investigate and establish the relationship between protein/peptide structures and their VCD spectra. The use of circular dichroism for the study of melittin and its isoform has been described. Wang and Polavarapu (2003) reported a VCD study of melittin in a solution of deuterated water (D_2O) at different conditions of pH, ionic strength, and 2,2,2-trifluoroethanol concentrations (Wang and Polavarapu, 2003). The spectra were taken in the amide I' region ($1850 - 1600\text{ cm}^{-1}$) using two models of a FT VCD spectrophotometer. Solutions of 6-10 mg/mL were used and at a path-length of 50 μm . The authors were able to show that melittin adopted mixed conformations at pH values of 1 to 9 in D_2O , low salt concentration ($\leq 0.06\text{ M KCl}$) or low TFE concentration ($\leq 0.1\%$), and that the structure changed to α -helix configuration at higher values of these parameters (pH of ≥ 11 , KCl concentration of $\sim 0.06\text{-}0.6\text{ M}$, or $\sim 25\%$ (v/v) TFE concentration), then subsequently aggregating as the conditions were further increased (Wang and Polavarapu, 2003).

On the other hand, Sciani *et al.* (2010) reported the use of a CD spectropolarimeter to study the structure conformation differences between melittin and its isoform, melittin-S, in 25% TFE (Sciani *et al.*, 2010). This isoform of melittin differs from the main peptide by having a Ser residue instead of Thr at position 10 (**Figure 2.4**, pp. 33). The authors were able to show that although the global appearance of the spectra was the same, there were noticeable differences pointing to varying secondary configurations of the two melittins. The conformational difference (helix of melittin vs. unordered for melittin-S) was also shown to be environment (buffer) dependent. The authors further speculated that this loss of conformational order might probably explain why the melittin-S isoform is less haemolytic (Sciani *et al.*, 2010). Other CD studies of BV have been reported by Monti *et al.* (2006) (Monti *et al.*, 2006).

2.4.7 Nuclear magnetic resonance spectroscopy

Nuclear Magnetic Resonance (NMR) spectroscopy has been employed previously to study the thermal stability of melittin's α -helix conformation in both ethanol and ethanol–water mixtures at different temperatures (Miura, 2011). The author showed that increase in the aqueous content of the solvent mixture (from 0 - 71.5 % w/w) and temperature (from RT to 60°C) led to destabilisation of the intramolecular hydrogen bonds in melittin, thus partially uncoiling the α -helical structure. However, the hydrogen bonds were found to have higher thermal stability in ethanol than in methanol pure solvents, probably indicating that their stability is enhanced by the increased size of the alkyl chain the alcohol (Miura, 2011).

2.4.8 Biological and functional assays

Past assays conducted on honey BV have included ELISAs and reverse transcription PCR in determining the expression of apidaecin genome in the venom gland of the worker bee (Van Vaerenbergh *et al.*, 2013). Furthermore, Funayama *et al.* (2012) presented a range of immunological and other bioassay tests for melittin and BV including ELISA, kinetic haemolysis assay using erythrocytes, as well as myotoxicity and lethality assays on mice (Funayama *et al.*, 2012). In addition to the SDS-PAGE immunoblot analysis of Api m 6 allergen, Kettner *et al.* (2001) also conducted proliferation assays using PBMCs isolated from heparinized blood via gradient density centrifugation (Kettner *et al.*, 2001). The PBMCs were isolated from both BV sensitive and non-sensitive patients but the proliferation results obtained were inconclusive (Kettner *et al.*, 2001). Another haemolytic assay has been described by Sciani *et al.* (2010) who showed melittin to have a significantly higher haemolytic activity compared to its isoform, melittin-S (Sciani *et al.*, 2010).

2.4.9 Other techniques for BV analysis

The other techniques which have been used in BV profiling studies or structural conformation of its main components include X-Ray crystallography (Sosa *et al.*, 2011;

Anderson *et al.*, 1980; Terwilliger and Eisenberg, 1982; Terwilliger *et al.*, 1982), IR and fluorescence spectroscopy, ion mobility mass spectrometry, HDX mass spectrometry, molecular modelling (Florance *et al.*, 2011), calorimetric binding assays, FTIR (Sosa *et al.*, 2011), and isoelectric focussing (Kettner *et al.*, 2001).

2.5 Bee venom as an active ingredient in cosmetics

Cosmetics are some of the most widely used consumer goods, with the market generating billions of pounds annually worldwide. Bee venom and its components are increasingly being used as primary ingredients in various cosmetic formulations including skin creams, balms, face masks, and serums, in Europe. Currently available honey BV products include the Manuka® Doctor *apinourish* range, which contains “Restoring Night Cream” and “Rejuvenating Face Mask” brands. Their other products are *apiclear* (Skin Balancing Serum) and *apirevive* (Rub Ease Balm), also marketed as containing purified BV, in addition to other ingredients. Other BV based cosmetic products on markets in the UK and EU include: *Nectar Balm* “Bee Venom Cream” manufactured by Nelson Honey New Zealand and *10 Natural Effects* “Bee Venom Essence” manufactured by Laboratorios DIET Esthetic S.A, Spain.

Marketing claims for the above cosmetic products include anti-wrinkle, skin rejuvenating, moisturising, skin relaxing/warming, skin balancing, and cell metabolism stimulating effects, among others. Given the complexity of the composition of these creams, it may be difficult to attribute any of these effects to a single constituent, given that the actual composition of the purified venom material is a company secret. However, it should be acceptable to believe that the relative success of a cosmetic product on an open free market can be an indicator of the efficacy it affords the user. At the very minimum, these products must be safe to the consumer who may be susceptible to risks of allergic reactions. Thus allergens have to be identified and removed; in addition, the end formulation has to be assayed to confirm the absence any unwanted components in the product before being passed for marketing and use.

It should be noted that, apart from cosmetic products, there are also BV based topical pharmaceutical creams both in Europe as well as on the globe. These include Forapin

in Germany, Virapin in Slovakia, Apiven in France, Melivenon in Bulgaria and Api-for in Russia which are used for pain-relieving effects (Matysiak *et al.*, 2011). Although these products have been on the market for quite some time, they have not been available as general use consumer products for a wide international market. Cosmetics are generally designed to fit the latter purpose but currently available ones have only appeared in the last few years. These products are being marketed as containing “purified bee venom” or “bee venom extracts” (e.g. 10 Natural Effects Bee Venom Essence by Laboratorios DIET Esthetic S.A.) without further specification. Despite this growing use of bee venom, current literature does not report a sufficient number of studies showing how to assess the composition of cosmetics in general (Gao *et al.*, 2012), let alone the BV content in these products.

The field of formulated BV cosmetics is likely to attract more interest from both manufacturers and consumers in the near future. This is partly due to: (1) the recent development of improved non-destructive BV harvesting technologies that ensure a steady supply of raw material; (2) an increasing proportion of the senior population and the resulting demand for age-defying products and technologies; and (3) the relative success of the existing products—factors which might inspire an influx of other manufacturers. At the same time, BV research maintains widespread mainstream scientific interest for potential applications in cancer therapy, arthritic disorders, and BV immunotherapy (Park *et al.*, 2015; Seppala *et al.*, 2012). The completion of the bee genome sequencing project could raise interest even higher (Nature, 2006; Elsik *et al.*, 2014). These trends point to an anticipated future where BV and related products could become ubiquitous. This could also increase incidences of BV allergic reactions, some of which can be life threatening. Methods for de-allergenisation of the venom through chromatographic purification before formulation are thus needed. In addition, screening studies for toxicity and anti-ageing efficacy are necessary in order to guarantee fit-for-purpose products.

2.6 Principles of chromatographic analysis

2.6.1 Theory of chromatography

Chromatography is a technique used to separate components of a mixture based on differences in their physical interactions between two phases, one being the stationary phase and the other, the mobile phase. Stationary phases used in chromatography consist of hydrophilic (neutral or charged) and hydrophobic materials held onto a rigid support, commonly silica. Based on the mobile phase, chromatography can be categorised as liquid chromatography (LC) or gas chromatography (GC). The mobile phases used in LC are solvents or, more commonly, miscible solvent mixtures of varying degrees of polarity. In GC, the mobile phase is a neutral gas, commonly nitrogen or helium (McNair and Miller, 2011). The mobile phase, as the name suggests, serves the purpose of transferring the analytes being assayed through the stationary phase contained in a column—either packed as is commonly the case in LC, or hollow as in GC—and during this time the separation of the components in the mixture takes place.

The success of a chromatographic run lies in fulfilling the condition that the components of a mixture introduced upstream onto the stationary phase column arrive at the downstream end of the column, where they are detected, at different times. The characteristic time it takes for a given compound to emerge from the column from the time of injection is called the retention time (t_R). The t_R of a given compound depends on the nature of the column, mobile phase composition, temperature, flow rate, mobile phase pH, and in some cases ionic strength of the buffer used. These factors can be optimised for a given compound mixture in order to achieve the most optimum separation, or resolution, required for the assay.

2.6.2 Modes of chromatography

Different modes of chromatography exist which can be distinguished on the basis of mobile and stationary phases employed, and the chemical interactions that define their retention mechanisms (Zhang *et al.*, 2012). Whereas mobile phase classifies

chromatographic separations broadly into LC and GC, stationary phase type and technical complexity broadly delineate thin layer chromatography (TLC), paper chromatography (PC), and high performance liquid chromatography (HPLC). HPLC itself can further be categorised into reversed phase (RP-HPLC), normal phase (NP-HPLC) or hydrophilic interaction liquid chromatography (HILIC), depending on the nature of mobile and stationary phases (Watson, 2012). RP-HPLC is different from NP-HPLC in that the former uses a nonpolar stationary phase (e.g. C18 and C8 hydrocarbons) with polar mobile phase mixtures (e.g. water and acetonitrile), while the latter uses polar stationary phases (e.g. amino or amide phases) with nonpolar mobile phase (e.g. hexane and chloroform). On the other hand, HILIC resembles NP-HPLC in that its stationary phase surface is hydrophilic but avoids the high organic mobile phases employed. Instead, HILIC employs the same mobile phases used in RP-HPLC but in an orthogonal manner, in that, whereas water is the weaker solvent in RP-HPLC, it is the stronger one in HILIC (Zhang *et al.*, 2014; Kumar *et al.*, 2013). Analytes are retained in HILIC phases by partitioning into a thin aqueous layer formed on the surface of the stationary phase by the water contained in the organic-rich mobile phase, but other mechanisms involving coulombic, π - π , van der Waals, and hydrogen bond interactions have also been described depending on the stationary phase types and analytes being assayed (Buszewski and Noga, 2012). The popularity of HILIC in the analysis of metabolites arose from the difficulties in achieving sufficient retention of polar compounds on reversed phase columns (Greco and Letzel, 2013). Whereas ion-pair approach would improve retention of such compounds in RP-HPLC, albeit only those with ionisable groups, it also leads to ion suppression in mass spectrometry which leads to decreased efficiency of ionisation during electrospray, thus low sensitivity of detection. Ion pairing agents can also be damaging to analytical columns as well (Watson, 2012).

On the basis of the retention mechanisms, chromatographic separations can be categorised into those based on partition, adsorption, ion-exchange, and size-exclusion (Harris, 2010; Watson, 2012). Partition chromatography involves the dynamic distribution of analytes between the stationary and mobile phases according to their partition coefficients. Analytes with high partition coefficients have more affinity for or-

ganic than aqueous phases and in this case will partition strongly into reversed phase stationary phases, leading to increased retention. On the other hand, hydrophilic analytes have low partition coefficients and this leads to low retention during separations on reversed phase columns. Adsorption chromatography occurs when the mechanism of separation mainly involves analyte molecules adhering to the stationary phase through electrostatic, hydrophobic, hydrogen bonding, or van der Waals interactions, so that those which are strongly held during those interactions are retained longer on the column than those which interact weakly. This mechanism of separation is employed in TLC and paper chromatography. In ion-exchange chromatography (IEC), charged analytes in the sample (e.g. amines) form transient ion pairs with oppositely charged ionic species (e.g. benzene sulfonic acid) bonded onto the silica surface as the stationary phase. Analytes which form stronger transient ion pairs are retained longer than those which form weaker ones. There are commercial columns which are manufactured with ion exchange resins as the stationary phases. In these columns, strong anion exchange resins are based on quaternary ammonium salts and are employed for the separation of organic acids while strong cation exchange resins based on benzene sulfonic acid are employed for the separation of basic organic compounds. Finally, size exclusion chromatography (SEC) employs, as the stationary phase, a polymer mesh of varying pore sizes in order to control the rate of movement of analytes through the column bed. This technique is usually applied in the separation of proteins and other large molecular weight (MW) compounds.

Of the methods described above, reversed phase chromatography is currently the most commonly applied technique in the pharmaceutical industry (Harris, 2010). This is partly due to the wide selection of stationary phases that can be reproducibly manufactured and which possess varying degrees of selectivity for reliable application to the analysis of several neutral and weakly ionisable non-volatile organic compounds. In general, however, the method of separation selected for a given analyte mixture depends on the nature of the analytes themselves. For instance, highly polar analytes unretained on RP-HPLC columns and which are insoluble in NP-HPLC phases can be reliably analysed by HILIC (Gama *et al.*, 2012); volatile analytes require GC analysis given its superior powers of resolution; strongly ionisable organic

compounds may be better separated using an IEC column; while SEC will be necessary to separate mixtures of high MW compounds which are too difficult to resolve, let alone elute, in packed columns and too involatile to even attempt their separation by GC.

2.6.3 Chromatographic resolution and performance

Chromatographic resolution (R_s) is a measure of how well separated individual analyte peaks are in a given chromatogram. The resolution is calculated using the formula given in the British Pharmacopoeia (BP)³ as follows:

$$R_s = 1.18 \left(\frac{t_{R2} - t_{R1}}{w_{h1} + w_{h2}} \right) \quad (1)$$

where: t_{R1} and t_{R2} ($t_{R2} > t_{R1}$) are the respective retention times of the two analytes 1 and 2, while w_{h1} and w_{h2} are the widths of the respective chromatograms at half height.

From equation (1) above, if the two analytes have exactly the same t_R , a resolution of zero is obtained, a situation that is referred to as *co-elution*. Co-eluting analytes can be resolved by optimising the separation conditions such as mobile phase composition, temperature, gradient time, and in some cases where the analytes are ionisable, pH. If resolution cannot be obtained with these changes, a column of different chemistry may be required to give different selectivity which might result in separation. A resolution of ≥ 1.5 is generally deemed appropriate for most analyses although most robust methods and impurity profiling studies require resolutions of 1.7 to 2.0. Any extra resolution above $R_s = 2.0$ is redundant as it unnecessarily prolongs analysis time.

³ British Pharmacopoeia (2012). Volume V: Appendix III, page A183.

Column performance during a chromatographic run can be calculated for each peak in the chromatogram as the number of theoretical plates (or simply plate number, N) using the following BP⁴ equation:

$$N = 5.54 \left(\frac{t_R}{w_h} \right)^2 \quad (2)$$

where: t_R is the retention time of the peak component and w_h is the peak width at half height.

The best chromatographic separation requires high N values; a high value of N implies that the component in question has interacted with the column stationary phase long enough (large t_R) while avoiding the risk of band broadening (small w_h). In packed columns, the latter can be more easily achieved with regularly spherical-shaped microporous particles, optimum flow rate, and in complex separations, use of gradient elution. Conversely, a large enough t_R value can be attained using a longer column or, more appropriately, by altering the mobile phase strength to avoid early elution of analytes. In this case, a minimum value of the retention factor (k), given by the BP⁵ formula below, of at least 2, is required.

$$k = \frac{t_R - t_0}{t_0} \quad (3)$$

where: t_R is the retention time of the compound and t_0 is the retention time of an unretained compound (also known as mobile phase holdup time) given by $t_0 \approx \frac{Ld_c^2}{2F}$, where L is the column length, d_c the diameter and F the flow rate (Harris, 2010).

Chromatographic performance and resolution are related in that large N values imply that peaks are narrow and sharp, and therefore less likely to overlap, especially since

⁴ British Pharmacopoeia (2012). Volume V: Appendix III, page A182.

⁵ British Pharmacopoeia (2012). Volume V: Appendix III, page A181.

they are also far removed from t_0 (i.e. $t_R \gg t_0$), where any unretained analytes elute. High resolution and performance are also linked to method robustness, in that such a method is “immune” to small perturbations in the experimental conditions, leading to reproducible analysis. A formula relating R_s and N shows that resolution varies as the square root of efficiency, as shown below:

$$R_s = \left(\frac{1}{4}\right) N^{0.5} \left(\frac{\alpha-1}{\alpha}\right) \left(\frac{k'}{k'+1}\right) \quad (4)$$

where: α is the selectivity factor defined as the ratio of retention factors (k) of the two analytes corresponding to the peaks in question (i.e. $\alpha = \frac{k_2}{k_1}$, $k_2 > k_1$) and k' is the mean of the retention factors (i.e. $k' = \frac{k_1+k_2}{2}$).

It can be observed from equation (4) above that doubling efficiency, N , (for example by using a longer column) only increases the resolution by a factor of $\sqrt{2} = 1.414$. On the other hand, the selectivity factor (α) has the greatest direct effect on resolution as it also affects the retention factor (k). Selectivity is dependent on both the chemistry of the column stationary phase and mobile phase composition (including buffer pH). Thus, an appropriate chromatographic separation should optimise both the selectivity and efficiency in order to obtain the best resolution.

Another important aspect of chromatographic performance which can have implications to resolution is the symmetry factor (A_s), defined in BP⁶ as follows:

$$A_s = \frac{w_{0.05}}{2d} \quad (5)$$

where: $w_{0.05}$ is the peak width at one-twentieth of the peak height and d is the distance between the perpendicular dropped from the peak maximum and the leading edge of the peak at one-twentieth of the peak height.

⁶ British Pharmacopoeia (2012). Volume V: Appendix III, page A183.

An A_s value of 1.0 signifies that the peak in question is perfectly symmetrical. Values of A_s above 1.0 indicate peak tailing while those below 1.0 suggest peak fronting. Tailing or fronting peaks can mask closely eluting minor peaks which is of key significance in impurity profiling studies. In RP-HPLC, peak tailing is normally observed in the analysis of bases due to interaction with residual silanol activity in bonded C8 or C18 phases. This can be minimised by using base deactivated silica which is acid treated to remove metallic impurities that activate silanol activity or by secondary methylation, a process known as end-capping. On the other hand, peak fronting is observed in cases where the injection solvent is stronger than the mobile phase composition (or the initial mobile phase composition in gradient elution) – a situation that leads to poor analyte focusing. In general, however, A_s values in the range of 0.9—1.5 are considered adequate for most chromatographic work (Harris, 2010).

2.6.4 Chromatographic elution profiles

There are three main forms of elution during chromatographic separations. These are: isocratic, step-wise and gradient profiles. In isocratic elution, the composition of the mobile phase stays the same during the entire run. On the other hand, step-wise profile is when elution is carried out in several successive isocratic intervals of gradually increasing solvent strength (e.g. by increasing the proportion of organic solvent in reversed phase HPLC). Gradient elution occurs when there is a constant rate of increase in mobile phase strength with time during the run (Watson, 2012; Harris, 2010).

Most chromatographic analyses employ either isocratic or gradient elutions. The choice on whether to use isocratic or gradient profiles during chromatography depends on the results of a *scouting* run (Dolan, 2013b). A broad scouting gradient (e.g. 10-90% acetonitrile in 40 min in reversed phase) is first performed so that the compounds in a sample mixture have all eluted. The retention time difference, Δt , between the most and least retained compounds, and the gradient time, t_G , are then noted. The criterion is that:

$$\text{if } \frac{\Delta t}{t_G} < 0.25 \gg \text{ use isocratic; and if } \frac{\Delta t}{t_G} > 0.25 \gg \text{ use gradient} \quad (6)$$

where: Δt is the retention time difference between the first and last peaks and t_G is the gradient time (time over which the solvent composition changes).

This implies that when all the analytes in a sample can be eluted over a narrow solvent range (i.e. small Δt), isocratic elution is possible, and it thus recommended. However, if a wide solvent range is required for the elution, gradient elution is more appropriate as an isocratic profile would mean longer analysis times. During analysis with isocratic elution, the retention of analytes is governed by the following empirically derived equation, relating the retention factor (k) and solvent strength (ϕ):

$$\log k \approx \log k_w - S\phi \quad (7)$$

where: k is retention factor of the analyte and k_w is the extrapolated retention factor for 100% aqueous eluent (in a plot of $\log k$ vs. ϕ), ϕ is the fraction of the organic solvent and S is a constant for a given compound, typically 4 for small molecules.

In gradient elutions, because the mobile phase is changing at any given point in time, analyte retention can be considered in terms of the average retention factor, k^* , which is the value of k when the analyte has travelled half-way through the column. The equation for calculating k^* is as follows:

$$k^* = \frac{t_G F}{\Delta\phi V_m S} \quad (8)$$

where: t_G is the gradient time (min), F is the flow rate (mL/min), $\Delta\phi$ is the change in solvent composition during the gradient, V_m is the volume of mobile phase in the column (mL), and S is the slope in the linear solvent-strength model.

A convenient starting point in method development for both isocratic and gradient elution profiles is a k (or k^*) of ~ 5 . In addition, a good starting mobile phase composition during isocratic method development is the solvent strength halfway through the interval, Δt , of the scouting gradient run. The developed method can then be optimized so that all the peaks are fully resolved ($R_s \geq 1.5$) from each other, with k values in the range of $0.5 \leq k \leq 20$ at reasonable back pressures of the pump (Harris, 2010).

2.6.5 Medium pressure liquid chromatography

Medium pressure liquid chromatography (MPLC) employs column back pressures of about 45psi (~ 3 bar) for rapid purification of complex samples. The Reveleris® flash chromatography system (Grace®) (**Figure 2.9**) is currently one of the latest reliable automated systems used for purification of complex mixtures. The instrument consists of an integrated UV/UV-Vis/ELSD detection system for the simultaneous detection of both chromophoric and non-chromophoric components in a given sample. Depending on the column used, it is possible to obtain pure components of a sample if the method is optimised to achieve proper resolution between individual peaks.

During a given run on the Reveleris® flash system, the dry-loaded sample in a cartridge is washed non-chromatographically onto the column within which separation occurs by mechanisms determined by the column and solvents used. Both isocratic and gradient elutions are possible.

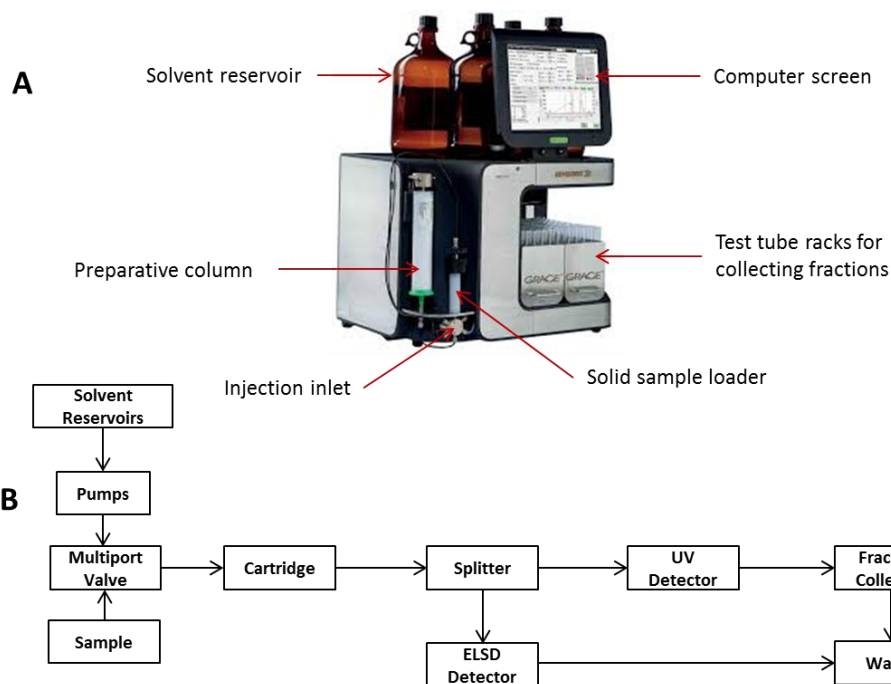


Figure 2.9: The Reveleris® flash chromatography system (Grace®) showing the main components (A) and a schematic diagram to show the flow of solvent through the main parts on the system (B).

The system automatically collects those portions of the eluate in which signals with intensities above threshold have been detected. The use of a dual detection approach ensures that most of the components of a given sample are collected as fractions in the eluate, rather than going to waste. The UV/Vis detectors depend on the ability of a compound to absorb in the ultraviolet or visible sections of the electromagnetic spectrum. Such compounds must possess chromophores, which are conjugated double-bond systems such as those present in benzenoids. However, many compounds do not absorb in the UV/Vis range and thus their detection by UV/Vis is not possible. For such compounds, evaporative light scattering detection (ELSD) facilitates their separation on the Grace® system. ELSD is a more universal detector than UV because its response is independent of the compound's spectral properties (Young and Dolan, 2003; Young and Dolan, 2004). In addition, unlike refractive index detection, another universal detector, it is compatible with a wide range of solvents and modifiers; thus it can be employed in gradient elutions.

2.6.6 Principle of detection by ELSD

The process of analyte detection by ELSD occurs in three stages: (1) nebulisation, (2) mobile phase evaporation, and finally (3) detection. The chromatographic column effluent is nebulised by mixing with a nebuliser gas, which may be nitrogen or air, in a nebulising chamber. The nebulised liquid then enters a heated drift tube region where the mobile phase evaporates, leaving behind solid particles of the analyte. Detection then occurs by means of the light scattered by the analyte particles when an incoming radiation strikes the analyte particles as they enter a light scattering cell at the end of the drift tube (Young and Dolan, 2003; Young and Dolan, 2004). Unlike in UV detection where the observed peak area (A) is proportional to analyte concentration (c) in accordance to Beer-Lambert's law, an ELSD signal is defined by the following relationship:

$$A = am^x \quad (9)$$

where: A is the observed peak area, m is the quantity of analyte, x is the slope of the response line and a is the response factor.

Thus, a plot of the logarithm of peak area A against m produces a straight line ($\log A = a + x \log m$). This lack of linear response limits the application of ELSD in high accuracy quantification. In addition, the on-column sensitivity of ELSD is lower than that of UV (for UV-absorbing compounds) and its mode of operation limits its use in the analysis of volatile and semi-volatile analytes which might be lost in the drift tube by evaporation, along with the mobile phase. In this case, one would need to decrease the operational temperatures of the drift tube in order to minimise such losses which would reduce signal intensities of such compounds (Young and Dolan, 2003; Young and Dolan, 2004).

2.6.7 Mode of operation of HPLC

High performance liquid chromatography (HPLC) is currently the most popular analytical technique used in the pharmaceutical industry, responsible for over 90% of all

chromatographic analyses. The basic instrument consists of a pump, an injection manifold, detector, and a recorder. Modern systems in use today employ pumps operating at backpressures of up to 400 psi (~6000bar) and capable of running up to four separate solvents, have an autosampler for injecting the samples unattended, can employ multiple detectors simultaneously, and are controlled via a computer running special software that also acts as the recorder (**Figure 2.10**).

During a HPLC run, the sample is injected near the top of the column and into the path of the mobile phase flowing under the pressure of the pump. The injected sample is carried by the mobile phase through the column during which separation occurs depending on the forces of interaction between the analytes in the sample, the mobile phase, and the stationary phase. Separated components are detected as they emerge from the column by an online detector or/and a hyphenated system. Mobile phase flow can be programmed via the computer to run isocratically, stepwise, or in gradient profiles. The most commonly used detectors are ultraviolet (UV), evaporative light scattering detector (ELSD), and mass spectrometers but systems based on fluorescence and refractive index detection are also available.

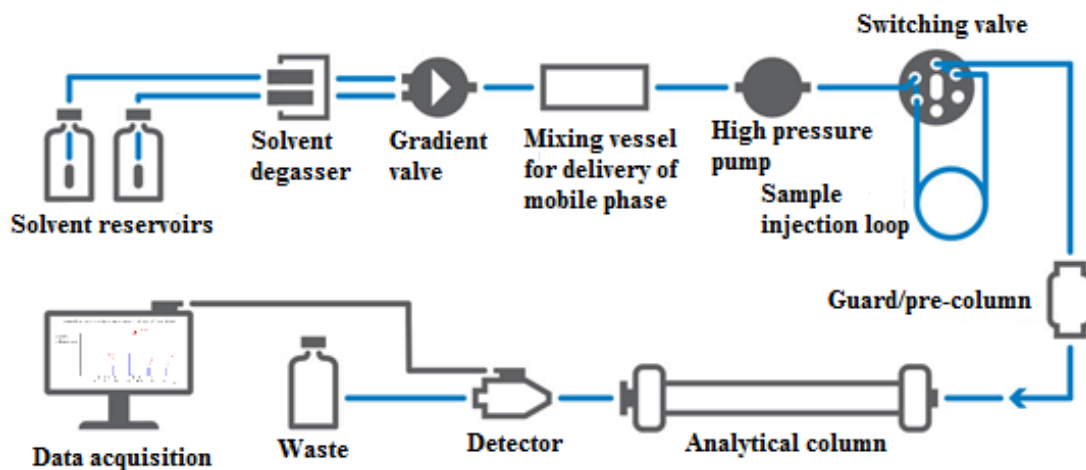


Figure 2.10: Schematic diagram of a modern HPLC system. The blue lines represent solvent lines while grey lines represent electrical connections. The guard column is optional.

Successful application of UV detection in HPLC is only possible for compounds that possess UV-absorbing moieties such as phenyl groups and conjugated double bond systems (known as chromophores). As a means of detection, the technique is cheap

and easy to use but it does not yield sufficient data to inform a structural elucidation process. On the other hand, fluorescence detectors can be used for compounds that possess fluorescence-emitting groups (fluorophores). For compounds whose chemical structures are not amenable to detection by UV or fluorescence, ELSD or RI detectors can be employed, albeit with their own limitations: That is, the former is not suitable for high volatility analytes (see section 2.6.6) and the RI detector cannot be employed in gradient applications. But perhaps the most powerful and versatile detection method is the use of mass spectrometry which offers higher levels of sensitivity and selectivity, and it can be used in different modes for a wide range of compounds. In addition, it provides supplementary data such as molecular formula predictions and mass spectra of analytes detected, all of which can offer valuable information for structural elucidation purposes.

2.7 Principles of mass spectrometry

Mass spectrometers measure molecular weights of compounds by calculating their gas-phase ionic trajectories after acceleration through electric and magnetic fields in vacuum (Schuberth, 2000). As a means of analyte detection in LC-MS systems, mass spectrometry is both selective and sensitive which minimises the need for rigorous sample preparation and complete chromatographic resolution of components as prerequisites for analysis of complex samples.

The deployment of mass spectrometry as an online detector for HPLC was initially frustrated by the high solvent pressures in the chromatographic system and the fact that liquid mobile-phase evaporation generates extremely high gas volumes [e.g. 18g of water (1 mole) generates 22.4L of gas phase at STP], with their accompanying pressures. In this case, the LC eluate would most likely overwhelm the pumping capabilities of the MS system, making vacuum stabilisation—a mandatory requirement to prevent molecular collisions, and hence reactions, during ion mass analysis—difficult to maintain. In order to overcome this challenge, there was a need to reduce the huge excess of matter in the interface between the LC and MS systems. This also called for avoidance of mobile phase additives that are difficult to volatilise such as

phosphate-containing buffers. Even with these measures, the MS could only be employed for relatively small, nonpolar, compounds that could be easily volatilised; its application to the analysis of large biological molecules (with molecular weights $\geq 1000\text{Da}$), such as large peptides and proteins, was still hampered by the impossibility of gas-phase ion formation in such molecules without extensive molecular deformation (Harris, 2010).

These major difficulties were later overcome through the development of two ionisation techniques: (1) electrospray ionisation (ESI) and (2) atmospheric pressure chemical ionisation (APCI). With these techniques, it was possible to generate a charged mist of the LC eluate from which the solvents could be quenched and gas-phase ions formed before introduction into the mass analyser compartment of the MS (see 2.7.1). This made it possible to conjugate HPLC systems to the mass spectrometer.

Thus the main components of a MS system are ion source, mass analyser, and detector (**Figure 2.11**). Analytes eluting from the LC column enter the ion source chamber and are converted into gas-phase ions (positive, negative, or both) (McLafferty, 1981). Following the ionization, ions are transferred to the mass analyser maintained under a high vacuum. The ions are separated within the mass analyser based on their mass to charge (m/z) ratios (Schuberth, 2000) and ion current detection occurs to produce a mass spectrum. Various types of mass analysers are currently available commercially and include: magnetic sector instruments, single and triple quadrupoles (Hoffmann and Stroobant, 2007; Schuberth, 2000), time-of-flight (ToF) instruments (Watson, 2012), ion traps, Fourier transform ion cyclotron resonance (FT-ICR) spectrometers (Scigelova *et al.*, 2011) and Orbitraps (Makarov and Scigelova, 2010). The latter is one of the latest technologies with the advantages of high mass resolution, mass accuracy and dynamic range (Hu *et al.*, 2005).

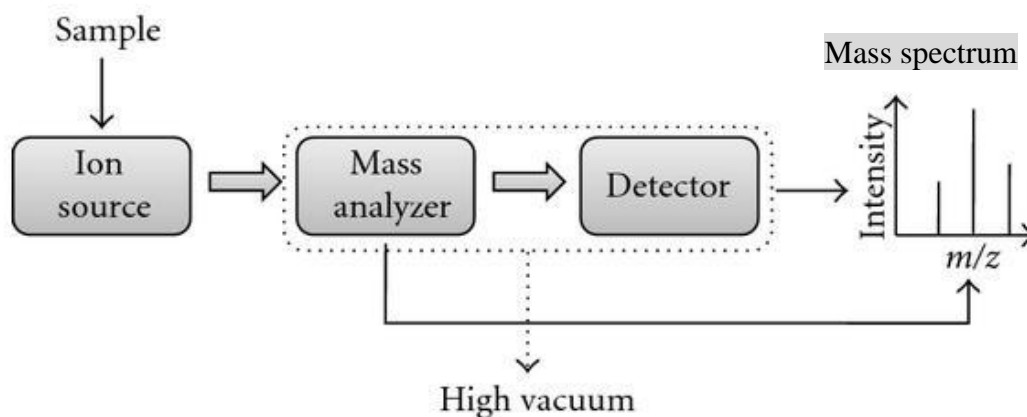


Figure 2.11: The main components of a mass spectrometer. The sample introduced into the ionisation chamber is ionised and then transferred to the mass analyser. The mass analyser separates ions according to their m/z ratios before being detected via ion image current to produce a mass spectrum.

The ionisation process in the mass spectrometer can be affected by various factors, including: type of analyte, nature and strength of buffer used, mobile phase composition, and mode of ion formation. The main mechanisms of ion formation in MS are electrospray ionisation (ESI) (Wilm, 2011), atmospheric pressure chemical ionisation (APCI), chemical ionisation (CI), matrix assisted laser desorption/ionisation (MALDI) (Matysiak *et al.*, 2011) and electron impact (EI) (Watson, 2012). While EI is known as a “hard” ionisation technique because of the molecular fragmentations that arise from high-energy collisions with electrons, the rest are “soft” ionisation techniques since no significant fragmentation occurs during ionisation which results in formation of molecular ions such as $[M+H]^+$ or $[M-H]^-$. Among the soft ionisation techniques, ESI is used for the majority of analytical assays because of its simplicity and applicability to a wide range of analytes.

2.7.1 The ESI technique

During electrospray ionization (ESI), the sample is introduced into the ionisation chamber via a fine, high voltage capillary needle (spray needle) surrounded by a flowing sheath gas of nitrogen (Wilm, 2011). As the analytes flow into the chamber, they are ionised by the high voltage (2-6kV) on the inner surface of the spray needle.

The charged ions first form a Taylor cone at the tip of the needle which then give rise to a charged aerosol—a process that is assisted by the sheath gas flow consisting of dry nitrogen gas (**Figure 2.12**).

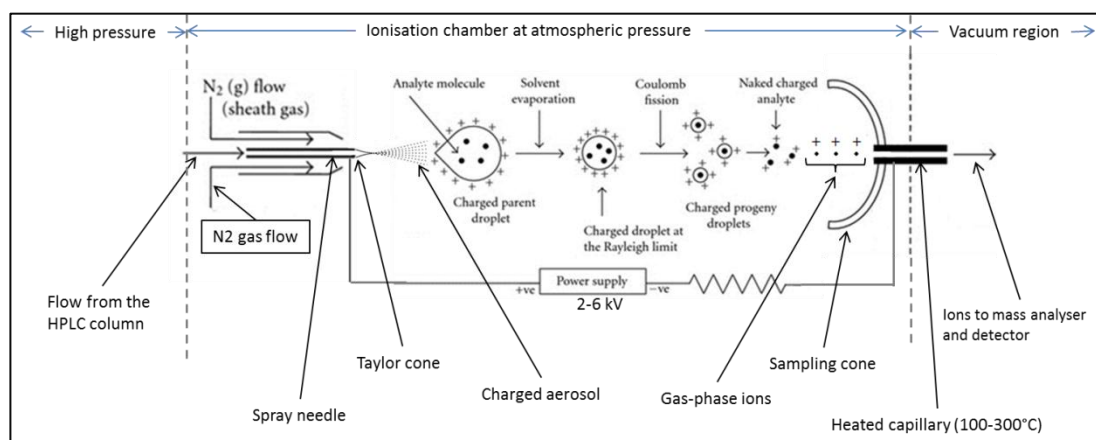


Figure 2.12: Mechanism of ESI as modified from (Banerjee and Mazumdar, 2012). The spray needle is kept at a high voltage of 2-6 kV relative to the surrounding source sampling cone and heated capillary. Analytes are charged as the HPLC eluate flows through the needle. Successive evaporation of charged droplets of the analyte and coulombic repulsion lead to formation of gaseous ions which are then sampled and directed to the mass analyser via a heated capillary.

Ions possessing a charge similar to that on the spray needle are repelled into the centre of the Taylor cone while those oppositely charged remain stuck on the needle. The charged liquid drops within the aerosol then evaporate and as they do so, they become smaller in size. This results into increased coulombic repulsion as similar charges in the drop are brought closer to each other. At a certain point, known as Rayleigh limit (Fenn *et al.*, 1989), the magnitude of the repulsive forces in the charged drop overcomes surface tension forces which causes the drop to break up, ejecting tiny droplets with diameters of ~10 nm. This process is enhanced by the flow of the nitrogen gas and heating, both of which cause evaporation of solvent until naked charged molecules are formed. It should be noted that mobile phases containing a high proportion of organic solvents, and therefore lower surface tension, and mobile phase additives such as formic acid, increase the efficiency of the ESI process. The charged gas molecules are then sucked into a high vacuum analyser region for mass measurement. The process of ion formation occurs at low energies and the desolvation process effectively lowers internal energies of analyte ions which leaves

them free from fragmentation as they enter the mass analyser (Banerjee and Mazumdar, 2012). This makes ESI a “soft” ionisation technique.

2.7.2 *The LTQ-Orbitrap MS*

The LTQ-Orbitrap is a hybrid system consisting of a linear ion trap mass spectrometer coupled to an Orbitrap mass analyser (Hu *et al.*, 2005). The LTQ—which stands for linear trap quadrupole—is a mass spectrometer in its own right (e.g. as LTQ-FT-MS, supplied by Thermo Electron Corporation). On its own, the LTQ is capable of detecting both MS and MSⁿ spectra with high sensitivity but with poor resolution and mass accuracy (Scigelova and Makarov, 2006). However, when it is coupled to the Orbitrap, far more superior mass detection occurs with higher resolution, increased mass accuracy, and higher sensitivity. The two components are linked through a curved, resonant frequency (rf)-only, voltage-gated trap known as C-trap—thus completing a triad of traps within the instrument (**Figure 2.13**).

Ions from the electrospray source are admitted via rf-only octapoles into the linear trap of the LTQ, wherein the ions are analysed and radially ejected to a pair of secondary electron multipliers. By means of a procedure known as automatic gain control (AGC), a short prescan is made to determine the ion current within the range of interest, in order to enable storage of a defined number of ions (known as AGC target value) in the subsequent analytical scan (Belov *et al.*, 2003). This circumvents the problem of space charging which would occur if the quadrupole were to store more ions than required as it has limited storage capacity. Space charging would be a problem since it compromises sensitivity and resolution (Makarov *et al.*, 2006). Thus by using the AGC procedure, both sensitivity and resolution are maximised by specifying the exact fill time of the trap.

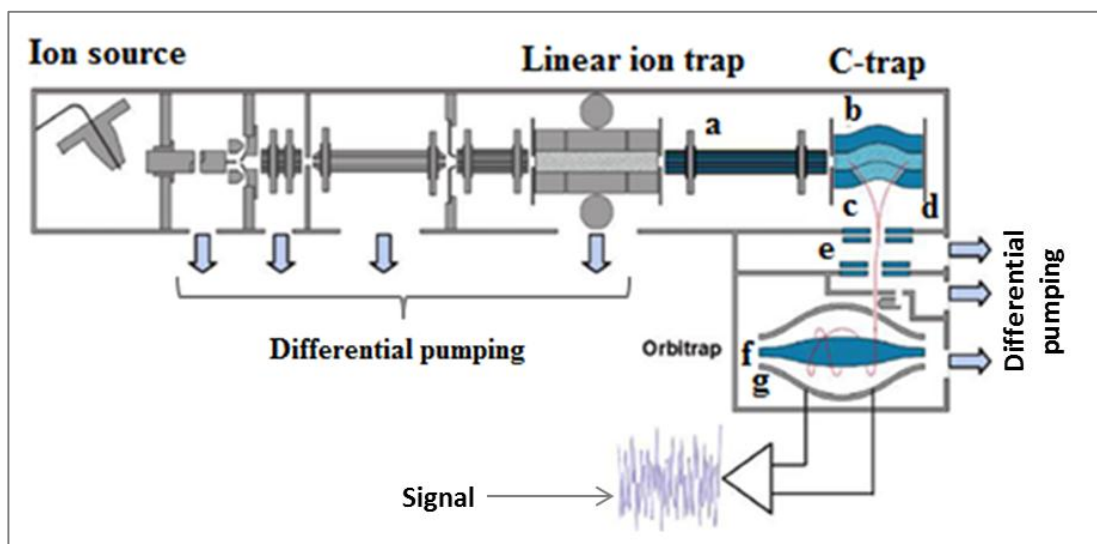


Figure 2.13: A schematic layout of the Orbitrap mass spectrometer. The main parts are: (a) Transfer octapole; (b) C-trap; (c) gate electrode; (d) trap electrode; (e) ion optics; (f) inner Orbitrap electrode;(g) outer Orbitrap electrodes.

The ions in the linear ion trap are then transferred into the C-trap which allows accumulation and transient storage of a significant ion population prior to injection into the Orbitrap analyser (Makarov and Scigelova, 2010; Scigelova and Makarov, 2006). This temporary ion storage improves the analytical capabilities of the instrument and permits additional high energy collision-induced dissociations (CIDs) to be carried out in the C-trap for MS^n spectra. From the C-trap, ions are injected into the Orbitrap mass analyser as short pulsed ion beams, allowing each mass/charge ratio subpopulation to form sub-microsecond pulses (Makarov and Scigelova, 2010). Once injected, these ion beams enter the Orbitrap mass analyser in the region between two electrodes: an inner (central) spindle-shaped electrode and outer barrel-shaped electrode coaxial with the first (Hu *et al.*, 2005). This region contains a rapidly changing electric field arising from a quadro-logarithmic electrostatic potential (equation 9) created by specially designed, axially symmetric electrodes (eqn. 10).

$$U_{(r,z)} = \frac{k}{2} \left(z^2 - \frac{r^2}{2} \right) + \frac{k}{2} \cdot (R_m)^2 \cdot \ln \left[\frac{r}{R_m} \right] + C \quad (10)$$

where: r and z are cylindrical coordinates, C is a constant, k is field curvature, and R_m is the characteristic radius (Hu *et al.*, 2005; Hardman and Makarov, 2003).

The ions from the C-trap are injected with such a tangential velocity as to avoid collision with the inner electrode; their velocity and the electric field intensity in the Orbitrap act in concert to cause the ions to undergo two forms of oscillations, concurrently, in order to become stable—one being the orbital oscillations around the central spindle-shaped electrode, and the other, the harmonic oscillations along the axis of the of the field. In this motion, the electrostatic attraction of the ions towards the central spindle-shaped electrode is counterbalanced by the centrifugal force of the ions resulting from their initial velocities (**Figure 2.14**).

Whereas rotational and radial frequencies of the ions in the beams are strongly dependent on their initial energies, positions or angles—which in turn results in the spread of the ion packet over the angular coordinate to form a thin ring (Makarov and Scigelova, 2010)—the frequency of harmonic oscillations along the axis of the central electrode is completely independent of these initial parameters, but depends solely on the mass-to-charge ratio (m/z) of the ions and the field curvature, k , as follows:

$$\omega = \sqrt{\left(\frac{z}{m}\right)k} \quad (11)$$

where: w is the frequency, z is the charge on the ion, m is the mass of the ion and k is the field curvature (Hu *et al.*, 2005; Hardman and Makarov, 2003).

Thus the m/z values of the ions can be determined by measuring the frequencies of the axial oscillations using fast Fourier transform mathematical algorithm of the broadband image current signal produced by the ions and detected on two split halves of the outer electrode of the trap. The technique gives high resolution ($\sim 150,000$ fwhm) spectra of the ions being measured along with good sensitivity, high mass accuracy (2-5ppm) and up to 8-fold relative mass range (Hu *et al.*, 2005; Hardman and Makarov, 2003).

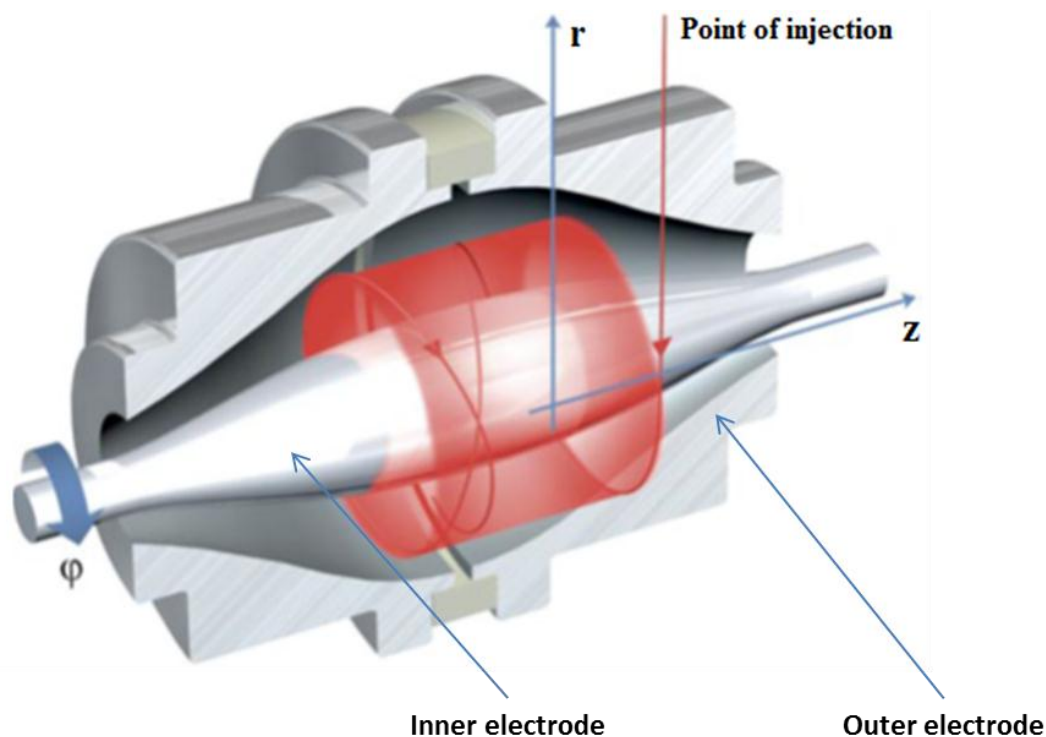


Figure 2.14: A section through the Orbitrap mass analyser. Ions enter the Orbitrap as shown by the red arrow perpendicular to the axis of the spindle-shaped electrode (z -axis). The point of injection is slightly offset from $Z = 0$ in order to give the ions axial potential energy, thus initiating harmonic axial oscillations, a term known as “excitation by injection”. The quadrupole-logarithmic field inside the analyser stabilises the axial oscillations through rotations around the central electrode.

The LTQ-Orbitrap mass spectrometer can be used for detecting analytes in biological samples because its high resolution, selectivity, and sensitivity come with potential for performing reaction monitoring in both selective ion monitoring (SIM) and selective reaction monitoring (SRM) functions as well. It is because of these strengths that the Orbitrap has seen increased applications, and led to significant advances, in proteomics (Ahlf *et al.*, 2012; Rosati *et al.*, 2012), metabolomics, lipidomics, in addition to phytochemistry and quality control analysis of pharmaceuticals (Makarov and Scigelova, 2010).

2.7.3 The quadrupole mass analyser

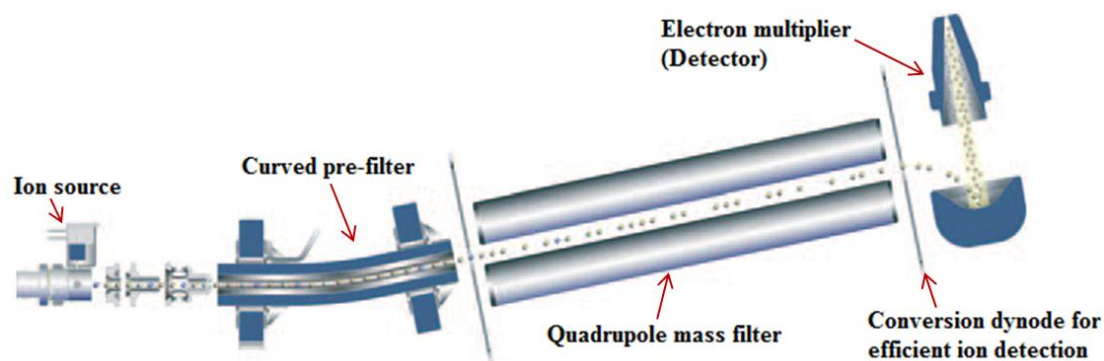


Figure 2.15: A schematic diagram for the structure of the DSQII mass spectrometer. Ions are formed in the ion source by electron impact ionisation (EI) and are directed towards the removable curved prefilter that traps any “dirt” present thus protecting the sensitive quadrupole mass filter. In the quadrupole, ions are separated according to their mass/charge ratios and then detected using an electron multiplier system to generate library-searchable spectra.

The quadrupole mass analyser consists of four, exactly similar, parallel, cylindrical electrodes arranged perfectly symmetrically, and in a square array, around a central axis (z -axis) (Miseki, 1993) (**Figure 2.15**). A constant direct current (D.C.) voltage, U , and a high frequency alternating current (A.C.) voltage, $V\cos\omega t$ (ω = frequency, t = time) are applied between pairs of diagonally-opposite electrodes located on the x and y axes (**Figure 2.16**).

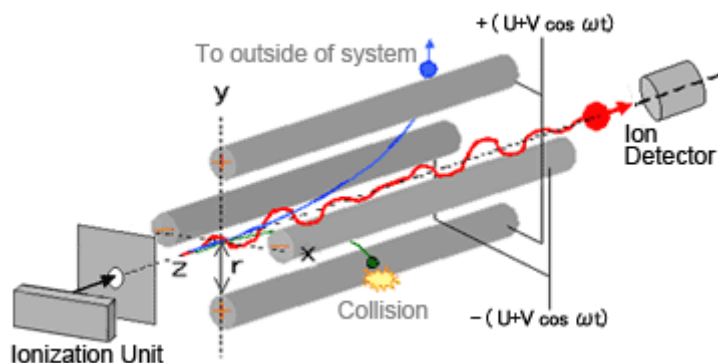


Figure 2.16: Action of the quadrupole mass analyser. Voltage of the same polarity is applied to diagonally-opposite poles and opposite voltage polarity is applied to adjacent poles. Only ions with specific m/z values can achieve stable oscillations inside the quadrupole thus being able to reach the detector. The rest of the ions either collide with the poles or fly out of the system. Different ions can be detected by varying the rf-voltage applied.

The combination of direct and high-frequency alternating voltages generates, within the space surrounded by the electrodes, an electric field with a rapidly varying phase. As a result, any ions entering this space along the z-axis are made to oscillate in the x and y directions by the action of the resonating electric field. At a given set of values of U , V and ω , ions with a specific mass to charge ratio (m/z) can go through the region by maintaining stable oscillations to reach the detector, while ions with different m/z ratios cannot, as their oscillations become unstable, leading either to collisions with the poles or dispersing out of the space. Mass spectrometric scanning is performed by changing the magnitudes of U and V , while maintaining a certain relationship between them, in order to obtain a mass spectrum for a given range of m/z values (Miseki, 1993; Taylor *et al.*, 2000).

The electric potential within a linear quadrupole $\phi(x, y)$ is given by the following equation:

$$\phi(x, y) = \left(\frac{x^2 - y^2}{r_0^2} \right) \phi_0 \quad (12)$$

where: x and y are Cartesian coordinates, and ϕ_0 is the applied potential to the electrodes. Since the potentials applied to the x and y electrodes are equal and opposite, the net potential in the centre of the quadrupole is zero (Douglas, 2009).

It has been shown that the motion of an ion within the quadrupole is in accordance with the Mathieu equation (equation 13) irrespective its initial velocity or position:

$$\frac{m}{z} = K \frac{V_{RF}}{r_0^2 \omega^2} \quad (13)$$

where: r_0 is the field radius (distance from the centre to any one electrode), ω is the frequency, and V_{RF} is the amplitude of the alternating voltage applied to the electrodes (March, 1997; Douglas, 2009).

The quadrupole system is an amazing device in that it can act both as an ion store and as a mass spectrometer, albeit with restrictions of mass range and mass resolution. It is capable of operating at lower vacuum levels (10^{-2} to 10^{-3} Pa) compared to other MS systems which are high vacuum instruments (March, 1997). This means that drops in vacuum levels caused by coupling to a chromatographic system have minimal effect on instrument performance, making it ideal for LC-MS. The trapping of gaseous ions in the absence of solvent occurs via establishment of a trapping potential within the quadrupoles in which the frequency is higher than necessary for the ions to escape (Miseki, 1993). This trapping ability, combined with high-speed switching, permits gas-phase ion studies for elucidation of molecular structures through selective ion and reaction monitoring as occurs in tandem mass spectrometry (MS/MS). Quadrupole MS systems are inexpensive; their simplicity and compactness make them easier to operate and maintain. For these reasons, they are widely used as general purpose MS instrument for both qualitative and quantitative analysis (March, 1997).

2.7.4 Electron impact (EI) ionisation

EI is a hard ionisation technique in which ions are formed as a result of collisions between analyte molecules in the gas phase and high energy electrons. The sample entering the EI source is bombarded with electrons produced by thermionic emission from a tungsten or rhenium filament (cathode) and accelerated towards the anode at a high energy of 70 eV. Collision between an analyte molecule M with an energetic electron e produces a radical cation M^+ . Extensive fragmentation occurs during the ionisation process because the collision energy used is higher than the bond strength (typically 4-7 eV). Fragmentation of the M^+ radical cation can occur via loss of a single radical and several neutral species (**Figure 2.17**). After the ionisation the molecular ion and its various fragments are ejected from the source by a repeller plate carrying the same charge (Watson, 2012).

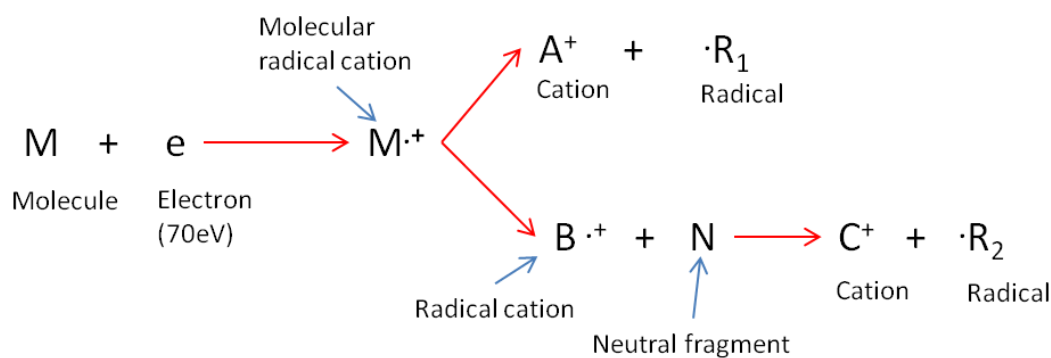


Figure 2.17: Ionisation and fragmentation processes during electron impact ionisation.

The formation of various fragment ions from electron collisions with the analyte molecule provides a means for structural elucidation, and library compilations and matching, since the spectrum acts as a unique fingerprint of the molecule (Watson, 2012).

2.8 Research hypothesis

2.8.1 Hypothesis one: BV can be formulated into a stable and safe cosmetic

The highly amphiphilic venom peptide, melittin, and other proteins present in the venom have potential to act as humectants and hydrophilic, water-binding agents to improve water retention of the skin, thereby keeping it hydrated for a smoother, less wrinkled appearance. The phospholipid fraction of the venom is capable of acting as an occlusive barrier to prevent trans-epidermal water loss (TEWL). The presence of (Z)-9-eicosen-1-ol in the venom has potential to confer anti-oxidant properties to the skin thereby minimising the tendency of oxidative stress to speed up the skin's ageing process.

2.8.2 Hypothesis two: BV contains useful biologically active compounds which can be used in medical treatment

The BV components including melittin may have potential as an anti-cancer, anti-inflammatory, antibacterial, anti-tumour, and anti-trypanosomal agent and also as a vaccine adjuvant.

2.9 Aims & objectives

2.9.1 Preliminary profiling studies

Aim 1: To develop reliable and robust techniques for the separation, detection, characterization and quantification of BV components in crude venom samples and BV-containing commercial cosmetic products.

Specific objectives

- To develop a suitable method for the efficient and reproducible fractionation and purification of the whole BV sample.
- To develop reproducible LC-ESI-MS and GC-MS methods for the analysis of the main components of BV.
- To apply MZMine and SIMCA-P statistical software in the analysis of the profile of the BV sample and its fractions based on LC-MS data.

2.9.2 Antimicrobial effects and selective toxicity

Aim 2: To assess the inhibitory effects of the major BV fractions on selected pathogenic microorganisms in order to determine any potential therapeutic uses.

Specific objectives

- To test for antiprotozoal effects of BV fractions on *Trypanosoma brucei*.
- To determine the antibacterial activity of BV fractions against *Norcardia farcinia* and *Mycobacterium marinum*.
- To evaluate the potential antiviral effects of BV fractions.

Aim 3: To investigate the viability of selected human cell lines on incubation with BV and its fractions in order to gauge their relative safety upon use as cosmetic ingredients.

Specific objectives

- To determine the minimum inhibitory concentrations (IC₅₀) of BV and its fractions against normal human keratinocytes, epithelial cells, and fibroblasts.
- To evaluate potential anti-inflammatory effects of the fractions on TNF- α -induced NF- κ B in normal human keratinocytes.

2.9.3 Assay of BV-containing cosmetics formulations

Aim 4: To develop a reliable method for the assay of melittin in commercially available cosmetic products containing BV.

Specific objectives

- To purify and characterize a reference standard of melittin for use in the analysis of BV-containing cosmetic products.
- To establish the range of BV content in commonly available BV-containing cosmetic products.

2.9.4 Stability and mechanisms for melittin degradation

Aim 5: To assess the factors affecting the stability of melittin in aqueous solutions of BV in order to determine how to control its potential degradation in formulations.

Specific objectives

- To determine the stability of melittin in aqueous BV solutions at different storage conditions.
- To investigate the possible mechanisms of spontaneous degradation of melittin in aqueous solution.

2.9.5 Pro-inflammatory and potential immuno-adjuvant effects

Aim 6: To evaluate the synergistic effects of BV and fractions on lipopolysaccharide (LPS)-induced cytokine production in phorbol-12-myristate-13-acetate (PMA)-differentiated U937 cells.

Specific objectives

- To measure the viability of U937 cells in the presence of BV and its fractions.
- To determine the levels of cytokines TNF- α , IL-1 β , and IL-6 produced by PMA-differentiated U937 cells when treated with BV and fractions in the presence and absence of LPS.
- To determine any potential synergistic effects of BV fractions and LPS in inducing cytokine release in the PMA-differentiated U937 cells.

Chapter Three

**Materials and Methods for Flash
Chromatography, LC-MS and GC-MS**

3 Materials and Methods for Flash Chromatography, LC-MS and GC-MS

3.1 Study samples

Two batches of crude *Apis mellifera* venom denoted “A” (*Bee Venom, 10 g*) and “B” (*Bee Venom, Lot No. WCBV010113, 10 g*), were supplied by Beesen Co. Ltd. (Dae Jeon, Korea). Batch “A” was contained in a stoppered plastic bottle while batch “B” was supplied in a stoppered amber glass bottle. Each of the samples appeared as a dark brown crystalline material. The samples were stored in the freezer at -30°C during the entire period of the experiments.

3.2 Instrumental systems and techniques

3.2.1 MPLC system

A Reveleris® X2 flash chromatography system (Grace®) supplied by Grace Davison Discovery Sciences (Carnforth, UK), was employed for the reversed phase chromatographic fractionation of the components of crude BV. The Grace® system employed commercial pre-packed C18 columns from Grace Davison Discovery Sciences, but self-packed reversed columns were also employed. The latter were prepared in-house by packing empty cartridges (Easyvarioflash D24 Empty Cart 20 g) from VWR International (Lutterworth, UK) with a polymer stationary phase material (Polymeric Retain PEP for SPE) supplied by Thermo Fisher Scientific (Bremen, Germany).

3.2.2 HPLC-ESI-MS systems

Two HPLC-ESI-MS systems were employed in this research. The first one employed, as the detector, an LTQ-Orbitrap mass spectrometer, and the second, an Orbitrap Exactive, respectively. In the case of the former, the LC system was a Finnigan HPLC consisting of a surveyor MS pump plus, a Finnigan surveyor autosampler plus, and a Finnigan surveyor PDA plus detector. In the case of the Exactive, an Ac-

cela 600 HPLC system was employed, with all the components similar to those of the Finnigan HPLC but being of the Accela brand. In both systems, the HPLC was interfaced to the mass spectrometer via an ESI interface and data acquisition was controlled by the Xcalibur 2.1.0 software. Both systems and the operating software were supplied by Thermo Fisher Scientific (Bremen, Germany).

The analytical HPLC columns used were: ACE 3 C18 column (150 × 3.0 mm, 3 μm particle size), supplied by Hichrom Ltd. (Reading, UK); Agilent PLRP-S (50 × 4.6 mm, 5 μm, 4000 Å) supplied by Agilent Technologies (Stockport, UK); and a Sequant® ZIC®-cHILIC; PEEK 150x4.6 mm, 3μm, 100Å supplied by Merck (Darmstadt, Germany). Both the ACE 3 C18 and Agilent PLRP-S were reversed phase columns but the latter's stationary phase was of polystyrene divinylbenzene (PS-DVB) chemistry. On the other hand, the Sequant® ZIC®-cHILIC was a hydrophilic interaction liquid chromatography (HILIC)-type column in which the silica surface was densely bonded with 1:1 charge-balanced phosphorylcholine functional groups. This column has previously been demonstrated to give improved chromatographic performance for acidic metabolites at low and medium pH (Zhang *et al.*, 2014). For the semi-preparative separation of samples, an ACE 5 C18 column (250 × 10 mm, 5 μm particle size), supplied by Hichrom Ltd. (Reading, UK), was employed.

3.2.3 *The GC-EI-MS system*

Gas chromatography (GC) was carried out using a Focus GC-DSQII system supplied by Thermo Fisher Scientific (Bremen, Germany). The Focus GC component was equipped with a full-size GC oven which could be operated at up to 350°C with ramp rates of 0.1-120°C/min and a split/splitless injector. On the other hand, the DSQII MS system employed a single quadrupole as the mass analyser with electron impact (EI) ionisation. Although positive and negative chemical ionisation (PCI and NCI respectively), as well as pulsed positive ionisation negative ionisation (PPINI) modes were also possible on the system, these were not employed. The system was also ca-

pable of performing selected ion monitoring (SIM), but throughout this work it was employed exclusively in a full scan mode.

The GC column employed was InertCap® capillary (FactorFour™, VF-1ms, 30 m length, 0.25 mm i.d., and 0.25 µm film thickness) manufactured by GL Sciences Inc. (Tokyo, Japan) and supplied by Hichrom Ltd (Reading, UK). The InertCap VF-1ms is an inert and nonpolar stationary phase whose chemistry is based solely on dimethylpolysiloxane (www.glsciences.com). The GC-MS system was controlled by Xcalibur data system (Thermo Scientific, Bremen, Germany) with a searchable library for compound matching of full-scan EI spectral data.

3.3 Other apparatus

The ultrasonic bath was a Branson 1510 from Branson Ultrasonics (Slough, UK). Automatic pipettes (Gilson) were from Anachem (Luton, UK). All glassware was Fisher Scientific (Loughborough, UK). The centrifuge was a Benchmark MyFuge Mini from Benchmark Scientific (Edison, NJ, USA). Acrodisc® syringes and filters were purchased from Fisher Scientific (Loughborough, UK). Pre-packed Hypersep C18 SPE cartridges were purchased from Thermo Scientific (Hempstead, UK).

3.4 Solvents and chemicals

The HPLC grade solvents including methanol, acetonitrile, chloroform and formic acid were purchased from Sigma-Aldrich (Dorset, UK). HPLC grade water was produced in the lab using a Direct-Q3 Millipore Ultrapure water purification system (Millipore, Watford, UK).

3.5 General sample preparation procedures

3.5.1 Preparation of filtered whole BV

Samples of BV from both batches were prepared at 10 mg/mL in aqueous solution and then double filtered serially with 5-13 μm VWR qualitative filters and 0.45 μm Millipore–Millex syringe filters (Millipore Ltd., Watford, UK) respectively. Then approx. 30mg (3mL) of each solution was transferred into 6 separate glass vials and frozen at -30°C for 24 h. Lyophilisation of the samples was done at -80°C for 48 h in a Christ Alpha 2-4 freeze dryer (SciQuip Ltd., Newton, UK). Recovery was determined by comparing the weight of freeze-dried material to that of the original crude sample.

3.5.2 Fractionation and lyophilisation of BV

A portion of crude BV of *ca.* 1.0 g was mixed with 3.0 g of purified calcium silicate (Celite®) and packed in a dry-loading cartridge (VWR International, Lutterworth, UK). The column used was manually packed with *ca.* 12.85 g of Polymeric Retain PEP for SPE. The run conditions were as follows: flow rate, 12 mL/min; equilibration time, 2 min; run length, 70 min; air purge time, 1 min; ELSD carrier, isopropanol; slope sensitivity, high; ELSD threshold, 20 mV; UV threshold, 0.05 AU; wavelength, 220 nm; collect peaks, on. A maximum per-vial volume of 20.0 mL was collected. The solvents used were: water (solvent A) and acetonitrile (solvent B) with the following gradient profile: 0-10 min (0% B), 10-20 min (20% B), 20-30 min (50% B), 30-60 min (60% B), 60-70 min (100% B). Run time was 70 min.

After fractionation, 100 μL aliquots were taken from each of the fractions collected for subsequent analysis by LC-MS on the LTQ-Orbitrap. Following LC-MS analysis, similar fractions were pooled together to form fractions F-1, F-2, F-4 and F-4. The fractions were transferred into separate pre-weighed glass vials and then frozen for ~24 h at -30°C . Thereafter, they were freeze-dried at -80°C for ~48 h. The lyophilised samples were re-weighed to determine the recovery and then stored at -30°C .

3.5.3 Melittin purification

Final purification of the melittin fraction, for the purposes of establishing an analytical standard, was achieved using semi-preparative HPLC (column 250mm length x 10 mm I.D., 5 μ m particle size) supplied by Hichrom Ltd. (Reading, UK). Approximately 100 μ L of a 0.1 g/mL (10 mg) aqueous solution of the melittin fraction were injected onto an equilibrated HPLC column. The injected sample was eluted with water:acetonitrile (60:40) at a flow rate of 5 mL/min. The dual UV detector was set at wavelengths 220 and 295 nm to monitor the peak as observed in ChromQuest software (Thermo Fischer Scientific, Hempstead, UK). The eluent corresponding to the melittin peak was repeatedly collected in a separate vial and lyophilised. Identity and purity profiles were characterised by quantitative NMR, using pure methanol as an external standard.

3.6 LC-MS analysis

3.6.1 LTQ-Orbitrap MS conditions

All the samples except F-4 were detected in the positive ESI ionisation mode as $[M+H]^+$ ions. The components of the F-4 fraction were detected in the negative ESI mode as $[M-H]^-$ ions. The spray needle voltages were set at 4.5 and -3.5 kV in positive and negative ion modes respectively. The sheath and auxiliary gas flow rates were 50 and 15 arbitrary units, respectively, while ion transfer capillary temperature was set at 275°C. Full scan MS spectral data were collected between m/z 100-2000. For F-4, the full scan m/z range was 200-1200 for the parental ion and MS/MS fragment ions were scanned in the m/z range of 200-700 in the negative ESI mode. The data was collected and processed using the XCalibur 2.1.0 software.

3.6.2 Reversed phase (C18) conditions

The mobile phases were A (0.1%, v/v, formic acid in water) and B (0.1%, v/v, formic acid in acetonitrile). All samples except the lipophilic fraction (F-4) were analysed using the following solvent gradient: 20-70% B (0-10 min), 70% B (10-16 min), 70-

20% B (16-20 min), and 20% B (20-25 min). On the other hand, F-4 was analysed using the gradient: 50% B (0-5 min), 95%B (6-15 min), 50% B (16-20 min). Finally, for investigations of the stability assay of melittin, the gradient used relative to B was 10-70% (0-15 min), 70% (15-20 min), 70-10% (20-25 min) and 10% (25-30 min) relative to solvent B, and at a flow rate of 0.3 mL/min. In each case, a constant flow rate of 0.3 mL/min was maintained and injection volume was 10 μ L.

3.6.3 Reversed phase (PS-DVB) conditions

The mobile phases A and B as described in section 3.4.3.1 were used. The gradient was 0-10 min (20-70% B), 10-11 min (70-50% B), 11-15 min (50% B), 15-16 min (50-20% B), 16-18 min (20% B) at a flow rate of 0.4 mL/min. Injection volume was 10 μ L and the total run time was 18 min.

3.6.4 HILIC (Sequant® ZIC®-cHILIC) conditions

The mobile phases A and B described in section 3.4.3.1 were employed in HILIC. The gradient was set up as follows: 0-30 min (20-95% A), 30-35 min (95% A), 35-40 min (95-20% A) and 40-45 min (20% A). The flow rate was 0.6 mL/min with 10 μ L injection volume.

3.7 GC-MS conditions

The sample was injected in splitless mode into an inlet maintained at 250°C and with a split flow of 11 mL/min (splitless time 1.0 min). Nitrogen (N₂) gas flow was maintained constant at 1.5 mL/min. The oven temperature was ramped from 80 to 350°C at a rate of 10°C/min after an initial hold of 1.0 min. The MS transfer line was maintained at 275°C. The full scan range of the EI spectra was m/z 50-650.

Chapter Four

Fractionation, Purification and Profiling of the Main Components of Bee Venom

4 Fractionation, Purification and Profiling of the Main Components of Honey Bee Venom

4.1 Introduction

Bee venom has been reported to possess therapeutic potential in the management of various pain-related disorders and cancerous tumours (Son *et al.*, 2007). Thus a significant amount of research has been focused on investigating and characterising the principal components in the venom responsible for the observed pharmacological effects. Crude honey BV is known to be a complex mixture whose composition can vary according to origin, season of harvest, bee type and age of sample among other factors (Ferreira Junior *et al.*, 2010b; Sciani *et al.*, 2010). Pioneering studies of characterisation of BV components by Banks *et al.* (1981), Shipolini *et al.* (1971), and Habermann (1972) used gel filtration and ion exchange chromatography. However, more recent studies have relied mainly on reversed phase chromatographic methods for separation and spectroscopic or mass spectrometric methods for detection, but the application of NMR in BV assays has been quite limited.

This chapter describes the studies carried out on two batches of crude BV supplied by Wissen Co. Ltd. (now Beesen Co. Ltd., Dae Jeon, Korea) in order to obtain their full chemical profiles. Retention properties of BV components were initially studied on both hydrocarbon and polymer-based reversed phase HPLC columns. A strategy for fractionation of the venom was developed by translating a solid phase extraction (SPE) method onto a medium pressure liquid chromatography (MPLC) system. All samples, including purified venom fractions, were analysed using a HPLC system interfaced to a mass spectrometer (LTQ-Orbitrap or Exactive) by way of an electrospray ionisation (ESI) manifold. Additional analysis of the lipophilic fraction was accomplished by means of GC-MS. Both limits of detection and quantification of the main peptide component, melittin, were also determined. Identification of two of the major BV allergens was performed using sodium dodecyl sulphate-polyacrylamide gel electrophoretic (SDS-PAGE) assay.

4.2 Methods

4.2.1 LC-MS analysis of BV and fractions

Filtered whole BV (prepared in section 3.5.1) was assayed at a final concentration of 0.1 mg/mL in water. Samples of the freeze-dried BV fractions were assayed after re-constitution in water (F-1 to F-3) or acetonitrile/water (1:1) (F-4) to achieve final concentrations of 0.1 mg/mL in each case. The samples were then analysed with reversed phase (C18) and HILIC columns using their respective methods already described in section 3.6 of Materials and Methods. MZMine version 2.1.0 software (<http://mzmine.github.io/>) was employed to extract all the ions in the chromatograms of whole BV samples whose intensity was above a 10^4 threshold. Subsequent principal component analysis (PCA) was performed in SIMCA version 14 (Umetrics, Crewe, UK).

4.2.2 GC-MS of BV and fraction F-4

The sample of whole BV or F-4 was dissolved in ethyl acetate to obtain a concentration of ~ 50 $\mu\text{g/mL}$. Only the BV solutions were filtered. Analysis was carried out on the GC-MS according to the method conditions described in section 3.7 and 1 μL of each sample was injected.

4.2.3 LoD and LoQ determination

Serial two-fold dilutions were made of the filtered BV in the range of 5 mg/mL to 1.0 $\mu\text{g/mL}$. Each solution was thoroughly mixed before any subsequent dilutions were made from it. When ready, all solutions were analysed immediately on the C18 column using the method described in section 3.6.2. Afterwards, calibration curves of peak area (y) versus concentration (x) were constructed and the LoD/LoQ values determined, according to the equations below, in accordance with ICH:

$$LoD = 3.3[\delta/s] \quad \text{and} \quad LoQ = 10[\delta/s] \quad (14)$$

where s is the slope of the calibration curve and δ is the standard deviation of the response (blank responses, or residual standard deviation of the regression line, or standard deviation of the intercept of the regression line, or standard error of the estimate $s_{y/x}$).

4.2.4 SDS-PAGE separation

A quantity of crude BV of *ca.* 5 mg was weighed and dissolved in 1 mL of de-ionised water to form a 5 mg/mL stock solution. Serial dilutions of the resulting stock solution were then prepared at final concentrations of 2.5, 1.5, 0.75, and 0.375 mg/mL respectively. Aliquots of 15 μ L of the stock solution and each dilution were separately mixed with 5 μ L of NuPAGE (4x LDS Sample Buffer) (Thermo Fisher Scientific, Hemel Hempstead, UK) in 1 mL Eppendorf tubes and vortex mixed. The running buffer was prepared by mixing 50 mL of 10x Tris/Glycine/SDS buffer (Bio-Rad Laboratories Ltd., Hemel Hempstead, UK) and 450 mL of de-ionised water to achieve a 10-fold dilution. The gel plate was placed in the electrophoresis tank (Thermo Fisher Scientific, Hemel Hempstead, UK) and filled with the prepared running buffer. Aliquots of 10 μ L (range of ~20 to 3 μ g BV loading) of each sample were loaded onto different lanes on the gel alongside a well with 10 μ L of Precision Plus ProteinTM Standards (Bio-Rad Laboratories Ltd., Hemel Hempstead, UK). The tank was connected to a power pack and electrophoresis carried out at 130 Volts. The current was stopped when the fastest migrating band reached the bottom of the gel. The gel plate was removed from the tank and the gel carefully removed. The gel was washed with water three times for 15 min and then stained with Bio-SafeTM Coomassie G-250 Stain (Bio-Rad Laboratories Ltd., Hemel Hempstead, UK) for 1 h prior to visualisation.

4.2.5 Western blot analysis

This assay was carried out through collaboration with ProteomeTech (Seoul, Korea). After SDS-PAGE (10 μ g BV loading), the separated protein bands were transferred onto a nitrocellulose membrane by electroblotting. The membrane was then blocked

with 5% skim milk in PBS containing 0.1% Tween-20 (PBS-Tween) at 4°C for 15 h. It was then incubated with seven BV-hypersensitive human sera (1:10 in PBS-Tween) for 45 min at RT, before washing with PBS-Tween. A non-atopic serum sample was included as a control. To detect the specific IgE binding, an alkaline phosphatase (AP)-conjugated monoclonal mouse anti-human IgE antibody was added, incubated at RT for 30 min, then washed with PBS-Tween, before carrying out the BCIP/NBT (5-bromo-4-chloro-3-indolyl phosphate/p-nitroblue tetrazolium chloride) reaction for 30 min at RT to form a purple colour. The membrane was then rinsed, dried and then its image was taken.

4.3 Results

4.3.1 Whole venom assay by LC-MS

Recoveries of 88.5% and 93.5% for batches A and B were obtained after filtration and freeze-drying. LC-MS analysis of these samples showed that melittin was the main component whose composition by dry weight in the venom was estimated from freeze-dried fractions to be 57% (section 4.3.3). In addition, there was a variety of other components identified such as histamine, apamin, secapin, phospholipase A₂, and many other unidentified components (**Figure 4.1**). MZMine 2.1.0 software (<http://mzmine.github.io/>) was employed to extract all the ions in the chromatograms of whole BV sample solutions whose intensity was above a 10⁴ threshold. Subsequent principal component analysis (PCA) using pattern recognition models (SIMCA-P) produced discrimination between the two batches of BV analysed. The two batches showed both intra- and inter-batch variability, with the latter being sufficiently more pronounced to result in batch classification (**Figure 4.2**).

The ability to discriminate between different batches of BV means that it would be possible to easily establish a batch uniformity standard in order to guarantee consistency of product formulations. It would also be possible to determine sample components that are responsible for the majority of observed batch variability in order to assess their potential value to the cosmetic formulation.

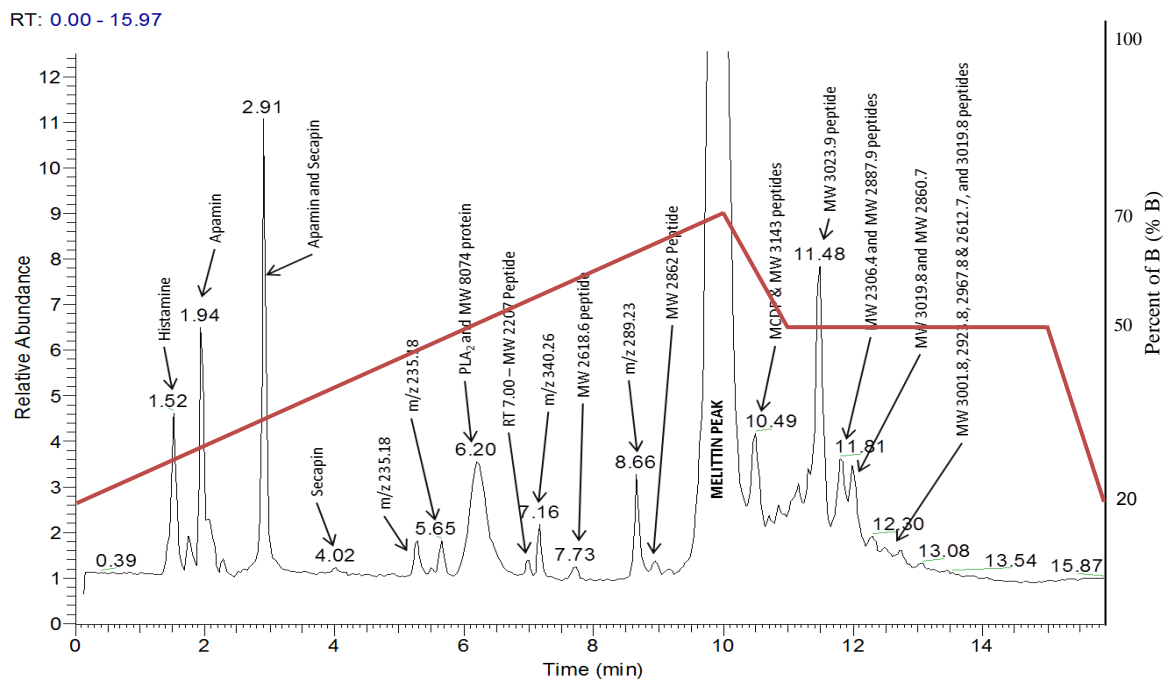


Figure 4.1: Some of the components identified in whole BV. Melittin was the main component accounting for approximately 55% of the dried weight of sample. The BV sample was analysed on a Finnigan HPLC-ESI-LTQ-Orbitrap using a reversed phase PLRP-S column (50 × 3.0 mm, 5 μm) with mobile phases: A (0.1% v/v formic acid) and B (0.1% v/v formic acid in acetonitrile) with gradient: 20-70% B (0-10 min), 50% B (10-15 min), 20% B (16-18) min at a flow rate of 0.4 ml/min as described in section 3.6.3.

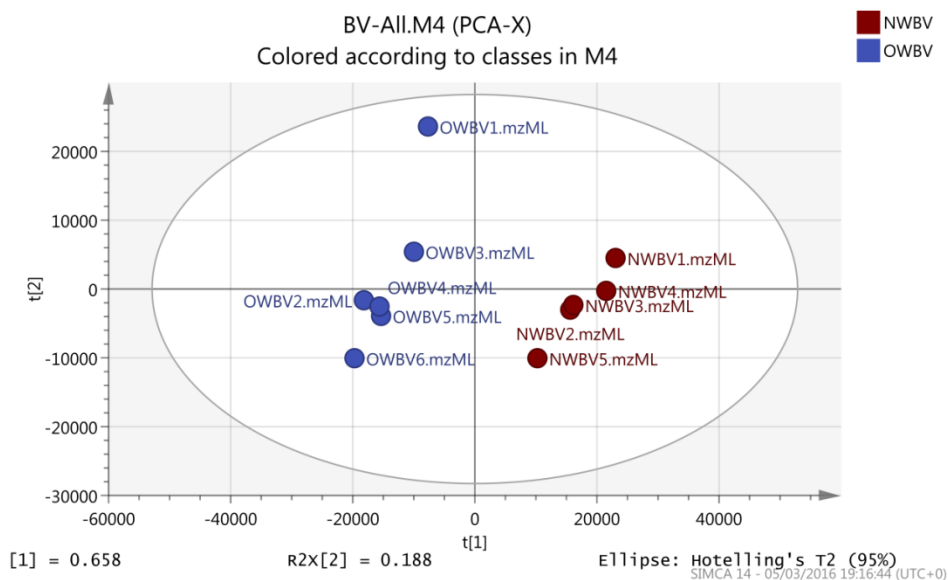


Figure 4.2: Scores plot of the replicate samples (n = 6) of the two batches A (blue circles) and B (red circles) of BV analysed with PCA-X modelling in SIMCA-P version 14. There was good separation between the two batches which signified inter-batch variation. Intra-batch variation was more prominent in the batch A than batch B samples.

4.3.2 GC-MS of whole BV

The ethyl acetate extract of whole BV gave at least 6 main peaks for each batch sample, with the main one eluting earliest at RT 16.35 min (**Figure 4.3**). A library search of the standard spectra corresponding to the main peak produced the following top 5 hits (% likelihood), all of which were mono-unsaturated long chain alcohols: (cis)-9-eicosen-1-ol (11.1%), (Z)-9-hexadecen-1-ol (6.0%), (Z)-11-hexadecen-1-ol (5.5%), (Z)-9-octadecen-1-ol (5.5%), and (E)-tetradecen-1-ol (5.2%). However, it would seem likely that the latter running peaks are alcohols with carbon numbers > 20 since their retention times are longer than that of eicosenol.

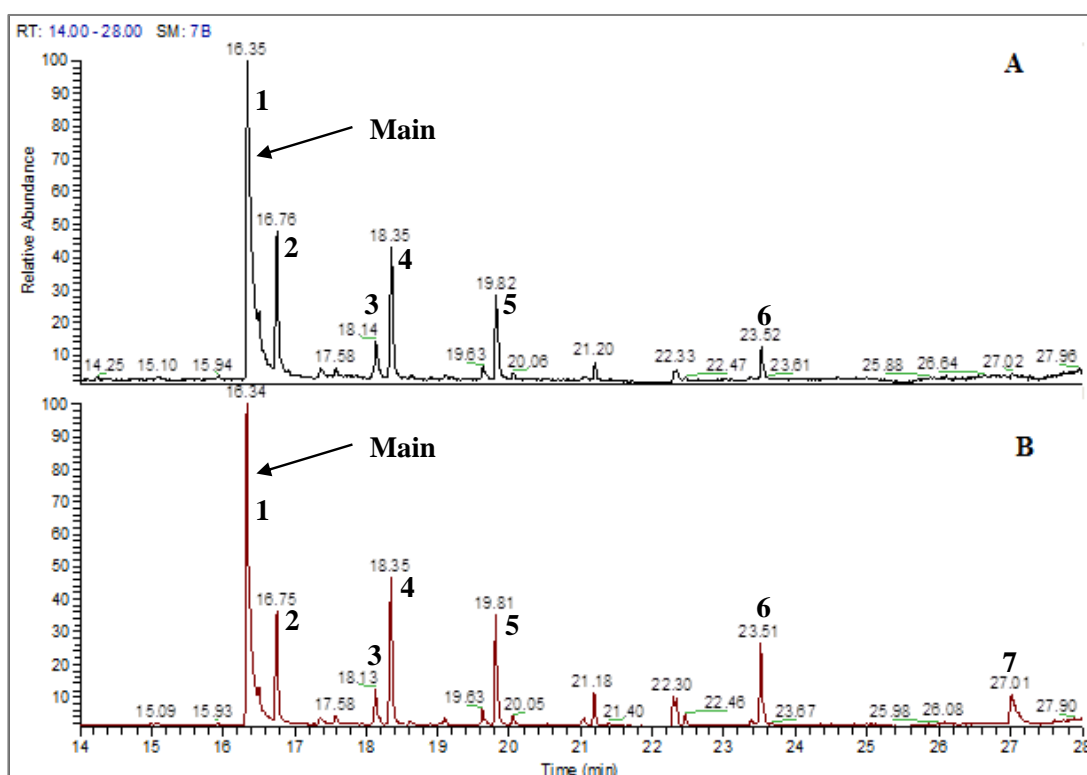


Figure 4.3: Full gas chromatogram of the ethyl acetate extract of whole BV sample batches **A** and **B**. The main peak is shown and the other peaks that could be observed are numbered 2 to 6 and 2-7 for the two batches respectively. Samples were analysed by injecting 1 μ L in splitless mode at N_2 flow rate of 1.5 mL/min, MS transfer line was maintained at 275°C, and oven temperature gradient was 80 to 350°C at a rate of 10°C/min. Full scan EI spectra collected in the m/z range of 50-650 as described in section 3.7.

4.3.3 Fractionation

The fractionation of the whole BV sample by flash chromatography (as described in section 3.5.2) yielded a recovery of *ca.* 60.8%. Four main fractions were obtained as shown in **Figure 4.4**. Fraction-1 (F-1) accounted for 26% of the total recovered freeze-dried sample. F-2 accounted for 15%, while the main fraction, F-3, accounted for 57% of the total dry venom recovered. On the other hand, fraction F-4 accounted for the remaining 2% of the total dry venom recovered. The losses of overall mass balance were expected to be due to non-collection of peaks with sub-threshold signals. LC-MS analyses of each fraction are described below.

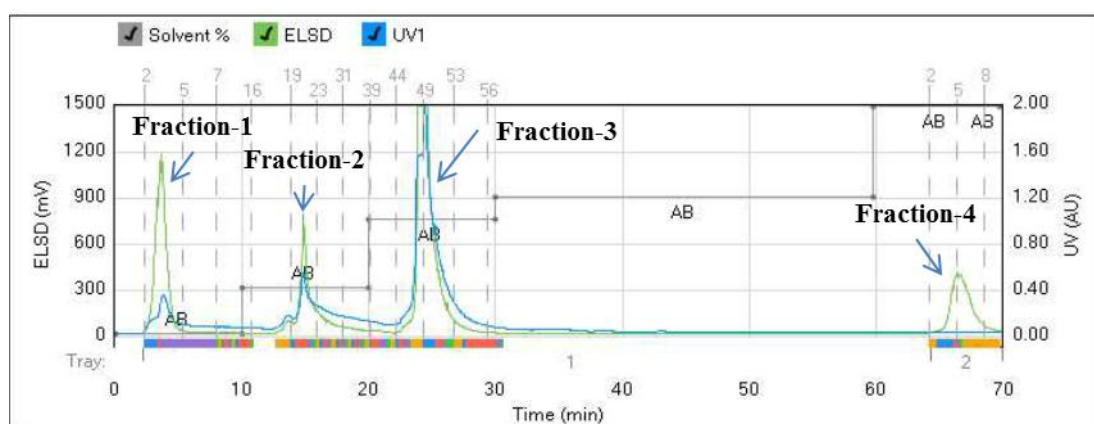


Figure 4.4: Chromatogram obtained in the MPLC separation of BV components using the Grace® system. Column: Generic C18, 24g; solvents: water (A) and acetonitrile (B) with a gradient of 0-10 min (0% B), 10-20 min (20% B), 20-30 min (50% B), 30-60 min (60% B), 60-70 min (100% B); flow rate 12mL/min, run length 70 min, slope detection: high, ELSD threshold: 5mV, UV threshold: 0.05 AU, UV1 wavelength 220 nm and maximum volume per vial: 20mL. The colours on the x-axis represent separate collections across with of the peak. (Further details of the method are described in section 3.5.2).

4.3.3.1 Fraction-1 (F-1):

Analysis, by LC-MS, of the components of the fraction corresponding to the first peak revealed a variety of constituents such as histamine (m/z 112.0871), proline (m/z 116.0707), 5-aminovaleric acid (5-AVA, m/z 284.0993), cellobiose (m/z 343.1243), and arginine (175.1193) (**Figure 4.5**). In addition, there were a number of other singly charged compounds in this fraction for example those with m/z ratios of 360.1510, 365.1061, and 210.0611 (**Figure 4.6**). These unknown compounds were

identified through PubChem search in MZMine as shown in **Table 4.1**. Some of them are probably just system peaks rather than genuine compounds.

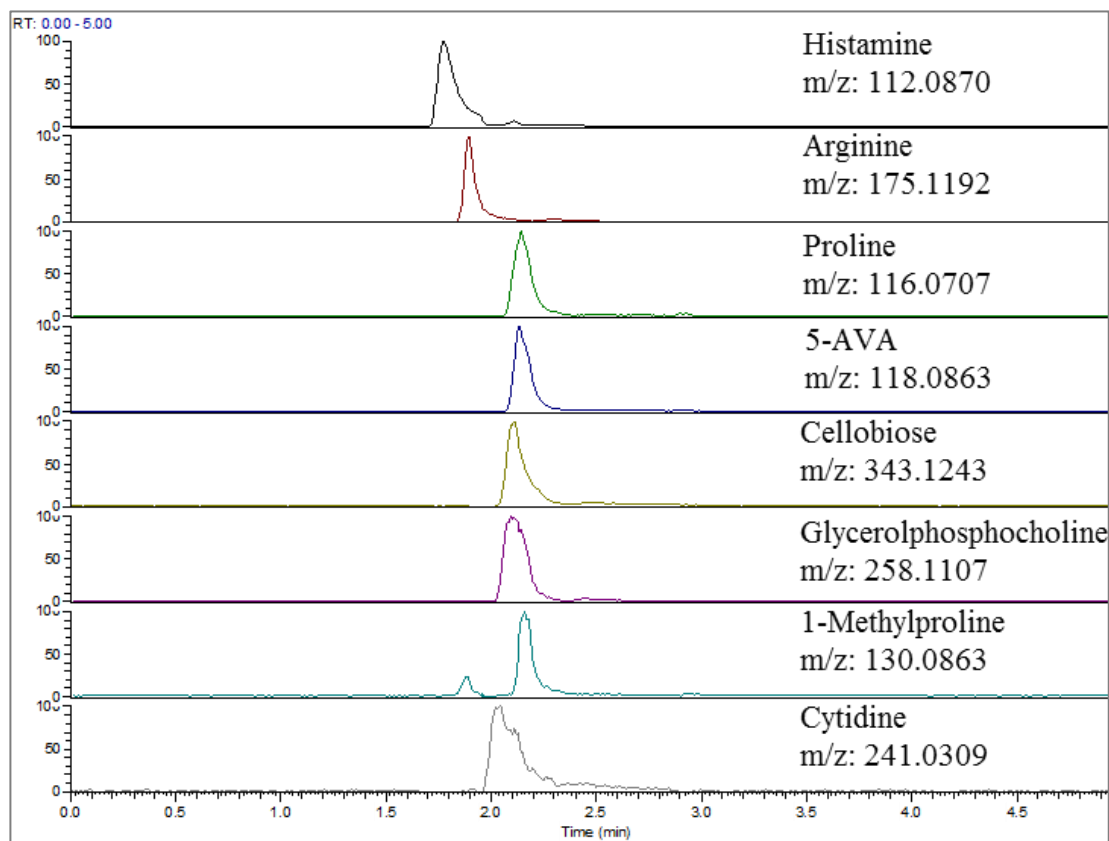


Figure 4.5: Some of the identified main components in the F-1 sample. The fraction was analysed by positive ion LC-ESI-MS on the Orbitrap mass spectrometer with an ACE 3 C18 column using mobile phases 0.1% formic acid in water (A) and 0.1% formic acid in acetonitrile (B) at a gradient of 20-70% (0-10 min), 70% (10-16 min), 70-20% (16-20 min) and 20% (20-25 min) relative to solvent B, and at a flow rate of 0.3 mL/min (as described in section 3.6.2). The extracted ion chromatograms (EICs) were obtained within ± 0.01 accuracy relative to the m/z of each ion.

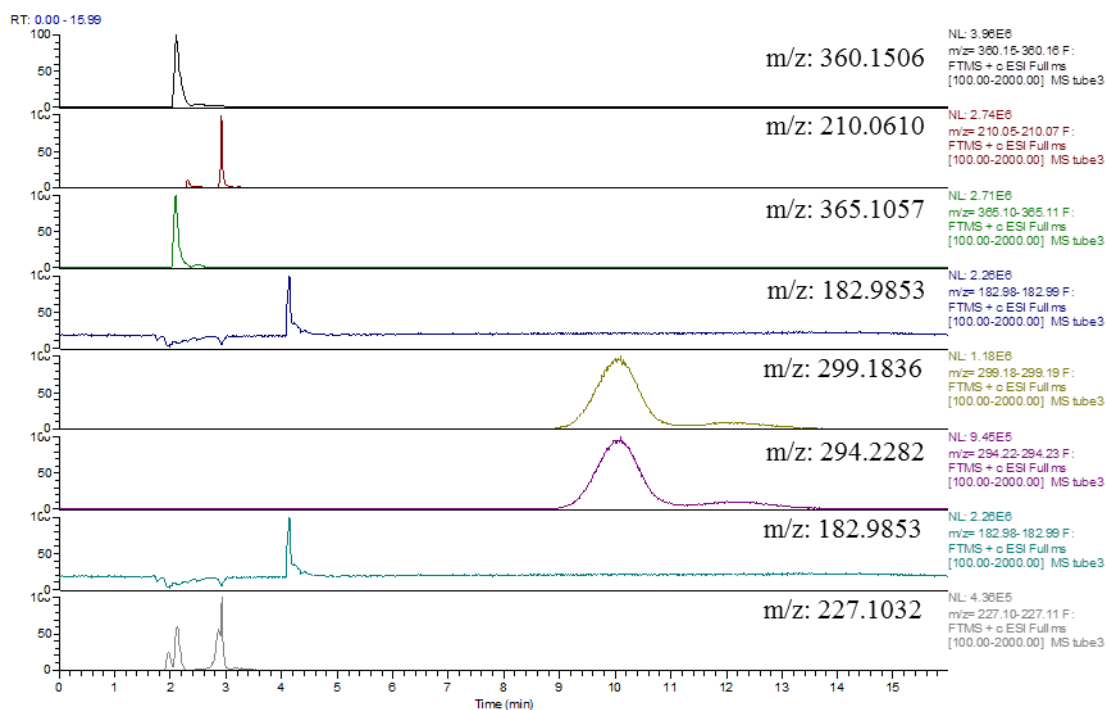


Figure 4.6: Some of the unidentified components in fraction F-1. The fraction was analysed by positive ion LC-ESI-MS on the Orbitrap mass spectrometer with an ACE 3 C18 column using mobile phases 0.1% formic acid in water (A) and 0.1% formic acid in acetonitrile (B) at a gradient of 20-70% (0-10 min), 70% (10-16 min), 70-20% (16-20 min) and 20% (20-25 min) relative to solvent B, and at a flow rate of 0.3 mL/min (as described in section 3.6.2). The extracted ion chromatograms (EICs) were obtained within ± 0.01 accuracy relative to the m/z of each ion.

Table 4.1: Summary of the main components identified in F-1, the polar fraction of BV. The chemical formulae and names of the compounds were obtained through a PubChem search.

<i>m/z</i>	<i>RT (min)</i>	<i>Formula</i>	<i>Chemical name</i>
360.1506	2.49	C ₁₃ H ₂₉ NO ₆ S ₂	Unidentified
210.0610	2.94	C ₇ H ₁₅ NO ₂ S ₂	3-(tert-Butyldisulfanyl)alanine
365.1057	2.28	C ₁₀ H ₂₄ N ₂ O ₈ S ₂	Ritrosulfan
215.0164	2.90	C ₅ H ₆ N ₆ S ₂	2-Azido-4,6-bis(methylsulfanyl)-1,3,5-triazine
182.9853	3.25	C ₈ H ₃ ClO ₃	3-Chlorophthalic anhydride
112.0870	2.18	C ₅ H ₉ N ₃	Histamine
175.1192	2.11	C ₆ H ₁₄ N ₄ O ₂	Arginine
299.1836	10.20	C ₁₄ H ₂₅ F ₃ O ₃	2-Decyloxy-ethanol, TFA
116.0707	2.31	C ₅ H ₉ NO ₂	Proline
141.9586	4.18	C ₃ H ₃ Cl ₂ O ₂ -	Methyldichloroacetate
294.2282	10.13	C ₁₄ H ₃₁ NO ₅	N-Octyl-D-glucamine

118.0863	2.45	C ₅ H ₁₁ NO ₂	5-Aminovaleric acid
154.0978	2.27	C ₇ H ₁₁ N ₃ O	Unidentified
277.2017	9.83	C ₁₄ H ₂₈ O ₅	(2R,3S,4R,5R)-2-(Hydroxymethyl)-6-octyloxane-3,4,5-triol
151.0966	3.18	C ₆ H ₁₄ O ₄	Triethylene glycol
522.2041	2.24	C ₃₀ H ₃₂ ClNO ₅	Unidentified
325.1135	2.35	C ₁₃ H ₁₆ N ₄ O ₆	Unidentified
194.1177	3.24	C ₁₁ H ₁₅ NO ₂	N-Methyl-3,4-methylenedioxyamphetamine
343.1243	2.10	C ₁₂ H ₂₂ O ₁₁	Cellobiose
258.1107	2.10	C ₈ H ₂₀ NO ₆ P	Glycerolphosphorylcholine
527.1596	2.06	C ₂₅ H ₂₆ N ₄ O ₇ S	2-(Ethyl(4-((2-(methylsulphonyl)-4-nitrophenyl)azo)phenyl)amino)ethyl phenoxyacetate
182.9853	5.99	C ₈ H ₃ ClO ₃	3-Chlorophthalic anhydride
157.0838	2.07	C ₆ H ₁₀ N ₃ O ₂ ⁺	1,2,3-Trimethyl-4-nitroimidazolium
201.0876	2.06	C ₉ H ₈ N ₆	Unidentified
227.1032	2.92	C ₁₀ H ₁₄ N ₂ O ₄	Porphobilinogen
245.1146	2.87	C ₁₁ H ₁₂ N ₆ O	2-amino-2-(5-phenyl-1,2,4-triazin-3-yl)acetohydrazide
360.1506	2.49	CH ₄ ClNO ₈ P ₂ S-2	Methoxy-[oxido-(perchlorylamino)-phosphoryl]sulfanylphosphate
132.0040	1.96	C ₂ HN ₃ O ₄	2,2-Dinitroacetonitrile
236.9985	2.79	C ₆ H ₆ Na ₂ O ₇	Disodium citrate
219.0981	2.06	C ₈ H ₁₄ N ₂ O ₅	N-nitrosodiethanolamine diacetate

The separation was initially carried out using a reversed phase column but there was co-elution of many compounds near the void time, t_0 , signifying that these components were not getting sufficiently retained in the C18 column (**Figure 4.7**). As all the compounds eluting in this fraction were highly polar (amines and amino acids) their poor retention on this column was not surprising since the C18 is a nonpolar phase that is less retentive for hydrophilic analytes.

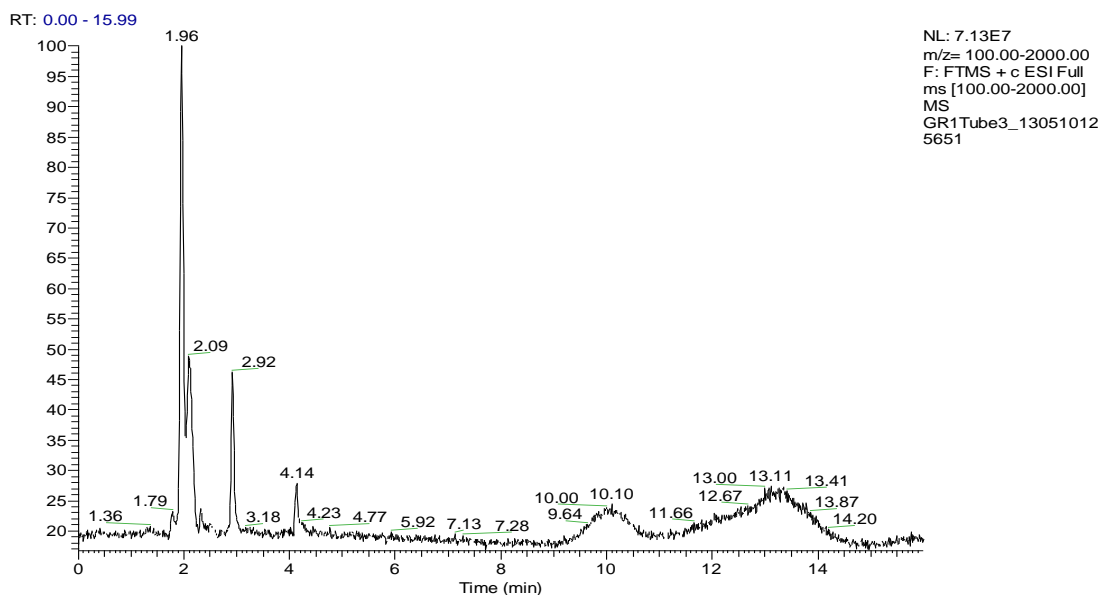


Figure 4.7: Chromatogram of sample fraction obtained from fraction F-1 of the MPLC showing early eluting small polar compounds in BV. The fraction was analysed by positive ion LC-ESI-MS on the Orbitrap mass spectrometer with an ACE 3 C18 column using mobile phases 0.1% formic acid in water (A) and 0.1% formic acid in acetonitrile (B) at a gradient of 20-70% (0-10 min), 70% (10-16 min), 70-20% (16-20 min) and 20% (20-25 min) relative to solvent B, and at a flow rate of 0.3 mL/min as described in section 3.6.2.

Thus in order to improve retention and therefore achieve the required separation of the components in this fraction, HILIC was carried out using the method described in section 3.6.4. Indeed, the separation on the ZICHILIC column led to increase in the retention times of the compounds as shown in **Figure 4.8**. For instance, the retention time of histamine increased from ~1.8 min obtained on the C18 to ~12.5 min when HILIC was employed. In general, all the components of F-1 had at least a 5-fold increase in retention time on the HILIC column compared to the C18 column.

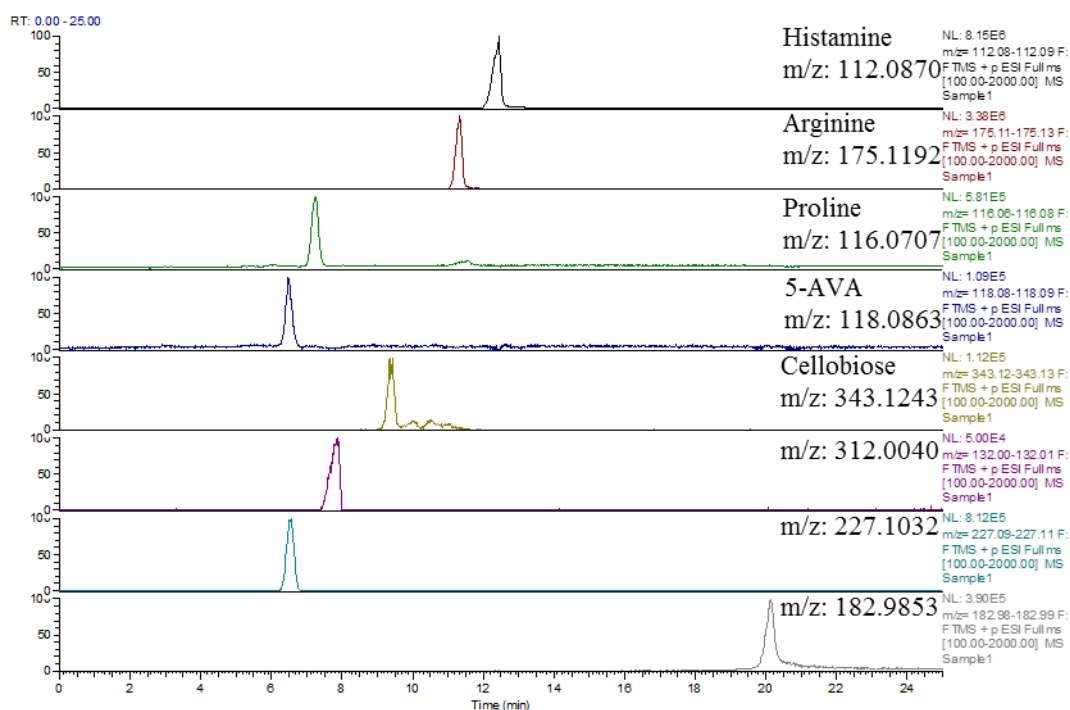


Figure 4.8: Some of the polar compounds identified in sample F-1 using the HILIC method. The fraction was analysed by positive ion LC-ESI-MS on the Orbitrap mass spectrometer with a Sequant® ZIC®-CHILIC column using mobile phases 0.1% formic acid in water (A) and 0.1% formic acid in acetonitrile (B) at a gradient of 20-95% (0-30 min), 95% (35-40 min), and 20% (40-45 min) relative to solvent A, and at a flow rate of 0.6 mL/min as described in section 3.6.4. There was obvious increase in the retention time of the components compared to the reversed phase method.

4.3.3.2 Fraction 2 (F-2):

The main components of this fraction were the peptide, apamin (MW 2026.92), and phospholipase A₂ (PLA₂), a 16 kDa protein and one of the main allergens present in BV. The other components were the BV peptides mast cell degranulating (MCD) peptide (MW 2586.45) and secapin (MW 2865.60), as well as traces of dopamine and noradrenaline (**Figure 4.9**). These compounds were identified based on their typical mass spectra which contained various multiply-charged ions as shown in **Table 4.2**.

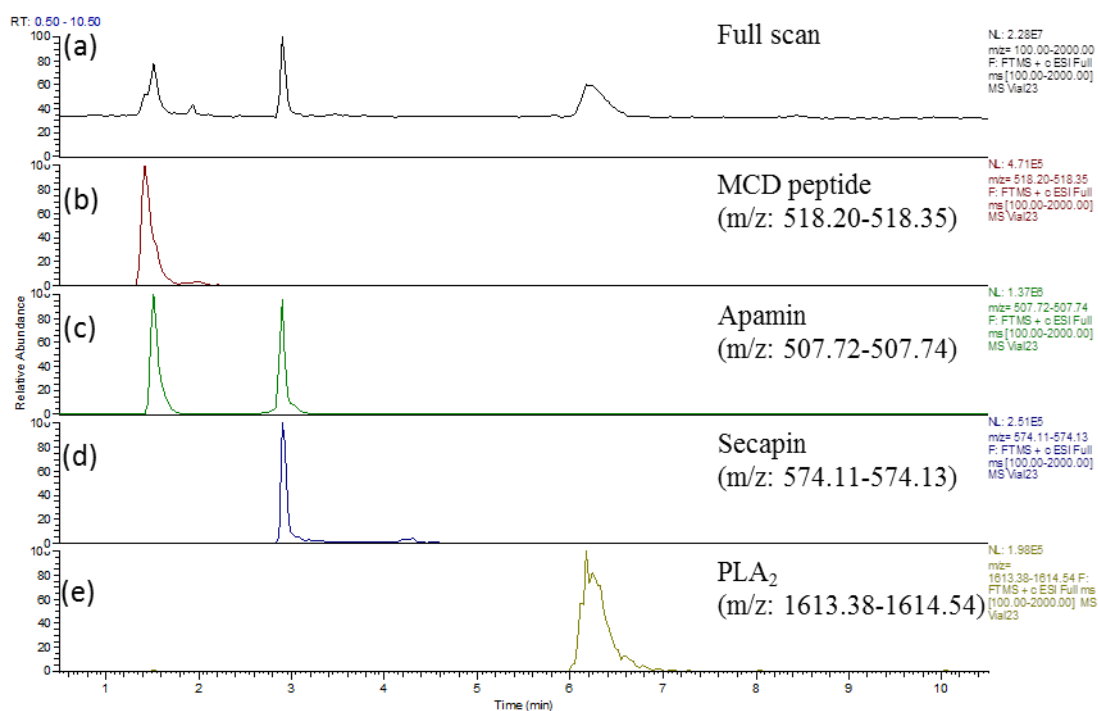


Figure 4.9: Chromatograms showing the full scan (a) and extracted ion chromatograms (b-e) of the components of F-2. The fraction was analysed by positive ion LC-ESI-MS on the Orbitrap mass spectrometer with an ACE 3 C18 column using mobile phases 0.1% formic acid in water (A) and 0.1% formic acid in acetonitrile (B) at a gradient of 20-70% (0-10 min), 70% (10-16 min), 70-20% (16-20 min) and 20% (20-25 min) relative to solvent B, and at a flow rate of 0.3 mL/min, as described in section 3.6.

Table 4.2: The main peptides identified in F-2 and their diagnostic ions in the mass spectra.

Peptide	Diagnostic ions (m/z)	Charge (+)	Calculated MW (Da)
Phospholipase A ₂	1077.5653	15	16150.2
	1154.3895	14	
	1243.1891	13	
	1346.6238	12	
	1468.9505	11	
	1615.6515	10	
	1795.1536	9	
Apamin	406.3849	5	2026.9
	507.7292	4	
	676.3021	3	
	1013.9509	2	

Table 4.2 (contd.): The main peptides identified in F-2 and their diagnostic ions in the mass spectra.

Peptide	Diagnostic ions (m/z)	Charge (+)	Calculated MW (Da)
MCD peptide	432.0726	5	2586.4
	518.2855	4	
	647.6055	3	
	863.4719	2	
Secapin	578.6031	6	2865.6
	574.1219	5	
	717.4001	4	
	956.1974	3	

In addition to the three main peptides identified, there were other minor co-eluting peptides in this fraction. For instance, apamin co-eluted with a minor peptide with a triply charged base ion of 709.2963 (MW 2124.89 Da) (**Figure 4.10**).

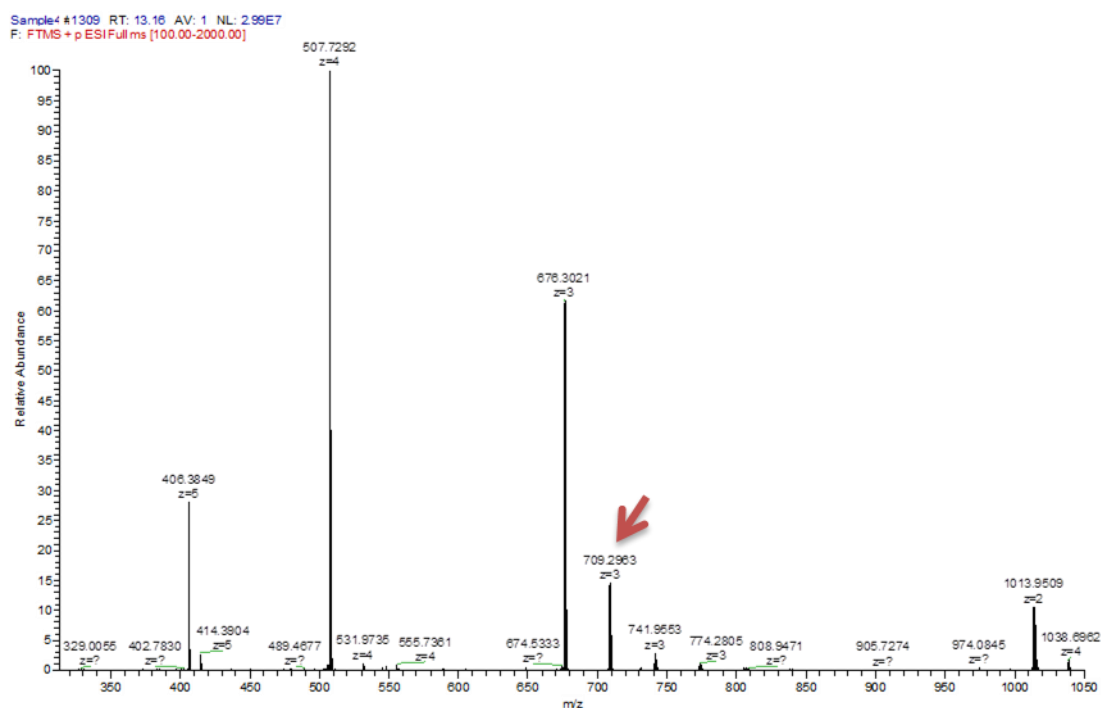


Figure 4.10: Mass spectrum of apamin showing a minor co-eluting peptide (red arrow) with a triply charged base ion of m/z 709.2963 (MW 2124.89 Da).

On the other hand, the mass spectrum of MCD peptide revealed two minor peptides of MWs 2684.40 and 2748.48 Da, each with a quintuply-charged base ion with m/z values of 537.8792 and 550.6965 respectively (**Figure 4.11**).

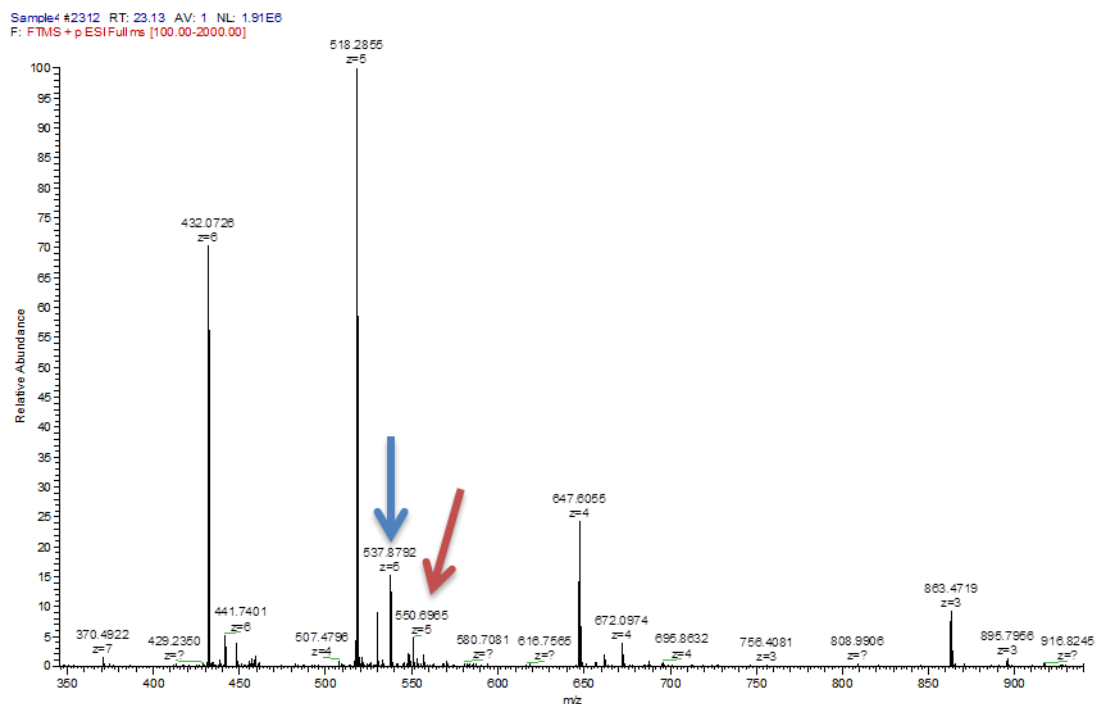


Figure 4.11: Mass spectrum of MCD peptide revealing 2 minor peptides (MW 2684.3960, Blue Arrow; and MW 2748.4825, Red Arrow) each with a quintuply-charged base ion with m/z 537.8792 and 550.6965 respectively.

There were a number of other relatively large peptides (polypeptides) with MWs ranging between 7,180-7,590 Da. The main ones were polypeptide-1 (MW ~7,179.6) and polypeptide-2 (MW ~7,586.8) (**Table 4.3** & **Figure 4.12**).

Table 4.3: The two polypeptides present in sample F-2 showing their diagnostic ions and approximate molecular weights.

<i>Polypeptide</i>	<i>Diagnostic ions (m/z)</i>	<i>Charge (+)</i>	<i>MW</i>
Polypeptide-1	1197.432	6	7,179.6
	1026.658	7	
	898.4521	8	
	798.6236	9	
Polypeptide-2	1265.794	6	7,586.8
	1084.826	7	
	949.3502	8	
	844.0901	9	

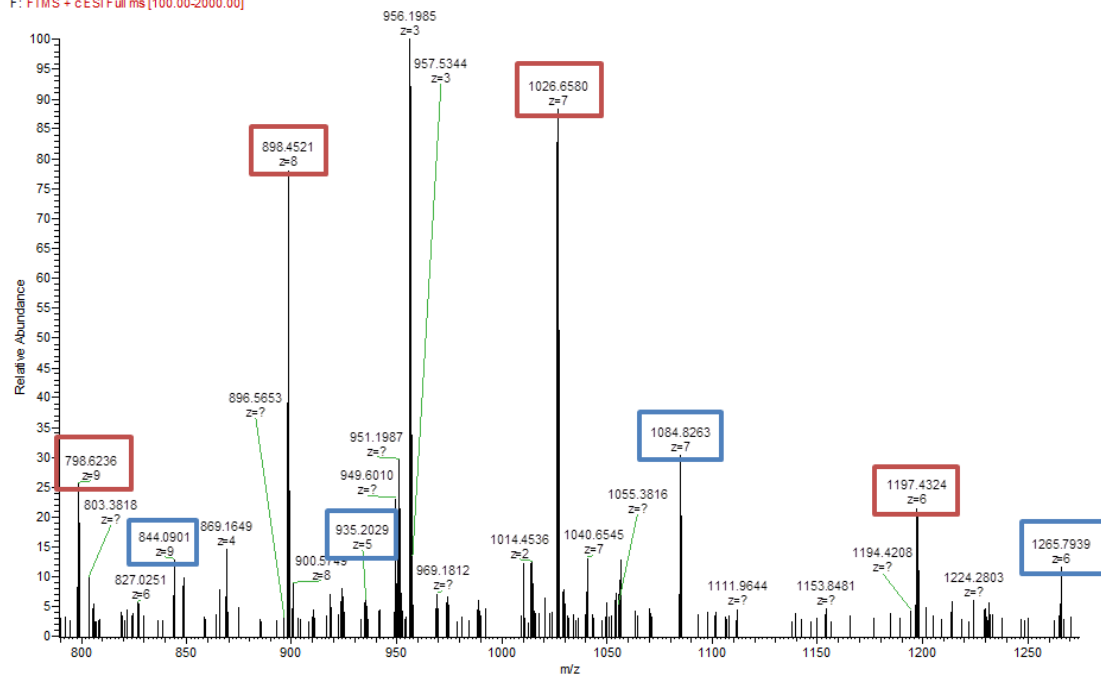


Figure 4.12: Mass spectrum of the two polypeptides showing the diagnostic m/z of the ions for polypeptide-1 (red) and polypeptide-2 (blue). The approximate MWs for the peptides are 7.2 and 7.6 kDa respectively.

The MWs of these two polypeptides matched those of two of the four isoforms of the small protein allergen (Api m6) (**Table 2.2**, pp. 43). The four isoforms of Api m6 (Api m6.01, Api m6.02, Api m6.03 and Api m6.04) possess equal levels of allergenicity. The MWs of the two polypeptides identified in F-2 matched those of Api m6.01 and Api m6.03 whose MWs are 7179.6 and 7588.1 respectively. Previous studies have reported that Api m6.02 and Api m6.04 differ from Api m6.01 and Api m6.03 respectively in that they have two extra amino acids at the C-terminus (Leu and Pro) and have MWs of 7389.9 and 7798.3 respectively. The Api m6 protein was reported to induce IgE antibodies in more than 40% of BV-hypersensitive patients (Kettner *et al.*, 2001).

4.3.3.3 Fraction-3 (F-3):

This fraction contained relatively pure melittin (MW 2845.6) (**Figure 4.13**) and some two minor peptides, with MWs 3007.85 and 3302.52 respectively, which are likely to be its precursors according to previous studies (Matysiak *et al.*, 2011). This fraction

was the largest in the chromatogram obtained from the Grace® system as shown previously in **Figure 4.4**.

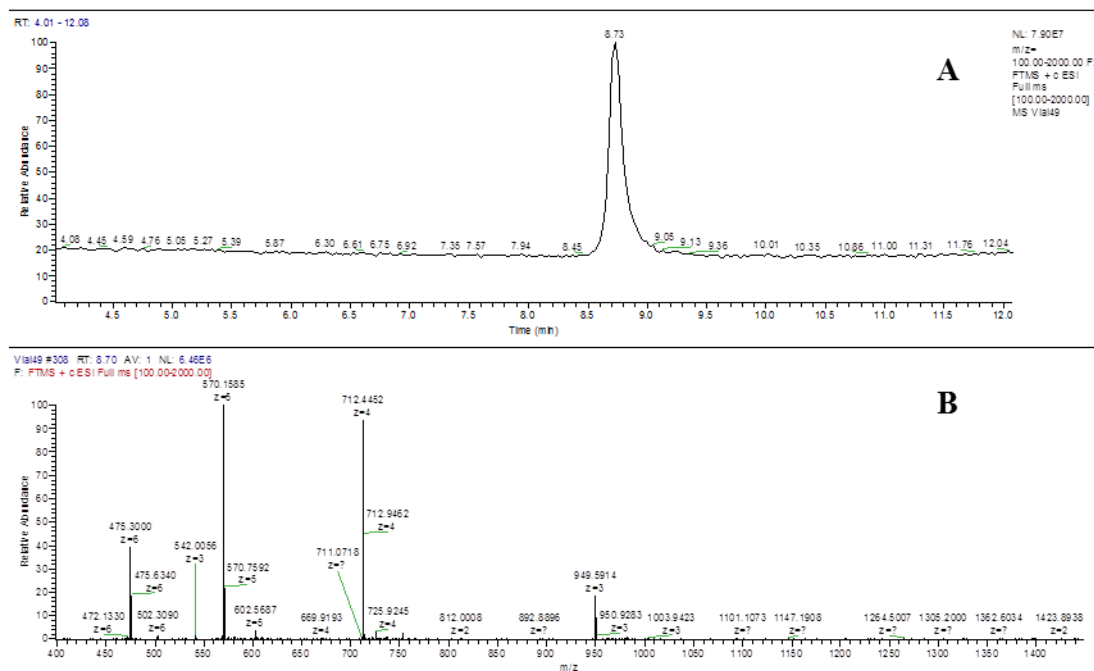


Figure 4.13: Chromatogram of sample from F-3 showing the melittin peak in a relatively pure form (**A**). The typical mass spectrum of melittin (**B**) shows a quintuply-charged base ion with m/z 570.1585. The sample was analysed by positive ion LC-ESI-MS on the Orbitrap mass spectrometer with an ACE 3 C18 column using mobile phases 0.1% formic acid in water (A) and 0.1% formic acid in acetonitrile (B) at a gradient of 20-70% (0-10 min), 70% (10-16 min), 70-20% (16-20 min) and 20% (20-25 min) relative to solvent B, and at a flow rate of 0.3 mL/min, as described in section 3.6.

In order to obtain purer fractions of melittin in F-3, the MPLC method was further optimised to achieve baseline resolution of the very broad peak (peak 2) preceding the melittin peak (**Figure 4.14**). This was mainly achieved by holding the mobile phase gradient at 20% of solvent B (acetonitrile) for longer than the 10 minutes that was used previously, so as to keep the melittin longer on the column. Melittin eluted when the proportion of acetonitrile in the mobile phase was then increased to 50% to yield a fraction whose purity was approximately 96% according to estimation by quantitative NMR (section 7.2.6).

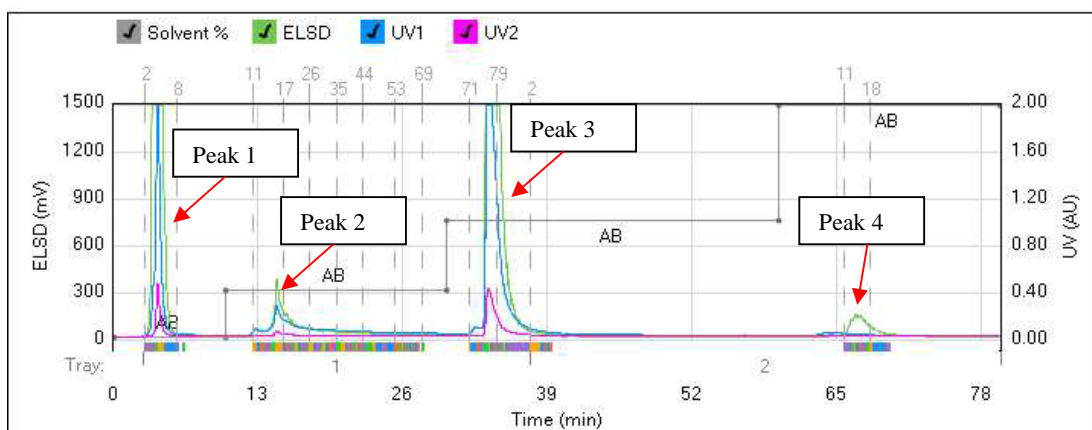


Figure 4.14: Chromatogram obtained in the MPLC separation of BV components using the Grace® system. The melittin peak (peak 3) was well resolved from the very broad and tailing peak 2. Column: Generic C18, 24g; solvents: water (A) and acetonitrile (B) with a gradient of 0-10 min (0% B), 10-20 min (20% B), 20-30 min (50% B), 30-60 min (60% B), 60-70 min (100% B); flow rate 12mL/min, run length 70 min, slope detection: high, ELSD threshold: 5mV, UV threshold: 0.05 AU, UV1 wavelength 220 nm and maximum volume per vial: 20mL. The colours on the x-axis represent separate collections across with of the peak. (Further details of the method. (Further details of the method are described in section 3.5.2).

4.3.3.4 Fraction-4 (F-4):

This final fraction was obtained from the peak that eluted at 100% acetonitrile on the MPLC system (peak 4), implying that it was highly lipophilic given that the column used was of the reversed phase type. Ample resolution was allowed between peaks 3 and 4 in order to obtain F-4 in a pure form.

The components of this fraction were determined both by GC-MS and LC-MS methods. A modified LC-MS method was required for this fraction since, being highly lipophilic, the components could not elute under the relatively weak solvent conditions used in the previous method, and it could not be reconstituted in water due to its limited aqueous solubility. In addition, unlike all the other components in the venom which ionised in positive mode, the main component in F-4 could only be detected in the negative ESI mode. Its lack of UV absorption on the Grace®, and its lipophilic nature, made us to suspect, initially, that it was probably either a large hydrocarbon or a lipid.

Following GC-MS analysis of the ethyl acetate solution of this fraction, a relatively pure compound with a mass spectral pattern closely related to that of (cis)-9-eicosen-1-ol (MW ~297) was obtained (**Figure 4.15**). The peak corresponded to the main and earliest eluting peak observed in the GC-MS chromatogram of the EtOAc extract of whole BV shown in **Figure 4.3**. Since the latter extract had already shown the presence of at least 6 peaks in each of the two batches of the crude venom samples, then it meant that during the fractionation process the rest of the components were not recovered probably because of their relatively lower content in the sample.

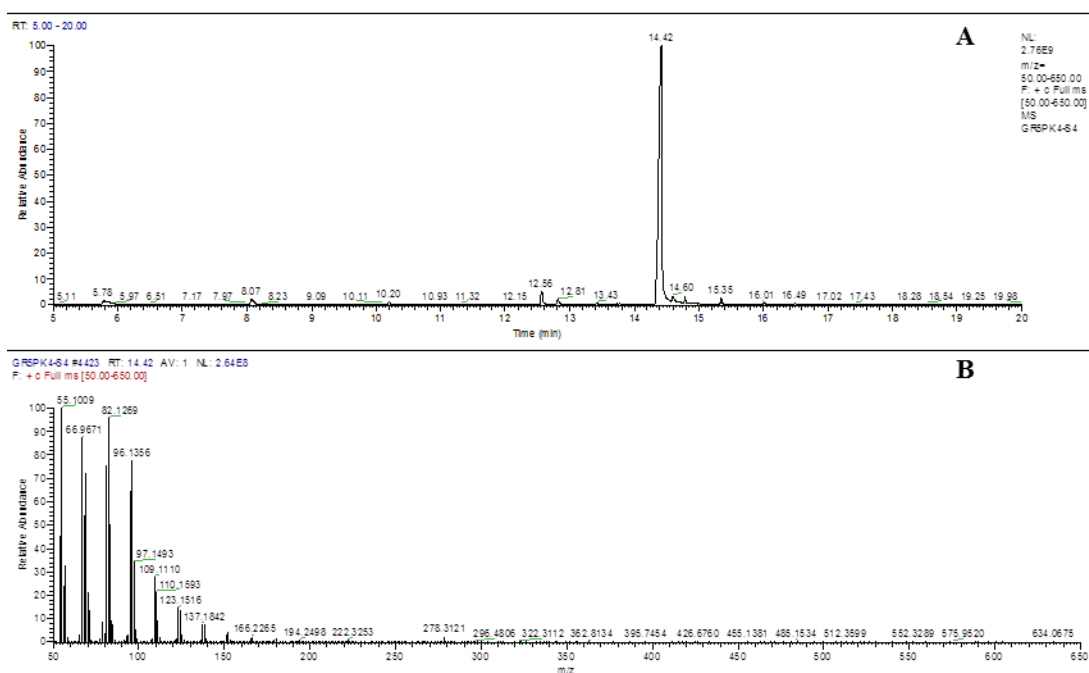


Figure 4.15: Gas chromatogram for the sample obtained from F-4 showing a single peak at 14.45 min (A). The corresponding mass spectrum shows a pattern similar to (Z)-9-eicosen-1-ol. The sample (1 μ L) was run in splitless mode a N_2 flow rate of 1.5 mL/min, MS transfer line was maintained at 275°C, and oven temperature gradient was 80 to 350°C at a rate of 10°C/min. Full scan EI spectra collected in the m/z range of 50-650.

The LC-MS assay of the same fraction showed a single compound with MW 794.5 that appeared to be a phospholipid (elemental composition, $C_{43}H_{70}O_{11}P$; 0.0783 ppm mass tolerance), detectable only in negative ESI mode (**Figure 4.16**). Given that the MW of the only compound that appeared in the GC-MS chromatogram of F-4 was approximately 297 (the MW of eicosenol), it was not immediately clear why the two techniques were giving totally conflicting information about the same sample. This

observation was later understood to arise from the inherent limitation of either technique: The LC-MS could not detect the eicosenol due to its absolute failure to ionise in the ESI, being a long chain neutral alcohol; on the other hand, the GC-MS could not detect the phospholipid due to its lack of volatility given its large size.

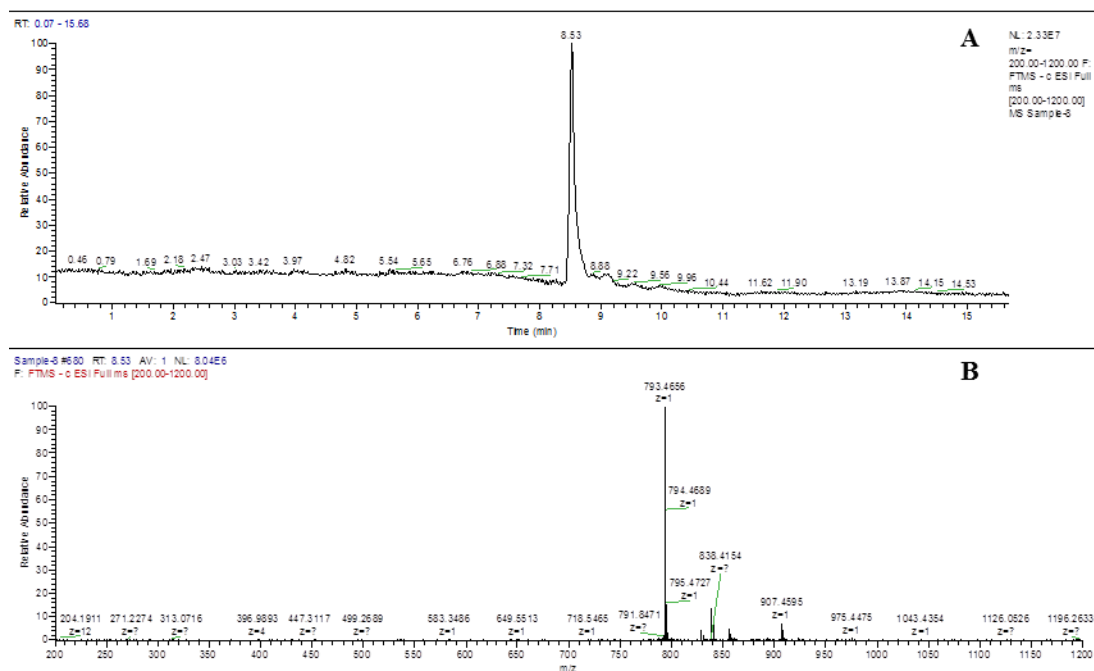
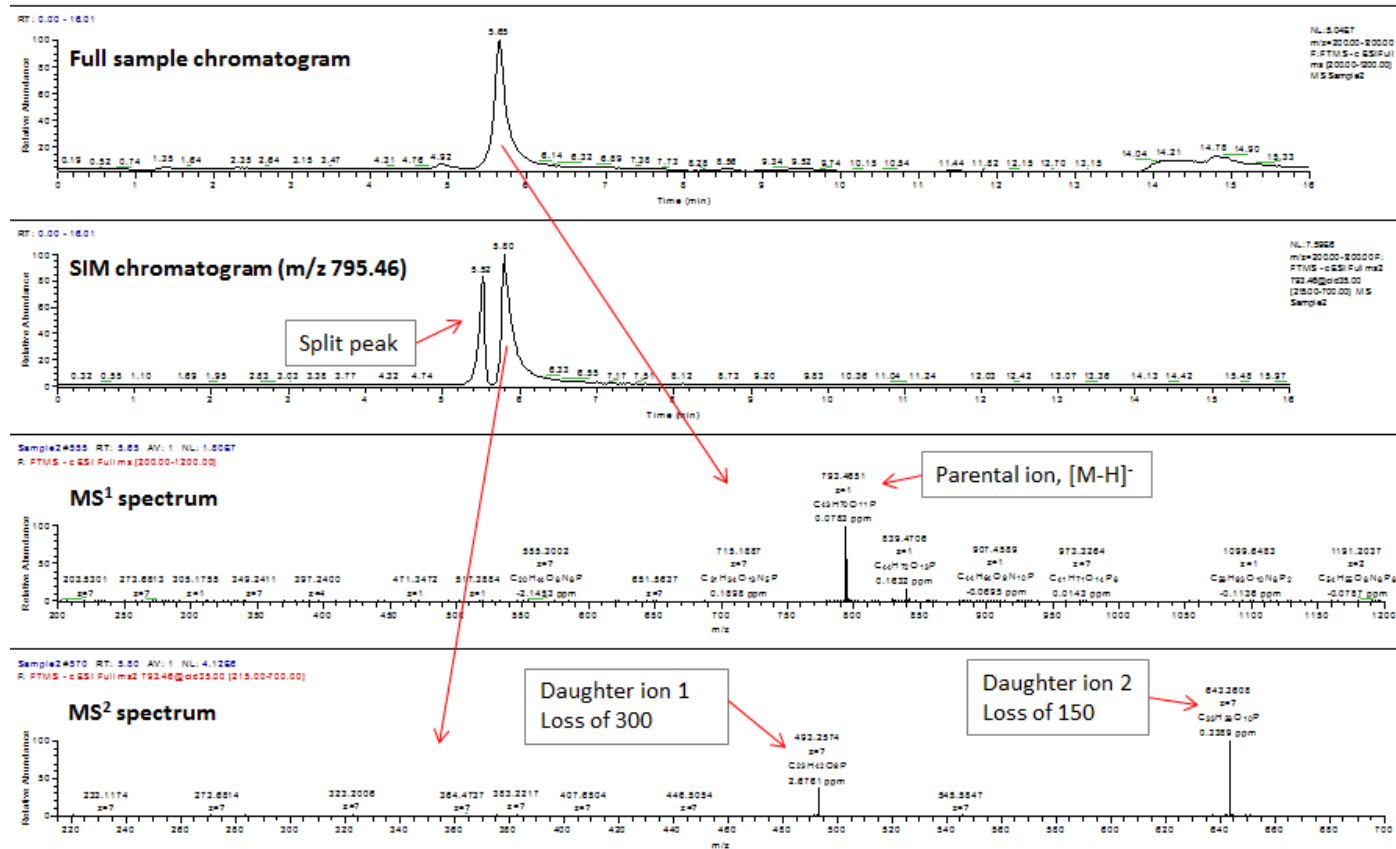


Figure 4.16: LC-MS assay of F-4 showing a single peak at 8.53 min (A) with a singly charged ion of m/z 793.4656 (B). The sample was analysed by negative ion LC-ESI-MS on the LTQ-Orbitrap mass spectrometer with an ACE 3 C18 column using mobile phases 0.1% formic acid in water (A) and 0.1% formic acid in acetonitrile (B) at a gradient of 50% B (0-5 min), 95%B (6-15 min), 50% B (16-20 min), and at a flow rate of 0.3 mL/min according to the method described in section 3.6.2.

In order to further characterize the phospholipid compound present in F-4, MS/MS was carried out using the LTQ-Orbitrap. The negative mode parental ion of m/z 793.46 was selected for collision-induced dissociation (CID) using a normalised collisional energy of 35.00. A product ion scan (PIS) of the resulting daughter ions was made in an m/z range of 215.00-700.00. The MS/MS spectrum contained two abundant daughter ions, one at m/z 493.2574 (40% relative abundance) with elemental composition of $C_{23}H_{42}O_9P$ (2.685 ppm mass tolerance) suggesting loss of an eicosahexanoic acid, while the second was m/z 643.3608 (60% relative abundance) with elemental composition of $C_{33}H_{56}O_{10}P$ (0.341 ppm mass tolerance) (Figure 4.17). This elemental composition, although inconclusive, suggested the possibility that the

unknown compound in F-4 might be a phospholipid. Through an extensive structure elucidation with NMR, the structure of the main component of F-4 was identified to be (*Z*)-9-eicosen-1-ol (Section 8.3.7). The unidentified phospholipid was thus confirmed to be a minor component of the fraction since it could not be detected by NMR at its concentration in F-4.



115

Figure 4.17: MS¹ and MS² of the unknown compound present in fraction F-4 of BV. The molecular ion [M-H]⁻ was selected for fragmentation using collision-induced dissociation (CID) to form two daughter ions of m/z 493.2574 and 643.3608 with 40% and 60% relative abundance respectively in a product ion scan spectrum.

4.3.4 Detection of phospholipase and hyaluronidase in BV

Electrophoretic bands for the two main BV proteins PLA₂ and hyaluronidase were observed in the sample (**Figure 4.18**). The former appeared as a dense band of MW ~20 kDa while the latter was seen as a trace band with MW ~60 kDa. These molecular weights matched those from literature (sections 2.2.2 and 2.2.3; pp.33-37). The Westernblot showed that all the BV-hypersensitive sera were reactive to PLA₂ except the sample in lane 5. On the other hand, only two BV-reactive serum samples in lanes 1 and 5 showed reactivity to hyaluronidase. Since these 7 reactive human sera had been obtained from 430 individuals, it means that BV reactivity was present in ~2% of the samples. In addition, it means that reactivity to PLA₂ occurs about 3 times as frequently as reactivity to hyaluronidase.

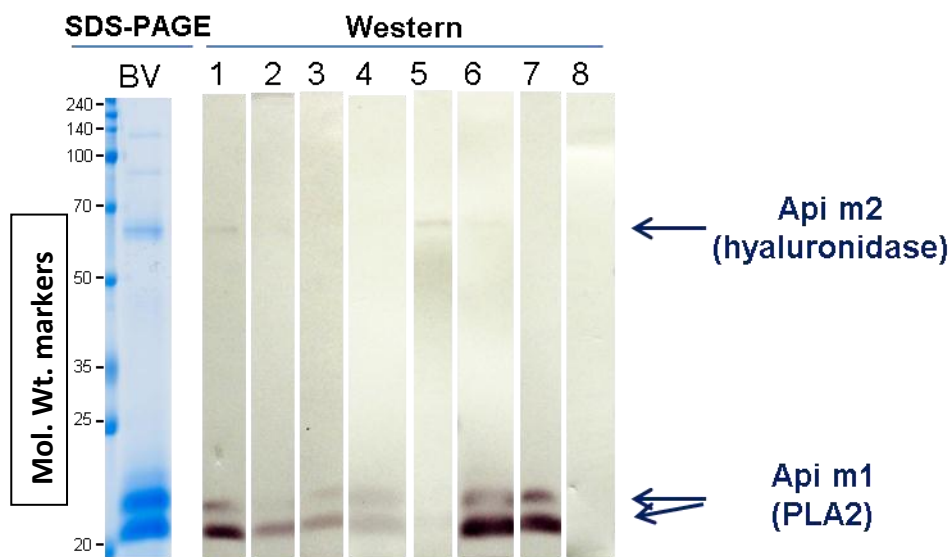


Figure 4.18: SDS-PAGE and immunoblot analysis of BV to detect the main allergens. The BV proteins were separated by SDS-PAGE and transferred to a nitrocellulose membrane. Lanes 1 to 7 of the Westernblot represent incubation with sera from BV-hypersensitive patients; lane 8 represents control serum. Specific IgE binding was detected by means of an AP-conjugated secondary antibody (IgE) followed by the BCIP/NBT substrate to obtain a purple colour in 30 min. Further details are described in sections 4.2.4 and 4.2.5 for SDS-PAGE and immunoblot analysis respectively. SDS-PAGE and Westernblot analysis were carried out though a collaboration with ProteomeTech (Seoul, Korea).

4.3.5 Determination of LoD and LoQ for melittin

The LoD and LoQ of melittin were determined in preparation for its analysis of in cosmetic formulations. The LoD and LoQ were approximately 1.3 and 4.0 ng/mL respectively (**Figure 4.19**). The limit of detection (LoD) specifies the least amount of analyte in a sample that the developed method is capable of detecting without being able to quantify it. This means that at the LoD value an analyte must produce a signal that is at least reliably distinguishable from background noise associated with the analytical method.

On the other hand, the limit of quantification (LoQ), which is also known as the lower limit of quantification (LLOQ), is taken to mean the least concentration of analyte in a sample that a developed method can accurately quantify with enough precision. The LoQ is expectedly higher than the LoD value by approximately a factor of 3. Equations for LoD and LoQ are given in section 4.2.3 above.

The regression lines used to compute LoD and LoQ values can be obtained from a set of calibration standards of the analyte being analysed prepared near the concentration range of the analyte's LoD value. The standard deviation parameters of any regression line can conveniently be computed using the LINEST function for plots made in Microsoft Excel®. Normally the calibration plot should be prepared from at least a 6-point calibration series.

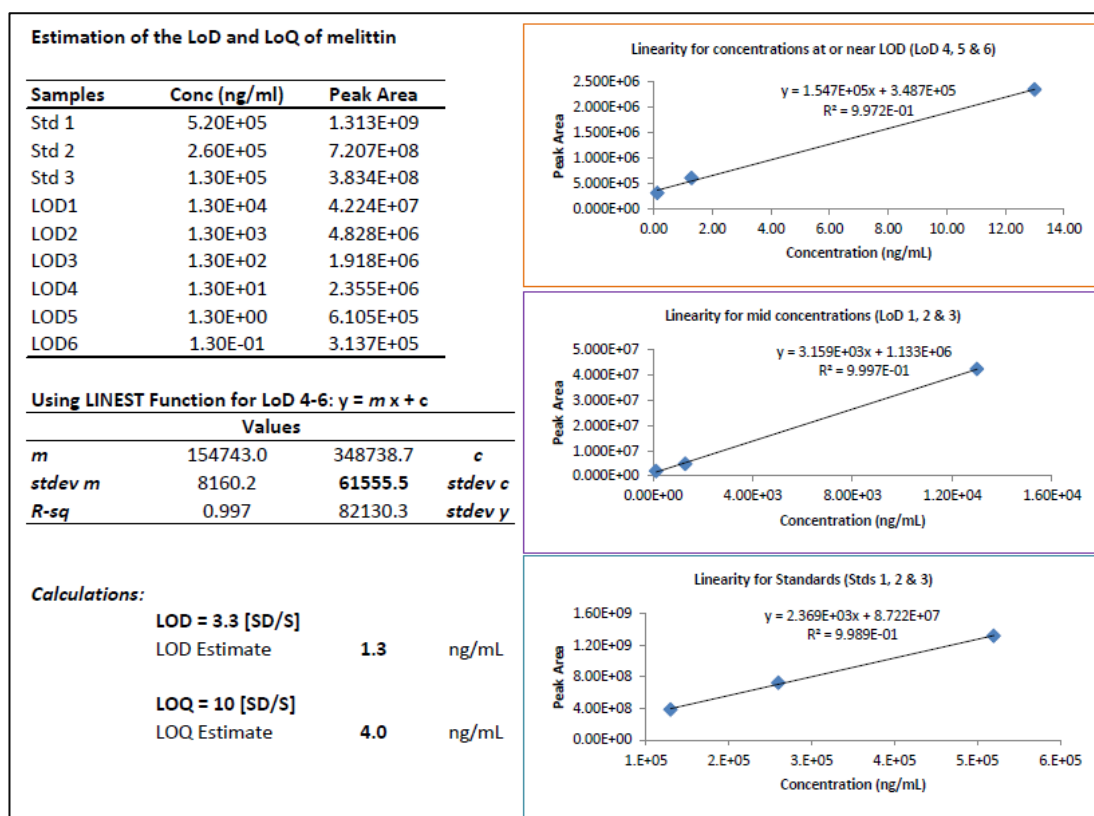


Figure 4.19: Determination of LoD and LoQ of melittin. The LoD and LoQ values approximated to 1.3 and 4.0 ng/mL respectively.

The use of mass spectrometry as a means of analyte detection in liquid chromatographic assays permits the achievement of relatively low levels of both detection and quantification, given that the technique is very selective and sensitive. Even then, the limits achievable also depend on the ionisation properties of the analyte, mobile phase characteristics, and the capabilities of the mass spectrometer used, including its ion source properties. For instance an easily ionisable analyte such as a strong base would be able to give low limits of both detection and quantification in positive mode on the LC-ESI-Orbitrap as compared to a weaker base. For easily ionisable analytes it is customary to achieve detection limits of 1 ng/mL or even less.

4.4 Discussion

The BV profiling showed multiple ingredients in the sample but melittin was the most abundant as expected. The most abundant components were peptides, amines, amino acids, and polypeptides. LC-MS analysis with the Orbitrap proved to be a versatile and comprehensive technique capable of detecting most of analytes,

including proteins. This technique can conduct MS/MS and full-scan functions concurrently, while yielding highly accurate mass data (Makarov and Scigelova, 2010). The mass spectrometer was set to detect ions in the mass range of m/z 100 to 2000. While this range suits most analytes, the molecular weights of some of the proteins in the sample ranged between MW 8 kDa to 50 kDa, which is above the m/z range used. Thus in order for the detection to be possible in this m/z range, the proteins and larger peptides have to become multiply charged. Because large proteins do not easily undergo ionisation in the ESI, their detection on the LC-MS can sometimes be a challenge—something that was observed with PLA₂ in this study.

Chapter Five

Antimicrobial and Cell Cytotoxicity Assays

5 Antimicrobial and Cell Viability Assays

5.1 Introduction

The biological effects of BV are well documented. Most of these effects are potentially therapeutic such as antimicrobial, antitumor, anti-inflammatory, anti-arthritis and other pain-relieving effects (Chen and Lariviere, 2010). However, some effects of BV are idiosyncratic and result when sensitive individuals are exposed to the venom, leading to allergic reactions. Most of the BV allergens are known and are listed in the database for International Union of Immunological Societies (Francese *et al.*, 2009). Given that this project sought to generate data that would contribute towards formulation of cosmetics containing BV, it was necessary to screen crude samples and their fractions for their effects on selected human cell lines and microbes in order to ensure that the intended product was safe and fit for purpose.

Biological testing was carried out *in vitro* on BV fractions for antimicrobial (antibacterial, antiprotozoal and antiviral), cytotoxic, and anti-inflammatory effects. Antibacterial effects were evaluated on two forms of bacteria, namely, *Mycobacterium marinum* and *Nocardia farcinia*, because they were readily available. The antiprotozoal activity was tested in *Trypanosoma brucei*, the causative agent of African trypanosomiasis in cattle (Hajduk *et al.*, 1989). On the other hand, the potential for antiviral activity in the samples was assessed indirectly via assay for α -glucosidase inhibition which has been shown to represent broad antiviral action (Mehta *et al.*, 1998). The cytotoxic activity of the venom and its fractions was investigated in “normal” human keratinocytes, epithelial cells, and fibroblasts in order to gauge its safety should it be introduced into the human body. Potential anti-inflammatory action was evaluated by determining the inhibition of Tumour Necrosis Factor- α (TNF- α)-induced Nuclear Factor-KappaB (NF- κ B) in human keratinocytes.

All biological testing were carried out within the Strathclyde Innovations in Drug Research (SIDR) laboratory. Sample stock solutions were prepared in purified water or DMSO at a concentration of 10 mg/mL and filter-sterilised. In the SIDR laborato-

ry, the samples were stored in standard 96-microwell storage plates at -20°C until required for assay.

5.2 Materials and methods

5.2.1 Test organisms and cells used in the assays

Antiprotozoal activity was tested against *Trypanosoma brucei* while antibacterial activity was tested against *Norcardia farcinia* and *Mycobacterium marinum*. Cell viability assays were performed using PNT2A (normal epithelial cells), NCTC 2544 (normal human keratinocytes), and HS27 (normal human fibroblasts) cell lines.

5.2.2 Test sample fractions and their preparation

Two different sets of three fractions (F-1, F-2 and F-3) were obtained from two separate fractionations on the Grace® system as already described in sections 3.5.2 (p. 90) and 4.3.3 (p. 100). The quantity of F-4 fraction available at this stage was only sufficient for HS27 assay. Each of the fractions tested had one or more separate samples based on the collection of fractions in several test tubes across the width of the peak obtained from the MPLC separation. From the first fractionation (G₁), the samples were F-1 (T₃), F-2 (T₆, T₈ & T₁₂), and F-3 (T₁₃ to T₁₆). The samples from the second fractionation (G₂) were F-1 (T₂ to T₄), F-2 (T₁₉), and F-3 (T₄₈ to T₅₀, T₅₂, T₅₃, and T₅₅). Test solutions were prepared by dissolving *ca.* 10 mg of the lyophilised samples in *ca.* 1 mL of DMSO or purified water to make final concentrations of exactly 10 mg/mL.

5.2.3 Assay for anti-trypanosomal activity

5.2.3.1 Measurement of protozoal cell viability

The anti-trypanosomal activity was tested using an already established Alamar Blue® assay on 96 micro-well plates. The samples were screened at a concentration of 20 µg/mL achieved by dilution, in HMI-9 medium, of the initial 10 mg/mL stock

solutions in DMSO. The stock solutions were first diluted ten-fold to 1 mg/mL with the HMI-9 medium. Then 4 μL of the resulting solutions were transferred to the plate and mixed with 96 μL of HMI-9 medium, resulting in 25-fold dilutions to give 40 $\mu\text{g}/\text{mL}$. The final assay concentrations of 20 $\mu\text{g}/\text{mL}$ were attained after 1:1 dilutions of the samples on addition of 100 μL of a suspension of *Trypanosoma brucei*, prepared and diluted to a concentration of 3×10^4 trypanosomes per mL established with the aid of a haemocytometer. A sterility well (A_1) and negative controls for media (A_1 to D_1), and DMSO (at 1% in E_1 to H_1) were included. Only the sterility well was not inoculated with the trypanosomes. After the inoculation, the micro-well plate was incubated at 37°C and 5% CO_2 in a humidified atmosphere for 48 h. Then 20 μL of Alamar Blue® dye were added to each well and the plate incubated for extra 4 h.

The fluorescence was measured by a Wallac Victor² microplate reader at an excitation wavelength (λ_{Ex}) of 560 nm and emission wavelength (λ_{EM}) of 590 nm. The final results were expressed as percentage of the mean DMSO control values, as follows:

$$Viability = \left[\frac{\text{Fluorescence of sample}}{\text{Fluorescence of blank}} \right] \times 100 \quad (15)$$

5.2.3.2 Determination of MICs

The minimum inhibitory concentration (MIC) was determined in duplicate for each of the samples that demonstrated less than 10% viability relative to the control. The assay plate was prepared as follows: To each of the micro-wells A_1 to D_1 (column 1) was added 100 μL of HMI-9 media; similarly, 100 μL of media containing 2% DMSO was added to the micro-wells E_1 to H_1 . In column 2, 200 μL of 200 $\mu\text{g}/\text{mL}$ solutions of the samples were prepared by 50-fold dilution of the original 10 mg/mL stock solutions in the HMI-9 medium. Then serial 1:1 dilutions of the resulting solutions were prepared in columns 3-11 of the plate by pipetting into each micro-well 100 μL of solution from the preceding well and then adding an equal volume (100 μL) of HMI-9 medium (**Table 5.1**). In column 12, a concentration range of suramin was prepared from 0.008 to 1.0 μM by dilution of the suramin stock solution with HMI-9 medium. Inoculation of the wells (except A_1) was carried out by adding 100 μL of a 3×10^4 cells/mL suspension of trypanosoma cells, leading to 1:1 dilutions of

the sample solutions on micro-well plate, so that the resulting concentrations were as shown in the table. Finally, incubation of the plate and subsequent addition of Alamar Blue® dye were carried out as already described in section 5.2.3.1 above.

5.2.4 *α-Glucosidase inhibition assay*

α -Glucosidase inhibitors have been shown to possess potential broad anti-viral activity (Mehta *et al.*, 1998). The virus life cycle is dependent on one or more viral glycoprotein(s) contained on the outer envelope which can be disrupted by α -glucosidase inhibitors resulting in inhibition of viral entry into mammalian cells. This property would be desirable in a *cosmeticeutical* product. Thus the α -glucosidase inhibitory assay was employed to evaluate potential antiviral activity of the BV fractions. Samples of the aqueous BV fractions were tested at a concentration of 30 $\mu\text{g/mL}$ (n=3) based on the method published by Dong *et al.* (Dong *et al.*, 2012). Samples which showed $\geq 60\%$ inhibition ($\leq 40\%$ control) were considered to be “active”. In addition, two purified melittin fractions (Melittin-1 and Melittin-2) were also tested. Both samples of melittin were assayed in the concentration range of 3-100 $\mu\text{g/mL}$ (n=3). The results were expressed as percentages of the enzyme-substrate reaction in the absence of the melittin. Lack of enzyme inhibition equals 100% control while 100% inhibition equals 0% control.

Table 5.1: Microwell plate set up for MIC determination

	1	2	3	4	5	6	7	8	9	10	11	12 (Suramin, μM)
A	SC	100	50	25	12.5	6.25	3.125	1.56	0.78	0.39	0.195	1.0
B	C ₁	100	50	25	12.5	6.25	3.125	1.56	0.78	0.39	0.195	0.5
C	C ₂	100	50	25	12.5	6.25	3.125	1.56	0.78	0.39	0.195	0.25
D	C ₃	100	50	25	12.5	6.25	3.125	1.56	0.78	0.39	0.195	0.125
E	DMSO	100	50	25	12.5	6.25	3.125	1.56	0.78	0.39	0.195	0.0625
F	DMSO	100	50	25	12.5	6.25	3.125	1.56	0.78	0.39	0.195	0.0313
G	DMSO	100	50	25	12.5	6.25	3.125	1.56	0.78	0.39	0.195	0.0156
H	DMSO	100	50	25	12.5	6.25	3.125	1.56	0.78	0.39	0.195	0.0078

Note: SC = Sterility control, C₁₋₃ = negative controls (HMI-9 media), and DMSO = negative control (1% DMSO).

5.2.5 Cell viability assays

5.2.5.1 Action on human epithelial cells (PNT2A)

The “normal” human epithelial cells (PNT2A) were incubated for 48 h (2 doubling times) in the presence of 30 and 100 µg/mL of each fraction sample (n=3). After 24 and 48 h, micrographs were taken of micro-wells where there was a change in cell viability as compared with the control well. The actions of two the purified melittin fractions were also assessed on these cells to give an indication of skin activity. Both fractions were assessed in the concentration range of 3 to 100 µg/mL (n=3) for 48 h to determine their effect on cell viability. Micrographs were taken to confirm the results obtained by the Alamar Blue® probe. Cell viability was expressed as a percentage of negative control, where 100% indicated complete viability and 0% indicated complete death, as shown in equation 15 in section 5.2.3.1.

5.2.5.2 Action on human keratinocytes (NCTC2544)

The “normal” human keratinocyte cells were incubated in the presence of 1, 3, 10 and 30 µg/mL (n=3) of each of the BV fraction samples for 48 h. Micrographs were taken at 5 min and 4 h in addition to 24 and 48 h. Alamar Blue® was utilised as already described in section 5.2.5.1 above in order to obtain meaningful numbers.

5.2.5.3 Action on human fibroblasts (HS27)

The culture media used for this normal human foreskin fibroblast cell line was Dulbecco’s Modified Essential Medium (DMEM) supplemented with 2 mM glutamine and 10% foetal bovine serum (FBS). Cell cultures were seeded at 10,000 cells/cm² and incubated at 37°C in a humidified atmosphere saturated with 5% CO₂. Sub-confluent cultures of the adherent cells were split every 2-3 days via trypsinisation. A haemocytometer was used as a cell counter. The cells were tested between passages 39-45.

The assays were performed on 96 micro-well plates. Cells were reconstituted in the culture media at 1×10^5 cells/mL and seeded in a volume of 75 µL/well at 7,500

cells/well on the plate. The plate was incubated for 48 h to allow the cells to adhere and grow. The 10 mg/mL sample stock solutions were diluted in media on a dilution plate to achieve serial concentrations in the range of 400 µg/mL to 40 ng/mL. After this, 25 µL aliquots of the diluted samples were then transferred to the assay plate which resulted into a 4-fold dilution to achieve final assay concentrations in the range of 100 µg/mL to 10 ng/mL. The plates were then incubated for a further 48 h before adding Alamar Blue® dye (10%, v/v) followed by a further incubation for 6 h. The plates were then read with a Wallac Victor² microplate reader to obtain fluorescence at $\lambda_{EX/EM}$ of 560/590 nm.

5.2.6 Assay for TNF- α -induced NF- κ B inhibition

The samples were tested at concentrations of 10 and 30 µg/mL (n=3) for anti-inflammatory properties by assessing the inhibition of TNF- α -induced NF- κ B in NCTC2544 cells (human keratinocytes) using the transient transfection and luciferase assay method published by Youn *et al.* (2011). In brief, approximately 60-80% confluent NCTC2544 cells (1×10^5 cells/well in a 24-well plate) were transiently co-transfected overnight with NF- κ B-luciferase construct (1µg per well) using the FuGene® transfection reagent (Promega, Southampton, UK). The cells were then treated with both concentrations of the BV fractions followed by TNF- α . Treatment with TNF- α alone served as the positive control. The luciferase assay was then carried out at room temperature on 20µL of cell lysates using 50µL of the luciferase substrate. The luciferase activity was measured with a luminometer and normalised to transfection efficiency monitored by renilla expression (Youn *et al.*, 2011). The data obtained were expressed as mean \pm SE for triplicate experiments. Samples which showed $\leq 40\%$ of the positive control values ($\geq 60\%$ inhibition) were considered to be potentially active.

5.3 Results

5.3.1 Antibacterial assays

The tables below show the results obtained from the assay for antibacterial effects of the fractions on *M. marinum* and *N. farcinia*, as well as the MICs obtained for fractions that demonstrated $\leq 10\%$ of microbe viability. *M. marinum* did not show appreciable sensitivity towards any of the samples tested at both 100 and 200 $\mu\text{g/mL}$ concentrations and thus the MICs were not determined in relation to it. For *N. farcinia*, sensitivity was observed only for samples of fraction F-3 from both fractionations which gave MICs of 25 or 50 $\mu\text{g/mL}$ for the aqueous stock solutions (**Table 5.2**). Similar MICs were obtained for the same F-3 sample stock solutions in DMSO except that sample G₁T₁₆ gave much less activity compared to the aqueous stock solution (**Table 5.3**). This difference in activity between aqueous and DMSO stock solutions of the G₁T₁₆ sample might be related to solubility differences of its components in these two solvents.

5.3.2 Activity against *T. brucei*

All the samples with the exception of aqueous stock solutions of G₂T₅₂, G₂T₅₃, and G₂T₅₅ of fraction F-3 were tested for MICs against *T. brucei* and similar results were obtained for both aqueous and DMSO stock solutions. As was observed for *N. farcinia*, the most active samples were those of fraction F-3 with MICs in the range of 0.78-1.56 $\mu\text{g/mL}$, except the DMSO sample of G₁T₁₆ which was not active at $\leq 100 \mu\text{g/mL}$.

Table 5.2 and **Table 5.3** summarise the biological activities of the BV fractions against *M. marinum*, *N. farcinia* and *T. brucei* for the samples reconstituted in water and DMSO respectively. The blue and purple colours represent different fractionations of BV. The different hues of each colour represent different fractions from the same fractionation experiment.

5.3.2.1 Sample stock solutions dissolved in water

Table 5.2: Biological activity of BV fractions against *M. marinum*, *N. farcinia* and *T. brucei*.

Fractions	Samples	<i>M. marinum</i>		<i>N. farcinia</i> [898 ATCC 3318]		<i>T. brucei</i>
		% of control		% of control		MIC
		200 µg/mL	100 µg/mL	200 µg/mL	100 µg/mL	(µg/mL)
F-1	G ₁ T ₃	91.8	61.0	98.9	94.3	>100
	G ₁ T ₆	62.2	95.5	90.9	91.5	100
F-2	G ₁ T ₈	40.5	59.4	93.4	95.0	12.5
	G ₁ T ₁₂	29.1	44.1	98.5	94.2	12.5
F-3	G ₁ T ₁₃	26.8	26.8	-2.2	-1.2	50
	G ₁ T ₁₄	27.0	28.8	3.1	-1.2	50
	G ₁ T ₁₅	26.9	28.1	-2.0	-1.3	50
	G ₁ T ₁₆	26.0	29.0	-1.4	23.4	25
F-1	G ₂ T ₂	122.9	92.5	91.0	95.2	>100
	G ₂ T ₃	119.9	88.4	94.2	93.5	>100
	G ₂ T ₄	66.4	67.5	92.3	89.8	>100
F-2	G ₂ T ₁₉	39.9	58.4	97.1	90.1	12.5
F-3	G ₂ T ₄₈	23.4	28.6	-2.4	21.4	25
	G ₂ T ₄₉	22.9	29.1	-2.3	-1.2	50
	G ₂ T ₅₀	21.8	48.9	-1.6	-1.0	50
	G ₂ T ₅₂	23.1	50.7	2.0	6.5	25
	G ₂ T ₅₃	25.3	57.4	1.2	-1.3	25
	G ₂ T ₅₅	24.1	65.3	14.8	15.8	-

5.3.2.2 Sample stock solutions dissolved in DMSO

Table 5.3: Biological activity of BV fractions on *M. marinum*, *N. farcinica* and *T. brucei*.

Fractions	Samples	<i>M. marinum</i>		<i>N. farcinica</i> [898 ATCC 3318]		<i>T. brucei</i>	
		% of control		% of control		MIC	
		200µg/mL	100µg/mL	200µg/mL	100µg/mL	(µg/mL)	
F-1	G ₁ T ₃	80.0	88.4	94.6	94.0	-	100
	G ₁ T ₆	14.6	29.5	16.5	47.9	-	1.56
F-2	G ₁ T ₈	31.0	75.0	88.8	92.9	-	25
	G ₁ T ₁₂	21.0	46.2	93.5	95.3	-	12.5
	G ₁ T ₁₃	20.2	36.0	-1.6	2.8	25	1.56
F-3	G ₁ T ₁₄	18.2	32.7	-1.6	-1.9	25	1.56
	G ₁ T ₁₅	16.2	30.1	15.2	2.0	25	1.56
	G ₁ T ₁₆	47.6	93.7	86.0	93.1	-	>100
F-1	G ₂ T ₂	71.2	98.6	95.0	100.6	-	>100
	G ₂ T ₃	91.4	118.3	97.3	102.3	-	>100
	G ₂ T ₄	67.4	122.8	95.8	95.4	-	>100
F-2	G ₂ T ₁₉	54.4	103.9	91.3	92.3	-	50
F-3	G ₂ T ₄₈	14.6	32.4	-1.6	1.7	50	1.56
	G ₂ T ₄₉	14.5	30.6	-1.4	-1.5	25	1.56
	G ₂ T ₅₀	15.7	34.1	-1.6	-2.6	25	1.56
	G ₂ T ₅₂	17.7	35.5	-1.6	-2.9	50	0.78
	G ₂ T ₅₃	18.8	35.0	14.7	-2.6	25	0.78
	G ₂ T ₅₅	19.7	40.2	15.3	75.2	-	1.56

5.3.3 α -Glucosidase activity

Figure 5.1 shows that none of the samples tested was able to inhibit α -glucosidase at the 30 $\mu\text{g}/\text{mL}$ concentration used in the assay. “Activity” of the sample was defined as the ability to produce at least 60% inhibition of α -glucosidase activity relative to the control (i.e. $\leq 40\%$ of the activity measured in the negative control). The melittin fractions (Melittin-1 and Melittin-2) which were tested in the concentration range of 3.0 to 100 $\mu\text{g}/\text{mL}$ ($n=3$) also did not demonstrate significant inhibitory effects on α -glucosidase activity (**Figure 5.2**).

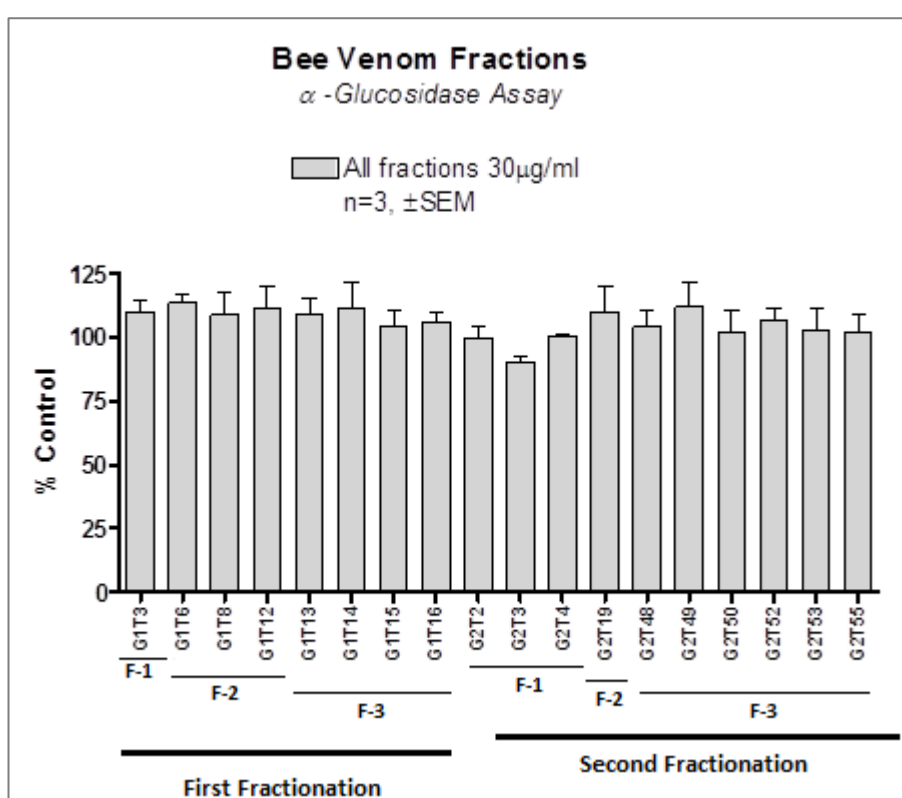


Figure 5.1: Inhibitory effect of aqueous BV fractions on α -glucosidase enzyme at 30 $\mu\text{g}/\text{mL}$ concentration. There was no significant enzyme inhibition detected in this assay system. This would imply no potential antiviral activity at this concentration.

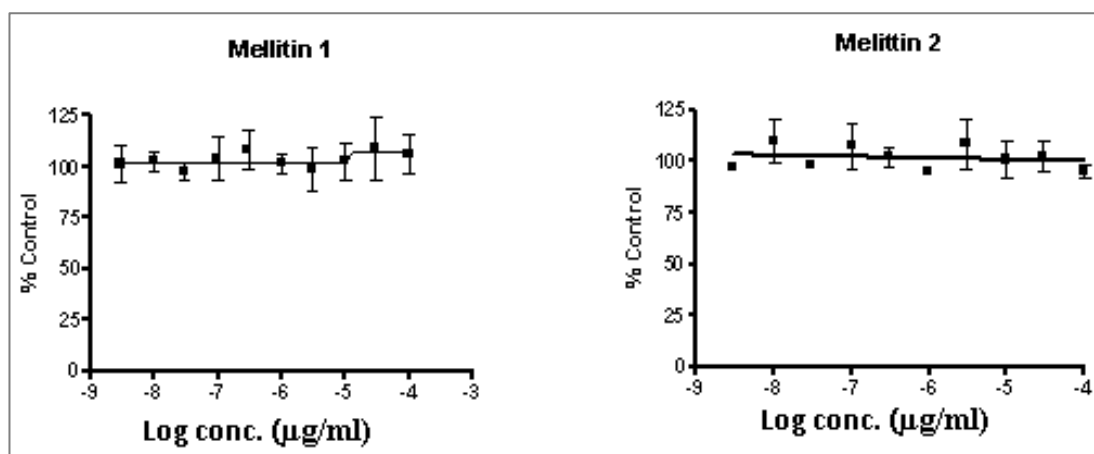


Figure 5.2: Action of melittin on α -glucosidase. No inhibitory effect was observed in the concentration range of 3 to 100 $\mu\text{g/mL}$. Values were expressed as a percentage of the enzyme-substrate reaction in the absence of the melittin samples. 100% control indicates zero inhibition whereas 0% control indicates 100% inhibition.

5.3.4 Effect BV fractions on cell viability

5.3.4.1 Effect of BV on PNT2A cell viability

Following incubation for 48 h in the presence of 30 and 100 $\mu\text{g/mL}$ of each of the fractions, the viability of the PNT2A cells was determined from fluorescence measurements representing the extent of reduction of resazurin to resorufin by cell respiration. Only samples of F-3 showed potential cytotoxic activity against the PNT2A cells at both concentrations tested as the cells lost their viability (**Figure 5.3**). In the presence of sample G₁T₁₂ of F-2, loss of cell viability was observed only at 100 $\mu\text{g/mL}$. The cytotoxic fractions were found to contain melittin following analysis by LM-CS. The samples that did not contain melittin were relatively nontoxic at the concentrations tested.

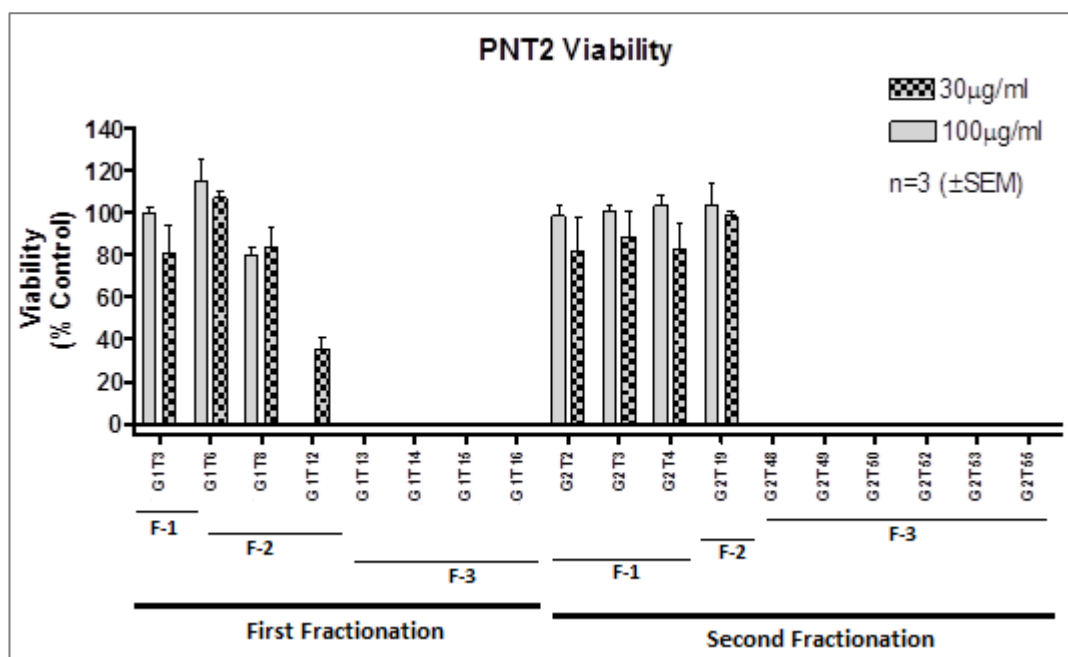


Figure 5.3: Effect of BV fractions on PNT2A normal epithelial cells at 30 and 100 µg/mL concentrations. The samples of fraction **F-3** can be seen to induce complete loss of cell viability at both concentrations. The active fractions are known to contain mainly melittin. Cell viability was measured as a ratio of the amount of fluorescence in test samples to that of the blank using resazurin reduction method.

From the micrographs of the wells taken after 24 and 48 h of incubation, the results of resazurin reduction in the **Figure 5.3** above could be confirmed. **Table 5.4** shows selected micrographs taken after 24 and 48 h incubation for two samples of F-3 that produced total loss of cell viability at 30 µg/mL.

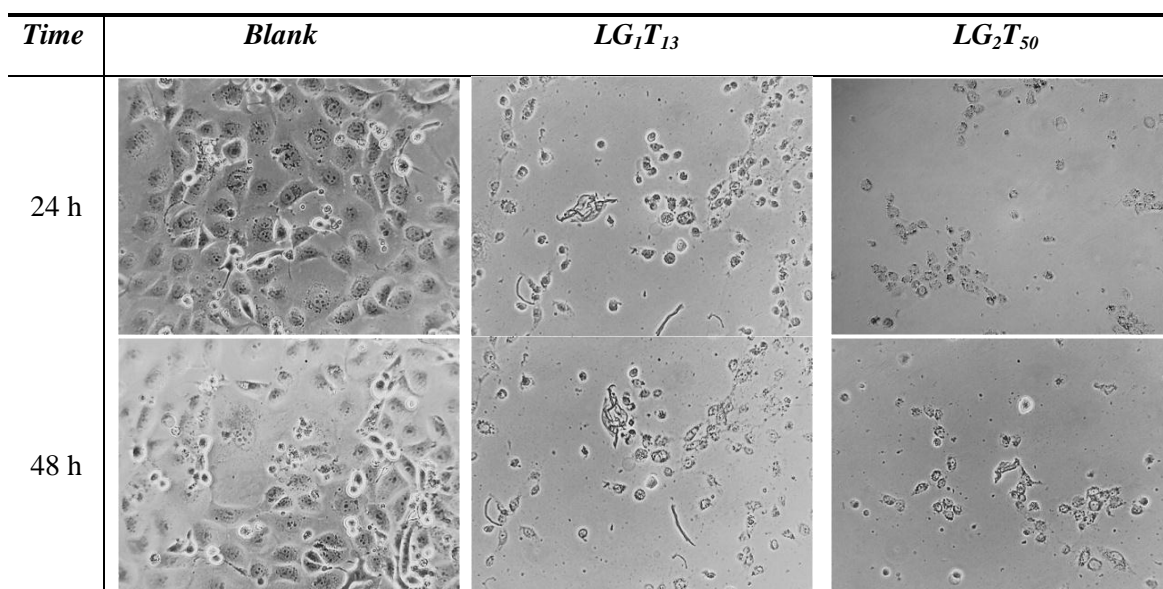


Table 5.4: Micrographs of wells containing PNT2A cells incubated with 30 $\mu\text{g}/\text{mL}$ concentration of F-3 samples G_1T_{13} and G_2T_{50} taken after 24 and 48 h. Compared to the blank, the micrographs of the treated cells depict a significantly more necrotic state, demonstrating the potential cytotoxic effect of the two samples at this concentration. (Magnification = 100X)

In order to confirm if the observed cytotoxic activity was due to melittin, two samples of melittin were also assessed using a similar approach. **Figure 5.4** showed that as the concentration of melittin in solution increased beyond 1.0 $\mu\text{g}/\text{mL}$, the percentage of viable cells began to fall drastically. The estimated MICs (as IC_{50} values) of the two melittin samples were 4.0 and 2.5 $\mu\text{g}/\text{mL}$ respectively. Complete cell death occurred at ≥ 10 $\mu\text{g}/\text{mL}$.

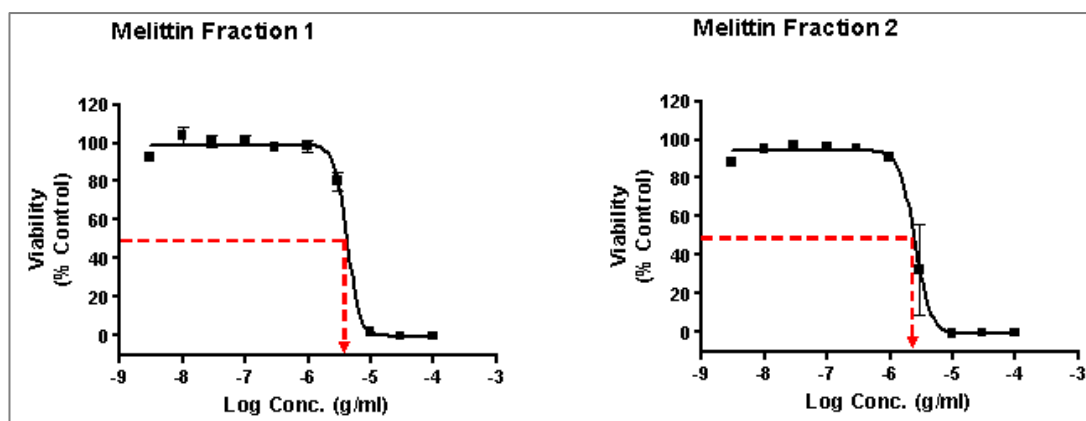


Figure 5.4: Action of melittin on PNT2A cells. The IC_{50} lies at log conc. of -5.4 for Melittin-1 and -5.6 for Melittin-2 giving IC_{50} values of 4.0 $\mu\text{g}/\text{mL}$ and 2.5 $\mu\text{g}/\text{mL}$ respectively.

The micrographs in **Figure 5.5** confirm the results obtained with the Alamar Blue® probe in the assay of Melittin-1. At 3 $\mu\text{g}/\text{mL}$ (panel D), there was a small decrease in the number of cells but at 10 $\mu\text{g}/\text{mL}$ and above (panels A-C), the cells displayed necrotic morphology.

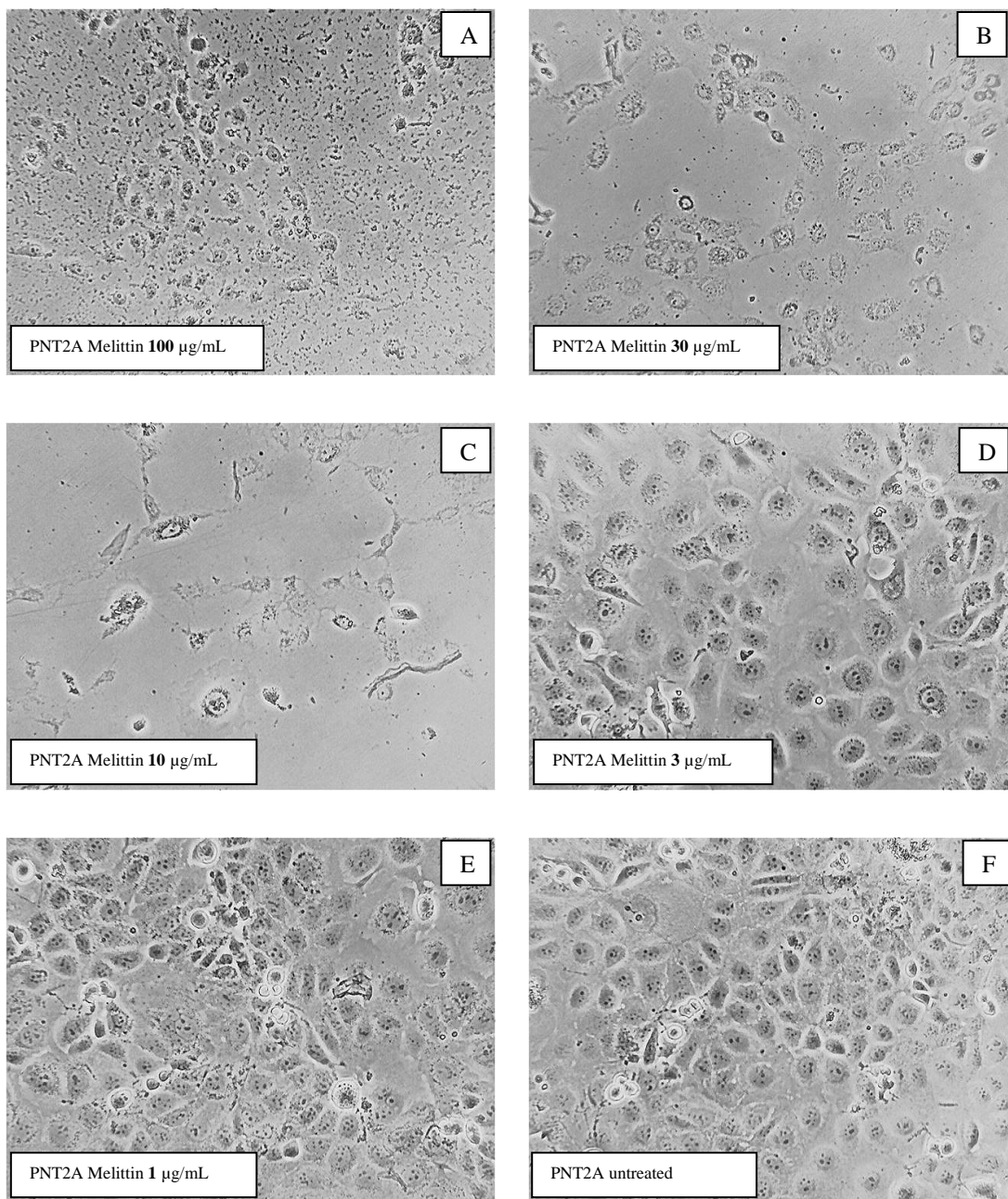


Figure 5.5: Micrographs showing the effect of Melittin-1 on PNT2A cells confirming the results obtained with the Alamar Blue® viability probe. At 3 $\mu\text{g}/\text{mL}$ there is a small change in the numbers of cells but at 10 $\mu\text{g}/\text{mL}$ and above the cells display necrotic morphology. (Magnification = 100X).

As was observed with Melittin-1, at the concentration of 3 $\mu\text{g/mL}$ of Melittin-2 (panel D), although there were reduced cell numbers, there were still some viable cells in accordance with the probe. At ≥ 10 $\mu\text{g/mL}$ concentrations (panels A-C), the cells were completely lysed (**Figure 5.6**).

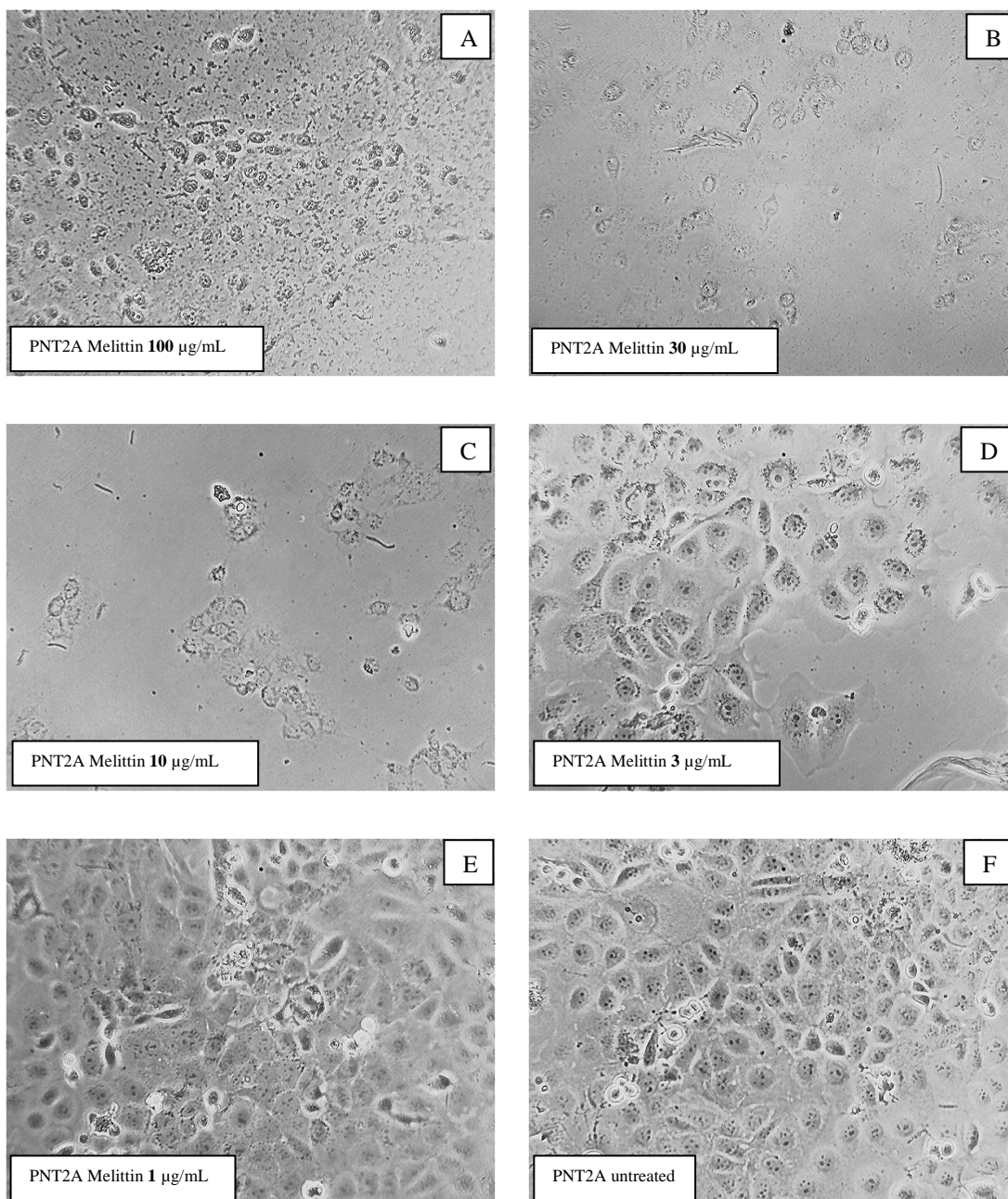


Figure 5.6: Micrographs showing the effect of Melittin-2 on PNT2A cells confirming the results obtained with the Alamar Blue® viability probe. At 3 $\mu\text{g/mL}$ there is a small change in the numbers of cells but at 10 $\mu\text{g/mL}$ and above the cells display necrotic morphology. (Magnification = 100X).

5.3.4.2 Effect of BV on NCTC2544 cell viability

The samples of F-3 fraction significantly affected the viability of the keratinocytes at concentrations of 10 and 30 $\mu\text{g}/\text{mL}$ as shown in **Figure 5.7**. It should be noted that these were the same samples that showed cytotoxic effects against the PNT2A (normal epithelial cells) and in which melittin was determined to be present from LC-MS analysis. The micrographs taken at 24 and 48 h confirmed the results obtained using the Alamar Blue® probe. In addition the micrographs taken at 5 min and 4 h demonstrated that necrosis of the cells caused by the “active” fractions was immediate.

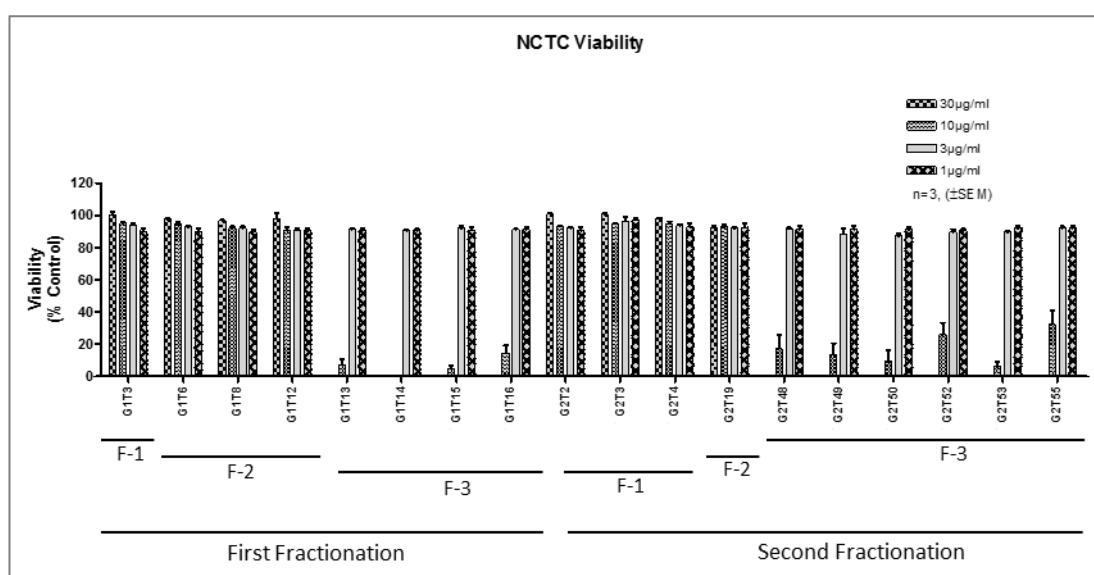


Figure 5.7: Effect of samples of BV fractions at 1, 3, 10 and 30 $\mu\text{g}/\text{mL}$ on normal human keratinocytes. The samples of F-3 can be seen to induce significant loss of cell viability at 10 and 30 $\mu\text{g}/\text{mL}$ concentrations. These are the fractions that contained melittin. Cell viability was measured as a ratio of the amount of fluorescence in test samples to that of the blank using the Alamar Blue® technique.

5.3.4.3 Effect of BV on HS27 cell viability

Fractions F-1 and F-2 did not show any loss of cell viability in the concentration range of 10 ng/mL to 100 $\mu\text{g}/\text{mL}$ (**Figure 5.8**) against fibroblasts. However, fractions F-3 and F-4 were potentially cytotoxic to the cells at concentrations of 30 and 100 $\mu\text{g}/\text{mL}$ respectively, due to the observed loss of cell viability and the appearance of cell death as observed in cell micrographs. The computed IC_{50} value for F-3 was 14.8

$\mu\text{g/mL}$ while that of F-4 was $89.0 \mu\text{g/mL}$. Micrographs taken after 24 h confirmed the results of the Alamar Blue® assay (**Figure 5.9**).

The HS27 cells are the principal cells for promoting skin regeneration by producing collagen, elastin and ECM. Skin regeneration/rejuvenation would be a desirable attribute of a product based on BV as it would increase potential for skin repair. Although skin cell proliferation & angiogenesis assays were not performed on these fractions, cytotoxic activity would be an unwelcome characteristic. Nevertheless these results show that melittin is not as toxic to HS27 cells as it is to PNT2A & NCTC2544 cell lines and, at concentrations of 5-40 ppm expected to be present in cosmetic formulations (Chapter **Error! Reference source not found.**), is potentially safe to HS27 cells of the skin.

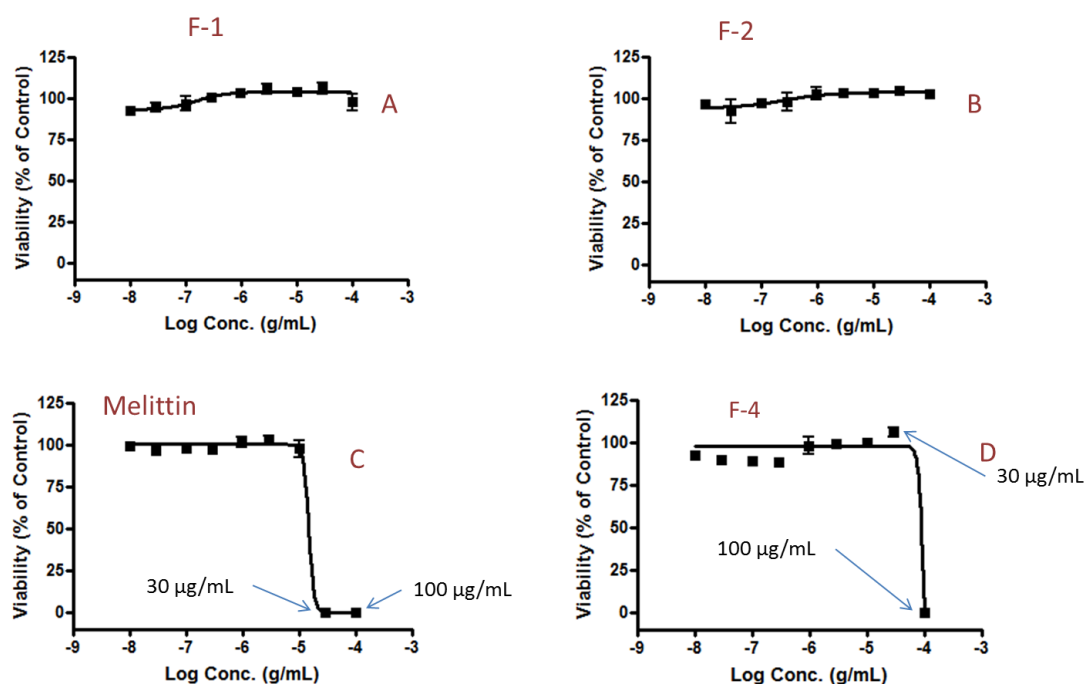


Figure 5.8: Graphs of viability of HS27 cells against log of concentration in g/mL. Fractions F-1 and F-2 had an $\text{IC}_{50} > 100 \mu\text{g/mL}$ while fraction F-3 which contained melittin was the most cytotoxic with IC_{50} of $14.8 \mu\text{g/mL}$. Manual estimate of fraction F-4 gave an IC_{50} value of $89.0 \mu\text{g/mL}$.

It was surprising to note that PLA_2 was nontoxic to the cells even at $100 \mu\text{g/mL}$. This observation might have been due to its separation from melittin with which it acts synergistically. Another possibility might arise from possible loss of the 3D structure

of PLA₂ during its fractionation in a solvent mixture containing 20% acetonitrile. An enzyme activity test, had it been performed, would have helped to confirm the latter.

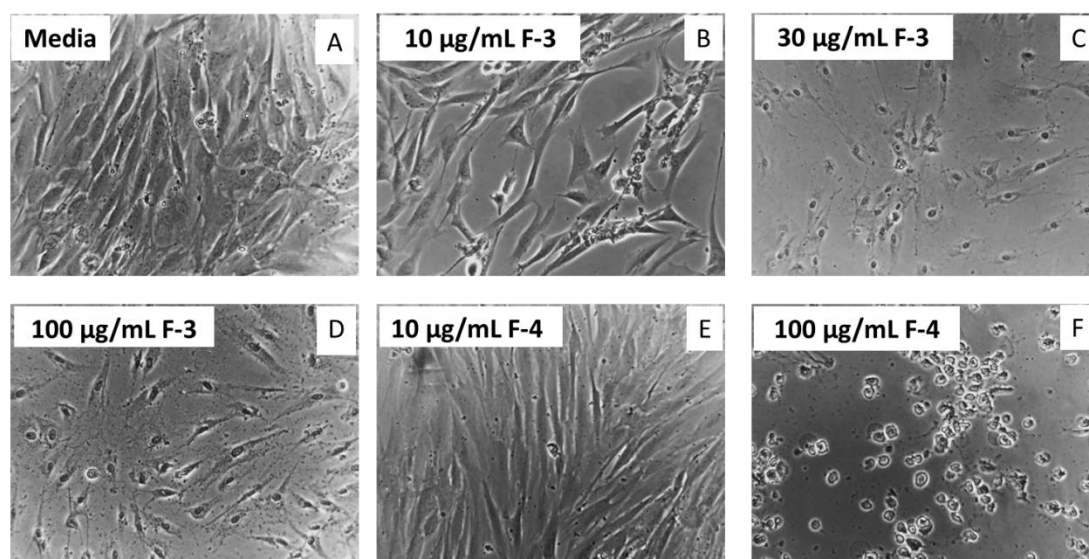


Figure 5.9: Micrographs of the HS27 cells after 24 h showing the effects of fractions F-3 and F-4 at different concentrations. With F-3, necrosis can be observed at concentration of 30 µg/mL and above while in F-4, necrosis was only observed at 100 µg/mL. (Magnification = 10X).

5.3.5 *TNF- α -induced NF- κ B inhibition assay*

Significant inhibition of TNF- α -induced NF- κ B was demonstrated only by F-3 samples at both 10 and 30 µg/mL concentrations as shown in **Figure 5.10**. Sample G₁T₁₂ of F-2 also showed significant inhibition at 30 µg/mL (~10% of control) but not at 10 µg/mL. As already mentioned in section 5.3.4 above, the “active” samples also demonstrated reduced cell viability against PNT2A and NCTC2544 cells. Therefore, in view of their demonstrated cytotoxic effects, especially those against the NCTC2544 cell line used in the anti-inflammatory screening, the observed anti-inflammatory effects might not be “real” but an effect of the cells being necrotic. However, given that other authors (Park *et al.*, 2004; Park *et al.*, 2007) have documented anti-inflammatory effects of BV which underlie its traditional use as an antiarthritic agent (Chen and Lariviere, 2010), there is a possibility that the same cytotoxic fractions also possess anti-inflammatory effects.

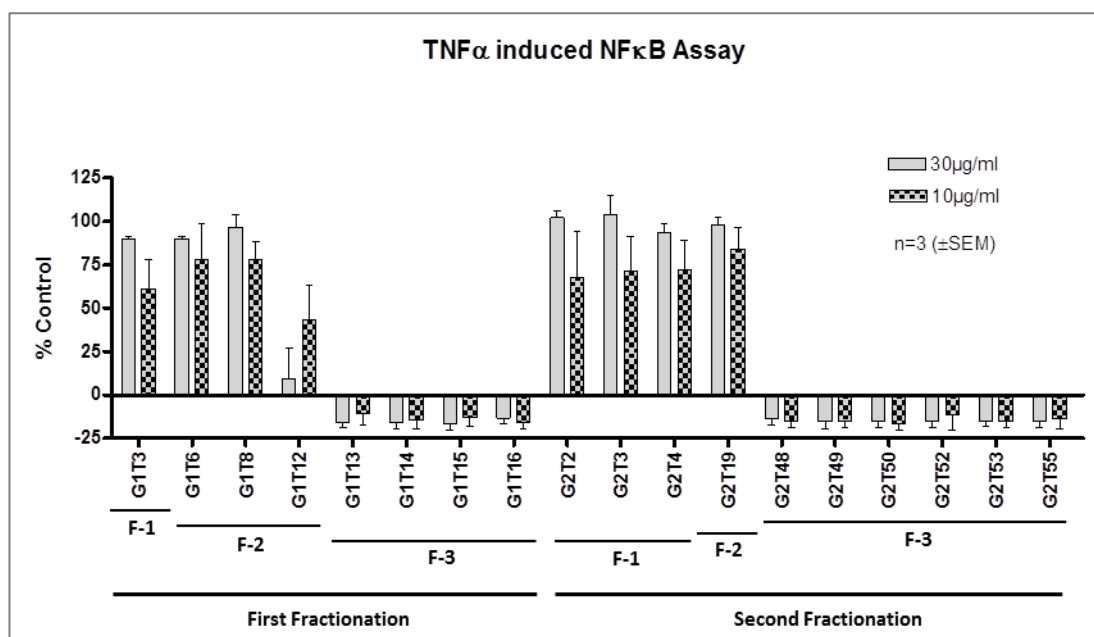


Figure 5.10: Inhibitory effect of aqueous BV on TNF- α -induced NF- κ B in NCTC2544 cells at 10 and 30 μ g/mL concentrations, expressed as % of TNF- α control. The samples of F-3 caused total inhibition at both concentrations. The active fractions contained melittin. Whereas the observed inhibition of NF- κ B in the cells might suggest that F-3 possesses potential anti-inflammatory activity, the results could be an outcome of cell necrosis induced by this fraction as evidenced by its toxicity at the concentrations used (discussed in section 5.3.4.2).

5.4 Discussion

When cells are exposed to a toxic compound, they can respond by undergoing necrosis (loss of cell membrane resulting in rapid cell death) or they may follow another pathway of cell death known as apoptosis (a slow and programmed form of cell death) (Nikoletopoulou *et al.*, 2013). Each of these forms of cell death occurs if the insult imposed on the cells is lethal, and this is termed cytotoxicity. However, cells exposed to sublethal insults may simply stop actively dividing/growing, leading to loss of cell proliferation and reduced viability. Cell viability may be determined through measurement of redox potentials, assessment of membrane integrity, and investigation of cellular enzymes such as esterases (Riss *et al.*, 2011). Whereas loss of cell viability is not necessarily an indication of cytotoxicity, in this experiment additional data with cell micrographs suggested that cell death occurred in those fractions in which cells lost their viability. For this reason, observations of reduced cell

viability have been interpreted as suggesting that the responsible fractions induced cell cytotoxicity.

The traditional Alamar Blue® assay was employed for the antimicrobial and cytotoxicity tests in 96-microwell plates. Commercially available Alamar Blue® dye is a redox indicator containing a blue pigment, resazurin, which is added to the assay plate at a level of 10-20% (v/v) per well. Metabolically active cells produce an oxygen-depleted, NADH-enriched, reducing environment that leads to the conversion of resazurin to resorufin, a pink pigment which yields fluorescent emission at 590 nm after excitation at 560 nm (Rampersad, 2012). Microwells in which the incubated cells have lost their ability to metabolise, whether through necrosis, apoptosis or other modes of cell death, produce no colour change and remain blue, thus yielding only background fluorescence readings.

The cell viability assays showed that the melittin-containing samples (F-3) were very cytotoxic against both “normal” keratinocytes and epithelial cells whereas sample G₁T₁₂ of F-2 which contained trace concentrations of melittin, only showed potential cytotoxic activity against normal epithelial cells. Since the IC₅₀ values obtained for melittin on PNT2A were estimated at 2.5-4.0 µg/mL, any formulations of BV for human application should be below this range in order to maintain safety and avoid toxic effects melittin which is the main component. The results obtained using the Alamar Blue® probe were confirmed from the micrographs taken during the incubation period. The micrographs taken at 5 min and 4 h demonstrated that melittin-induced cell necrosis in keratinocytes was immediate. It should be noted that the observed toxicity of melittin towards HS27 cells (IC₅₀ = 14.8 µg/mL) was less compared to PNT2A cells.

The anti-inflammatory assay on TNF- α -induced NF- κ B in NCTC2544 cells showed activity only in melittin-containing samples. Given that these samples also showed potential cytotoxicity at the concentrations evaluated for anti-inflammatory activity, it was not possible to rule out the observed effects as being due to cells becoming necrotic. Anti-inflammatory effects have been reported previously for BV and melit-

tin at concentrations in the range of 0.5-2.0 µg/mL in murine cell lines, where its inhibitory effects on LPS-induced inflammation were reported (Moon *et al.*, 2007; Srivastava *et al.*, 2012). However, it should be noted that many components of BV are inducers of inflammation, including histamine (Park *et al.*, 2014), mast cell degranulating peptide (MCDP) (Buku, 1999; Buku *et al.*, 2005), and apamin (Regnier-Vigouroux *et al.*, 1988). In addition, a study by Stuhlmeier (2007) suggested that neither BV nor melittin blocked IL-1 β -induced activation of NF- κ B but led to significant increase in mRNA levels of several pro-inflammatory genes in fibroblast-like synoviocytes, dermal fibroblasts and mononuclear cells (Stuhlmeier, 2007). In fact, as reported in Chapter 8, melittin and other fractions of BV demonstrated synergistic effects with LPS in inducing cytokine release in phorbol-12-myristate-13-acetate (PMA) stimulated U937 cells. Thus in view of these facts, caution is required during interpretation of BV or melittin's anti-inflammatory data. The α -glucosidase inhibition test was negative for all the fractions at the 30 µg/mL concentration used in the assay system, suggesting that there was no significant antiviral activity at this concentration.

From the antibacterial tests, it was observed that BV fractions did not significantly inhibit *Mycobacterium marinum* (MIC >100 µg/mL) but melittin-containing fractions showed sufficient inhibitory effect on *Norcardia farcinia* with MICs of 25-50 µg/mL. The latter fractions showed relatively high activity against *Trypanosoma brucei* with MIC values of 0.78-1.56 µg/mL. The activity against *T. brucei* was particularly interesting since melittin's cytotoxicity levels, although only determined in human cells lines, were well above the MIC range for *T. brucei*. *Trypanosome brucei brucei* is the cause of African trypanosomiasis in cattle and is transmitted by tsetse flies (Hajduk *et al.*, 1989). Although there are human infective subspecies of *Trypanosoma brucei* (i.e. *T.b. gambiense* and *T.b.rhodesiense*), the *T.b.brucei* does not infect humans because of the presence of trypanosome lytic factors (TLFs) in the human innate defence system (Stephens *et al.*, 2012). Thus it would be necessary to assess the efficacy of melittin in human infective forms or its cytotoxicity in bovine cells in order to determine its potential as a treatment alternative for African trypanosomiasis in humans or cattle, respectively.

Mycobacteria possess a cell wall that is generally more intricate than that of both Gram positive and Gram negative bacteria, of which the genus is neither. The cell wall consists of a hydrophobic layer of mycolic acids and a peptidoglycan layer bound by a polysaccharide, arabinogalactan (Bhamidi et al., 2009). This cell wall structure is largely responsible for the hardness of the genus, which makes Mycobacterial infections difficult to treat with conventional antibiotics such as penicillins, to which these pathogens are naturally resistant. The unique cell wall structure and composition make these bacteria able to survive harsh conditions such as exposure to antibiotics, alkalis, acids, detergents, and lysis by complement. Although most of the species are rather susceptible to clarithromycin and rifamycin (Forsgren, 1993; Aubry et al., 2000), resistant strains have also emerged. *Mycobacterium marinum* is a non-tuberculous mycobacterium with worldwide prevalence found in non-chlorinated water. It is the most common atypical Mycobacterium that causes opportunistic cutaneous infections in humans (Rallis and Koumantaki-Mathioudaki, 2007). As with other mycobacteria, this species is multidrug resistant. Interference with the biosynthetic pathways of the cell wall components has emerged as a potential target for novel anti-Mycobacterial drugs. (Bhamidi et al., 2009).

Given the membrane activity of melittin, the observed differences in the activity against different bacteria and against protozoa suggest that melittin may be interacting differently with the microbes' cell envelopes. This implies that the low activity against *Mycobacterium marinum* may be related to the fact that this microorganism has a complex protective layer (Cantrell *et al.*, 2013; Esin *et al.*, 2013) which remains stable even after the cells have been treated with melittin.

Chapter Six

Investigation of the Stability and Biochemical Activity of Bee Venom

6 Investigation of Stability and Biochemical Activity of Bee Venom

6.1 Introduction

The behaviour of BV in aqueous solutions has been widely reported in literature, including the ability of melittin to form tetramers at high ionic strength (Anderson *et al.*, 1980; Terwilliger and Eisenberg, 1982). However, in this work, it was necessary to investigate the solution stability of melittin in order to determine the most appropriate storage conditions and lifetimes of analytical sample solutions. In addition, given the high content of water in most gels and creams, and the potential liability of peptides and proteins to aqueous hydrolysis, it was deemed fit to focus this investigation on aqueous solutions. To this end, different experiments were carried out by LC-MS on whole BV and melittin. The aqueous stability was evaluated at different storage temperatures. In addition, susceptibility of melittin towards selected proteases was also tested. Finally, the utility of three different enzyme inhibitors for blocking the spontaneous degradation of melittin was also evaluated.

6.2 Materials and methods

6.2.1 Protease enzymes

The degradation profile of melittin was investigated using the proteases: subtilisin A, proteinase K, trypsin and dipeptidylpeptidase IV (DPP_{IV}). Subtilisin A is a serine protease which belongs to the S8 endoproteinase family. It hydrolyzes native and denatured proteins under alkaline conditions. DPP_{IV} is a post-proline dipeptidyl aminopeptidase and to a lesser extent a post-alaninyl dipeptidyl aminopeptidase (Kreil *et al.*, 1980; Matteucci and Giampietro, 2009). The enzymes were all obtained from Sigma-Aldrich (Dorset, UK).

6.2.2 *Protease inhibitors*

Two protease inhibitors [P32/98 for DDP_{IV} and PMSF (phenyl methane sulfonyl fluoride)] were investigated for their inhibition of melittin degradation in BV solution. The enzyme inhibitors were both obtained from Sigma-Aldrich (Dorset, UK).

6.2.3 *Melittin auto-degradation in BV*

Two batches of filtered BV and melittin were separately prepared at a concentration of 0.1 mg/mL in de-ionised water. They were then aliquoted into capped HPLC vials each containing 1.5 mL of solution. These were stored in duplicates at four different conditions: laboratory bench at room temperature (RT), laboratory window exposed to direct sunlight at RT, fridge at 2°C and freezer at -20°C. Then at intervals of 3 days these samples were analysed on the Orbitrap Exactive using a previously described method (section 3.6). The resulting chromatograms were then analysed for time-dependent variation over a period of 3 months when the original signals almost disappeared. The main degradation products were observed by looking for newly emerging peaks on the chromatograms. These degradants were then identified based on their MWs and mass spectra. The resulting information was analysed to determine the sites of degradation of the original melittin molecule, leading to elucidation of the possible class of enzymes involved.

6.2.4 *Enzymatic degradation of melittin*

Four commercially available proteases subtilisin A, proteinase K, dipeptidyl peptidase IV (DPP_{IV}) and trypsin; and two inhibitors P32/98 and PMSF were treated with melittin and BV samples respectively. The enzymes were used to determine which of them produced the same pattern of degradation on melittin as that observed in aqueous BV solutions. On the other hand, the inhibitors were employed to check which of them could inhibit the observed autolysis of melittin in the whole venom solution.

For this study, solutions of BV and melittin were prepared at a nominal concentration of 0.1 mg/mL in 10mM ammonium bicarbonate (NH₄HCO₃) buffer at pH 8.0. Then each was separately aliquoted into eight 1-mL portions in 2 mL Eppendorf

tubes. 10 μL portions of enzyme and inhibitor solutions were then added to the melittin and BV aliquots respectively according to **Table 6.1**, before incubation at 37°C for 24 h.

Table 6.1: Investigation of melittin-degrading enzyme activity in BV.

<i>Aliquot</i>	<i>1</i>	<i>2</i>	<i>3</i>	<i>4</i>	<i>5</i>
Melittin	Buffer	Subtilisin A	Proteinase K	Trypsin	DPP _{IV}
BV	Water	PMSF	PMSF	P32/98	P32/98

After the incubation, the solutions were transferred into HPLC auto sampler vials containing 500 μL of acetonitrile to deactivate enzyme activity. The samples were then run on the LC-MS system (Orbitrap Exactive) using a previously described method (section 3.6).

6.3 Results

6.3.1 Spontaneous degradation of melittin in BV solution

The aqueous solutions of BV showed gradual temperature-dependent degradation of the melittin component over time during storage at ambient temperatures (**Figure 6.1**). Microbiological evaluation of the solutions ruled out any microbial contamination of the sample.

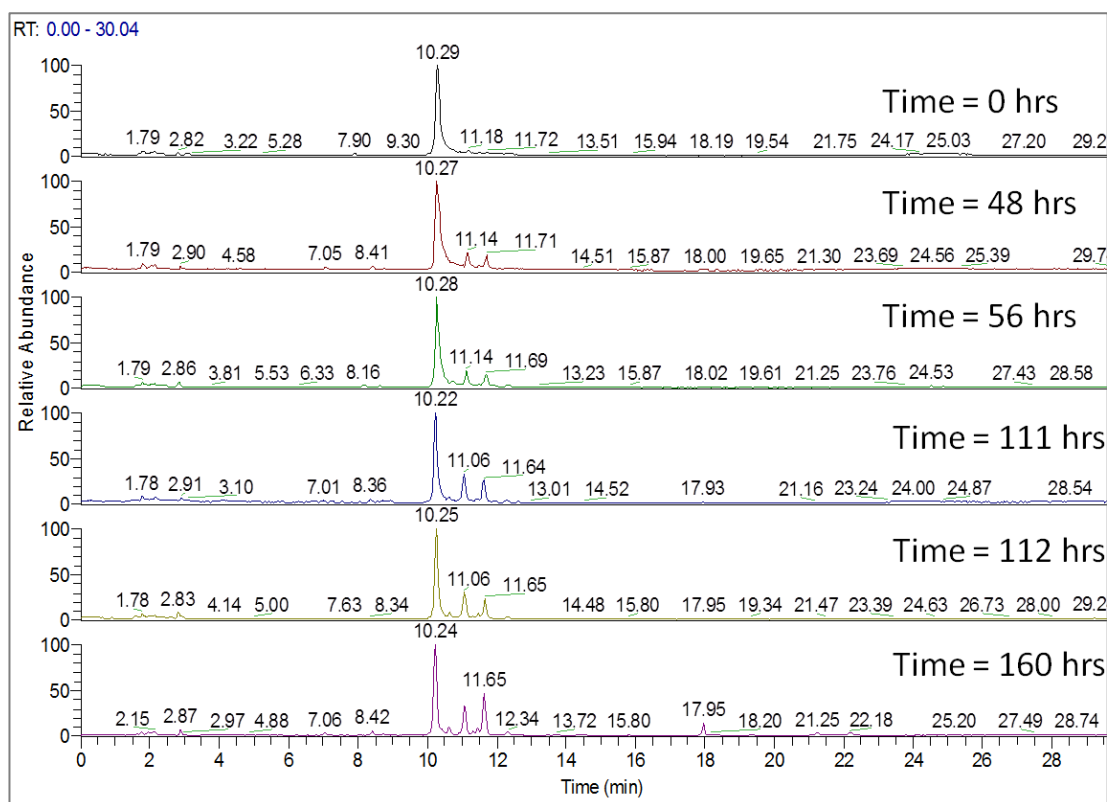


Figure 6.1: Time-dependent degradation of melittin in a solution of BV from 0 – 160 hours. The sample of whole BV was prepared at 0.1 mg/mL and stored at room temperature. Aliquots were taken at different time intervals and analysed. The analysis was performed in positive ion LC-ESI-MS on the Orbitrap mass spectrometer with an ACE 3 C18 column using mobile phases 0.1% formic acid in water (A) and 0.1% formic acid in acetonitrile (B) at a gradient of 10-70% (0-15 min), 70% (15-20 min), 70-10% (20-25 min) and 10% (25-30 min) relative to solvent B, and at a flow rate of 0.3 mL/min (as described in section 3.6.2).

The rate of melittin degradation was estimated by assuming first order kinetics (equation 16) as follows:

$$\frac{dA}{dt} \propto A, \text{ implying that } \frac{dA}{dt} = -\lambda A. \text{ Rearrangement gives: } \frac{dA}{A} = -\lambda dt.$$

$$\text{After integration, } \ln A = \ln A_0 - \lambda t \quad (16)$$

where: A if the peak area of melittin, $\frac{dA}{dt}$ is the degradation rate, λ is decay constant, \ln is natural logarithm (\log_e), A_0 is the peak area at time, $t = 0$, and t is the duration of degradation.

The plot of $\ln A$ against t was approximately linear with a slope of -0.002635 h^{-1} and intercept on the $\ln A$ axis of 19.66 (**Figure 6.2**).

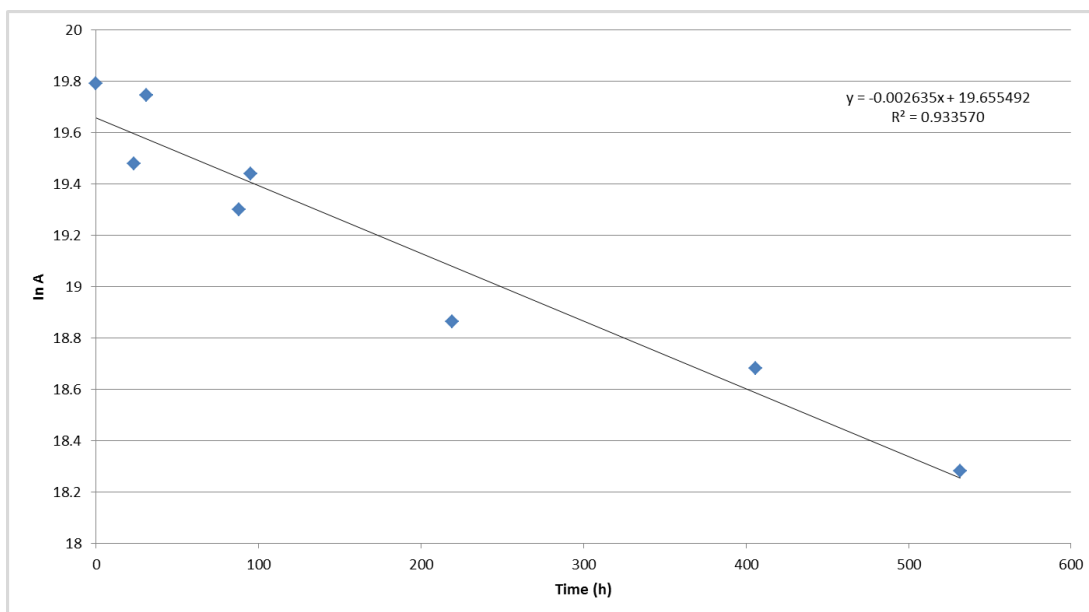


Figure 6.2: Plot of $\ln A$ versus time (in hrs) to estimate the rate of melittin degradation in solution at ambient temperatures. The plot is approximately linear with R^2 of 0.934 and intercept of the $\ln A$ axis of 19.66.

The decay constant, λ , given by $\lambda = -\text{slope}$ was thus $2.635 \times 10^{-3} \text{ h}^{-1}$ while half-life ($t_{1/2}$) and $t_{0.9}$ of melittin (in h) were estimated to be 263 and 40 (equation 17) respectively, as follows:

$$t_{\frac{1}{2}} = \frac{\ln 2}{\lambda} = \frac{0.693}{2.635} \times 1000 = 263 \text{ h} \quad (17)$$

$$t_{0.9} = \frac{\ln(1.1)}{\lambda} = \frac{0.1054}{2.635} \times 1000 = 40 \text{ h}$$

The degradation of melittin appeared to occur within the ^{21}Lys - ^{22}Arg - ^{23}Lys - ^{24}Arg region of its amino acid sequence (**Figure 6.3**).

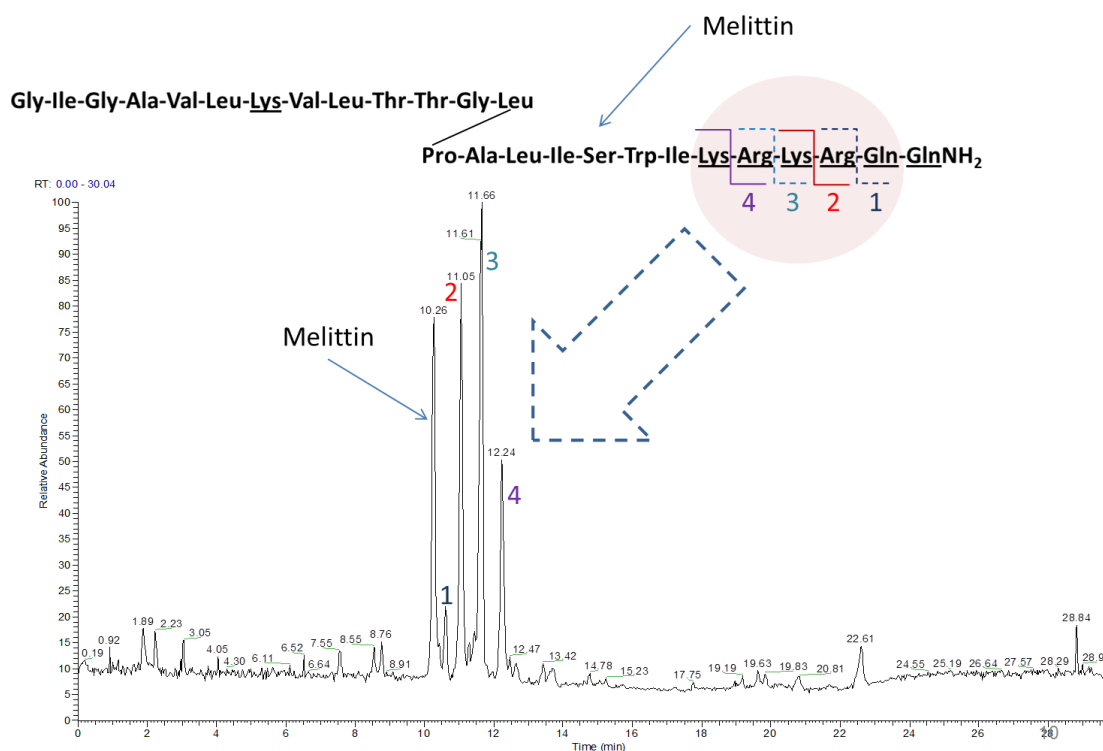


Figure 6.3: Chromatogram of BV showing the peaks of the main fragments of melittin after 40 days of storage at room temperature (25°C). The sample of whole BV was prepared at 0.1 mg/mL and stored at room temperature. An aliquot was taken at after 40 days and analysed. The analysis was performed in positive ion LC-ESI-MS on the Orbitrap mass spectrometer with an ACE 3 C18 column using mobile phases 0.1% formic acid in water (A) and 0.1% formic acid in acetonitrile (B) at a gradient of 10-70% (0-15 min), 70% (15-20 min), 70-10% (20-25 min) and 10% (25-30 min) relative to solvent B, and at a flow rate of 0.3 mL/min (as described in section 3.6.2).

The products of this degradation were identified based on their molecular weights calculated from their accurate masses. Product 1 (*pI*) gave a molecular weight of 2590.66 Da which corresponded to the loss of the two carboxyl-terminal glutamine residues along with the terminal amide group (**Figure 6.4**). This assignment was based on the fact that loss of ^{25}Q - ^{26}Q -NH₂ from melittin theoretically leaves a fragment of molecular weight 2591.17Da based on amino acid sequence, assuming there is OH transfer from water to the terminal carboxyl group of the remaining fragment (hydrolysis reaction) to form a free acid, with the remaining proton from water accompanying the departing group. Based on the amino acid sequence, the molecular weight of melittin is 2846.44.

The degradant was multiply charged (maximum positive charge = 6, similar to melittin) since the bond cleavage to form *p1* occurs before any of the positively charged amino acid residues in melittin (K and R). Thus the mass spectrum of *p1* contains ions (*m/z* scan range 100-2000) of 519.13 (+5), 648.66 (+4), 864.55 (+3), and 1296.82 (+2). The +1-charged ion is expected to be the 2591.17 molecular ion which does not appear in the mass spectrum since it is above the scan range used. In any case such a molecular ion would be very low in intensity since under the conditions of the experiment, the peptide is largely ionised on all its basic amino groups.

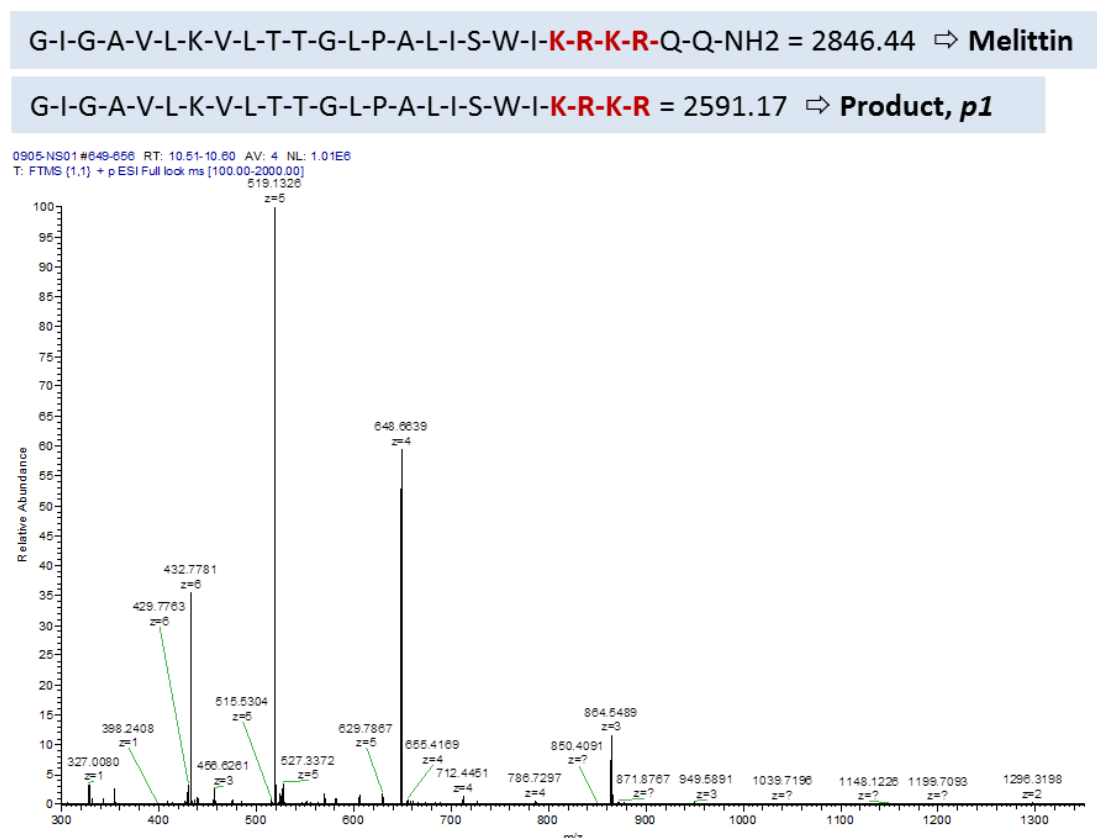


Figure 6.4: Possible site of degradation of melittin to yield *p1*. The molecular weight calculated from accurate mass of the multiply charged melittin fragment is 2590.66 which is close to the theoretical value (2591.17) corresponding to loss of terminal QQNH₂ group from melittin.

The second degradant (*p2*) corresponded to loss of an additional amino acid (arginine) from the carboxyl terminal of *p1* (**Figure 6.5**). The *p2* fragment has a molecular weight of 2434.55 Da based on accurate mass measurement. This value corresponds to the theoretical molecular weight of 2434.99 Da based on the amino acid

sequence in the peptide. In fact, the molecular weight difference between *p1* and *p2* (156.11 Da) corresponds to the molecular weight of arginine (174.2 Da) less water (18.02 Da). The mass spectrum of *p2* shows that it is charged at 5 sites rather than 6 of *p1* due to loss of the basic arginine residue.

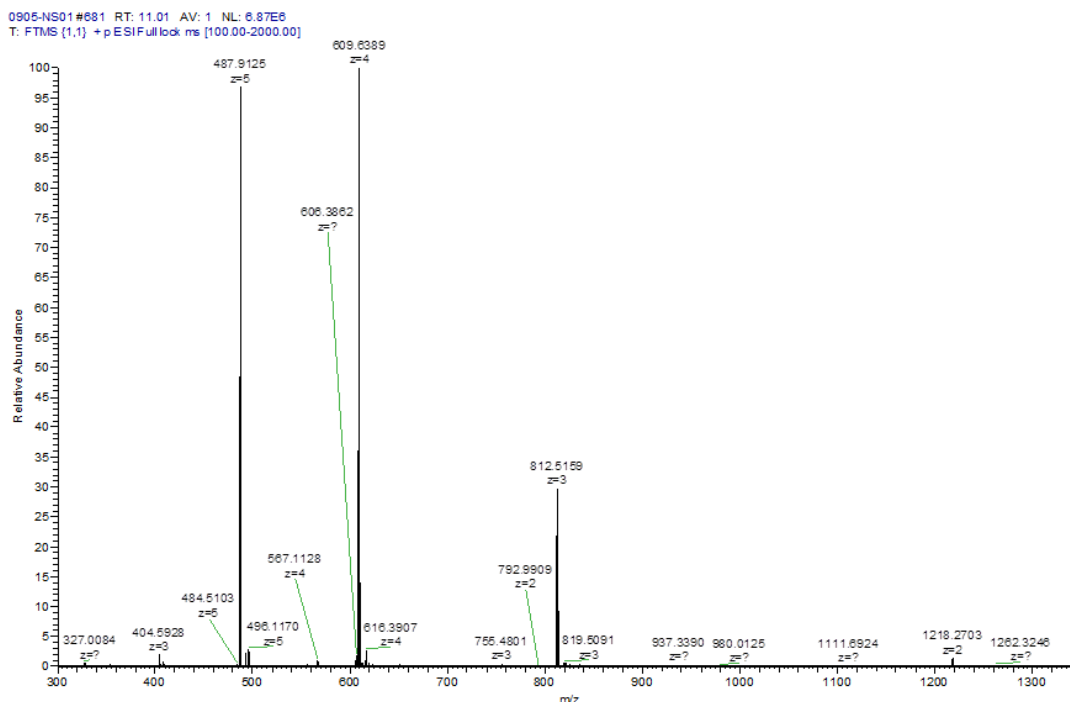
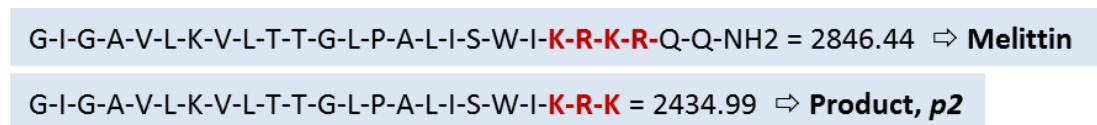
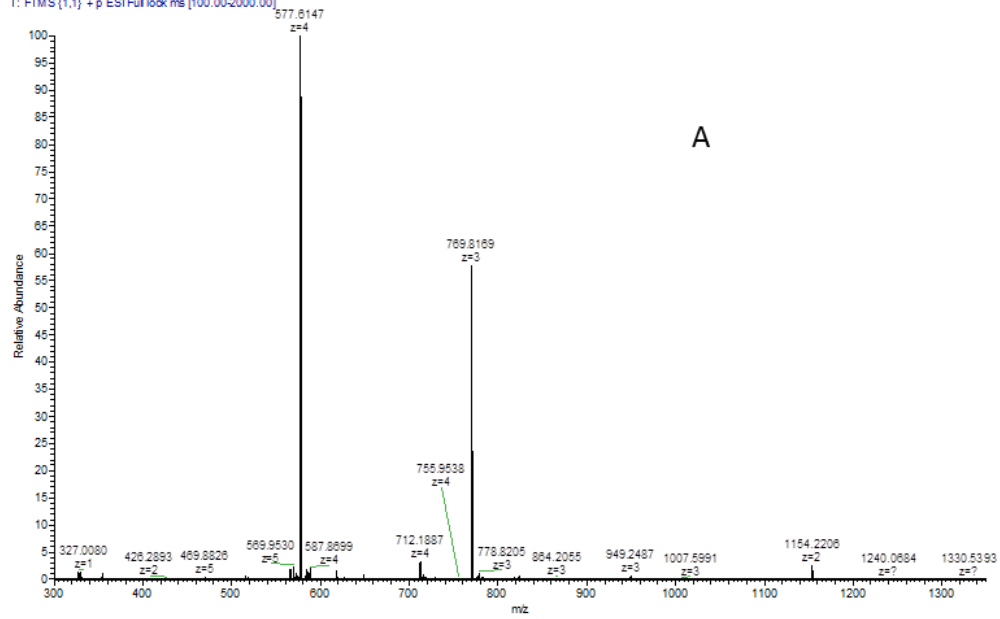


Figure 6.5: Possible site of degradation of melittin to yield *p2*. The MW difference between *p1* and *p2* (156.11 Da) corresponds to the molecular weight of arginine (174.2 Da) less water (18.02 Da).

Following the same reasoning, *p3* (MW 2306.45) and *p4* (MW 2150.35) were determined to correspond to sequential losses of carboxyl-terminal K and R residues from *p2* and *p3* respectively (**Figure 6.6**). Because both the K and R residues are positively charged, their loss means that *p3* carries a maximum of four charges while *p4* carries 3; the latter due to two lysine residues—the only remaining amino acids with positively charged side-chains—and the N-terminal amino group on glycine.

G-I-G-A-V-L-K-V-L-T-T-G-L-P-A-L-I-S-W-I-K-R = 2306.82 ⇨ Product, *p3*

0905-NS01#705-729 RT: 11.38-11.73 AV: 13 NL: 2.41E9
T: FTMS (1,1) + p ESI Full lock ms [100.00-2000.00]



G-I-G-A-V-L-K-V-L-T-T-G-L-P-A-L-I-S-W-I-K = 2150.64 ⇨ Product, *p4*

0905-NS01#766 RT: 12.20 AV: 1 NL: 9.84E5
T: FTMS (1,1) + p ESI Full lock ms [100.00-2000.00]

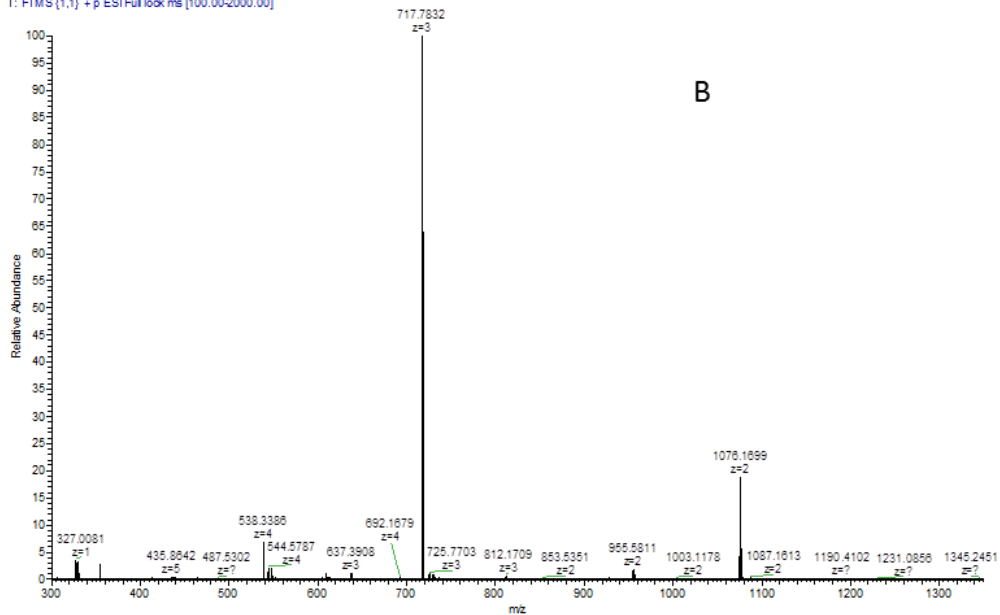


Figure 6.6: Possible sites of degradation of melittin to yield *p3* and *p4*. While *p3* has a maximum charge of 4, *p4* has a maximum of 3 due to the extra loss of lysine from the carboxyl terminal. The final charge on *p4* is due to the two lysine residues located at y^7 and y^{21} and the N-terminal amine on glycine.

Table 6.2 summarises the major products of melittin degradation with their accurate and theoretical masses, the latter being calculated based on amino acid sequences.

Table 6.2: Summary of interpretation of the degradation of melittin.

<i>Amino acid sequence</i>	<i>MW (Da)</i>			<i>Fragment</i>
	<i>MS*</i>	<i>AA**</i>	Δ	
G-I-G-A-V-L-K-V-L-T-T-G-L-P-A-L-I-S-W-I-K-R-K-R-Q-Q-NH ₂	2845.80	2846.44	0.64	Melittin
G-I-G-A-V-L-K-V-L-T-T-G-L-P-A-L-I-S-W-I-K-R-K-R	2590.66	2591.17	0.51	<i>p1</i>
G-I-G-A-V-L-K-V-L-T-T-G-L-P-A-L-I-S-W-I-K-R-K	2434.55	2434.99	0.44	<i>p2</i>
G-I-G-A-V-L-K-V-L-T-T-G-L-P-A-L-I-S-W-I-K-R	2306.45	2306.82	0.37	<i>p3</i>
G-I-G-A-V-L-K-V-L-T-T-G-L-P-A-L-I-S-W-I-K	2150.35	2150.64	0.29	<i>p4</i>
* As determined on the Orbitrap Exactive MS	** Calculated from amino acid sequence			

Note: The most intense signals were due to fragments p2 and p3 of MWs 2434 and 2306 Da respectively.

6.3.2 Effect of storage temperature

The degradation of melittin during storage occurred only in solutions of whole BV rather than those of the melittin fraction (**Figure 6.7**). This implied that during the purification process, when melittin was separated from the rest of the venom, the enzyme responsible for this degradation was either also removed from the melittin or irreversibly denatured.

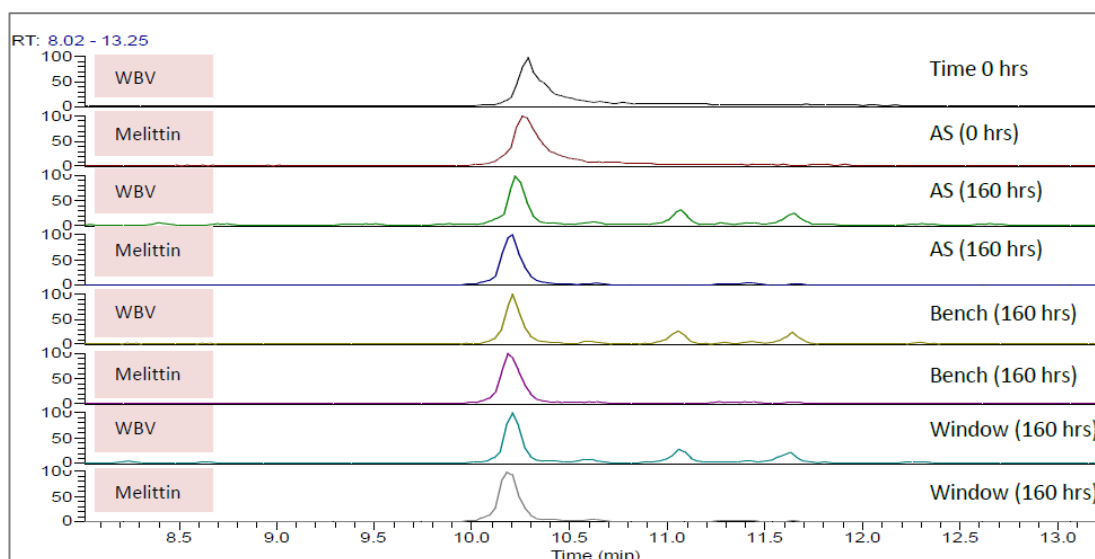


Figure 6.7: Effect of storage conditions on melittin stability. WBV is filtered whole BV; AS represents samples residing in the LC-MS auto-sampler. The samples of whole BV and melittin were prepared at 0.1 mg/mL and stored at different conditions of temperature. Aliquots were taken at different time intervals and analysed. The analysis was performed in positive ion LC-ESI-MS on the Orbitrap mass spectrometer with an ACE 3 C18 column using mobile phases 0.1% formic acid in water (A) and 0.1% formic acid in acetonitrile (B) at a gradient of 10-70% (0-15 min), 70% (15-20 min), 70-10% (20-25 min) and 10% (25-30 min) relative to solvent B, and at a flow rate of 0.3 mL/min (as described in section 3.6.2).

At the same time this spontaneous degradation activity was significantly lower at 4°C, compared to room temperature, providing further evidence that the degradation was probably enzyme mediated (**Figure 6.8**).

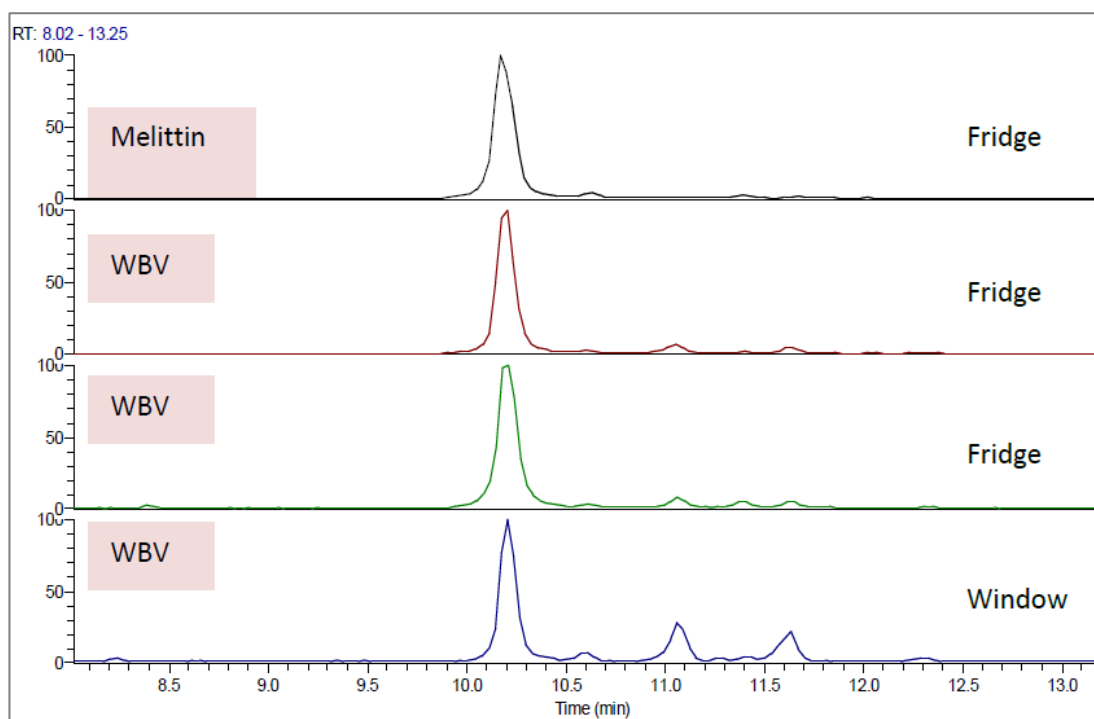


Figure 6.8: Effect of storage on melittin degradation. Samples analyzed after 7 days from date of preparation. WBV stands for filtered whole BV. Three samples of whole BV and a control melittin sample were prepared at 0.1 mg/mL and stored at different conditions of temperature. Aliquots were taken at different time intervals and analysed. The analysis was performed in positive ion LC-ESI-MS on the Orbitrap mass spectrometer with an ACE 3 C18 column using mobile phases 0.1% formic acid in water (A) and 0.1% formic acid in acetonitrile (B) at a gradient of 10-70% (0-15 min), 70% (15-20 min), 70-10% (20-25 min) and 10% (25-30 min) relative to solvent B, and at a flow rate of 0.3 mL/min (as described in section 3.6.2).

6.3.3 Effect of added proteolytic enzymes

Given that the rate of degradation of melittin was significantly higher in the whole venom than in the purified melittin fraction, and that it was slower at low temperatures, the instability was linked to a proteolytic enzyme activity in the venom that could have been removed during the fractionation process. To characterise this activity further, a selection of four proteases namely: subtilisin A, proteinase K, DPP_{IV} and trypsin were spiked into the melittin and BV samples respectively, and incubated. The enzymes selected represented both the specific protease activity (trypsin), as well as non-specific/broad protease action (proteinase K/subtilisin A) respectively. On the other hand, although there was no evidence of N-terminal shortening resembling DPP_{IV}-like activity (**Table 6.2**), the latter was included to rule out any intrinsic

BV DPP_{IV} activity. These four proteases were then used to determine if any of them caused a similar pattern of degradation of melittin.

Consequently, melittin degradation was observed with subtilisin A, proteinase K, and trypsin enzymes. The subtilisin A produced a much slower degradation rate compared to the other two (**Figure 6.9**). The chromatogram of the sample spiked with DPP_{IV} did not give noticeable differences compared to that of the melittin blank, indicating no activity. None of the former three enzymes produced a degradation pattern of melittin similar to the one observed spontaneously in the crude venom. This suggests that the likely enzyme(s) involved may be different from the ones tested in this experiment.

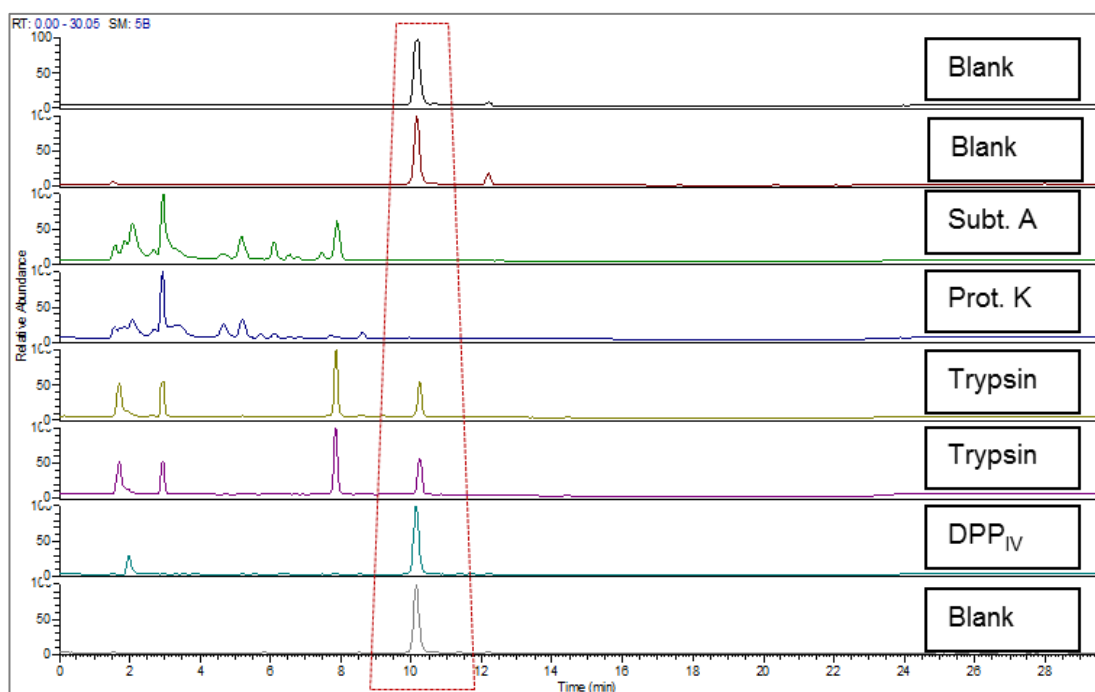


Figure 6.9: Chromatogram for melittin spiked with different proteolytic enzymes. The melittin peaks are highlighted by the red box. The samples of melittin were prepared at 0.1 mg/mL and incubated with different proteases at 30°C for 24 h. The samples were then treated with acetonitrile and analysed in positive ion LC-ESI-MS on the Orbitrap MS with an ACE 3 C18 column using mobile phases 0.1% formic acid in water (A) and 0.1% formic acid in acetonitrile (B) at a gradient of 10-70% (0-15 min), 70% (15-20 min), 70-10% (20-25 min) and 10% (25-30 min) relative to solvent B, and at a flow rate of 0.3 mL/min (as described in section 3.6.2).

6.3.4 Effect of added enzyme inhibitors

Two protease inhibitors P32/98 (also known as CD26, a DPP_{IV} inhibitor) and phenylmethylsulfonyl fluoride (PMSF, a serine protease inhibitor) were spiked into the melittin and BV samples respectively, and incubated. These inhibitors were used to test for the involvement of the proteases already known to be present in BV (i.e. Api m7 and Api m9, both serine dependent catalytically, and Api m5, known to be similar to DPP_{IV}) (Blank *et al.*, 2010). Degradation of melittin in the BV was observed to be inhibited by PMSF, but not by P32/98 (DPP_{IV} inhibitor) (**Figure 6.9** and **Figure 6.10**).

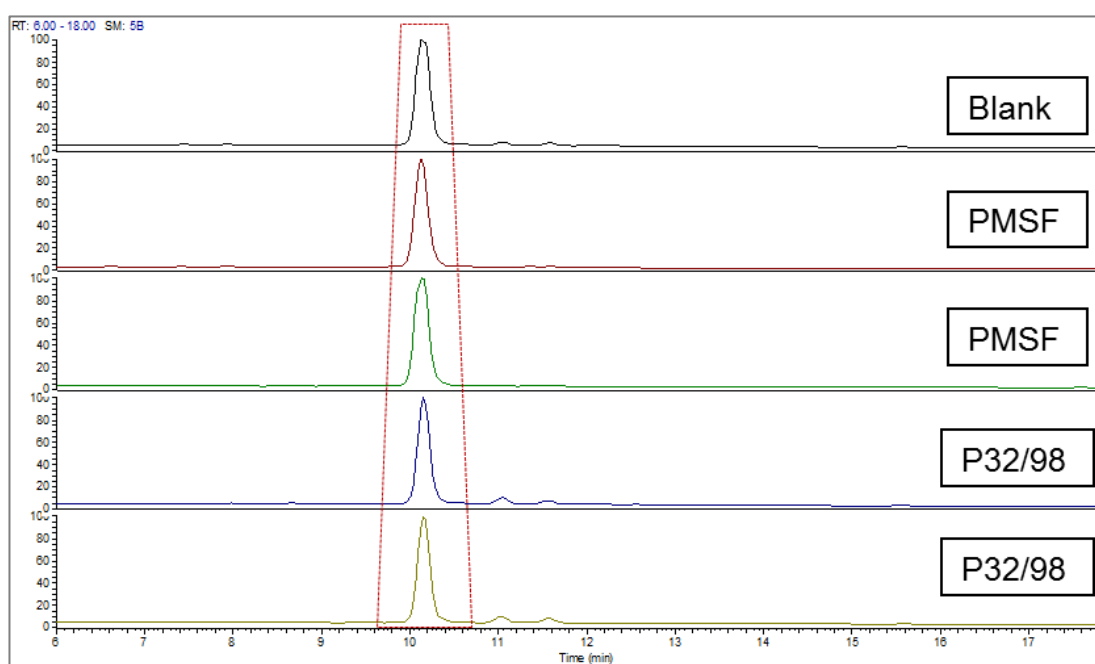


Figure 6.10: Chromatograms for BV with inhibitors after 24 h of incubation. The melittin peaks are highlighted by the red box. The samples of whole BV were prepared at 0.1 mg/mL and incubated with the two protease inhibitors at 30°C. Final samples were then analysed in positive ion LC-ESI-MS on the Orbitrap MS with an ACE 3 C18 column using mobile phases 0.1% formic acid in water (A) and 0.1% formic acid in acetonitrile (B) at a gradient of 10-70% (0-15 min), 70% (15-20 min), 70-10% (20-25 min) and 10% (25-30 min) relative to solvent B, and at a flow rate of 0.3 mL/min (as described in section 3.6.2).

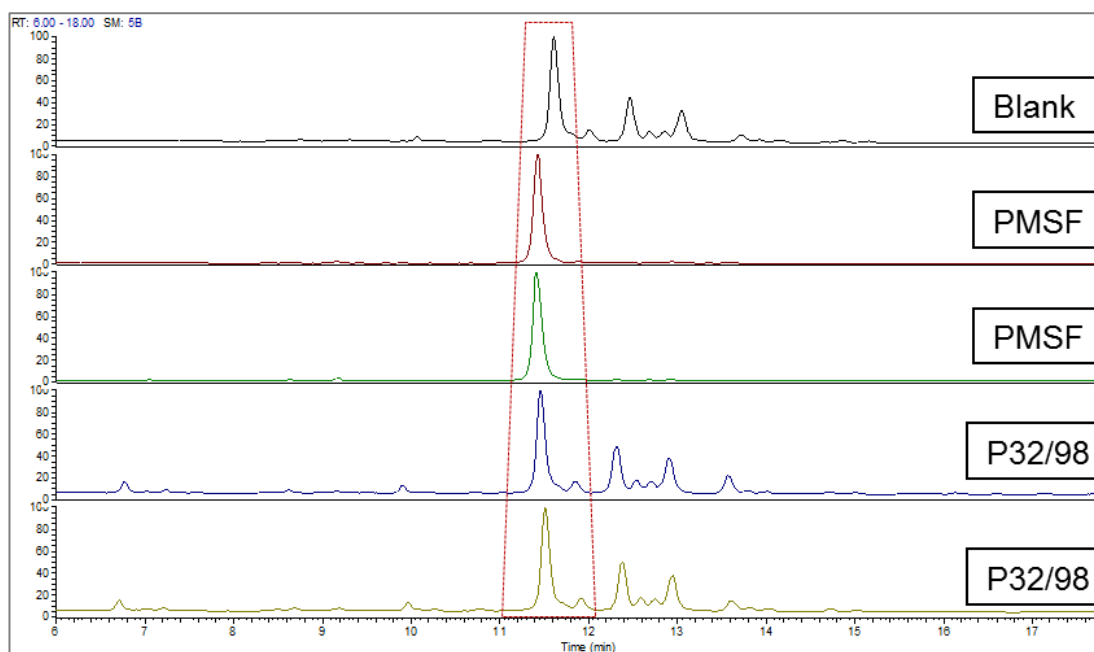


Figure 6.11: Chromatogram obtained 14 days following incubation. The melittin peaks are highlighted by the red box. The samples of melittin were prepared at 0.1 mg/mL and incubated with the two protease inhibitors at 30°C. Final samples were then analysed in positive ion LC-ESI-MS on the Orbitrap MS with an ACE 3 C18 column using mobile phases 0.1% formic acid in water (A) and 0.1% formic acid in acetonitrile (B) at a gradient of 10-70% (0-15 min), 70% (15-20 min), 70-10% (20-25 min) and 10% (25-30 min) relative to solvent B, and at a flow rate of 0.3 mL/min (as described in section 3.6.2).

These results indicated that the degradation of the melittin in BV was enzymatic, and was caused by a serine dependent protease because it could be inhibited by PMSF. Two such proteases are known to be present in BV and they are CUB serine protease and serine carboxypeptidase which are known bee allergens (see **Table 2.2**, page 43).

6.4 Discussion

The investigations revealed that sterile aqueous solutions of whole BV suffered a gradual, temperature-dependent, degradation of melittin within the ²¹Lys-²²Arg-²³Lys-²⁴Arg region of the amino acid sequence. Given the specificity for Lys and Arg, if an enzyme was involved, it is likely to be trypsin-like, with an endo- or exo-peptidase action selective for positively charged side chains. From the peptidases identified in BV through genetic analysis, CUB serine proteinase (Api m7) is an endopeptidase that hydrolyses long peptides/proteins at internal peptide bonds

(Georgieva *et al.*, 2011; Georgieva *et al.*, 2010; Levine *et al.*, 2001). Thus it is unlikely to be responsible for the observed spontaneous degradation. On the other hand, serine carboxypeptidase (Api M9) shows broad specificity by removing amino acids from the C-terminus (Agarwal *et al.*, 2012). This enzyme has the theoretical capability to remove residues sequentially from the C-terminal of melittin in the fashion observed, given its broad specificity. Although Api M5 (DPP_{IV}) is also a serine dependent protease, it removes the first two N-terminal amino acids from peptides, cleaving after Pro, Ala, Gly (Kreil *et al.*, 1980) which does not correspond to what was observed.

As Api M9 is a known human allergen, if indeed it is responsible for the observed degradation of melittin in aqueous BV solutions, its presence or absence in a BV preparation could be judged by the structural stability of melittin; where C-terminal shortening of melittin is observed, the enzyme/allergen is present. This has potential as a commercial test to ensure the allergen is absent. In terms of the effect on the properties of melittin of removal of its C-terminal residues, previous work has shown that the inflammatory capability will be reduced (Owen, 2008). Whether C-terminal shortening of melittin to create a population of native and C-terminal shortened melittin-like peptides with different lengths and inflammatory power is an intended or accidental consequence of the presence of Api M9 is not clear.

Chapter Seven

Development of a Method for Assay of Bee Venom in Cosmetics

7 An LC-MS Method for the Assay of Melittin in Cosmetic Formulations Containing Bee Venom

Tusiimire, J.,¹ Wallace, J.,² Dufton, M.,² Parkinson, J.,² Clements, C. J.,¹ Young, L.,¹ Park, J. K.,³ Jeon, J. W.,³ & Watson, D. G.^{1,*}

¹ Strathclyde Institute of Pharmacy and Biomedical Sciences, University of Strathclyde, 161 Cathedral Street, Glasgow G4 0RE, U.K.

² WestCHEM Department of Pure and Applied Chemistry, University of Strathclyde, 295 Cathedral Street, Glasgow G1 1XL, U.K.

³ #204, Beesen Co. Ltd., Bio Venture Town, Yuseong Daero 1662, 34054 Dae Jeon, Korea.

* Correspondence: d.g.watson@strath.ac.uk; Tel.: +44-141-548-2651; Fax: +44-141-552-6443

This chapter constitutes a published research article:

Tusiimire, J., Wallace, J., Dufton, M., Parkinson, J., Clements, C. J., Young, L., Park, J. K., Jeon, J. W. & Watson, D. G. 2015. An LC-MS method for the assay of melittin in cosmetic formulations containing bee venom. *Analytical and Bioanalytical Chemistry*, **407**, 3627-3635.

Wallace J., Dufton, M. and Parkinson, J. contributed towards NMR analysis. Clements, C. J. and Young, L. contributed towards manuscript review. Park, J. K. and Jeon, J. W. provided the crude bee venom samples. Watson, D. G. contributed towards both NMR and LC-MS analyses, and provided overall guidance and supervision.

Abstract

There is a growing interest in the potential of bee venom (BV) in cosmetics as a rejuvenating agent. Products currently on the market do not specify exactly their content of BV. Therefore we developed a method for the detection and quantification of melittin, as a marker of BV content, in selected commercial creams which contained BV according to their marketing claims, in order to gauge the relative quality of such formulations. A quantitative method was achieved following a rigorous extraction procedure involving sonication, liquid-liquid extraction (LLE) and solid phase extraction (SPE) since carryover of excipients was found to cause a rapid deterioration in the chromatographic performance. The method employed a standard additions approach using, as spiking standard, purified melittin isolated from BV and standardized by quantitative NMR. The aqueous extracts of the spiked creams were analysed by reversed phase LC-MS on an LTQ-Orbitrap mass spectrometer. The purity of the melittin spiking standard was determined to be 96.0%. The lowest measured mean melittin content in the creams was 3.19ppm (± 1.58 ppm 95% CI) while highest was 37.21 ppm (± 2.01 ppm 95% CI). The method showed adequate linearity ($R^2 \geq 0.98$) and a recovery of 87.7-102.2% from a spiked blank cream. An assay precision of <20% RSD was achieved for all but one sample where the RSD value was 27.5%. The method was sensitive enough for use in routine assay of BV-containing cosmetic creams. Differences in the melittin content of the commercial products assayed were nearly tenfold.

Key words: Melittin; bee venom; extraction; LC-MS; creams; cosmetics; quantitative NMR.

7.1 Introduction

The venom of *Apis mellifera* and its components are increasingly being used as primary ingredients in various cosmetic formulations including skin creams, balms, face masks, and serums. Cosmetics are some of the most widely used consumer goods (Gagliardi *et al.*, 2007), with the market annually generating billions of pounds worldwide (Gao *et al.*, 2012), and so their testing must be thorough in view of their widespread usage. Although the separate testing of constituents may not necessarily indicate properties of the final formulation, appropriate methods are needed for the routine assay, stability monitoring and quality control of primary ingredients in order to set a quality standard for a particular product even though there is no prescribed content for BV in such creams (Kokot and Matysiak, 2009).

Apis mellifera venom contains various ingredients ranging from relatively low MW amines, such as histamine (MW ~111), to relatively large-sized proteins such as phospholipase (MW ~16000) and hyaluronidase (MW ~53000) enzymes. Melittin (MW ~2800) is the main constituent of the venom, constituting approximately 45-60% of the bulk venom material and is a 26-amino acid peptide (Terwilliger and Eisenberg, 1982). The other components are the peptides apamine, mast cell degranulating peptide (MCDP), secapin, adolapin, and apidaecin (Van Vaerenbergh *et al.*, 2013; Chen and Lariviere, 2010; Kokot and Matysiak, 2009). Both phospholipase (api m1) and hyaluronidase (api m3) are classified as major allergens according to the International Union of Immunological Societies (IUIS) (WHO/IUIS, 2014). The other BV allergens include dipeptidyl dipeptidase IV (api m5), serine carboxypeptidase (api m9), CUB serine protease (api m7), and vitellogenin (api m12) among others. A host of other ingredients including amino acids, carbohydrates, amines and lipids have also been described (Chen and Lariviere, 2010; Orsolic, 2012; Ferreira Junior *et al.*, 2010a). The presence of ionisable free primary amino and the highly basic guanidino groups (on lysine and arginine respectively), in addition to polar amido (on N-terminal glycine and both C-terminal glutamines) and hydroxyl (on threonine and serine residues) groups in melittin reduce its retention on a hydrophobic C18-type column, particularly when ionised in an acidic medium (0.1 % v/v formic acid). However, due to the presence of valine (2), leucine (4) and isoleucine (3) resi-

dues (all with non-polar side chains) in its amino acid sequence, the molecule is retained long enough for analysis by a reversed phase method.

Recent advances in cosmetic analysis have focused on developing new methods for determining cosmetic preservatives, fragrance allergens and plasticizers such as phthalates, using chromatographic and mass spectrometry techniques (Alvarez-Rivera *et al.*, 2013). New methods become more necessary when new ingredients are used in formulations for general use. Thus although BV based products have been on the European markets for quite some time (such as Forapin in Germany, Virapin in Slovakia, Apiven in France, Melivenon in Bulgaria and Apifor in Russia) (Matysiak *et al.*, 2011), these have been available more as topical medications rather than as general use consumer products in the wider international market. Products designed to fit the latter category (e.g. the Manuka cosmetics range) have only recently appeared on the EU markets. These products are being marketed as containing “purified bee venom” or “bee venom extracts” (e.g. 10 Natural Effects Bee Venom Essence by Laboratorios DIET Esthetic S.A.) without further specification. Despite this growing use of BV, the current literature does not report a sufficient number of studies showing how to assess the composition of cosmetics in general (Gao *et al.*, 2012), let alone the BV content in these products.

Analysis of cosmetic products may be considered as relating to that of non-oral semi-solid dosage forms (which include ointments, gels, creams, and pastes) in pharmaceutical formulations and whose sample preparation methods for analysis have been previously reviewed (Bu *et al.*, 2011). It would appear from The Cosmetic, Toiletry and Perfumery Association (CTPA) (CTPA, 2013) that the main difference, at least in practical terms, between a cosmetic product and its corresponding pharmaceutical counterpart is the purpose of application and composition. Both cosmetics and topical pharmaceutical products have common sites of application although the former tend to be more complex in composition.

Directive 93/35/EEC, the Sixth Amendment to the original Cosmetic Directive of 1976, incorporates the following definition of a cosmetic product:

A "cosmetic product" shall mean any substance or mixture intended to be placed in contact with the various external parts of the human body (epidermis, hair system, nails, lips and external genital organs) or with the teeth and the mucous membranes of the oral cavity with a view exclusively or mainly to cleaning them, perfuming them, changing their appearance and/or correcting body odours and/or protecting them or keeping them in good condition.

Cosmetics are not expected to contain substances with systemic therapeutic action, but are instead only formulated for topical applications exerting local effects. Thus the level of emphasis placed on exact proportions of their chemical constituents (i.e. content uniformity) is lower than for pharmaceutical products. In addition the control of how many constituents there are in a single formulation (complexity), component compatibility and susceptibility to degradation, and the general requirement for standardisation is also lower than for pharmaceuticals. Even the labelling requirement does not expect the manufacturer to specify quantities of ingredients while “top secret” ones are not even included on the label (Llompert *et al.*, 2013). A cosmetic product tends to be considered acceptable as long as it does not contain banned substances (or restricted substances beyond allowed limits), is nontoxic, does not make unjustified marketing claims, and generally satisfies the customer’s needs.

Although current legislation does not require full profiling of all constituents in a cosmetic product, but only focuses on controlling restricted or banned ingredients (Tullo, 2013), it is likely that such requirements will be invoked in future as technologies advance, and new molecules or formulations, such as nanoparticles, become more commonly available.

Thus in order to meet current and anticipated formulation and regulatory requirements for BV formulated skin products, it is important to be able to detect, quantify and control the amount of active BV material. Since BV is only present in small amounts in creams, the current work focussed on developing a reliable sample preparation and clean-up procedure in order to isolate melittin, the most abundant marker compound for the presence of BV, from the formulation excipients with subsequent

analysis of the extracts by LC-MS using a standard additions technique. For an analytical method based on an efficient separation technique such as reversed phase HPLC and highly selective and sensitive detection systems such as Orbitrap mass spectrometry (Denisov *et al.*, 2012), one would ideally not have to worry much about co-eluting compounds in the extract solution (Zhou *et al.*, 2010). However, because cosmetic products are generally very complex in composition (Bu *et al.*, 2011), with most of the ingredient structures unknown but likely to be comprised of varying proportions of lipophilic and hydrophilic materials, the whole process of analytical method development may become unpredictable even when employing some of the latest highly selective analytical devices. At the very least, in order to protect the analytical column and detection system, there is a need to attempt to selectively extract and concentrate the analyte of interest from the matrix of the complex product. This paper reports a method based on liquid-liquid extraction in a ternary solvent system followed by solid phase extraction (SPE) on a reversed phase (C18) cartridges to obtain relatively clean samples for analysis of melittin, which gives an indication of BV content, in BV containing cosmetics by LC-MS.

7.2 Materials and methods

7.2.1 Study samples

Six commercial cosmetics which were stated to contain BV were analysed. Throughout the experiments the samples were stored in a cool, dry environment and away from direct sunlight as recommended by the manufacturers. Prepared solutions for analysis were run immediately to avoid any sample degradation.

7.2.2 Solvents and chemicals

HPLC grade acetonitrile and methanol were purchased from Fisher Scientific, UK while chloroform was from Sigma-Aldrich Ltd. (Dorset, UK). Deionised purified water was produced in the lab using a Direct-Q 3 Millipore Ultrapure water purification system (Millipore, UK). AnalaR grade formic acid (BDH-Merck, UK) was used

as a pH modifier. D₂O was obtained from Sigma Aldrich (Dorset, UK). Crude BV from which melittin was purified was supplied by Beesen Co. Ltd. (Dae Jeon, Korea).

7.2.3 Instrumentation and Consumables

The syringes and filters were obtained from Fisher Scientific, UK. The following equipment was also used: a micro-centrifuge, a vortex mixer, an ultrasonic bath (Fisher Scientific, UK) and Automatic pipettes (Gilson, Anachem, UK). The Reveleris® Flash Chromatography was supplied by Alltech, UK. The Reveleris system uses two variable wavelengths and evaporative light scattering (ELSD) detectors to detect both chromophoric and non-chromophoric compounds in a single run. The LC-MS system consisted of a Surveyor pump connected to a LTQ Orbitrap (Thermo Fisher, Hemel Hempstead, UK). The HPLC column used was a reversed phase ACE 3 C18 column; 150 x 3.0mm, 3µm, supplied from Hichrom, Reading, UK. For sample purification of melittin, a reversed phase semi-prep HPLC column (250mm length x 10mm I.D., 5µm particle size, supplied by HiChrom Ltd, UK) was used.

7.2.4 LC-MS method conditions

Final diluted and filtered sample solutions were run on the LC-MS under these conditions. Mobile phases consisted of 0.1% (v/v) formic acid in water (A) and 0.1% (v/v) formic acid in acetonitrile (B). The solvent gradient used was 20-70 %B (from 0-10 min), 70% (10-16 min), 70-20% (16-20 min), and finally 20% (20-25 min) at a flow rate 0.3 mL/min. Injection volume was 10µL. The ESI interface was employed in positive ionisation mode for detection of [M+H]⁺ ions, with a spray voltage of capillary and cone at 4.5 and 35kV respectively. The sheath and auxiliary gas flow rates were 50 and 15 arbitrary units, ion transfer capillary temperature was set at 275°C and full scan data were collected between m/z 100-2000. The data was collected and processed using Xcalibur 2.1.0 software (Thermo Fisher Scientific, UK).

7.2.5 Melittin isolation from bee venom

The melittin used in the spiking standard solution was prepared by medium pressure liquid chromatographic (MPLC) fractionation of a BV sample on a Reveleris® Flash chromatography system. Approximately 800 mg of BV sample was mixed with 3g of purified silica (Celite) in a dry-loading cartridge prior to the fractionation. The column used was prepared by packing an empty 20g Easyvarioflash D24 cartridge (VWR International, UK) with *ca.* 13 g of Polymeric Retain PEP for SPE (Thermo Scientific, UK). The mobile phases used were water (solvent A) and acetonitrile (solvent B) under the following gradient conditions: 0-10 min (0% B), 10-20 min (20% B), 20-30 min (50% B), 30-60 min (60% B), and 60-70 min (100% B) at a flow rate of 12 mL/min. The melittin peak eluted between 22 and 28 minutes. Following LC-MS analysis on the Orbitrap, similar fractions were pooled together and further purification of the melittin fraction was achieved by semi-preparative HPLC using a Thermo Separations P2000 pump and ACE C18 column (250mm length x 10mm I.D., 5µm particle size; HiChrom Ltd, UK). To this end, aliquots of the pooled melittin fractions from MPLC (100 µL of a 0.1 g/mL aqueous solution) were injected onto the HPLC column. The injected samples were eluted with water:acetonitrile (60:40) at a flow rate of 5mL/min. The dual UV detector was set at wavelengths 220 and 295 nm and data was collected using the ChromQuest software. The melittin peak was collected and lyophilised.

7.2.6 Melittin purity measurement by NMR

A solution of the melittin spiking standard was made by dissolving 14.23 mg of the sample in 1 mL of D₂O to give a final concentration of 5.0 mM. A portion of exactly 600µL of this solution was then taken for NMR analysis. After this, 30 µL of a 50 mM solution of MeOH in D₂O was then spiked into the melittin sample to give a final methanol concentration of *ca.* 2.5 mM. The samples were each run in triplicate at 310K for 16 scans with a pre-saturation pulse programme which had a long recovery time (D1=58s) and a short pre-saturation time (D2=2s). This long recovery time allowed for all the resonances to be fully detected. One dimensional ¹H NMR data were acquired under Topspin (version 2.1, Bruker Biospin, Karlsruhe) using a meth-

od analogous to that previously described by Evstigneev *et al.* (2010) (Evstigneev *et al.*, 2010). A Bruker AVANCE III 600 NMR spectrometer operated at a proton resonance frequency of 600.13 MHz was equipped with a TBI [^1H , ^{13}C , ^{31}P - ^{15}N]-z triple resonance probe head fitted with an actively shielded gradient coil for delivery of pulsed-field gradients.

7.2.7 Assay method for the creams

A sample of cream (*ca* 1 g) was weighed into a 20 mL glass vial and dispersed in 10mL of methanol-chloroform (1:2) mixture. The mixture was then sonicated, with intermittent shaking, for 30 min in an ultrasonic bath until homogenous. A portion (1 mL) of the extraction solvent was pipetted and transferred into a 2 mL centrifuge tube and spiked with a known quantity of melittin standard reconstituted in 0.1% (v/v) formic acid, and then made up to 2 mL with 0.1% (v/v) formic acid. The mixture was then shaken on a vortex mixer for about 2-3 min to allow complete mixing. Thereafter it was centrifuged at 6000 rpm for 15 min upon which the supernatant was transferred into a separate vial for solid phase extraction (SPE). SPE was performed on Strata C18, 100 mg/mL packed columns (Phenomenex, UK). The sample was loaded onto the SPE column and washed with 1 mL of 30/70 (acetonitrile/water) and then eluted with 1 mL of 50/50 (acetonitrile/water). Final eluted solutions were run on the LC-MS according to the method described earlier. Peak area was obtained by integrating extracted ion chromatograms of the abundant +4 (m/z 712.45 \pm 0.01) and +5 (570.16 \pm 0.01) melittin ions (Zhou *et al.*, 2010) using the XCalibur software.

7.2.8 Calibration with standard additions

Sample extracts were spiked with aliquots of 0.1 mg/mL of a freshly prepared standard spike solution of melittin. Spike weights of 0.0, 2.5, 5.0, 7.5, 10.0, 12.5 and 15.0 μg of melittin corresponded to 0, 25, 50, 75, 100, 125 and 150 μL of the spiking standard solution. Following the spiking, samples were gently vortexed and mixed thoroughly before liquid-liquid extraction by centrifugation and later solid phase extraction. A calibration curve of analyte response versus amount of spiked standard

melittin was then constructed using the un-spiked sample as the lowest point on the curve. From this curve the content of melittin in each cream sample was then determined by extrapolating the line to meet the concentration (horizontal) axis.

7.3 Results

7.3.1 Melittin purity determination

The NMR spectra obtained showed clear distinction at $\sigma 3.4$ ppm chemical shift between melittin spiking standard and that of its solution after spiking with pure methanol internal standard (**Figure 7.1** & **Figure 7.2**). The methyl protons in methanol overlapped with some unidentified protons in melittin and thus they could not be integrated independently. However, the aromatic region of melittin clearly showed the 5 protons corresponding to the single tryptophan residue in melittin. Integrating this reference region to 5 protons, the rest of the standard melittin spectrum integrated to 174 protons—representing the other non-exchangeable protons in melittin. In addition, the methanol-spiked standard solution integrated to 174 protons plus the contribution from the extra 3 non-exchangeable protons from methanol.

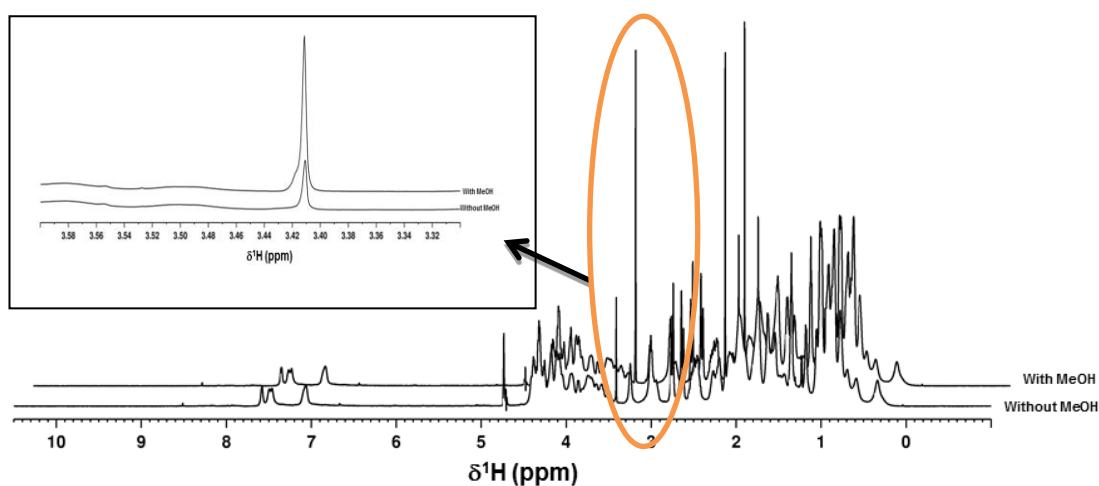


Figure 7.1: NMR spectra of melittin with and without methanol spike. The insert shows where the methyl protons in methanol appear on the spectrum at $\sim\sigma 3.4$ ppm. There is noticeable signal amplification following addition of methanol in the solution. The signal in the unspiked sample at $\sigma 3.4$ ppm is perhaps due to a methyl group on one of the amino acids in melittin.

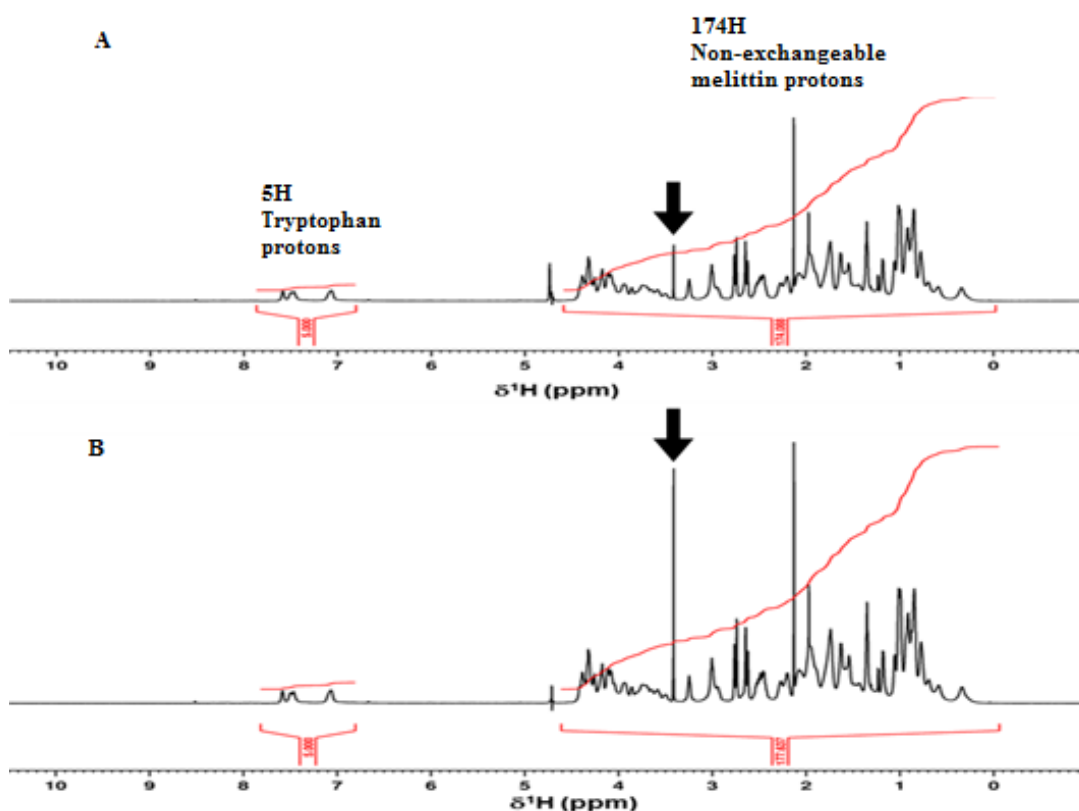


Figure 7.2: NMR spectra of melittin (A) and melittin + methanol (B). The arrow in each case shows the position of the methyl protons in methanol at $\sigma 3.4$ ppm chemical shift. By comparing the area integrals before and after addition of methanol standard, the number of protons in unspiked melittin was determined.

The purity of the standard melittin was calculated by using the formula proposed by Malz and Jancke (2005) (Malz and Jancke, 2005) given in equation 18 as follows:

$$P_x = \frac{I_x}{I_{std}} \frac{N_{std}}{N_x} \frac{M_x}{M_{std}} \frac{m_{std}}{m_x} P_{std} \quad (18)$$

where I, N, M, m and P represent magnitude of signal response (area integral), number of resonant nuclei (protons), molar mass, sample weight and purity of the unknown and standard compounds respectively.

For this experiment, the following values apply for the unknown sample (melittin) and calibration standard (methanol) (**Table 7.1**). Although melittin has 229 protons in total, 50 of them are exchangeable with deuterium atoms from the D_2O used as solvent so that the resonant ones are only 179.

Table 7.1: Values used in the calculation of melittin purity.

<i>Parameter</i>	<i>Calibration standard (MeOH)</i>	<i>Unknown (melittin)</i>
Signal response (I)	3 (177 less 174)	174
Number of resonant nuclei (N)	3	174 (179 less 5 of Trp)
Molecular weight (M)	32.04	2846.46
Sample weight in mg (m)	0.09649	8.9649
Purity % (P)	99.9	P _x

Substituting the values in **Table 7.1** into equation 19 above gives P_x, the purity of melittin, as 96.0%. Since the mass spectrum of the melittin spiking solution showed only a single peak representing melittin, it is likely that any impurity present might be due to water or counter anions associated with the basic side chains in melittin.

7.3.2 Mean melittin content in creams

Table 7.2 shows a summary of results obtained after assay of six samples of each cream on three separate occasions. Each analysis was conducted by running seven spiked 1 mL aliquots of extract, each prepared from 1 g of cream, on the LC-MS and using the melittin peak areas obtained to plot a straight line from which the content in the un-spiked extract was estimated by extrapolation of the standard additions plot.

Table 7.2: Triplicate assays of commercial facial creams claimed to contain unstated amounts of BV. The values represent complete assays performed on three separate occasions using a 7-point standard additions technique with spikes of 0-15 µg in 2.5-point increments.

<i>Sample</i>	<i>Assay of melittin content (in ppm)</i>				<i>RT (min)</i>	<i>Linearity</i>
	I	II	III	Mean (RSD)	Mean (RSD)	Mean R ² (RSD)
A	3.90	4.21	5.42	4.51 (17.8)	6.29 (0.56)	0.989 (0.35)
B	4.37	3.98	3.51	3.95 (10.8)	6.26 (0.88)	0.985 (0.60)
C	36.60	37.21	32.55	35.45 (7.1)	6.36 (0.55)	0.979 (0.18)
D	15.53	17.03	14.45	15.61 (8.9)	6.35 (0.24)	0.992 (0.35)
E	32.59	35.06	34.55	34.07 (3.8)	6.37 (0.24)	0.990 (0.54)
F	3.19	5.62	4.45	4.42 (27.5)	6.69 (0.09)	0.981 (0.82)

7.3.3 Assay precision

Analytical precision was determined both between and within runs. Inter-assay precision was checked by testing, on 3 separate occasions, each of the cream samples using the developed method and then calculating the relative standard deviation (**Table 7.2**). The calculated between-run precisions were found to be less than 20% except for product F where the RSD was 27.5% perhaps due to the melittin content being close to the limit of quantification of the method. The between sample variations could also be due to variation in the uniformity of content within the creams rather than the analytical precision of the method.

Intra-assay precision was calculated using equation 19, as previously described by Bruce and Gill (Bruce and Gill, 1999), to calculate the standard error (s_c) in the concentration (c_x) of the assay mixture obtained by extrapolation of the linear regression standard additions plot.

$$s_c^2 = \frac{s_y^2}{m^2} \left(\frac{1}{N} + \frac{\bar{y}^2}{m^2 S_{xx}} \right) \quad (19)$$

where s_y is the standard deviation around the regression line (standard deviation of the residuals), m is the slope of the regression line, N is the number of samples for each plot, \bar{y} is the response mean and S_{xx} is the corrected sum of squares of the independent variable (spiked concentration).

Table 7.3 shows the margin of error (precision) estimates calculated for each assay using the equation above and the 95% confidence intervals for the determined melitin content in the cosmetic products assayed. **Table 7.4** gives a summary of the calibration equations obtained for all the samples assayed in triplicate.

Table 7.3: Intra-assay precision estimates at 95% confidence level ($p=0.05$, $df=5$). The t -value for a 2-tailed t -test is ± 2.5706 from the Student t -table. The 95% confidence interval was calculated as (95% CI = tsc) as described by (Bruce and Gill, 1999).

<i>Product</i>	<i>Run</i>	<i>Assay</i> (ppm)	<i>Standard</i> <i>error</i> (s_e)	<i>Margin of</i> <i>error</i> (%)	\pm 95% CI ($\pm t s_e$) (ppm)	<i>Lower CI</i> (ppm)	<i>Upper CI</i> (ppm)
A	1	3.90	0.3952	26.05	1.0159	2.88	4.92
	2	4.21	0.4173	25.48	1.0727	3.14	5.28
	3	5.42	0.5270	25.00	1.3548	4.07	6.77
B	1	4.37	0.4683	27.54	1.2037	3.17	5.57
	2	3.98	0.4447	28.72	1.1431	2.84	5.12
	3	3.51	0.6230	45.63	1.6015	1.91	5.11
C	1	36.60	0.7662	5.38	1.9697	34.63	38.57
	2	37.21	0.7817	5.40	2.0094	35.20	39.22
	3	32.55	0.8060	6.37	2.0720	30.48	34.62
D	1	15.53	0.3310	5.48	0.8509	14.68	16.38
	2	17.03	0.3656	5.52	0.9398	16.09	17.97
	3	14.25	0.4927	8.89	1.2664	12.98	15.52
E	1	32.59	0.6143	4.85	1.5790	31.01	34.17
	2	35.06	0.4388	3.22	1.1281	33.93	36.19
	3	34.55	0.4624	3.44	1.1885	33.36	35.74
F	1	3.19	0.6138	49.46	1.5778	1.61	4.77
	2	5.62	0.4211	19.26	1.0826	4.54	6.70
	3	4.45	0.6801	39.28	1.7481	2.70	6.20

Table 7.4: Summary of the equations of calibration curves (in the form of $y = mx + c$) obtained during the assay of the 6 creams (A-F).

<i>Samples</i>	<i>Slope, m (μg^{-1})</i>	<i>y- intercept, c</i>	<i>/x-intercept/ (μg)</i>	<i>Linearity, R²</i>
A	82462.4629	32135.2843	0.3897	0.9911
	82367.8220	34708.6236	0.4214	0.9902
	79832.8949	43257.5386	0.5419	0.9847
B	85601.1771	37387.7843	0.4368	0.9877
	83035.3569	33012.0036	0.3976	0.9888
	85052.6091	29889.6814	0.3514	0.9781
C	6567.3226	24035.9279	3.6599	0.9807
	6513.4514	24235.4514	3.7208	0.9802
	6970.9136	22688.1725	3.2547	0.9774
D	89737.9669	139404.2871	1.5535	0.9949
	86782.1707	147767.1025	1.7027	0.9929
	76890.2507	109605.3996	1.4255	0.9885
E	65242.3570	212602.9011	3.2587	0.9868
	62561.6680	219322.2243	3.5057	0.9935
	63100.6986	218032.7721	3.4553	0.9927
F	339024.0249	108079.3764	0.3188	0.9786
	322348.3874	181137.1043	0.5619	0.9902
	359450.2041	159968.0232	0.4450	0.9744

From **Table 7.3**, it can be seen that the margin of error was, unsurprisingly, high for products where the melittin content was below 10 ppm (A, B and F). However, for the rest of the products, the margin of error was well below the 10% threshold set for mass fraction of $\geq 1,000 \mu\text{g}/\text{kg}$ in accordance with CD2002/657/EC (Communities, 2002), although the direct application of this standard in a standard additions technique does not seem feasible given the complexity of the sample, nor has it been reported previously. The observed degradation of precision is expected in standard additions procedures as described by Ellison and Thompson (2008) (Ellison and Thompson, 2008), although such variations are also expected to arise from the detailed extraction procedures required for this type of formulation (Bu *et al.*, 2011; Bishop *et al.*, 2011).

7.3.4 Recovery, specificity and linearity

Since no appropriately matched matrix samples were available, extraction recovery of the method was determined using a spiked base cream (Nivea) because it was expected to offer comparable extraction challenges to those exhibited by the samples assayed. The blank cream samples were fortified at 5.0, 10.0 and 15.0 µg per 100mg with melittin and assayed in triplicate. The peak areas obtained were compared to those of external standards prepared in triplicate at the mid-point of the expected concentration range (10.0 µg/mL). The mean recovery obtained was 94.0 % (range: 87.7-102.2%) with a coefficient of variation (RSD) of 4.6% (**Table 7.5** & **Table 7.6**).

Table 7.5: Recovery data obtained using a blank cream fortified at three different levels of 5, 10 and 15 µg per mL of extract containing 100mg cream.

<i>Replicates</i>	<i>Fortification level</i> (µg per 100 mg)	<i>Area</i>	<i>RT(min)</i>	<i>Recovery (%)</i>	<i>Mean (%)</i>	<i>RSD (%)</i>
1	5.0	425882	6.22	87.7	95.1	7.7
2	5.0	463353	6.24	95.4		
3	5.0	496710	6.25	102.2		
1	10.0	918056	6.24	94.5	92.4	2.2
2	10.0	896992	6.25	92.3		
3	10.0	877902	6.24	90.3		
1	15.0	1413491	6.24	97.0	94.5	3.7
2	15.0	1398745	6.26	96.0		
3	15.0	1318737	6.27	90.5		
Overall mean			6.25	94.0		4.6

Table 7.6: Peak areas of standard melittin assayed at 10µg/mL concentration

<i>Replicates</i>	<i>Conc (µg/mL)</i>	<i>Peak Area</i>	<i>RT (min)</i>	<i>Mean Area</i>	<i>RSD %</i>
1	10.0	978938	6.24	971682.3	0.79
2	10.0	963628	6.24		
3	10.0	972481	6.25		

Specificity of detection was accomplished by using extracted ion chromatograms for the melittin molecule using two of its abundant ions its mass spectrum (**Figure 7.3**), filtering within a tight range of m/z 712.445 ± 0.005 and 570.165 ± 0.005 . This was fur-

ther confirmed by looking at the ion spectrum of the peak within the retention time range of the melittin standard. No other compounds from the samples appeared in the chromatogram at the retention time of melittin under these conditions. This was further confirmed by running blank samples.

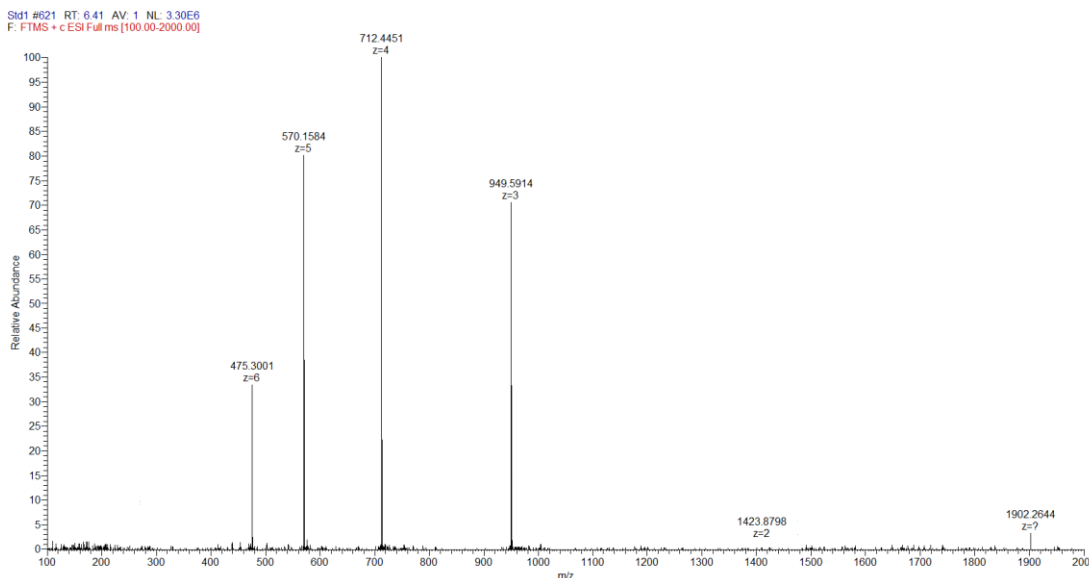


Figure 7.3: The mass spectrum of melittin. Melittin molecules can acquire up to 6 positive charges during electrospray ionisation (ESI) in the mass spectrometer. The most abundant ions in the spectrum are m/z: 712.45 (+4) and 570.16 (+5) species.

Linearity of the response was evaluated by using a spiked blank matrix at 6 calibration points i.e. 2.5, 5.0, 7.5, 10.0, 12.5 and 15.0 $\mu\text{g/mL}$ and then carrying out a linear regression analysis of the analyte peak areas obtained versus concentration. The method showed good linearity in the analytical range with correlation coefficient (R^2) ≥ 0.99 . Standard melittin peaks were stable with a retention time mean 6.26 min (RSD ≤ 1.0 %). The mean chromatographic efficiency for the melittin was calculated at $\sim 75,000$ plates per metre. The limits of detection (LOD) and quantification (LOQ) of melittin in the spiking solution, determined according to ICH guidelines (ICH, 1996) were 50 ng/mL and 150 ng/mL respectively.

7.4 Discussion

The standard additions method is used to eliminate matrix effects in samples that would lead to biased results during analysis (Danzer and Currie, 1998). This is par-

ticularly likely to occur with trace amounts of a chemically complex moiety such as melittin in the complex cream matrix. It has been proposed that the method of standard additions solves a particular type of matrix effect, called the rotational effect which is a proportional bias depending on the amount of matrix, but not translational effects, a constant bias, which must be separately dealt with (Ellison and Thompson, 2008). In the method of standard additions, known quantities of the analyte being assayed are spiked into a sample containing the analyte at increasing concentrations, starting from zero, and then extracted. Final solutions are subsequently analysed and the peak areas obtained are plotted against the spiked volumes or concentration of spiked samples. Provided that the area response is directly proportional to concentration, a straight line is obtained. This straight line crosses the response (vertical) axis at the response value of the un-spiked sample; extrapolating this straight line to the concentration (horizontal) axis gives, numerically, the weight of analyte in the un-spiked sample (**Figure 7.4** and Appendix I). The main advantage of using standard additions is that there is no need for complete extraction of analyte from matrix provided all the samples have been subjected to exactly the same extraction process. It is important that the samples are not spiked to levels exceeding linearity limits of the analyte response. The amount of standard added depends on the approximate concentration of the unspiked samples. Ideally, samples should be spiked at evenly spaced concentrations of standard solutions within the linear range, although it has been recommended that spiked concentrations should be at least 4 times the concentration of analyte (Ellison and Thompson, 2008).

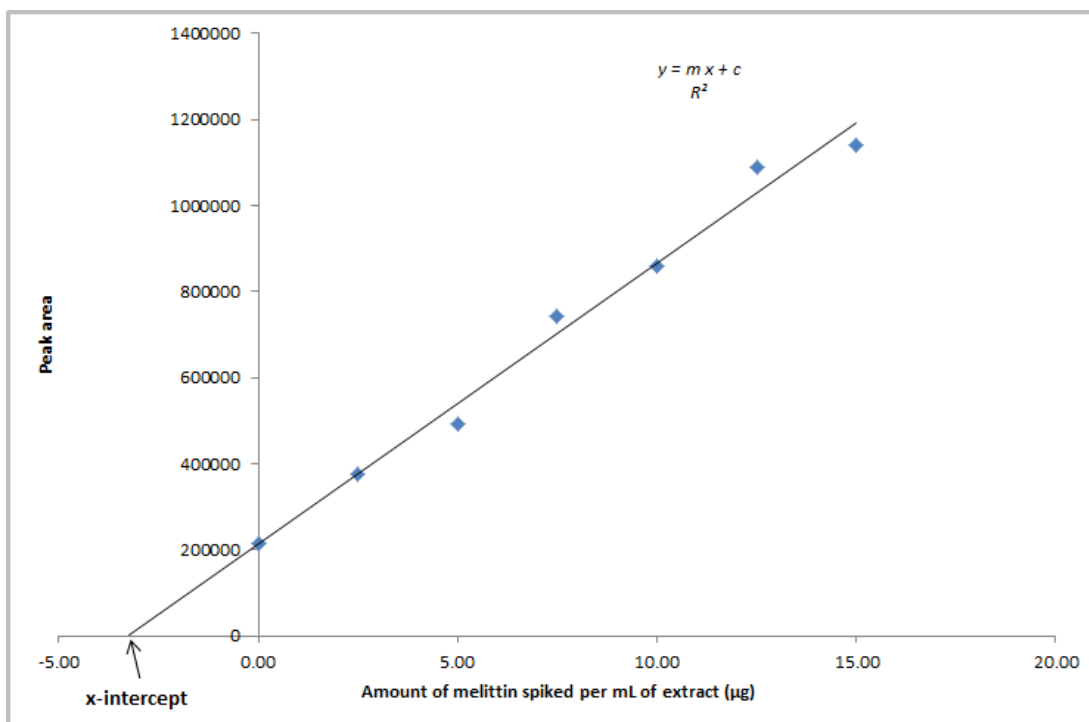


Figure 7.4: Calibration plot of peak area versus amount of melittin spiked into the extract of cream E replicate 1. The values of m , c and R^2 for this assay were 65242.4, 212602.9 and 0.9868 respectively.

In this experiment initial analyses had given us varying composition of melittin in the creams ranging from approximately 5 to 100 ppm ($\mu\text{g/g}$). This translates to a melittin content of about 0.5-10 μg per 100mg of the cream. Thus in this work, the samples were spiked with the melittin standard at 0, 25, 50, 75, 100, 125, and 150 μg per 100mg. These spiking levels conform to the sequence $x_1 \approx x_0$, $x_2 = 2x_1, \dots$, $x_p = px_1$ (x being analyte amount) which is generally acceptable (Danzer and Currie, 1998). The levels are nevertheless slightly below those recommended by Ellison and Thompson (2008) where at least 5 times the expected concentration of analyte should be used with repetitive measurements, if necessary, to improve precision (Ellison and Thompson, 2008). Clearly the latter approach also reduces the total amount of sample preparation time required. Based on results obtained and observations made during this assay, it is quite clear that the extraction and determination of melittin in the creams is a complex and laborious process which might introduce some errors depending on the degree of control of extraction conditions. The liquid layers formed after solvent extraction centrifugation were quite distinctly separated, but with a white precipitate forming at the liquid-liquid interface for 3 of the samples analysed

(C, E and F). This was thought to be possibly due to lignin from the herbal components stated to be present in these products. Preliminary LLE extracts without SPE had exhibited poor compatibility with the reversed phase analytical column leading to significant peak distortions. This was understood to arise from matrix interferents that probably suppressed melittin ionisation or its ability to chromatograph properly leading to poor chromatographic efficiency as peaks became broader and noisier, especially at spiked analyte concentrations $\leq 2.5 \mu\text{g/mL}$. Extraction with either aqueous or organic solvent alone proved inadequate as this led to incomplete dispersion of the creams. Ideally a good SPE method should achieve strong enough retention of an analyte on the column during sample loading and washing steps so that it can be concentrated and eluted in a more controlled manner to obtain relatively clean fractions (Moldoveanu and David, 2015). The initial lack of adequate retention of melittin on the SPE cartridge was found to be associated with fast loading under vacuum. Allowing the sample to load slowly, freely under gravity, overcame this problem. Attempts at preventing early breakthroughs by using high pH (at which the melittin was less ionised) during LLE proved fruitless due to low extraction recovery. This observation concerning the role of low pH (with formic acid) in the extraction of melittin from the cream might have been expected since a basic amphiphilic peptide such as melittin needs to be ionised in order to effectively partition into the aqueous layer that was analysed in this assay. Complete elimination of formic acid thus prevents such ionisation leading to insufficient extraction.

Aqueous solutions of whole BV demonstrated gradual degradation of melittin within the ²¹Lysine-²²Arginine-²³Lysine-²⁴Arginine region of the amino acid sequence under sterile conditions at room temperature (Chapter 6). Zhou *et al.* (2010) have previously reported a similar behaviour in pure melittin and apamin aqueous samples as well as in aqueous crude BV extracts (Zhou *et al.*, 2010). It was observed that purified melittin degrades comparatively much more slowly, if at all, than when it is in the crude venom. The observed activity appears to be enzyme catalysed and the enzyme involved seems to be trypsin-like. It is probable that the observed activity is due to a serine carboxy-peptidase already identified in BV as an allergen through genome analysis. That would mean that the method of purification of melittin either removes

or denatures this peptidase activity. Indeed, this is not surprising given that phospholipase and a number of other proteases were found in fraction F-2 (not F-3, which contained melittin) after purification as discussed in Chapter 4, Section 4.3.3.2. Currently it cannot be confirmed whether or not such degradation does occur in the formulated products and, if it does, the extent of such degradation. Thus the results of this assay can only confirm the melittin content of the creams at the time of analysis which may differ from the original amount incorporated.

7.5 Conclusion

A reversed phase LC-MS method was developed for the assay of melittin in 6 commercially available creams containing unspecified amounts of purified BV. Given that the proportions of BV in the products were not specified, it is not possible to comment on how well the products conform to a label claim. Extraction recovery suggests the accuracy of the assay method to be acceptable, although the blank matrix was an entirely different cream altogether, but with no BV in it. This might have biased the results of extraction recovery since this can vary across different blank matrices. Nevertheless there, certainly, is significant variation in the amount of melittin measured in the creams which ranged between 3.2-37.2 ppm, which is more than tenfold but with satisfactory intra and inter- assay precisions. These levels fall close to the IC_{50} values of melittin of 2.5-4.0 $\mu\text{g/mL}$ in human epithelial (PNT2A) cells and 14.8 $\mu\text{g/mL}$ in normal human fibroblasts (HS27 cells) as determined *in vitro* (Chapter 5). Production of a good quality product requires adequate quality control for the finished product. The chemical and physical stability of BV in cream matrices would require careful assessment and this is something which can now be done with this method.

Chapter Eight

Effect of Bee Venom and its Fractions on the Release of Pro-Inflammatory Cytokines in PMA-Differentiated U937 Cells Co-Stimulated with LPS

8 Effect of Bee Venom and its Fractions on the Release of Pro-Inflammatory Cytokines in PMA-Differentiated U937 Cells Co-Stimulated with LPS

Jonans Tusiimire¹, Jennifer Wallace², Nicola Woods¹, Mark J. Dufton², John A. Parkinson², Grainne Abbott¹, Carol J. Clements¹, Louise Young¹, Jin Kyu Park³, Jong Woon Jeon³, Valerie A. Ferro¹ and David G. Watson^{1,*}

¹ Strathclyde Institute of Pharmacy and Biomedical Sciences, University of Strathclyde, 161 Cathedral Street, Glasgow G4 0RE, U.K.

² WestCHEM Department of Pure and Applied Chemistry, University of Strathclyde, 295 Cathedral Street, Glasgow G1 1XL, U.K.

³ #204, Beesen Co. Ltd., Bio Venture Town, Yuseong Daero 1662, 34054 Dae Jeon, Korea

* Correspondence: d.g.watson@strath.ac.uk; Tel.: +44-141-548-2651; Fax: +44-141-552-6443

This chapter constitutes a published research article:

Jonans Tusiimire, Jennifer Wallace, Nicola Woods, Mark J. Dufton, John A. Parkinson, Grainne Abbott, Carol J. Clements, Louise Young, Jin Kyu Park, Jong Woon Jeon, Valerie A. Ferro and David G. Watson (2016). Effect of Bee Venom and its Fractions on the Release of Pro-Inflammatory Cytokines in PMA-Differentiated U937 Cells Co-Stimulated with LPS. *Vaccines*, **4**(2): 11.

Wallace J., Parkinson J. A. and Dufton M. J. contributed towards NMR analyses; Woods N., Young L., Abbott G. and Clements C. J. contributed towards bioassays; Park J. K. and Jeon J. W. supplied the crude bee venom; and Watson D. G. and Ferro V. A. conceived the project and contributed towards the writing of the manuscript.

Abstract

The venom of *Apis mellifera* (honey bee) is a complex mixture, composed of peptides, proteins, biogenic amines, and lipids, which produces powerful toxic effects in vertebrates and invertebrates. It is reported to have application in immunotherapy, but consistent evidence to support its immunomodulatory claims is lacking. Four fractions from whole bee venom (BV) were prepared by reversed phase medium pressure chromatography. Their ability to induce production of cytokines TNF α , IL-1 β and IL-6 in phorbol-12-myristate-13-acetate (PMA) treated U937 cells was assessed. The aim of this study was to evaluate the effect of co-stimulation of the cells with lipopolysaccharide (LPS) and BV fractions at sub-toxic levels. Cell viability tests showed that fractions F-1 and F-2 were relatively non-cytotoxic with IC₅₀ values >100 $\mu\text{g/mL}$. Fraction F-3, which contained melittin, was the most cytotoxic with an IC₅₀ value of 5.4 $\mu\text{g/mL}$ (95% confidence interval, CI: 4.43-6.66 $\mu\text{g/mL}$). The lipid-containing organic fraction, F-4, had an IC₅₀ value of 68.8 $\mu\text{g/mL}$. The levels of the three cytokines produced by stimulation with the four fractions and crude BV without LPS were not significantly different from negative control values. However, co-stimulation of the cells with LPS and F-4 induced a 1.6-fold increase in TNF- α level ($p < 0.05$) compared with LPS alone. Likewise, LPS-induced IL-1 β production was significantly synergised in the presence of F-1 (9-fold), F-2 (6-fold), F-3 (4-fold) and F-4 (2-fold) fractions, but was only slightly enhanced with crude BV (1.5-fold) relative to LPS. Furthermore, the LPS-stimulated production of IL-6 was not significantly increased in cells co-treated with F-2 and F-3, but the organic fraction (F-4) showed an inhibitory effect ($p < 0.05$) on IL-6 production. The latter was found to contain a lipid whose structure was elucidated by NMR spectroscopy to be (Z)-9-eicosen-1-ol. The effects observed with the purified BV fractions were more marked than those obtained with the whole venom. These findings demonstrate that BV may have potential as a vaccine adjuvant.

Key words: Bee venom, pro-inflammatory cytokines, adjuvants, LPS stimulation, U937 cells, *Apis mellifera*, PMA, ELISA, (Z)-9-eicosen-1-ol.

8.1 Introduction

Bee venom (BV) is mainly used as a defensive tool by the honey bee and its primary function is to inflict distracting pain and incapacity on any intruders into the hive (Moreau, 2013). Despite its toxic effects, it has been claimed that sub-cutaneous administration to humans can bring about relief from the pain arising from arthritis and rheumatism (Hider, 1988, Lee *et al.*, 2005), tendonitis, multiple sclerosis, wounds, and gout (Chen and Lariviere, 2010; Rho *et al.*, 2009; Zhou *et al.*, 2010). The chemical composition of BV is complex, but the primary ingredients are bioactive peptides, proteins, and several other biomolecules (Baracchi *et al.*, 2011; Ferreira Junior *et al.*, 2010; Sciani *et al.*, 2010; Van Vaerenbergh *et al.*, 2013; Zhou *et al.*, 2010). The principal component is a 26 amino acid haemolytic peptide, melittin, which accounts for about 50-60% of the venom by dry weight and is responsible for most of the observed effects. The other peptides/polypeptides (and their composition by dry weight) are apamin (1-3%), mast cell degranulating peptide (MCDP) (1-3%), secapin (1-2%) and adolapin (2-5%). The two main proteins present in BV are phospholipase A₂ (PLA₂; 10-12%) and hyaluronidase (1-3%) that are considered to be its principal allergens. The venom also contains variable amounts of histamine (0.5-2%), dopamine (0.2-1%), norepinephrine (0.1-0.7%), glucose/fructose (2%), phospholipids (5%), aminobutyric acid (0.5%) and α -amino acids (1%) (Matysiak *et al.*, 2011; Sciani *et al.*, 2010; Vick and Shipman, 1972).

Some of the BV components have been reported to possess various, and sometimes conflicting, immune-related effects. Available evidence suggests that apamin (Regnier-Vigouroux *et al.*, 1988), histamine (Park *et al.*, 2014), MCD peptide (Buku, 1999; Buku *et al.*, 2005) and PLA₂ (Bourgeois *et al.*, 2015), significantly increase the inflammatory response. The small neurotoxic peptide apamin (MW 2.0 kDa) is a Ca²⁺-activated K⁺-channel blocker, which has been reported to increase murine T-cell proliferation (Regnier-Vigouroux *et al.*, 1988). However, it has also been reported to inhibit histamine release in lung tissues, suggesting that it could decrease allergic airway inflammation through mast cell stabilisation (Ichinose *et al.*, 1995). Park *et al.* (2004) also demonstrated that histamine increased the production of IL-6 in nasal fibroblasts and induced nuclear factor kappa B (NF- κ B) (Park *et al.*, 2014), a

transcriptional factor for many pro-inflammatory genes (Lawrence, 2009). On the other hand, MCD peptide was reported to inhibit histamine release from mast cells (Buku, 1999) by binding, in a dose related manner, to mast cell receptors thereby partially inhibiting IgE binding to these receptors (Buku *et al.*, 2001). Similarly, PLA₂ was shown to activate T-cells via its action on phosphodiacylglycerides to form small neoantigenic factors *in vivo*, in a process dependent on antigen presentation by CD1a proteins (Bourgeois *et al.*, 2015).

Conversely, some components of BV have been reported to possess anti-inflammatory actions. For instance, the basic polypeptide adolapin (MW 11.5 kDa) was reported to possess anti-inflammatory and analgesic activities in carrageenan-, prostaglandin- and adjuvant-induced rat oedema and adjuvant polyarthritis (Shkenderov and Koburova, 1982). These effects were attributed to inhibition of prostaglandin synthesis, via cyclooxygenase inhibition, as well as through central mechanisms (Shkenderov and Koburova, 1982). Adolapin was also shown to inhibit the activity of BV PLA₂ and human lipoxygenase from platelets, and possessed anti-pyretic effects (Koburova *et al.*, 1985).

Regarding the principal component melittin, past reports on its immuno-modulating effects are rather contradictory. For instance, whereas Bramwell *et al.* (2003) reported dose-dependent mucosal adjuvant action of intranasal melittin co-administered with tetanus and diphtheria toxoids in mice (Bramwell *et al.*, 2003), a number of other studies have reported its “neutralising” effects on LPS in murine macrophage cell lines (Park *et al.*, 2004; Park *et al.*, 2007). The adjuvant effects of melittin were linked to its enhancement of vaccine absorption across the mucosal lining, which led to higher antibody (IgG) titres than those of either component alone (Bramwell *et al.*, 2003). On the other hand, its antagonistic effects on LPS were linked to inhibition of NF-κB binding to DNA (Park *et al.*, 2004) and phosphorylation of IκB kinase (Park *et al.*, 2007), respectively. In addition, treatment of LPS-stimulated BV2 immortalized murine microglial cells with BV or melittin, decreased the expression of pro-inflammatory cytokines (IL-1β, IL-6 and TNF-α) and inhibited inducible nitric oxide synthetase (iNOS) production and nitric oxide (NO) expression, as was the expres-

sion of cyclooxygenase-2 (COX-2) and prostaglandin E₂ (PGE₂) (Moon *et al.*, 2007; Srivastava *et al.*, 2012). These anti-inflammatory effects were linked mainly to melittin's leucine zipper sequence, which contains two leucine residues since Leu-Ala substitution in this sequence progressively reduced this neutralising effect (Srivastava *et al.*, 2012). Jang *et al.* (2005) also reported anti-inflammatory effects of BV in RAW 264.7 macrophages that were attributed to a down regulation of iNOS, COX-2, NF- κ B and mitogen-activated protein kinases (MAPKs) (Jang *et al.*, 2005). In addition, Park *et al.* (2004) also reported that BV and melittin decreased carrageenan-induced oedema and adjuvant-induced arthritis in rat models consistent with their inhibitory effects on LPS-induced expression of COX-2, cytosolic PLA₂ and iNOS, and on the generation of PGE₂ and NO (Park *et al.*, 2004). BV and melittin also prevented LPS-induced transcriptional and DNA binding activity of NF- κ B via inhibition of I κ B release (Hider, 1988).

Since upregulation of most pro-inflammatory genes (e.g. cytokines and chemokines) relies on activation of NF- κ B (Lawrence, 2009), inactivation of the latter by BV or its components would be a key mechanism for exerting anti-inflammatory effects (Vick *et al.*, 1972). However, in a previous study, no significant inactivation of IL-1 β -induced NF- κ B was observed in fibroblast-like synoviocytes from rheumatoid arthritis patients, as well as in dermal fibroblasts and red blood cells from healthy volunteers, after treatment with BV and melittin (Stuhlmeier, 2007). In addition, there was no effect on the phosphorylation or degradation of I κ B, and even at high concentrations of BV and melittin no effects on NF- κ B-p50-DNA interactions were observed. Instead, significant increases in mRNA levels of several pro-inflammatory genes (including COX-2, IL-1 β , TNF- α) and large quantities of oxygen radicals were observed following exposure to BV or melittin (Stuhlmeier, 2007). This suggested that melittin alone and BV as a whole are pro- rather than anti-inflammatory.

In the current study, the effects of BV and its fractions on the production of cytokines TNF- α , IL-1 β and IL-6 were investigated in PMA-treated U937 cells. The latter belong to a monocytic differentiation lineage derived from malignant cells of a patient with generalised histiocytic lymphoma (Sundstrom and Nilsson, 1976), and

their differentiation with PMA, a potent tumour promoting agent (Minta and Pambrun, 1985), is known to impart functional properties typical of macrophages (Passmore *et al.*, 2001; Verhoeckx *et al.*, 2004; Minta and Pambrun, 1985). The presence of synergy between BV and LPS, a standard antigen, in inducing the production of the pro-inflammatory mediators would suggest the potential application of BV as a source of immuno-modulating agents for use as vaccine adjuvants.

8.2 Materials and methods

8.2.1 Cell culture

U937 cell cultures (obtained from ECACC, Porton Down, Salisbury) were seeded at 3×10^5 cells/mL in RPMI-1640 (Lonza, Verviers, Belgium) supplemented with 2 mM L-glutamine (Life Tech, Paisley, UK), 100 IU/100 µg/mL penicillin/streptomycin (Life Tech, Paisley, UK) and 10% (v/v) foetal bovine serum (FBS) (Sigma-Aldrich, Dorset, UK). Cells were subcultured every 2-4 days and maintained at 37 °C in a humidified atmosphere of 5% CO₂.

8.2.2 Test sample isolation, preparation and analysis

Crude BV (supplied by Beesen Co. Ltd, Dae Jeon, Korea) was prepared by dissolving 10 mg in 1 mL of dimethyl sulphoxide (DMSO, Sigma-Aldrich) followed by filtration through a 0.2 µm filter (Millex®, Sigma-Aldrich). Venom fractions F-1 to F-4 were isolated from 800 mg of crude BV by reversed phase medium pressure liquid chromatography (MPLC) on a Reveleris® iES flash chromatography system (Grace Davison Discovery Sciences, Carnforth, UK) with dual UV ($\lambda = 220/280$ nm) and evaporative light scattering (ELSD) detection. The sample was mixed with 3g of Celite® before loading it into a dry-loading cartridge. The column used was an Easyvarioflash D24 cartridge (VWR International, Lutterworth, UK) packed with *ca* 13 g of Polymeric Retain PEP for SPE (Thermo Scientific, Paisley, UK) as previously described (Tusiimire *et al.*, 2015). Fraction F-1 was eluted with 100% water and F-4 with 100% acetonitrile (Sigma-Aldrich), both solvents being of HPLC grade.

Fractions F-2 and F-3 were eluted in water/acetonitrile mixtures of 80/20% and 50/50%, respectively. The resulting purified fractions were freeze-dried and reconstituted at 10 mg/mL in DMSO. Liquid chromatography-mass spectrometry (LC-MS) analysis of F-4 was carried out on a Surveyor HPLC system interfaced to an Orbitrap Mass Spectrometer (Thermo Fisher Scientific, Bremen, Germany) using an ACE 3 C18 column (150 × 3.0 mm, 3 µm particle size) supplied by Hichrom Ltd (Reading, UK).

8.2.3 Cell viability assay

U937 cells were seeded at 2.25×10^4 cells/well in 96-well plates (Corning®, Sigma-Aldrich) and incubated in the presence and absence of BV or its fractions at final concentrations ranging from 100 µg/mL to 3 ng/mL ($n = 3$) in 100 µL volumes per well. Triton X at 1% (v/v) Triton X to serve as a positive control. The plate was then incubated at 37 °C and 5% CO₂ in a humidified atmosphere for 48 h. After incubation, Alamar® Blue (VWR International, Lutterworth, UK) was added at a final concentration of 10% and the plate incubated for a further 6 h. Fluorescence readings of the plate were taken using a Wallac Victor 2 microplate reader ($\lambda_{\text{EX/EM}}$: 560/590 nm). All readings were corrected for background by subtracting the mean fluorescence of the Triton X wells. Cell viability was then calculated for each well as a percentage of fluorescence readings in the presence of test sample relative to the value of the negative controls. The resulting data were analysed with GraphPad Prism 3 (San Diego, USA) to obtain dose-response curves for each sample and their corresponding mean inhibitory concentration (IC₅₀) values.

8.2.4 Induction of cell differentiation

U937 cells were seeded at 4.5×10^4 cells/well in a volume of 450 µL in 24-well tissue culture plates (Corning®, Sigma-Aldrich, UK) ($n = 3$) in media containing 60 ng/mL PMA (Sigma-Aldrich, UK). A control well containing cells in media without PMA was also included. The cells were then incubated in a humidified atmosphere at 37 °C and 5% CO₂ for 48 h. Micrographs of the cells were taken with a Moticam

1000 (1.3 M Pixel) camera, mounted on an Olympus IM microscope, after 24 and 48 h for evidence of differentiation.

8.2.5 Stimulation of cytokine release by PMA

After 48 h differentiation, the media was aspirated and replaced with fresh media, without PMA, and the cells incubated for a further 24 h. At this point, samples of BV or fractions, with or without *Escherichia coli* (*E. coli*) LPS (Sigma-Aldrich), were then added from a separate sample dilution plate prepared using 10 mg/mL stock solutions (**Table 8.1**). The final concentrations of the samples on the cell culture plate were 100 µg/mL (F-1 and F-2), 3 µg/mL (F-3 and BV) and 30 µg/mL (F-4), respectively. The final LPS concentration in the LPS-containing samples was 1 µg/mL.

Table 8.1: Volumes of LPS, fractions and media used to stimulate cytokine production in PMA-differentiated U937 cells.

Sample	Volume added (µL)			Concentration (µg/mL)	
	Stock solution (10mg/mL)	LPS (1 mg/mL)	Media	Fraction	LPS
F-1	80.0	8.0	1912.0	400.0	4.0
F-2	80.0	8.0	1912.0	400.0	4.0
F-3	2.4	8.0	1989.6	12.0	4.0
F-4	24.0	8.0	1968.0	120.0	4.0
BV	2.4	8.0	1989.6	12.0	4.0
LPS	-	8.0	1992.0	-	4.0

8.2.6 Assessment of cytokine release

Three ELISA kits from R&D Systems (Abingdon, UK) were used to assess release of interleukin (IL)-1β/IL-1F-2, IL-6, and tumour necrosis factor (TNF)-α from LPS-stimulated and non-stimulated U937 cells. The ELISA assay was carried out according to the kit manufacturer's instructions, except that the colour substrate used (3,3',5,5'-tetramethylbenzidine, TMB) was from Sigma-Aldrich (Dorset, UK) and came ready for use. The reaction was stopped with 2N sulphuric acid (H₂SO₄) and the absorbance was measured immediately at 450 nm wavelength using a Spectra-

Max Pro 5 (Wokingham, UK) with wavelength correction by subtracting readings taken at 570 nm.

8.2.7 Data analysis

Standard calibration curves were plotted by fitting the optical density data of TNF- α , IL-1 β and IL-6 to 4-parameter logistic (4-PL) regression curves (**Table 8.2** & Figures B1-B9 in Appendix II). Each of these standards was prepared in duplicate at each of the concentrations in the ranges recommended by the manufacturer. The 4-PL regression equation is given by the equation:

$$y = d + \frac{a-d}{1+\left(\frac{x}{c}\right)^b} \quad (20)$$

where: y is the response value (i.e. measured optical density), x is the concentration (in pg/mL) and a , b , c , and d are constants. The regression analysis also computes the R^2 value which gives an indication of how best the fitted curve agrees with the data. From equation 20, the unknown concentration, x , of a sample of optical density, y , can be calculated according to the equation:

$$x = c \left(\frac{a-d}{y-d} - 1 \right)^{\frac{1}{b}} \quad (21)$$

Using equation 21, the concentrations of TNF- α , IL-1 β and IL-6 induced by each of the samples assayed (with and without LPS) were calculated and expressed as ratios of the mean cytokine level induced by LPS (positive control), assayed in triplicate ($n=3$). The resulting data were then analysed with GraphPad Prism to obtain bar graphs whose statistical significances were tested at 95% confidence level relative to the mean positive control ratio of 1.0.

Table 8.2: The constant values of the 4-PL regression curve fitted to the data of TNF- α , IL-1 β and IL-6 standards respectively (n=3).

<i>Constants</i>	<i>TNF-α</i>			<i>IL-1β</i>			<i>IL-6</i>		
	<i>n = 1</i>	<i>n = 2</i>	<i>n = 3</i>	<i>n = 1</i>	<i>n = 2</i>	<i>n = 3</i>	<i>n = 1</i>	<i>n = 2</i>	<i>n = 3</i>
a	0.265	0.194	0.114	0.132	0.184	0.103	0.104	0.0708	0.0377
b	1.11	1.07	1.2	1.02	1.14	1.25	1.33	1.08	1.16
c	711	1180	541	191	222	136	165	444	364
d	5.15	6.03	4.6	5.72	5.24	4.35	3.95	5.21	4.82
R ²	1.000	1.000	1.000	1.00	1.000	1.000	0.999	1.000	1.000

8.2.8 NMR spectroscopy

NMR spectroscopy studies were carried out on 7.4 mg of a sample of fraction F4 from BV. This was dissolved in 600 μ L DMSO- d_6 contained in a 5 mm \varnothing standard NMR tube.

NMR data were acquired on a Bruker AVANCE II⁺ NMR spectrometer equipped with a 14.1 T Ultrashield superconducting magnet operating at a ¹H resonance frequency of 600.13 MHz. All data were acquired using a BBO-z-atm probehead operating at ambient temperature (298 K) regulated by means of a BCU-05 chiller unit.

1D ¹H NMR spectra were acquired with 16 transients over a frequency width of 7.2 kHz (12.0 ppm) centred at a frequency offset of 5.0 ppm into 32 K data points for an acquisition time of 2.27 s using a 30 degree radio frequency (r.f.) pulse and a recycle delay of 2.0 s.

1D ¹³C-¹H NMR spectra were acquired with 1024 transients over a frequency width of 33.33 kHz (220.8 ppm) centred at a frequency offset of 100.0 ppm into 32 K data points for an acquisition time of 491.5 ms using a 30 degree r.f. pulse with continuous composite pulse decoupling applied at the ¹H resonance frequency and using a recycle delay of 0.7 s.

2D [¹H, ¹H] phase-sensitive double quantum filtered COSY and TOCSY NMR data were acquired with 8 and 4 transients respectively for each of 360 TPPI t_1 increments

into 2 K complex data points over ω_2 and ω_1 frequency widths of 3.6 kHz (6 ppm, ω_2 acquisition time = 284.7 ms) centred at a frequency offset of 3.0 ppm and using zero-quantum suppression to reduce interference from zero-quantum effects (Thrippleton and Keeler, 2003).

2D [^1H , ^{13}C] HSQC NMR spectra were acquired in both traditional mode and over a reduced ω_1 frequency width using non-uniform sampling (NUS) to increase F1 resolution. Traditional low resolution NMR data were acquired using a multiplicity edited, echo-antiecho gradient selected approach with sensitivity improvement (Bruker pulse program hsqcedetgpsisp2.3). Data were acquired into 2 K complex data points over an ω_2 frequency width of 3.6 kHz (6.0 ppm) centred at a frequency offset of 3.0 ppm and an ω_1 frequency width of 24.9 kHz (165.0 ppm) centred at a frequency offset of 70.0 ppm with 8 transients for each of 256 t_1 increments. High resolution data were acquired with the ω_1 frequency width set to 4.5 kHz (30.0 ppm) centred at a frequency offset of 30.0 ppm nominally using 2048 t_1 increments sampled at 25% NUS (equivalent to 256 NUS t_1 increments) using a random generator seed of 54321 for NUS purposes.

2D [^1H , ^{13}C] HMBC NMR spectra were also acquired in both traditional and NUS modes into 2 K complex data points over an ω_2 frequency width of 3.6 kHz (6.0 ppm) centred at a frequency offset of 3.0 ppm and an ω_1 frequency width of 33.55 kHz (222.4 ppm) centred at a frequency offset of 100.0 ppm with 8 transients for each of 256 traditional and NUS (25% sampled) t_1 increments respectively. Data were acquired with gradient coherence selection and used a low-pass filter to reduce the appearance of artefacts from $^1J_{\text{HC}}$ coupling.

NUS data were processed using the MDD (multidimensional decomposition) algorithm developed by Orekhov *et al.* followed by Hilbert transformation to allow traditional phase correction and processing of the data (Jaravine *et al.*, 2008).

8.3 Results

The fractions revealed mixed components in F-1 and F-2, while F-3 and F-4 contained single components respectively. The major constituents of F-1 were putatively identified to be histamine, proline, noradrenaline, 5-aminovaleric acid, cellobiose, and arginine. Fraction F-2 contained mainly PLA₂ as well as varying amounts of apamin, secapin, and MCD peptide. On the other hand, melittin was the principal component of F-3 (96% purity) while the organic fraction, F-4, mainly contained a new compound identified through NMR analysis as (Z)-9-eicosen-1-ol, and trace levels of an unidentified phospholipid.

8.3.1 Viability of U937 cells incubated with BV fractions

Cell viability studies were carried out ($n = 3$) to obtain IC₅₀ values (**Figure 8.1**). Samples F-1 and F-2 gave IC₅₀ of greater than 100 µg/mL. In contrast, F-3 gave the lowest IC₅₀ value at 5.4 µg/mL (or 1.9 µM). The IC₅₀ value of F-4 was 68.8 µg/mL. Micrographs of the cells taken after 24 and 48 h confirmed the assay results obtained with the Alamar® Blue assay (**Figure 8.2**). These micrographs also revealed significant microscopic differences in the appearance of cells treated with F-3 and F-4 even in wells where Alamar® Blue readings were comparable. Unlike necrosis caused by melittin, which revealed the cells to have burst to release their protoplasm, non-viable F-4-treated cells appeared to have an intact cell outline, implying that the mechanism by which the lipid exerts its cytotoxic effect on U937 cells may be different from that of melittin, which acts through cell lysis (Gajski and Garaj-Vrhovac, 2013).

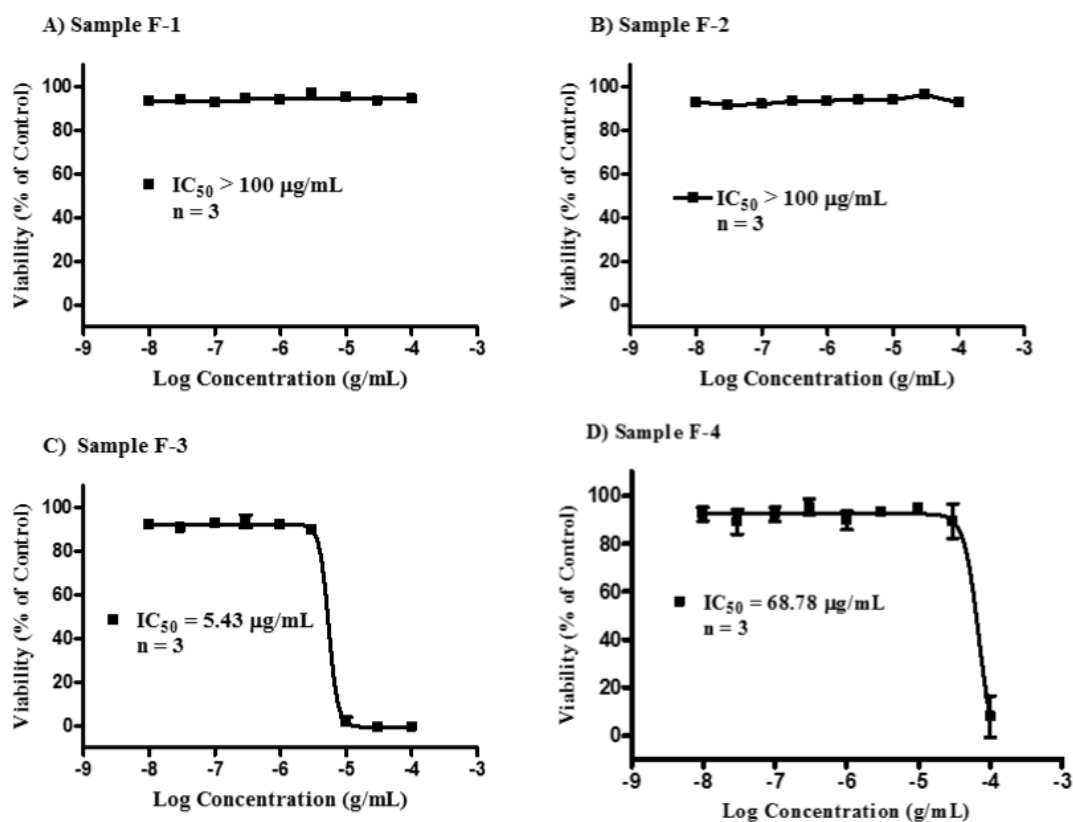
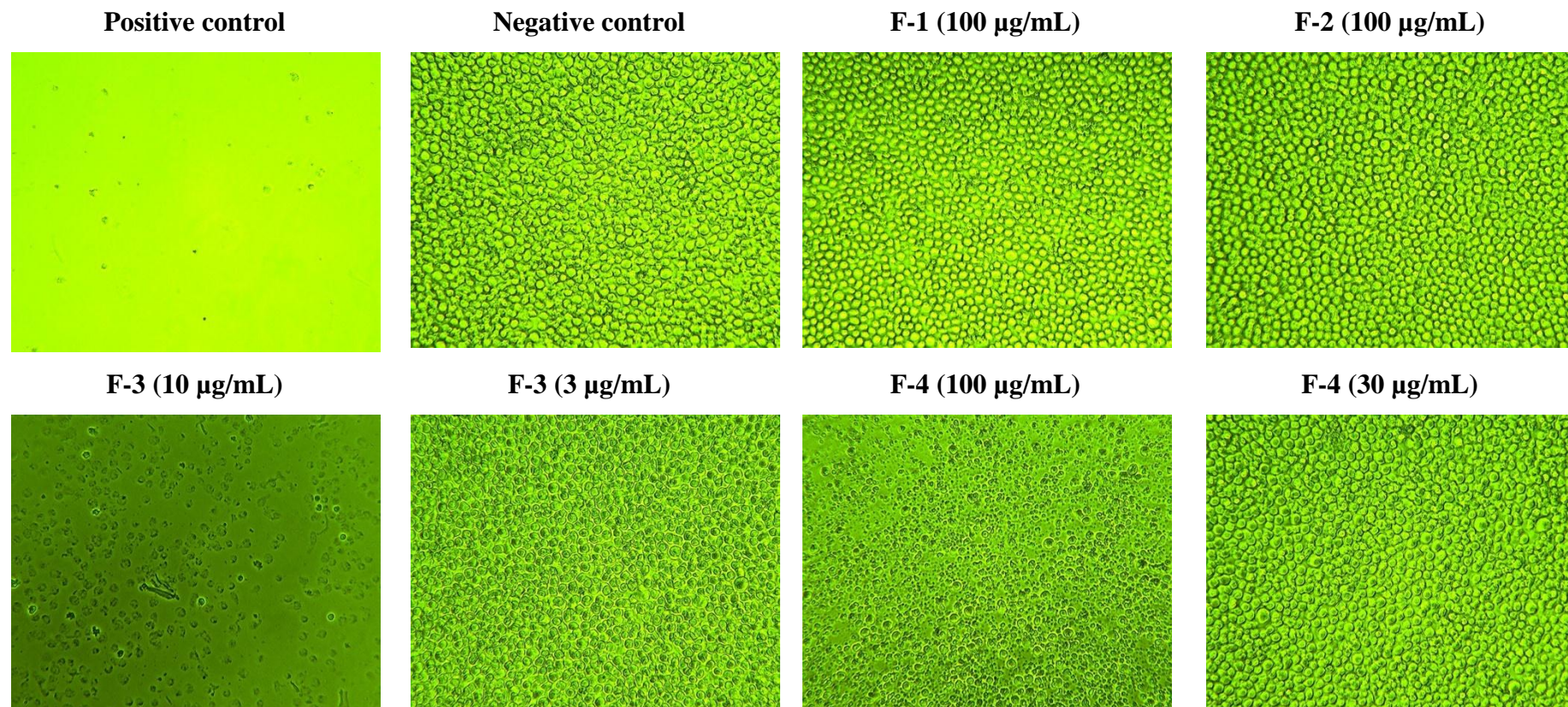


Figure 8.1: Viability of U937 cells incubated with BV sample fractions F-1 to F-4. Fraction samples F-1 (A) and F-2 (B) were non-cytotoxic each with IC_{50} value $>100 \mu\text{g/mL}$. Fraction sample F-3 (C, melittin) was the most cytotoxic with IC_{50} of 5.43 (95% CI 4.43-6.66) $\mu\text{g/mL}$ while fraction sample F-4 (D, lipid) had an IC_{50} value of 68.78 $\mu\text{g/mL}$.



197

Figure 8.2: Cytotoxic effects of BV fractions on U937 cells. Fractions F-1 and F-2 were non-cytotoxic at the highest concentration of 100 µg/mL used while F-3 was the most cytotoxic on the cells as necrotic effects were observed even at 10 µg/mL (IC₅₀ 5.4 µg/mL). On the other hand, F-4 was cytotoxic above 30 µg/mL with IC₅₀ of 68.8 µg/mL (n=3). (Magnification = 100X).

8.3.2 Selection of BV and fraction concentrations for assay

ELISAs were carried out in order to determine the effect of the fractions on PMA-differentiated cells with respect to the production of three inflammatory mediators TNF- α , IL-1 β and IL-6. Since investigation of immunomodulatory effects had to be conducted using concentrations of the fractions where the cells remained viable, concentrations were selected for each fraction that were below their respective IC₅₀ values. Specifically, the highest concentration in the dilution series at which 100% viability of cells had been observed was used. Thus, since fractions F-1 and F-2 showed no potential cytotoxicity to the cells at 100 $\mu\text{g}/\text{mL}$, the highest concentration used in the assay for both fractions was 100 $\mu\text{g}/\text{mL}$. F-3 was assayed at 3 $\mu\text{g}/\text{mL}$ as it was cytotoxic at 10 $\mu\text{g}/\text{mL}$ (IC₅₀ 5.4 $\mu\text{g}/\text{mL}$) and 3 $\mu\text{g}/\text{mL}$ was the next concentration in the dilution series. By the same principle, F-4, which was cytotoxic at 100 $\mu\text{g}/\text{mL}$ (IC₅₀ 68.8 $\mu\text{g}/\text{mL}$) was assayed at 30 $\mu\text{g}/\text{mL}$ (Table 8.3). The mean viability (n = 3) of the cells at the concentrations selected for each of the fractions in the assay were F-1 (93%), F-2 (94%), and F-3 and F-4 (90% each), respectively, relative to the media.

Table 8.3: Concentrations of the fractions used in the assay of immunomodulatory effects on PMA-differentiated U937 cells.

<i>SN</i>	<i>Fraction</i>	<i>IC₅₀ ($\mu\text{g}/\text{mL}$)</i>	<i>Selected concentration ($\mu\text{g}/\text{mL}$)</i>
1	F-1	>100	100
2	F-2	>100	100
4	F-3	5.4	3.0
3	F-4	68.8	30.0

Note: For each fraction, the concentration selected was the highest non-toxic one.

8.3.3 Observed effects of PMA on U937 cells

After the cells had been incubated at 10⁵ cells/mL in the presence of PMA, they were observed microscopically at 24 and 48 h for the presence of features that confirmed whether or not they had differentiated (Otte *et al.*, 2011). The most marked effects of PMA observed in the cells which constituted differentiation were: cessation of cell

division, presence of a more regular cell outline, and a bigger cell size after 24 and 48h. In addition, differentiated cells formed some clusters, although these were not numerous in any given well. As expected, the cells became more adherent to the plate resulting in no visible lateral movement upon agitation. Micrographs were also taken of the treated cells and compared with those of U937 cells in control wells (absence of PMA) on the same plate (**Figure 8.3**) which confirmed the above morphological changes.

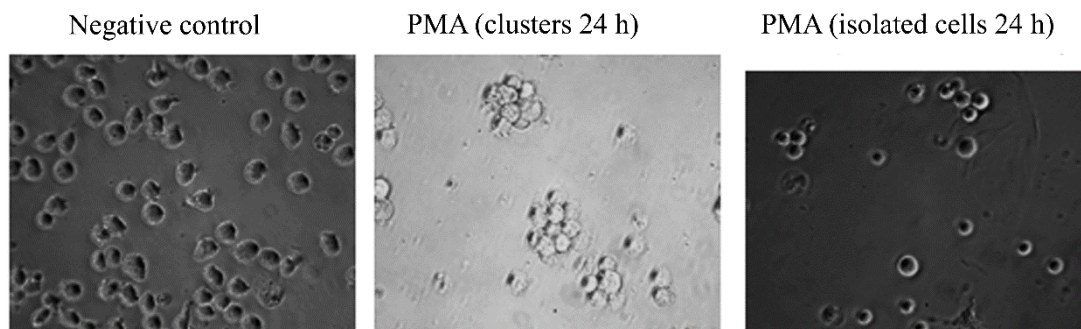
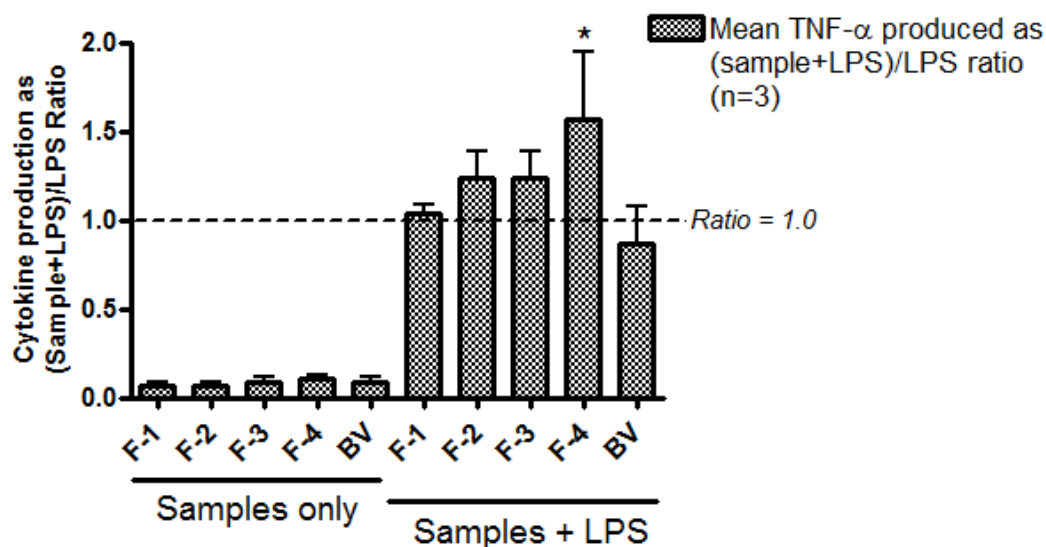


Figure 8.3: Effect of PMA on U937 cells. PMA was added to the cells at 60 ng/mL (n=3). (Magnification = 400X).

8.3.4 Effect on TNF- α production

All the BV fractions on their own did not induce significant TNF- α production in PMA-differentiated U937 cells relative to the negative control (culture media). However, when used in combination with LPS, there was noticeable enhancement (ratio > 1.0) in the amount of TNF- α produced compared to LPS alone (Table B1, Appendix II). This was statistically significant ($p < 0.05$) only with F-4, which produced a 1.6-fold increase in TNF- α in the cells (**Figure 8.4**).

Effect of bee venom fractions on TNF- α production in LPS-stimulated PMA-differentiated U937 cells



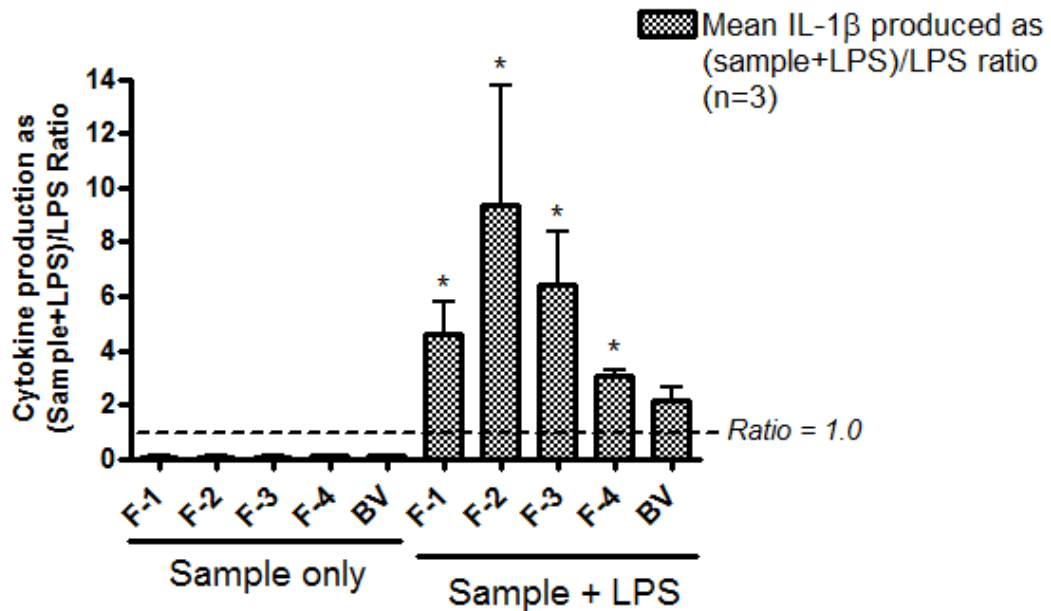
* Significant synergistic effect ($p < 0.05$) at 95% CI

Figure 8.4: Effect of BV and its fractions of TNF- α production in PMA-differentiated U937 cells. All the 5 samples tested produced slightly more than background levels of TNF- α but not significantly different from those of negative control (media). The level of TNF- α was significantly higher in fractions co-stimulated with F-4 and LPS compared to LPS but the other fractions did not show any significant changes in the levels of the cytokine ($n=3$).

8.3.5 Effect on IL-1 β production

The enhancement of IL-1 β /IL-1F2 by BV fractions in LPS co-stimulated U937 cells was much more pronounced than that observed with TNF- α . Fractions F-2 and F-3 greatly enhanced IL-1 β /IL-1F2 release in the cells by approximately 9- and 6-fold, respectively (Table B2, Appendix II). Additionally, F-1 (4-fold), F-4 (3-fold), and whole BV (2-fold) also enhanced the level of this cytokine with LPS co-stimulation, although the increase obtained with BV was not statistically significant (**Figure 8.5**). As can be seen from the figure, the fractions on their own did not induce any significant levels of the cytokine.

Effect of bee venom fractions on IL-1 β production in LPS-stimulated PMA-differentiated U937 cells



* Significant synergistic effect ($p < 0.05$) at 95% CI

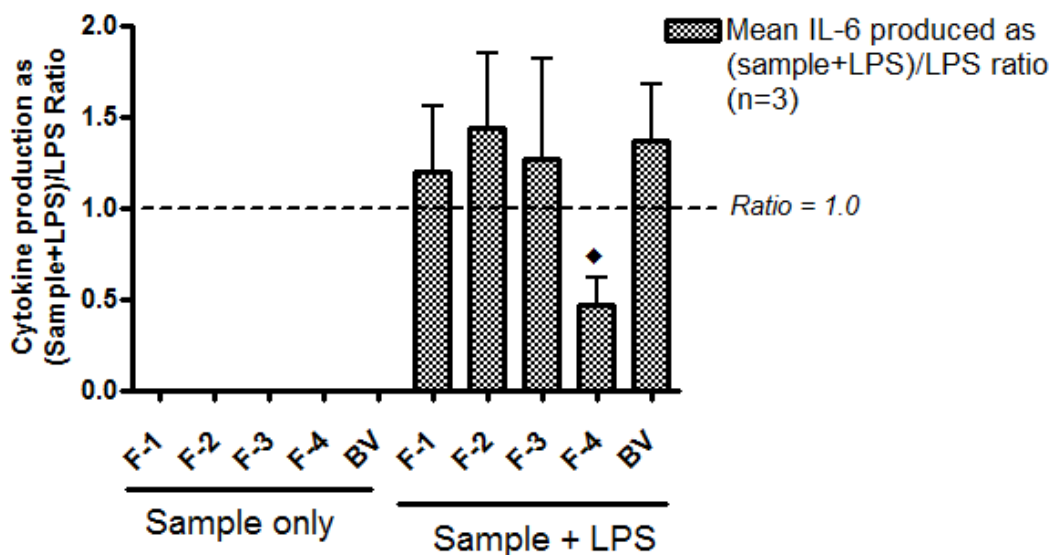
Figure 8.5: Effect of BV and its fractions of IL-1 β production in PMA-differentiated U937 cells. All the 5 BV fractions tested produced only background levels of IL-1 β when used alone. In the presence of LPS, there was significant synergy especially with F-2 and F-3 which resulted in 9- and 6-fold increase in production of the cytokine respectively. Significant synergy was also observed with F-1 (4-fold) and F-4 (3-fold) but not with BV despite a 2-fold increase in the latter (n=3).

8.3.6 Effect on IL-6 production

As with TNF- α and IL-1 β production, the amount of IL-6 produced by the cells in the presence of BV fractions alone was undetectable (F-1 to F-3) or not significantly different from levels observed in negative controls (F-4 and BV). Yet when the same fractions were incubated together with LPS, the amount of IL-6 produced by the cells was raised, compared to that of stimulation with LPS alone, by 20, 40, 30 and 30% with F-1, F-2, F-3 and BV, respectively; although these were not statistically significantly different from positive control values (Table B3, Appendix II). Surprisingly, and contrary to observations with TNF- α and IL-1 β , F-4 significantly decreased the

amount of IL-6 released with LPS co-stimulation in the PMA differentiated U937 cells by about 50% (Figure 8.6).

Effect of bee venom fractions on IL-6 production in LPS-stimulated PMA-differentiated U937 cells



◆ Significant antagonistic effect ($p < 0.05$) at 95% CI

Figure 8.6: Effect of BV and its fractions with and without LPS on IL-6 production in PMA-differentiated U937 cells. The level of IL-6 produced by BV fractions alone was undetectable. However, in combination with LPS, fractions F-1 to F-3 and BV enhanced the level of cytokine produced by LPS though not significantly. Interestingly, F-4 significantly inhibited cytokine production by about 50% of the mean positive control (LPS) value ($n=3$).

8.3.7 Identification of active compound in BV fraction F-4

Given its unusual effect on $\text{TNF-}\alpha$ and IL-6 release in PMA-differentiated U937 cells, we sought to identify the component present in F-4 by NMR spectroscopy. The one-dimensional (1D) ^1H NMR spectrum of F-4 (acquired at 298K in $\text{DMSO-}d_6$, Figure 8.7) gave 10 distinguishable signals with chemical shifts and integrals as detailed in

Table 8.4. Signal A, which corresponded to a ^1H chemical shift associated with a proton attached to an sp^2 -hybridized carbon centre (alkene), integrated to two proton equivalents. Multiplicity-edited 2D [^1H , ^{13}C] HSQC NMR data revealed that the signal was associated with a methine (CH) group, allowing the conclusion to be drawn that the molecule was likely to be a structure with close to two-fold symmetry about a double bond. Thus, based on this information, the two A protons were each assigned to either of the two carbon atoms sharing the double bond located approximately at the line of symmetry of the entire molecule. The signal envelope designated H integrated to twenty two proton equivalents and suggested the presence of long chains of methylene groups typical of a lipid.

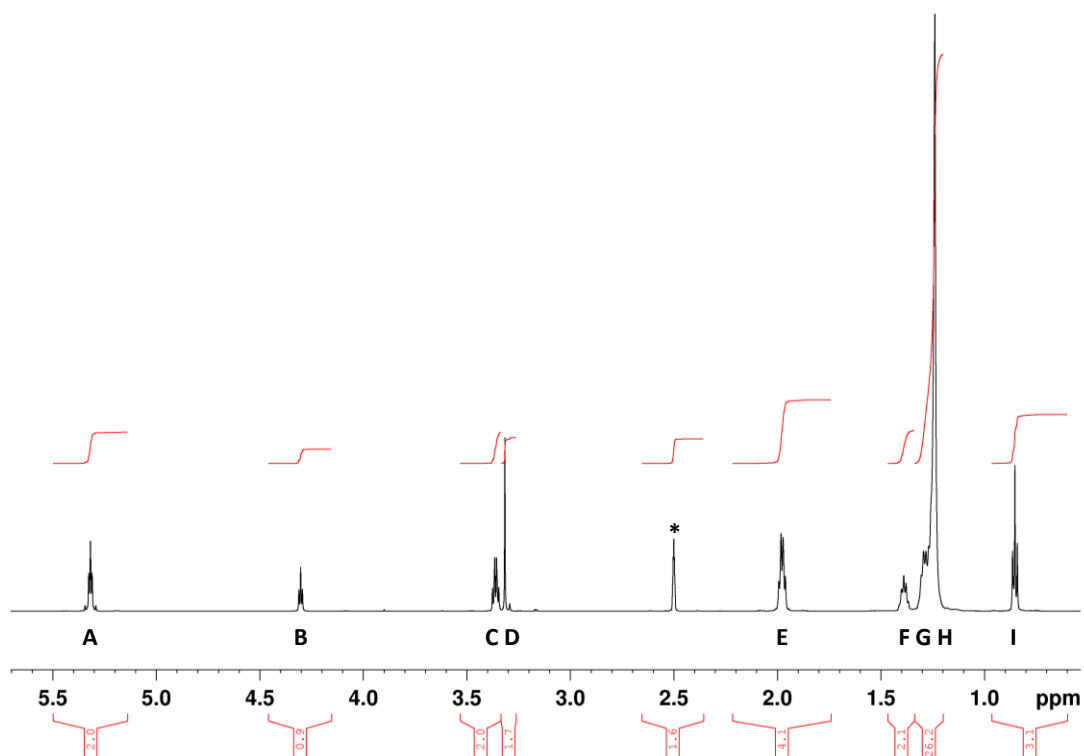


Figure 8.7: 600 MHz 1D ^1H NMR spectrum of the lipid component from fraction F-4 showing signal integrals. The signal indicated by * arises from the solvent and signal **D** is ascribed to water in $\text{DMSO}-d_6$.

Table 8.4: Data arising from the 1D ^1H NMR spectrum of the lipid component. Reference to the “Link to ^{13}C ” arises from analysis of the 2D [^1H , ^{13}C] HSQC NMR spectrum that reveals $^1J_{\text{HC}}$ correlations where labels *a-q* correspond to ^{13}C resonances shown in (Figure 8.8).

<i>Label</i>	δ (ppm)	<i>Integral</i>	<i>Type</i>	<i>Multiplicity</i>	<i>Link to ^{13}C</i>	<i>Proposal</i>
A	5.32	2	Alkene <u>CH</u>	Second order	a	Symmetric Alkene
B	4.30	1	- <u>OH</u>	t	-	- <u>CH₂-OH</u>
C	3.36	2	-CH ₂ -	dt	b	
D	3.32	1.7	H ₂ O	s	-	Water in DMSO
E	1.98	4	-CH ₂ -	q	m	
F	1.39	2	-CH ₂ -	pentet	c	
G	1.29	4	-CH ₂ -	q	f	
H	1.24	22	-CH ₂ -	-	d,e,g,h,i,j,k,l,n,o	
I	0.85	3	-CH ₃	t	q	-CH ₂ - <u>CH₃</u>

To establish how many types of carbon centres existed within the molecule, ^{13}C - $\{^1\text{H}\}$ NMR data (Figure 8.8) were examined. The data gave rise to 16 NMR signals corresponding to sixteen different types of ^{13}C environments. Many of these showed similar chemical shifts (signals *e-l*). Additionally the intensities revealed that a number of carbon centres (*a, f, l, m*) were twice as abundant, resulting from symmetry within the structure. It was clear in particular from these data that the carbon signal (*a*) was due to two alkene carbons with identical chemical shifts, confirming the expectation that the structure would be roughly symmetrical about a central double-bond, the symmetry of which would remain largely unaffected by remote tail groups.

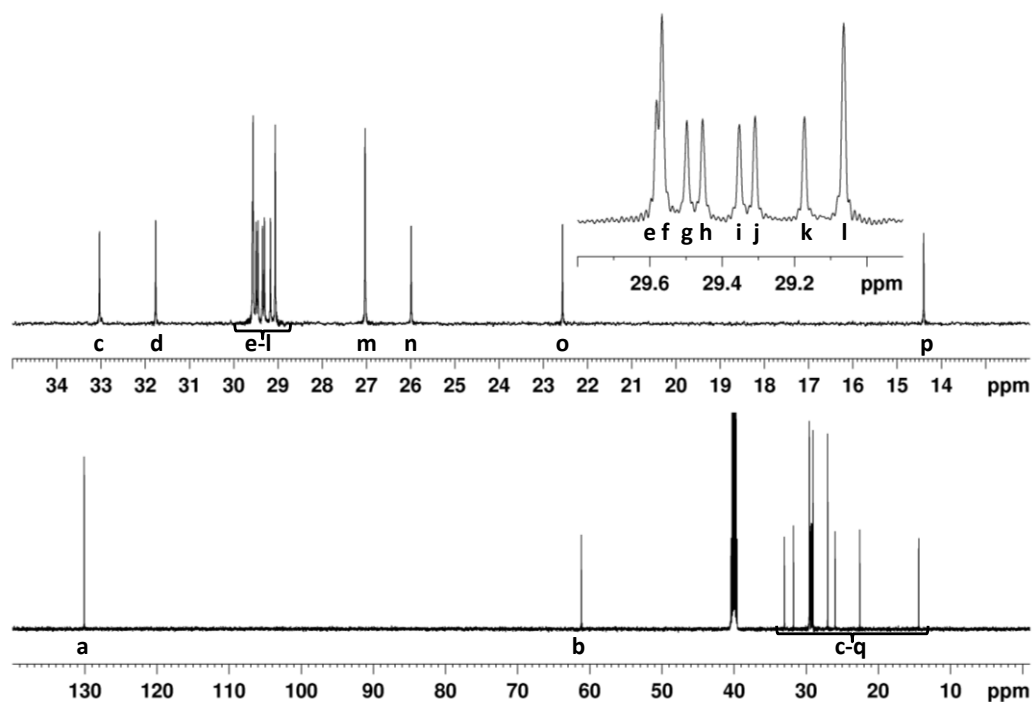


Figure 8.8: $^{13}\text{C}\{-^1\text{H}\}$ NMR spectrum of the lipid component from fraction F-4 with expansions shown to reveal details of crowded region. The expansion immediately above the full NMR spectrum shows expansion of the signal region *c-p*. Further expansion of the region *e-l* within this is shown inset as the topmost expansion.

2D [^1H , ^{13}C] HSQC NMR data (**Figure 8.9**) at both low and high resolution allowed the types of carbon to be distinguished for every centre as well as editing the data to reveal protons that were not attached to carbon. As well as enabling the identification of H/C correlations within each magnetic environment, these data also made it possible to confirm the number of protons associated with the lipid chain. These data also revealed that protons giving rise to resonances B and D were not attached to carbon given that their signals did not show any H/C correlations in the HSQC data. By analogy with literature examples, it was clear that resonance D was associated with water in DMSO and could therefore be discounted from the analysis. A summary of the ^{13}C NMR data is shown in **Table 8.5**. These data are summarized to provide a molecular formula of $\text{C}_{20}\text{H}_{40}\text{O}$, yielding a molecule weight $\text{MW} = 296$. Integration of the ^1H NMR spectrum is consistent with this formula and the number of protons ‘counted’ using the 2D [^1H , ^{13}C] HSQC NMR data.

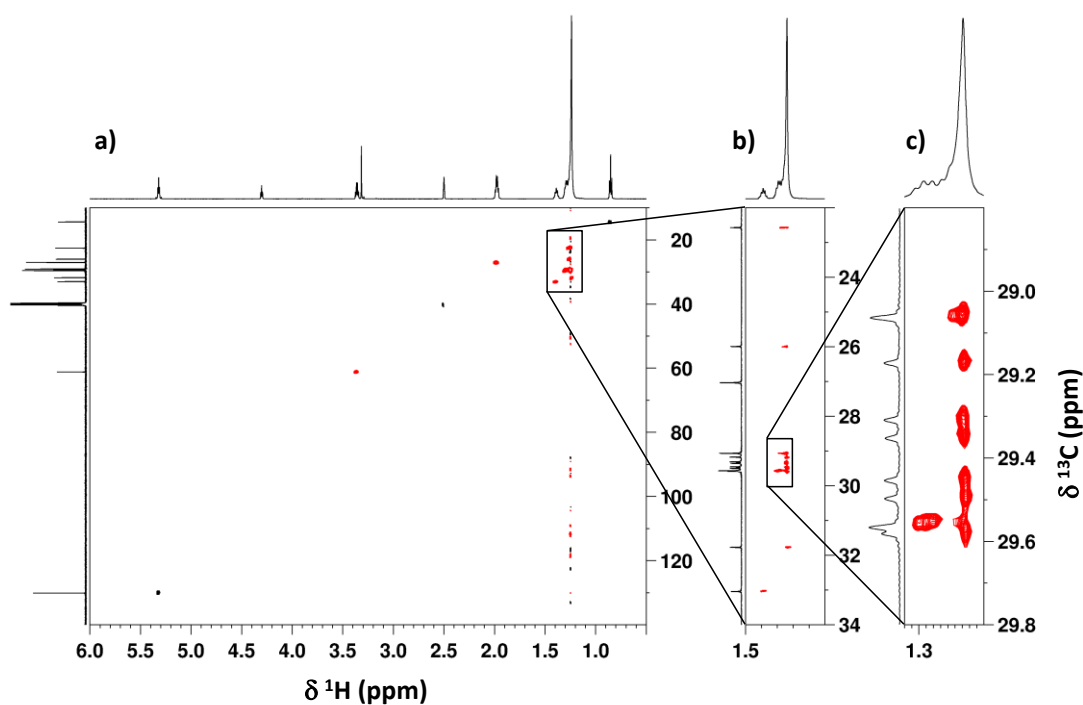


Figure 8.9: 600 MHz 2D [^1H , ^{13}C] HSQC NMR data for the lipid component of fraction F-4. **a)** Low resolution data showing the complete data set. **b)** Expansion of the boxed region of data shown in (a) from data acquired at high F1 resolution using non-uniform sampling. **c)** Further expansion of the boxed region shown in (b) to reveal high resolution data in F1 allowing individual correlations between protons and carbons of each methylene group to be distinguished for unique carbon resonance assignment and proton counting. Black cross-peaks (positive) correspond to methine (CH) and methyl (CH_3) groups; red cross-peaks correspond to methylene (CH_2) groups.

Table 8.5: Summary of ^{13}C NMR data for the lipid molecule as revealed by 1D ^{13}C - $\{^1\text{H}\}$ and 2D [^1H , ^{13}C] HSQC NMR data.

<i>Label</i>	<i>σ (ppm)</i>	<i>No. of Carbons</i>	<i>Type</i>	<i>Link to ^1H</i>
a	130.09	2	CH	A
b	61.18	1	CH_2	C
c	33.03	1	CH_2	F
d	31.76	1	CH_2	H
e	29.58	1	CH_2	H
f	29.56	2	CH_2	G
g	29.50	1	CH_2	H
h	29.45	1	CH_2	H

i	29.35	1	CH ₂	H
j	29.31	1	CH ₂	H
k	29.17	1	CH ₂	H
l	29.06	2	CH ₂	H
m	27.03	2	CH ₂	E
n	25.99	1	CH ₂	H
o	22.57	1	CH ₂	H
p	14.40	1	CH ₃	I

Analysis of the remaining 2D [¹H, ¹H] COSY and TOCSY and 2D [¹H, ¹³C] HSQC and HMBC NMR data are summarized in **Table 8.6** and **Table 8.7** respectively. (See also Figures B10-B12 in Appendix II). The triplet character of ¹H resonance B and its correlation with resonance C by COSY and TOCSY indicated that the hydroxyl group was a terminal –OH attached to a methylene whose protons gave rise to resonance C. The triplet character of proton signal I similarly enabled the identity of this resonance to be associated with a terminal methyl group. Correlations were traced as far as possible from both the terminal positions and the alkene proton resonances (A) until these assignment pathways merged at resonance H. 2D [¹H, ¹³C] HMBC NMR data were used to establish longer range H/C correlations to reinforce the assignments, which remained incomplete owing to the degeneracy at signal H.

Table 8.6: Coupling partners revealed through 2D [¹H, ¹H] COSY (C) and TOCSY (T) NMR data.

<i>Label</i>	<i>A</i>	<i>B</i>	<i>C</i>	<i>D</i>	<i>E</i>	<i>F</i>	<i>G</i>	<i>H</i>	<i>I</i>
A					C, T				
B			C, T						
C		C, T				C, T			
D									
E	C, T						C, T	C, T	
F			C, T					C, T	
G					C, T			C, T	
H					C, T	C, T	C, T		C, T
I								C, T	

Table 8.7: Coupling partners revealed by analysis of 2D [¹H, ¹³C] HSQC (HS) and HMBC (HM) NMR data for the lipid component.

<i>Labels</i>	<i>A</i>	<i>B</i>	<i>C</i>	<i>D</i>	<i>E</i>	<i>F</i>	<i>G</i>	<i>H</i>	<i>I</i>
a	HS				HM		HM		
b		HM	HS			HM		HM	
c		HM	HM			HS		HM	
d								HSHM	HM
e								HS	
f	HM				HM		HS		
g								HS	
h						HM		HS	
i								HS	
j								HS	
k								HS	
l					HM		HM	HS	
m	HM				HS		HM	HM	
n			HM			HM		HS	
o								HS	HM
p								HM	HS

Following identification of coupling partners and piecing the structural evidence together, the proton and carbon assignments were allocated to a basic structure as

shown (**Figure 8.10**). It was not clear from the NMR data whether the double bond would be at the 9- or 10-position (shown in the 10-position in **Figure 8.10**). Neither was it clear from the data whether the double bond was of *E* or *Z* configuration. For this reason, computer simulations were carried out based on both *E* and *Z* isomers of 9- and 10-eicosen-1-ol and the data obtained were compared with the experimental data in order to throw some light on the conformation of the double bond. Particular attention was paid to the appearance of proton resonances A and E in these simulations, which would reflect directly on the conformation about the centralised double bond. The results of these simulations with their equivalent experimental counterparts are shown in **Figure 8.11**.

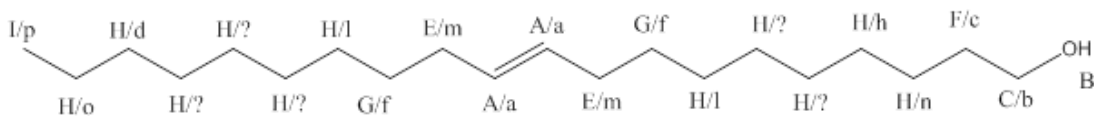


Figure 8.10: Basic lipid structure from an analysis of the NMR data showing the signal assignments associated with protons (upper case labels) and carbons (lower case labels) at each position. The *E*-layout about the double bond is purely for convenience and has no bearing on the final structure.

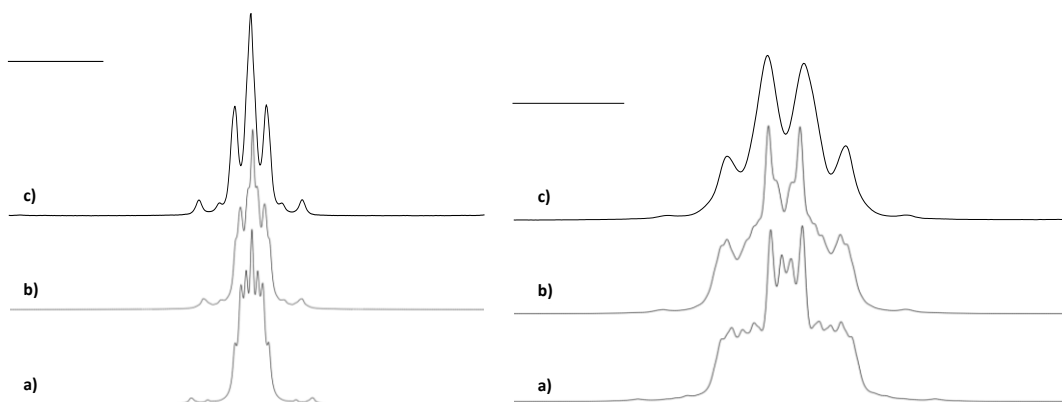


Figure 8.11: Simulations and experimental data for two possible configurations of the lipid molecule for ¹H resonances A (left) and E (right). **a)** Simulated signals for the *E*-configuration; **b)** simulated signals for the *Z*-configuration; **c)** experimental data.

On balance these data suggest a greater likelihood of the lipid existing in the (*Z*)-configuration as shown in **Figure 8.12**. The position of the double bond is not revealed through these simulations or by experiment. Comparison with information

provided directly through Beesen Co. Ltd., suppliers of the venom, suggests that the material and data are consistent with (Z)-eicos-9-en-1-ol.

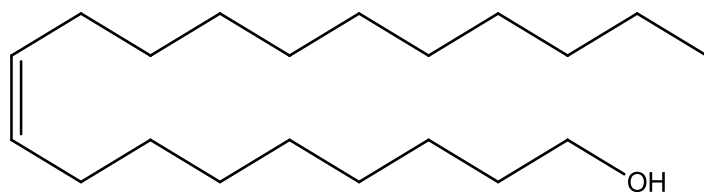


Figure 8.12: (Z)-eicos-9-en-1-ol.

8.3.8 Identification of minor impurity in F-4

Fraction F-4 was found to contain trace levels of an unidentified minor component with $[M-H]^-$ elemental composition of $C_{43}H_{70}O_{11}P$ (0.0783 ppm mass tolerance) and MW 794.47. Collisional induced dissociation (CID) of the parental ion (m/z 793.46) at a normalised collisional energy (NCE) of 35.0 produced two daughter ions with m/z 493.2574 ($C_{23}H_{42}O_9P$, 2.685 ppm mass tolerance, 40%) and 643.3608 ($C_{33}H_{56}O_{10}P$, 0.341 ppm mass tolerance, 60%) (**Figure 8.13**). This elemental composition, though inconclusive, suggested the likelihood that the unknown impurity might be a phospholipid.

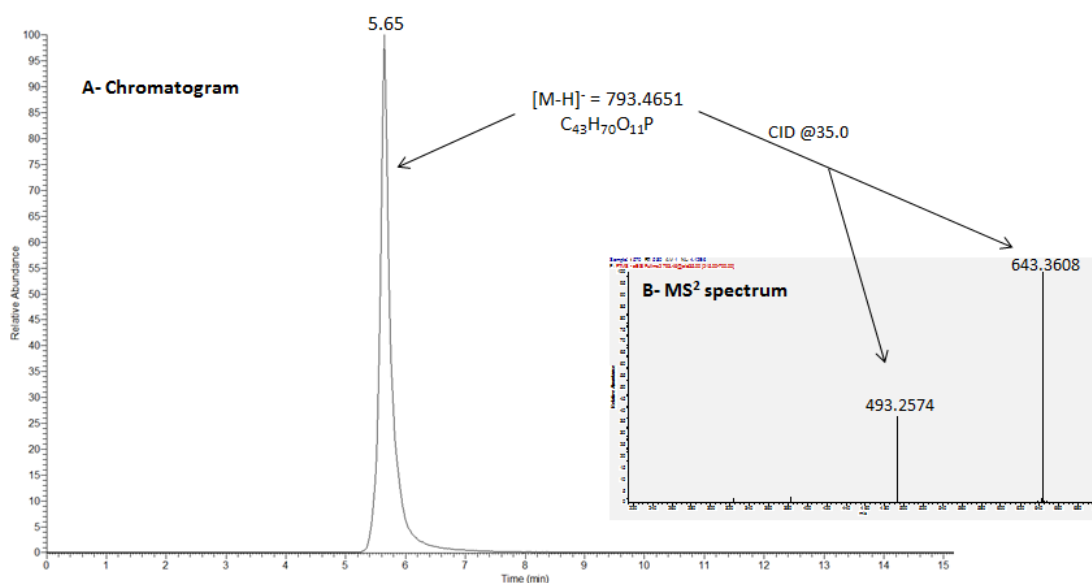


Figure 8.13: Chromatogram of the impurity in F-4 with $[M-H]^-$ of 793.4651 and elemental composition $C_{43}H_{70}O_{11}P$. CID of m/z 793.46 parental ion at a NCE of 35.0 gave two fragment ions of m/z 493.2574 and 643.3608 respectively. Sample analysed by reversed phase LC-MS on the LTQ-Orbitrap using the method described in section 3.6 for fraction F-4.

8.4 Discussion

8.4.1 Cell viability

The two fractions which were cytotoxic to U937 cells with IC_{50} values below 100 $\mu\text{g/mL}$ contained melittin (F-3, IC_{50} 5.4 $\mu\text{g/mL}$) and (Z)-9-eicosen-1-ol (F-4, IC_{50} 68.8 $\mu\text{g/mL}$). The latter also contained trace levels of an unidentified phospholipid. F-1 and F-2 were relatively non-toxic to U937 cells at the concentrations tested. The former contained mainly low MW amines such as histamine, dopamine and norepinephrine, while the latter contained mainly PLA_2 , a major BV allergen (Dhillon *et al.*, 1992; Ameratunga *et al.*, 1995). Although one would have expected fraction F-2 to be cytotoxic due to its PLA_2 content, it may be that the enzymatic activity reduced because of its separation from melittin since the venom PLA_2 and melittin act synergistically (Habermann, 1972), or as a result of loss of its 3D configuration during the fractionation. Fraction F-2 also contained variable amounts of the peptides apamin, MCD peptide and secapin, which were also detected in trace amounts in F-1.

Whereas the cytotoxicity of melittin is generally known in normal human and cancer cells (Son *et al.*, 2007; Gajski and Garaj-Vrhovac, 2013), the biological activities of the organic fraction of BV are less well known. Melittin's cytotoxicity is thought to be due to membrane-disruption (Lee *et al.*, 2013) and apoptotic actions mediated via mitochondrial and caspase activities (Lee and Lee, 2014). During the experiments, the toxicity of F-4 (at 100 µg/mL) was also observed in adherent normal human fibroblast (HS27) cells in which growth inhibition appeared to be associated with loss of cell attachment to the cell culture well plate (data not shown). Because of this, it had been anticipated that with suspended U937 cells the F-4 fraction would have no such cytotoxic effect below 100 µg/mL, since adherency was not a prerequisite for cell division and growth. Thus the observed toxicity in U937 cells might suggest that F-4 acts within the cell, at least partially, rather than exclusively externally to it. Its amphiphilic structure would be consistent with an ability to penetrate and pass through cell membranes.

8.4.2 Effect on cytokine release

The enhancement of LPS-stimulated release of IL-1 β in U937 cells was by far the most pronounced effect induced by all four BV fractions and crude BV, while the effects on TNF- α and IL-6 release were less marked, with variability between the fractions. The only significant effect on TNF- α release was due to F-4, while F-2 and F-3, which contained PLA₂ and melittin respectively, were the most potent enhancers of IL-1 β release by the cells following co-stimulation with LPS. Interestingly, F-4 showed anti-IL-6 effects. The IL-1 family of cytokines is closely linked to innate inflammatory and immune responses more than any other cytokine family, and IL-1 β mediates auto-inflammatory diseases (Dinarello, 2013). In the context of bees, the observed several-fold enhancement of IL-1 β release by all its fractions is thus logical given the defensive function of the venom. However, unlike the fractions, crude BV did not stimulate IL-1 β as much as did the individual fractions, perhaps due to lower concentration thresholds for the active components or/and antagonistic effects from components with IL-1 β inhibitory activities. Stimulation of IL-6 production is a key target for adjuvants due to its role in promoting B-lymphocyte differentiation into

antibody producing cells (Beagley *et al.*, 1989; Bertolini and Benson, 1990; Hilbert *et al.*, 1989), T-cell proliferation (Tosato and Pike, 1988), and development of cell mediated cytotoxicity by CD8⁺ cells (Okada *et al.*, 1988; Houssiau and Van Snick, 1992; Van Snick *et al.*, 1988). Thus inhibition of IL-6 production by F-4 would suggest an immunosuppressive action, but its concomitant stimulatory effect on TNF- α , an important cytokine involved in development of resistance to infection and cancer with roles in necrosis and apoptosis (Idriss and Naismith, 2000), suggests a more subtle mechanism.

Among the major components of F-1, histamine was reported to increase production of IL-6, expression of histamine receptors, expression of the kinases pp38, pERK and pJNK, and induction of NF- κ B in nasal fibroblasts when assayed at 200 μ M (~22.2 μ g/mL) (Park *et al.*, 2014). This concentration level was significantly higher than that present in the assay solutions of both F-1 fraction and BV, which might explain their non-significant effects on IL-6. Bee venom PLA₂, a major allergen and main component of F-2, and apamin have been shown to possess immune-inducing effects by activating T-cells (Bourgeois *et al.*, 2015) and promoting T-cell proliferation (Regnier-Vigouroux *et al.*, 1988), respectively. Thus the effects observed with F-2 on IL-1 β and IL-6 production might be related to the effects of both PLA₂ and apamin on the cells.

Additionally, melittin, the sole component of F-3 has been reported to possess adjuvant properties by enhancing the absorption of intranasal tetanus and diphtheria toxoids (Bramwell *et al.*, 2003). This would support its effect on IL-1 β observed in this study. However, these findings do not suggest that melittin could reduce the effect of LPS on cells contrary to some previous studies (Moon *et al.*, 2007; Srivastava *et al.*, 2012). The concentration used in the current study (3 μ g/mL) was sub-lethal to the U937 cells but at 10 μ g/mL, the concentration used in a previous study (Srivastava *et al.*, 2012), melittin was found in the current study to be 100% cytotoxic. This was observed previously in dermal fibroblasts, mononuclear cells, and fibroblast-like synoviocytes (Stuhlmeier, 2007). On the other hand, the study by Moon *et al.* (Moon *et al.*, 2007) assayed both BV and melittin at 0.5-2.0 μ g/mL—levels which are all

markedly lower than those employed in the current study. In the same study, LPS was assayed at 0.5 µg/mL compared to 1.0 µg/mL used in this study, and the cells were initially treated with BV or melittin for 1 h before treatment with LPS, rather than being simultaneously exposed (Moon *et al.*, 2007). Thus the differences observed in these *in vitro* studies in relation to melittin's role in immuno-modulation might be related to the different experimental designs and/or concentrations of melittin and LPS used. In a previous study by Stuhlmeier (2007), neither BV nor melittin was found to inhibit IL-1 β -induced activation of NF- κ B. Instead, there were significant increases in the levels of the mRNA of several pro-inflammatory genes and COX-2 in synoviocytes, dermal fibroblasts, and mononuclear cells (Stuhlmeier, 2007). The results obtained in this study corroborate these findings.

The main component of F-4, identified in this study as (Z)-9-eicosen-1-ol, resembled the lipid-soluble compound reported by Pickett *et al.* (1982) in *A. mellifera* venom and structurally elucidated as (Z)-11-eicosen-1-ol (Pickett *et al.*, 1982). The latter was described as a natural pheromone, which acted synergistically with amyl acetate, another pheromone produced by the bees [1]. Schmidt *et al.* (1997) also reported the same long chain monounsaturated alcohol to be the main component of the oily fraction of *Apis cerana* venom (Schmidt *et al.*, 1997), a species related to *A. mellifera*. The compound isolated in F-4 appears to differ from that previously described with respect to the double bond position, although it could not be confirmed with 100% certainty whether it was on position 9 or 10. Nevertheless, variations in double bond placement might be a means of conveying subtle differences in message recognition among the bees (Boch and Morse, 1974).

8.4.3 Conclusion

Inflammatory responses mediated by pro-inflammatory cytokines are a key component of protective immunity against many infections. This study shows that treatment of PMA-differentiated U937 cells with BV fractions significantly enhances the cytokine release effect of LPS in these cells. However, neither BV nor its fractions could induce any significant cytokine release on their own. The largest synergistic effect

was observed for IL-1 β release, which was promoted by all fractions, while only the lipid fraction, F-4, enhanced TNF- α production in the cells co-stimulated with LPS. Although fraction F-4, identified to contain (Z)-9-eicosen-1-ol, was stimulatory for IL-1 β and TNF- α release, it produced an inhibitory effect on IL-6 production. The commercial availability of this compound in larger amounts than can be isolated from the venom will enable further work to explore potential synergies between it and fractions F-1 to F-3. In addition, it provides a lead compound for exploring the effects of other long chain alcohols, since they are accessible via reduction of the wide range of long chain fatty acids that are commercially available. Taken together, these results do not support some studies in the literature which suggest that BV and melittin possess potential anti-inflammatory activity by antagonising LPS-stimulation of cytokine production. Instead BV fractions synergise with LPS in the induction of the IL-1 β cytokine release in U937 cells and the lipophilic fraction has additional orthogonal effects on TNF- α and IL-6 whereby it induces the former and inhibits the latter. Overall, these effects provide valuable preliminary information to support further evaluation of purified BV as a potential source of natural adjuvants for some vaccines.

General Discussion and Conclusion

General Discussion and Conclusion

From the outset, the main objectives of this project were threefold, namely: (1) To develop reliable and robust methods for the separation, detection and characterization of bee venom (BV) components in crude samples, including their quantification in commercial BV-containing cosmetic products; (2) To study the chemical and biological properties of BV that would support its application in the development of skin anti-ageing cosmetic applications; and (3) To investigate the immunomodulatory potential of BV in stimulating the production of cytokines in PMA-differentiated U937 cells and their synergistic action with lipopolysaccharide (LPS).

The first objective was accomplished through studies involving medium pressure liquid chromatography (MPLC), and employing both UV/Vis and ELSD detectors, to separate BV samples into fractions based on their varying degrees of polarity. This MPLC method was developed by scaling up a preliminary fractionation procedure developed on solid phase extraction (SPE) columns. Reversed phase columns based on both C18 and polar enhanced polymer (PEP) columns were found to be the most effective at separating BV components on the Grace® with a recovery of approximately 60%. The fractionation method developed yielded four major fractions of which melittin, the main fraction of the venom, had a purity of about 96% as determined through a quantitative NMR (qNMR) assay. All the components of each of the fractions were identified using robust LC-MS analysis methods developed for this purpose. The first one of these three methods employed a ZICHILIC column and was developed to analyse components of the most polar fraction (F-1) which contained compounds so hydrophilic that they eluted in the void volume of the standard C18 analytical column. The HILIC method improved their retention times which allowed baseline resolution and increased their sensitivity of detection. The second and third methods were based on reversed phase and employed a standard C18 column but the difference was in the ionisation mode and gradient elution profile. The second method employed positive ionisation mode of the ESI and was applied to the analysis of components of F-2 and F-3 which contained mainly peptides/proteins and some amines—compounds that could be detected in the positive ESI mode. On the other

hand, the third method was applied to F-4 to analyse a compound observed using negative ion ESI which was putatively identified to be a phospholipid. All the three methods gave reproducible chromatograms and proved to be reliable. Finally, a protocol for the assay of melittin in commercial BV-containing cosmetic formulations was developed (Tusiimire *et al.*, 2015) and also applied to several in-house formulations. The developed method, which employed liquid-liquid (LLE) and solid phase (SPE) extractions, was applicable to the assay of most of the cosmetic samples but with limited reproducibility owing to the difficulty in obtaining homogenous solutions for chromatography, the many extraction steps involved, and the low levels of BV contained in the formulations. It is recommended that, in order to improve the robustness and reproducibility of the method, the sample should be initially dispersed in 1% formic acid before methanol/chloroform (1:1) is added and that the melittin-containing supernatant from the LLE be reconstituted in acetonitrile to make a clear solution.

The fractions obtained from MPLC fractionation were evaluated for their biological and chemical activities in subsequent investigations that addressed the second objective of this study. Biological tests performed consisted of assays for antibacterial, antiprotozoal, and antiviral effects, as well as effects on human cell lines. For antibacterial assays, the organisms employed were *Mycobacterium marinum* and *Nocardia farcinia* while antiprotozoal assays employed *Trypanosoma brucei brucei*, the causative agent for African trypanosomiasis. The antiviral effects were determined indirectly by testing for presence of α -glucosidase inhibitory activity in the fractions since α -glucosidase inhibitors have been reported to possess potent antiviral action. In human cell lines, the BV fractions were evaluated for their cytotoxic effects against normal human keratinocytes, epithelial cells, and fibroblasts in order to determine their selective toxicity and predict any potential safety issues of the venom after formulation into cosmetic products. In addition, potential anti-inflammatory effects of the fractions were assessed by their ability to inhibit TNF- α -induced NF- κ B in normal human keratinocytes. Among the chemical investigations carried out on BV was the assessment of the factors affecting stability of melittin in aqueous solutions and in cosmetic formulations in order to determine how to control its degrada-

tion. Aqueous stability was studied at different temperatures including fridge, freezer, and laboratory bench through determination of orders and rates of degradation. Such information was required to determine the most appropriate storage conditions and approximate lifetimes of analytical aqueous BV solutions.

The final objective to evaluate pro-inflammatory effects of BV was undertaken in PMA-differentiated U937 cells in assays utilising ELISAs. Determination of U937 cell viability in the presence of the venom fractions enabled the estimation of doses nontoxic to the cells. The levels of the cytokines TNF- α , IL-1 and IL-6 produced by the cells when treated with BV fractions in the presence and absence of LPS were also determined. Comparisons between the levels of cytokines produced by cells treated with the fractions against those of negative controls were made to determine any presence of immuno-stimulation by BV and its components. Comparison of levels of cytokines produced by cells treated with LPS alone with those produced by co-stimulation with LPS and the fractions enabled the detection of any synergistic effects (Tusiimire *et al.*, 2016). Although neither BV nor its fractions, on their own, induced any significant cytokine release in the cells, significant synergy was observed in the presence of lipopolysaccharide (LPS) co-stimulation particularly for IL-1 β and TNF- α which suggests that BV might act as a potential source for immuno-adjuvants.

In conclusion, this study has filled many gaps identified at the beginning of the project and has in the process improved the general understanding of the chemical composition and stability of BV and the implications of the latter in the analysis of both crude BV samples and cosmeceuticals based BV extracts. The biological effects of BV have been evaluated in some bacteria and protozoa although a wider scope of organisms would be more appropriate in future studies. The effect of melittin on cisplatin-sensitive (A2780) and resistant (A2780cis) cancer cell lines has also been evaluated via collaboration with another PhD student (Alonezi *et al.*, 2016; in prep.). The effects on cytokine production observed do not corroborate many of the studies in literature that suggest BV and melittin possess anti-inflammatory potential (Moon *et al.*, 2007; Srivastava *et al.*, 2012). Instead, BV fractions seem to possess synergis-

tic immuno-stimulatory effects by inducing IL-1 β , and to some extent TNF- α , release in U937 cells—an observation that corroborates the study by Stuhlmeier (Stuhlmeier, 2007). Such effects would support the potential use of purified BV components, or their mixtures, as natural adjuvants for some vaccines.

References

- ABDEL-RAHMAN, M. A., ABDEL-NABI, I. M., EL-NAGGAR, M. S., ABBAS, O. A. & STRONG, P. N. 2011. Intraspecific variation in the venom of the vermivorous cone snail *Conus vexillum*. *Comp Biochem Physiol C Toxicol Pharmacol*, 154, 318-325.
- ABDEL-RAHMAN, M. A., ABDEL-NABI, I. M., EL-NAGGAR, M. S., ABBAS, O. A. & STRONG, P. N. 2013. *Conus vexillum* venom induces oxidative stress in Ehrlich's ascites carcinoma cells: an insight into the mechanism of induction. *J Venom Anim Toxins Incl Trop Dis*, 19, 1-10.
- AGARWAL, V., TIKHONOV, A., METLITSKAYA, A., SEVERINOV, K. & NAIR, S. K. 2012. Structure and function of a serine carboxypeptidase adapted for degradation of the protein synthesis antibiotic microcin C7. *Proc Natl Acad Sci USA*, 109, 4425-4430.
- AHLF, D. R., COMPTON, P. D., TRAN, J. C., EARLY, B. P., THOMAS, P. M. & KELLEHER, N. L. 2012. Evaluation of the compact high-field Orbitrap for top-down proteomics of human cells. *J Proteome Res*, 11, 4308-4314.
- ALONEZI, S., TUSIIMIRE, J., WALLACE, J., DUFTON, M., PARKINSON, J. A., YOUNG, L., CLEMENTS, C. J., PARK, J. K., JEON, J. W., FERRO, V. A. & WATSON, D. G. 2016. Metabolomic profiling of the effects of melittin on cisplatin resistant and cisplatin sensitive ovarian cancer cells. In Prep: University of Strathclyde.
- ALVAREZ-RIVERA, G., LORES, M., LLOMPART, M. & GARCIA-JARES, C. 2013. Cosmetics and Toiletries: Chromatography. *Reference Module in Chemistry, Molecular Sciences and Chemical Engineering*. Elsevier.
- AMERATUNGA, R. V., HAWKINS, R., PRESTIDGE, R. & MARBROOK, J. 1995. A high efficiency method for purification and assay of bee venom phospholipase A₂. *Pathology*, 27, 157-160.

- ANDERSON, D., TERWILLIGER, T. C., WICKNER, W. & EISENBERG, D. 1980. Melittin forms crystals which are suitable for high resolution X-ray structural analysis and which reveal a molecular 2-fold axis of symmetry. *J Biol Chem*, 255, 2578-2582.
- ARDA, O., GOKSUGUR, N. & TUZUN, Y. 2014. Basic histological structure and functions of facial skin. *Clin Dermatol*, 32, 3-13.
- AUBRY, A., JARLIER, V., ESCOLANO, S., TRUFFOT-PERNOT, C. & CAMBAU, E. 2000. Antibiotic susceptibility pattern of *Mycobacterium marinum*. *Antimicrob Agents Chemother*, 44, 3133-6.
- BANERJEE, S. & MAZUMDAR, S. 2012. Electrospray ionization mass spectrometry: a technique to access the information beyond the molecular weight of the analyte. *Int J Anal Chem*, 2012, 1-40.
- BANKS, B. E., DEMPSEY, C. E., PEARCE, F. L., VERNON, C. A. & WHOLLEY, T. E. 1981. New methods of isolating been venom peptides. *Anal Biochem*, 116, 48-52.
- BARACCHI, D., FRANCESE, S. & TURILLAZZI, S. 2011. Beyond the antipredatory defence: Honey bee venom function as a component of social immunity. *Toxicon*, 58, 550-557.
- BARACCHI, D. & TURILLAZZI, S. 2010. Differences in venom and cuticular peptides in individuals of *Apis mellifera* (Hymenoptera: Apidae) determined by MALDI-TOF MS. *Journal of Insect Physiology*, 56, 366-375.
- BÁRÁNY, E., LINDBERG, M. & LODÉN, M. 2000. Unexpected skin barrier influence from nonionic emulsifiers. *International Journal of Pharmaceutics*, 195, 189-195.
- BEAGLEY, K. W., ELDRIDGE, J. H., LEE, F., KIYONO, H., EVERSON, M. P., KOOPMAN, W. J., HIRANO, T., KISHIMOTO, T. & MCGHEE, J. R. 1989. Interleukins and IgA synthesis. Human and murine interleukin 6 induce high rate IgA secretion in IgA-committed B cells. *J Exp Med*, 169, 2133-2148.

- BELOV, M. E., RAKOV, V. S., NIKOLAEV, E. N., GOSHE, M. B., ANDERSON, G. A. & SMITH, R. D. 2003. Initial implementation of external accumulation liquid chromatography/electrospray ionization Fourier transform ion cyclotron resonance with automated gain control. *Rapid Commun Mass Spectrom*, 17, 627-636.
- BENEDETTO, A. V. 1999. The cosmetic uses of Botulinum toxin type A. *Int J Dermatol*, 38, 641-655.
- BENTINGER, M., TEKLE, M. & DALLNER, G. 2010. Coenzyme Q--biosynthesis and functions. *Biochem Biophys Res Commun*, 396, 74-79.
- BERNHARD, D., MOSER, C., BACKOVIC, A. & WICK, G. 2007. Cigarette smoke--an aging accelerator? *Exp Gerontol*, 42, 160-165.
- BERTOLINI, J. N. & BENSON, E. M. 1990. The role of human interleukin-6 in B-cell isotype regulation and differentiation. *Cell Immunol*, 125, 197-209.
- BHAMIDI, S., SCHERMAN, M. S. & MCNEIL, M. R. 2009. Mycobacterial Cell Wall Arabinogalactan: a Detailed Perspective on Structure, Biosynthesis, Functions and Drug Targeting. In: ULLRICH, M. (ed.) *Bacterial Polysaccharides: Current Innovations and Future Trends*. Norfolk, UK: Caister Academic Press.
- BISHOP, J. E., KOU, D., MANIUS, G. & CHOKSHI, P. H. 2011. Sample Preparation Method Validation. In: NICKERSON, B. (ed.) *Sample Preparation of Pharmaceutical Dosage Forms: Challenges and Strategies fo Sample Preparation and Extraction*. 1 ed.: American Association of Pharmaceutical Scientists.
- BISSETT, D. L. 2009. Common cosmeceuticals. *Clinics in Dermatology*, 27, 435-445.
- BLANES-MIRA, C., CLEMENTE, J., JODAS, G., GIL, A., FERNANDEZ-BALLESTER, G., PONSATI, B., GUTIERREZ, L., PEREZ-PAYA, E. & FERRER-MONTIEL, A. 2002. A synthetic hexapeptide (Argireline®) with antiwrinkle activity. *Int J Cosmet Sci*, 24, 303-310.

BLANK, S., SEISMANN, H., BOCKISCH, B., BRAREN, I., CIFUENTES, L., MCINTYRE, M., RUHL, D., RING, J., BREDEHORST, R., OLLERT, M. W., GRUNWALD, T. & SPILLNER, E. 2010. Identification, recombinant expression, and characterization of the 100 kDa high molecular weight Hymenoptera venom allergens Api m5 and Ves v3. *J Immunol*, 184, 5403-5413.

BOCH, R. & MORSE, R. 1974. Discrimination of familiar and foreign queens by honey bee swarms. *Ann Entomol Soc Am*, 67, 709-711.

BOTTAI, G., MANCINA, R., MURATORI, M., DI GENNARO, P. & LOTTI, T. 2013. 17beta-estradiol protects human skin fibroblasts and keratinocytes against oxidative damage. *J Eur Acad Dermatol Venereol*, 27, 1236-1243.

BOURGEOIS, E. A., SUBRAMANIAM, S., CHENG, T. Y., DE JONG, A., LAYRE, E., LY, D., SALIMI, M., LEGASPI, A., MODLIN, R. L., SALIO, M., CERUNDOLO, V., MOODY, D. B. & OGG, G. 2015. Bee venom processes human skin lipids for presentation by CD1a. *J Exp Med*, 212, 149-163.

BRAMWELL, V. W., SOMAVARAPU, S., OUTSCHOORN, I. & ALPAR, H. O. 2003. Adjuvant action of melittin following intranasal immunisation with tetanus and diphtheria toxoids. *J Drug Target*, 11, 525-530.

BRUCE, G. R. & GILL, P. S. 1999. Estimates of precision in a standard additions analysis. *J Chem Educ*, 76, 805-807.

BU, X., CHANDRAN, S., SPIRIG, J. & WANG, Q. 2011. Sample Preparation for Selected Nonsolid Dosage Forms. In: NICKERSON, B. (ed.) *Sample Preparation of Pharmaceutical Dosage Forms: Challenges and Strategies for Sample Preparation and Extraction*. American Association of Pharmaceutical Scientists.

BUKU, A. 1999. Mast cell degranulating (MCD) peptide: a prototypic peptide in allergy and inflammation. *Peptides*, 20, 415-420.

BUKU, A., CONDIE, B., PRICE, J. & MEZEI, M. 2005. [Ala12] MCD peptide: a lead peptide to inhibitors of immunoglobulin E binding to mast cell receptors. *J Pept Res*, 66, 132-137.

- BUKU, A., PRICE, J. A., MENDLOWITZ, M. & MASUR, S. 2001. Mast cell degranulating peptide binds to RBL-2H3 mast cell receptors and inhibits IgE binding. *Peptides*, 22, 1993-1998.
- BURKE, J. E. & DENNIS, E. A. 2009. Phospholipase A2 structure/function, mechanism, and signaling. *J Lipid Res*, 50, S237-S242.
- BUSZEWSKI, B. & NOGA, S. 2012. Hydrophilic interaction liquid chromatography (HILIC)--a powerful separation technique. *Anal Bioanal Chem*, 402, 231-47.
- CANTRELL, S. A., LEAVELL, M. D., MARJANOVIC, O., IAVARONE, A. T., LEARY, J. A. & RILEY, L. W. 2013. Free mycolic acid accumulation in the cell wall of the mce1 operon mutant strain of *Mycobacterium tuberculosis*. *J Microbiol*, 51, 619-626.
- CAPSONI, F., ONGARI, A. M., LONATI, C., ACCETTA, R., GATTI, S. & CATANIA, A. 2015. Alpha-Melanocyte-stimulating-hormone (alpha-MSH) modulates human chondrocyte activation induced by proinflammatory cytokines. *BMC Musculoskelet Disord*, 16, 154.
- CASEWELL, N. R., WUSTER, W., VONK, F. J., HARRISON, R. A. & FRY, B. G. 2013. Complex cocktails: the evolutionary novelty of venoms. *Trends Ecol Evol*, 28, 219-229.
- ČEŘOVSKÝ, V., HOVORKA, O., CVAČKA, J., VOBURKA, Z., BEDNÁROVÁ, L., BOROVIČKOVÁ, L., SLANINOVÁ, J. & FUČÍK, V. 2008. Melectin: A Novel Antimicrobial Peptide from the Venom of the Cleptoparasitic Bee *Melecta albifrons*. *ChemBioChem*, 9, 2815-2821.
- CHAO, K. L., MUTHUKUMAR, L. & HERZBERG, O. 2007. Structure of human hyaluronidase-1, a hyaluronan hydrolyzing enzyme involved in tumor growth and angiogenesis. *Biochemistry*, 46, 6911-6920.
- CHEN, J. & LARIVIERE, W. R. 2010. The nociceptive and anti-nociceptive effects of bee venom injection and therapy: A double-edged sword. *Prog Neurobiol*, 92, 151-183.

CHOI, C. M. & BERSON, D. S. 2006. Cosmeceuticals. *Semin Cutan Med Surg*, 25, 163-168.

COMMUNITIES, C. O. T. E. 2002. Commission Decision 2002/657/EC. In: UNION, E. (ed.) L221/8. Official Journal of the European Communities: Luxembourg: Office for Official Publications of the European Communities.

CRAMER, J. A., BAILEY, L. C., BAILEY, C. A. & MILLER, R. T. 1994. Kinetic and mechanistic studies with bovine testicular hyaluronidase. *Biochim Biophys Acta*, 1200, 315-321.

CTPA. 2013. *How are cosmetics regulated?* [Online]. CTPA Website: CTPA. Available: <http://www.ctpa.org.uk> [Accessed 01 October 2013].

DANZER, K. & CURRIE, L. A. 1998. Guidelines for calibration in analytical chemistry - Part 1. Fundamentals and single component calibration (IUPAC recommendations 1998). *Pure And Applied Chemistry*, 70, 993-1014.

DENISOV, E., DAMOC, E., LANGE, O. & MAKAROV, A. 2012. Orbitrap mass spectrometry with resolving powers above 1,000,000. *International Journal of Mass Spectrometry*, 325, 80-85.

DHILLON, M., ROBERTS, C., NUNN, T. & KUO, M. 1992. Mapping human T cell epitopes on phospholipase A₂: the major bee venom allergen. *J Allergy Clin Immunol*, 90, 42-51.

DINARELLO, C. A. 2013. Overview of the interleukin-1 family of ligands and receptors. *Semin Immunol*, 25, 389-393.

DOLAN, J. W. 2013a. Gradient Elution, Part I: Intuition. *LC-GC North America*, 31, 204-209.

DOLAN, J. W. 2013b. Making the Most of a Gradient Scouting Run. *LC-GC North America*, 31, 30-35.

DONG, H.-Q., LI, M., ZHU, F., LIU, F.-L. & HUANG, J.-B. 2012. Inhibitory potential of trilobatin from *Lithocarpus polystachyus* Rehd against α -glucosidase and α -amylase linked to type 2 diabetes. *Food Chemistry*, 130, 261-266.

DOUGLAS, D. 2009. Linear quadrupoles in mass spectrometry. *Mass Spectrom Rev*, 28, 937-960.

DRAELOS, Z. D. 2008. The cosmeceutical realm. *Clinics in Dermatology*, 26, 627-632.

DRAINAS, D. & LAWRENCE, A. J. 1980. Albumin mediates lysis of erythrocytes by bee venom phospholipase A₂ activated with oleoyl imidazolide. *FEBS Letters*, 114, 93-97.

EDMOND, D. H. 1996. Tandem mass spectrometry: A primer. *J Mass Spectr*, 31, 129-137.

EGBERT, M., RUETZE, M., SATTLER, M., WENCK, H., GALLINAT, S., LUCIUS, R. & WEISE, J. M. 2014. The extracellular matrix protein periostin contributes to proper collagen function and is downregulated during skin aging. *J Dermatol Sci*, 73, 40-48.

Eisenberg, D., Gribskov, M. & Terwilliger, T.C., 1990. MELITTIN. Available at: <http://dx.doi.org/10.2210/pdb2mlt/pdb>.

EL-DOMYATI, M., ATTIA, S., SALEH, F., BROWN, D., BIRK, D. E., GASPARRO, F., AHMAD, H. & UITTO, J. 2002a. Intrinsic aging vs. photoaging: a comparative histopathological, immunohistochemical, and ultrastructural study of skin. *Experimental Dermatology*, 11, 398-405.

EL-DOMYATI, M., ATTIA, S., SALEH, F., BROWN, D., BIRK, D. E., GASPARRO, F., AHMAD, H. & UITTO, J. 2002b. Intrinsic aging vs. photoaging: a comparative histopathological, immunohistochemical, and ultrastructural study of skin. *Exp Dermatol*, 11, 398-405.

ELLISON, S. L. & THOMPSON, M. 2008. Standard additions: myth and reality. *Analyst*, 133, 992-7.

ELSIK, C. G., WORLEY, K. C., BENNETT, A. K., BEYE, M., CAMARA, F., CHILDERS, C. P., DE GRAAF, D. C., DEBYSER, G., DENG, J., DEVREESE, B., ELHAIK, E., EVANS, J. D., FOSTER, L. J., GRAUR, D., GUIGO, R., HOFF, K. J., HOLDER, M. E., HUDSON, M. E., HUNT, G. J., JIANG, H., JOSHI, V., KHETANI, R. S., KOSAREV, P., KOVAR, C. L., MA, J., MALESZKA, R., MORITZ, R. F., MUNOZ-TORRES, M. C., MURPHY, T. D., MUZNY, D. M., NEWSHAM, I. F., REESE, J. T., ROBERTSON, H. M., ROBINSON, G. E., RUEPPELL, O., SOLOVYEV, V., STANKE, M., STOLLE, E., TSURUDA, J. M., VAERENBERGH, M. V., WATERHOUSE, R. M., WEAVER, D. B., WHITFIELD, C. W., WU, Y., ZDOBNOV, E. M., ZHANG, L., ZHU, D. & GIBBS, R. A. 2014. Finding the missing honey bee genes: lessons learned from a genome upgrade. *BMC Genomics*, 15, 86.

ESIN, S., COUNOUPAS, C., AULICINO, A., BRANCATISANO, F. L., MAISETTA, G., BOTTAI, D., DI LUCA, M., FLORIO, W., CAMPA, M. & BATONI, G. 2013. Interaction of *Mycobacterium tuberculosis* cell wall components with the human natural killer cell receptors NKp44 and Toll-like receptor 2. *Scand J Immunol*, 77, 460-469.

EVSTIGNEEV, M. P., PARKINSON, J. A., LANTUSHENKO, A. O., KOSTJUKOV, V. V. & PAHOMOV, V. I. 2010. Hexamer oligonucleotide topology and assembly under solution phase NMR and theoretical modeling scrutiny. *Biopolymers*, 93, 1023-1038.

EZURE, T. & AMANO, S. 2011. Negative regulation of dermal fibroblasts by enlarged adipocytes through release of free fatty acids. *J Invest Dermatol*, 131, 2004-2009.

FALCAO-PIRES, I., CASTRO-CHAVES, P., MIRANDA-SILVA, D., LOURENCO, A. P. & LEITE-MOREIRA, A. F. 2012. Physiological, pathological and potential therapeutic roles of adipokines. *Drug Discov Today*, 17, 880-889.

FALLA, T., J., ZHANG, L. & HARRIS, S. 2008. *Antimicrobial hexapeptides*. United States patent application 11/350,192. Aug 05, 2008.

FENN, J. B., MANN, M., MENG, C. K., WONG, S. F. & WHITEHOUSE, C. M. 1989. Electrospray ionization for mass spectrometry of large biomolecules. *Science*, 246, 64-71.

FERREIRA JUNIOR, R. S., SCIANI, J. M., MARQUES-PORTO, R., LOURENCO JUNIOR, A., ORSI, R. D. O., BARRAVIERA, B. & PIMENTA, D. C. 2010a. Africanized honey bee (*Apis mellifera*) venom profiling: Seasonal variation of melittin and phospholipase A₂ levels. *Toxicon*, 56, 355-362.

FISHER, G. J., DATTA, S., WANG, Z., LI, X.-Y., QUAN, T., CHUNG, J. H., KANG, S. & VOORHEES, J. J. 2000. c-Jun-dependent inhibition of cutaneous procollagen transcription following ultraviolet irradiation is reversed by all-trans retinoic acid. *The Journal of Clinical Investigation*, 106, 663-670.

FISHER, G. J., TALWAR, H. S., LIN, J., LIN, P., MCPHILLIPS, F., WANG, Z., LI, X., WAN, Y., KANG, S. & VOORHEES, J. J. 1998. Retinoic acid inhibits induction of c-Jun protein by ultraviolet radiation that occurs subsequent to activation of mitogen-activated protein kinase pathways in human skin *in vivo*. *J Clin Invest*, 101, 1432-1440.

FISHER, G. J., TALWAR, H. S., LIN, J. & VOORHEES, J. J. 1999. Molecular Mechanisms of Photoaging in Human Skin *In vivo* and Their Prevention by All-Trans Retinoic Acid. *Photochemistry and Photobiology*, 69, 154-157.

FLORANCE, H. V., STOPFORD, A. P., KALAPOTHAKIS, J. M., MCCULLOUGH, B. J., BREATHERICK, A. & BARRAN, P. E. 2011. Evidence for alpha-helices in the gas phase: A case study using Melittin from honey bee venom. *Analyst*, 136, 3446-3452.

FLYNN, T. C., PETROS, J., CLARK, R. E. & VIEHMAN, G. E. 2001. Dry skin and moisturizers. *Clinics in Dermatology*, 19, 387-392.

- FORSGREN, A. 1993. Antibiotic susceptibility of *Mycobacterium marinum*. *Scand J Infect Dis*, 25, 779-82.
- FRANCESE, S., LAMBARDI, D., MASTROBUONI, G., LA MARCA, G., MONETI, G. & TURILLAZZI, S. 2009. Detection of Honeybee Venom in Envenomed Tissues by Direct MALDI MSI. *Journal of the American Society for Mass Spectrometry*, 20, 112-123.
- FUNAYAMA, J. C., PUCCA, M. B., RONCOLATO, E. C., BERTOLINI, T. B., CAMPOS, L. B. & BARBOSA, J. E. 2012. Production of Human Antibody Fragments Binding to Melittin and Phospholipase A2 in Africanised Bee Venom: Minimising Venom Toxicity. *Basic & Clinical Pharmacology & Toxicology*, 110, 290-297.
- GAGLIARDI, L., DE ORSI, D. & DORATO, S. 2007. General review of official methods of analysis for cosmetics in different countries. In: SALVADOR, A. & CHISVERT, A. (eds.) *Analysis of Cosmetic Products*. Amsterdam: Elsevier.
- GAJSKI, G. & GARAJ-VRHOVAC, V. 2013. Melittin: a lytic peptide with anticancer properties. *Environ Toxicol Pharmacol*, 36, 697-705.
- GAMA, M. R., DA COSTA SILVA, R. G., COLLINS, C. H. & BOTTOLI, C. B. G. 2012. Hydrophilic interaction chromatography. *Trends Analyt Chem*, 37, 48-60.
- GAO, W., GRAY, N., HEATON, J., SMITH, N. W., JIA, Y. & LEGIDO-QUIGLEY, C. 2012. UV gradient combined with principal component analysis: Highly sensitive and specific high performance liquid chromatography analysis of cosmetic creams. *Journal of Chromatography A*, 1228, 324-328.
- GAULDIE, J., HANSON, J. M., SHIPOLINI, R. A. & VERNON, C. A. 1978. The Structures of Some Peptides from Bee Venom. *Eur J Biochem*, 83, 405-410.
- GEORGIEVA, D., GREUNKE, K., ARNI, R. K. & BETZEL, C. 2011. Three-dimensional modelling of honeybee venom allergenic proteases: relation to allergenicity. *Z Naturforsch C*, 66, 305-12.

- GEORGIEVA, D., GREUNKE, K. & BETZEL, C. 2010. Three-dimensional model of the honeybee venom allergen Api m 7: structural and functional insights. *Molecular BioSystems*, 6, 1056-1060.
- GMACHL, M. & KREIL, G. 1993. Bee venom hyaluronidase is homologous to a membrane protein of mammalian sperm. *Proc Natl Acad Sci U S A*, 90, 3569-3573.
- GOROUHI, F. & MAIBACH, H. I. 2009. Role of topical peptides in preventing or treating aged skin. *Int J Cosmet Sci*, 31, 327-345.
- GRECO, G. & LETZEL, T. 2013. Main interactions and influences of the chromatographic parameters in HILIC separations. *J Chromatogr Sci*, 51, 684-93.
- GUNIN, A. G., KORNILOVA, N. K., VASILIEVA, O. V. & PETROV, V. V. 2011. Age-related changes in proliferation, the numbers of mast cells, eosinophils, and cd45-positive cells in human dermis. *J Gerontol A Biol Sci Med Sci*, 66, 385-392.
- GUNIN, A. G., PETROV, V. V., GOLUBTZOVA, N. N., VASILIEVA, O. V. & KORNILOVA, N. K. 2014a. Age-related changes in angiogenesis in human dermis. *Exp Gerontol*, 55, 143-151.
- GUNIN, A. G., PETROV, V. V., VASIL'eva, O. V. & GOLUBTsoVA, N. N. 2014b. Blood vessels in human dermis during aging. *Adv Gerontol*, 27, 54-61.
- HABERMANN, E. 1972. Bee and wasp venoms. *Science*, 177, 314-322.
- HAJDUK, S. L., MOORE, D. R., VASUDEVACHARYA, J., SIQUEIRA, H., TORRI, A. F., TYTLER, E. M. & ESKO, J. D. 1989. Lysis of *Trypanosoma brucei* by a toxic subspecies of human high density lipoprotein. *J Biol Chem*, 264, 5210-5217.
- HARDMAN, M. & MAKAROV, A. A. 2003. Interfacing the orbitrap mass analyzer to an electrospray ion source. *Analytical Chemistry*, 75, 1699-1705.
- HARRIS, D. C. 2010. *Quantitative Chemical Analysis*, New York, W. H. Freeman.

HARRIS, S., M. , FALLA, T., J. & ZHANG, L. 2011. *Peptide fragments for inducing synthesis of extracellular matrix proteins*. United States patent application 13/339,606. Feb 25, 2014.

HARRIS, S., M., ZHANG, L. & FALLA, T., J. 2010. *Short bio-active peptides for cellular and immunological modulation*. United States patent application 12/005,653. Apr 13, 2010.

HARRISON, P. L., ABDEL-RAHMAN, M. A., MILLER, K. & STRONG, P. N. 2014. Antimicrobial peptides from scorpion venoms. *Toxicon*, 88, 115-37.

HIDER, R. C. 1988. Honeybee venom: a rich source of pharmacologically active peptides. *Endeavour*, 12, 60-65.

HILBERT, D. M., CANCRO, M. P., SCHERLE, P. A., NORDAN, R. P., VAN SNICK, J., GERHARD, W. & RUDIHOFF, S. 1989. T cell derived IL-6 is differentially required for antigen-specific antibody secretion by primary and secondary B cells. *J Immunol*, 143, 4019-4024.

HOFFMAN, D. R. 2006. Hymenoptera venom allergens. *Clin Rev Allergy Immunol*, 30, 109-28.

HOFFMANN, E. & STROOBANT, V. 2007. *Mass spectrometry: Principles and applications*, Chichester, England, John Wiley & Sons, Ltd.

HOPKINSON, S. B., HAMILL, K. J., WU, Y., EISENBERG, J. L., HIROYASU, S. & JONES, J. C. 2014. Focal contact and hemidesmosomal proteins in keratinocyte migration and wound repair. *Adv Wound Care (New Rochelle)*, 3, 247-263.

HOUSSIAU, F. & VAN SNICK, J. 1992. IL6 and the T-cell response. *Res Immunol*, 143, 740-743.

HU, Q. Z., NOLL, R. J., LI, H. Y., MAKAROV, A., HARDMAN, M. & COOKS, R. G. 2005. The Orbitrap: a new mass spectrometer. *J Mass Spectr*, 40, 430-443.

- HUILGOL, S. C., CARRUTHERS, A. & CARRUTHERS, J. D. 1999. Raising eyebrows with botulinum toxin. *Dermatol Surg*, 25, 373-376.
- ICH 1996. Validation of analytical procedures: methodology, ICH Topic Q2B (CPMP/ICH/281/95). The European Agency for the Evaluation of Medicinal Products.
- ICHINOSE, M., MIURA, M., TAKAHASHI, T., YAMAUCHI, H., KAGEYAMA, N., TOMAKI, M., ENDOH, N., SAKURAI, E., WATANABE, T. & SHIRATO, K. 1995. Allergic airway response and potassium channels: histamine release and airway inflammation. *Methods Find Exp Clin Pharmacol*, 17 (Suppl. C), 36-39.
- IDRISS, H. T. & NAISMITH, J. H. 2000. TNF alpha and the TNF receptor superfamily: structure-function relationship(s). *Microsc Res Tech*, 50, 184-195.
- ISBELL, L. A. 2006. Snakes as agents of evolutionary change in primate brains. *J Hum Evol*, 51, 1-35.
- JANG, H. S., KIM, S. K., HAN, J. B., AHN, H. J., BAE, H. & MIN, B. I. 2005. Effects of bee venom on the pro-inflammatory responses in RAW264.7 macrophage cell line. *J Ethnopharmacol*, 99, 157-160.
- JARAVINE, V. A., ZHURAVLEVA, A. V., PERMI, P., IBRAGHIMOV, I. & OREKHOV, V. Y. 2008. Hyperdimensional NMR spectroscopy with nonlinear sampling. *Journal of the American Chemical Society*, 130, 3927-3936.
- JONES, S. L., JONES, H. R. & THRASYVOULOU, A. 2011. Disseminating research about bee products. A review of articles published in the Journal of Apicultural Research over the past fifty years. *Journal of ApiProduct & ApiMedical Science*, 3, 105-116.
- KAMAKURA, M. 2011. Royalactin induces queen differentiation in honeybees. *Nature*, 473, 478-83.
- KAPOOR, S. 2012. Bee Venom Therapy: Neuro Therapeutic Benefits Besides Pain Amelioration. *Journal of Pain*, 13, 608-608.

- KEMENY, D. M., DALTON, N., LAWRENCE, A. J., PEARCE, F. L. & VERNON, C. A. 1984. The purification and characterisation of hyaluronidase from the venom of the honey bee, *Apis mellifera*. *Eur J Biochem*, 139, 217-223.
- KENDALL, A. C. & NICOLAOU, A. 2013. Bioactive lipid mediators in skin inflammation and immunity. *Prog Lipid Res*, 52, 141-164.
- KETTNER, A., HUGHES, G. J., FRUTIGER, S., ASTORI, M., ROGGERO, M., SPERTINI, F. & CORRADIN, G. 2001. Api m 6: a new bee venom allergen. *J Allergy Clin Immunol*, 107, 914-20.
- KOBUROVA, K. L., MICHAILOVA, S. G. & SHKENDEROV, S. V. 1985. Further investigation on the antiinflammatory properties of adolapin--bee venom polypeptide. *Acta Physiol Pharmacol Bulg*, 11, 50-55.
- KOKOT, Z., MATYSIAK, J. & MATYSIAK, J. 2009. Simultaneous Determination of Major Constituents of Honeybee Venom by LC-DAD. *An International Journal for Rapid Communication in Chromatography, Electrophoresis and Associated Techniques*, 69, 1401-1405.
- KOKOT, Z. J. & MATYSIAK, J. 2009. Simultaneous determination of major constituents of honeybee venom by LC-DAD. *Chromatographia*, 69, 1401-1405.
- KOKOT, Z. J., MATYSIAK, J., URBANIAK, B. & DEREZINSKI, P. 2011a. New CZE-DAD method for honeybee venom analysis and standardization of the product. *Analytical and Bioanalytical Chemistry*, 399, 2487-2494.
- KOKOT, Z. J., MATYSIAK, J., URBANIAK, B. & DEREZIŃSKI, P. 2011b. New CZE-DAD method for honeybee venom analysis and standardization of the product. *Analytical and Bioanalytical Chemistry*, 399, 2487-2494.
- KREIL, G., HAIML, L. & SUCHANEK, G. 1980. Stepwise cleavage of the pro part of promelittin by dipeptidylpeptidase IV: Evidence for a new type of precursor--product conversion. *Eur J Biochem*, 111, 49-58.

- KUMAGAI, C., OKANO, M. & KITAGAWA, Y. 2000. Three heterotrimeric laminins produced by human keratinocytes. *Cytotechnology*, 33, 167-174.
- KUMAR, A., HEATON, J. C. & MCCALLEY, D. V. 2013. Practical investigation of the factors that affect the selectivity in hydrophilic interaction chromatography. *J Chromatogr A*, 1276, 33-46.
- LAI, C.-C. & HER, G.-R. 2000. Analysis of phospholipase A2 glycosylation patterns from venom of individual bees by capillary electrophoresis/electrospray ionization mass spectrometry using an ion trap mass spectrometer. *Rapid Communications in Mass Spectrometry*, 14, 2012-2018.
- LAWRENCE, T. 2009. The Nuclear Factor NF- κ B Pathway in Inflammation. *Cold Spring Harbor Perspectives in Biology*, 1, a001651.
- LEE, J. & LEE, D. G. 2014. Melittin triggers apoptosis in *Candida albicans* through the reactive oxygen species-mediated mitochondria/caspase-dependent pathway. *FEMS Microbiol Lett*, 355, 36-42.
- LEE, J. D., PARK, H. J., CHAE, Y. & LIM, S. 2005. An overview of bee venom acupuncture in the treatment of arthritis. *Evid Based Complement Alternat Med*, 2, 79-84.
- LEE, M. T., SUN, T. L., HUNG, W. C. & HUANG, H. W. 2013. Process of inducing pores in membranes by melittin. *Proc Natl Acad Sci U S A*, 110, 14243-14248.
- LEE, S. H., JIN, S. Y., SONG, J. S., SEO, K. K. & CHO, K. H. 2012. Paracrine effects of adipose-derived stem cells on keratinocytes and dermal fibroblasts. *Ann Dermatol*, 24, 136-143.
- LEVINE, M. Z., HARRISON, P. J., WALTHALL, W. W., TAI, P. C. & DERBY, C. D. 2001. A CUB-serine protease in the olfactory organ of the spiny lobster *Panulirus argus*. *J Neurobiol*, 49, 277-302.
- LIPOTEC 2008. Serilesie® solution GC: An adhesion sequence for laminin. *In*: LIPOTEC (ed.).

LIPOTEC. 2014a. *Eyeseryl® peptide* [Online]. Company Website: The Lubrizol Corporation. Available: <http://www.lipotec.com/en/products> [Accessed November 02, 2014 2014].

LIPOTEC. 2014b. *Liporeductyl® functional ingredient* [Online]. Company Website: The Lubrizol Corporation. Available: <http://www.lipotec.com/en/products> [Accessed November 02, 2014 2014].

LLOMPART, M., CELEIRO, M., PABLO LAMAS, J., SANCHEZ-PRADO, L., LORES, M. & GARCIA-JARES, C. 2013. Analysis of plasticizers and synthetic musks in cosmetic and personal care products by matrix solid-phase dispersion gas chromatography–mass spectrometry. *Journal of Chromatography A*, 1293, 10-19.

LODÉN, M. 2003. The skin barrier and use of moisturizers in atopic dermatitis. *Clinics in Dermatology*, 21, 145-157.

LOTFI, R. A., EL ZAWAHRY, K. M., KAMAR, Z. A. & HASHEM, Z. 2014. Effects of smoking on human telomerase reverse transcriptase expression in the skin. *Int J Dermatol*, 53, 1205-1212.

LUCASMEYERCOSMETICS. 2014a. *ChroNoline™: The anti-wrinkle peptide* [Online]. Company Website: Unipex Group Inc. Available: <http://lucasmeyercosmetics.com/en/products> [Accessed October 16, 2014 2014].

LUCASMEYERCOSMETICS. 2014b. *ECM-Protect®: Firmness & elasticity* [Online]. Company Website: Unipex Group Inc. Available: <http://lucasmeyercosmetics.com/en/products> [Accessed October 16, 2014 2014].

LUCASMEYERCOSMETICS. 2014c. *Kollaren™: The dermis enhancer* [Online]. Company Website: Unipex Group Inc. Available: <http://www.lucasmeyercosmetics.com/en/products> [Accessed October 16, 2014 2014].

LUCASMEYERCOSMETICS. 2014d. *Melanostatine™ 5: Focus on whitening* [Online]. Company Website: Unipex Group Inc. Available: <http://lucasmeyercosmetics.com/en/products> [Accessed October 16, 2014 2014].

- LUPO, M. P. 2005. Cosmeceutical peptides. *Dermatol Surg*, 31, 832-836.
- MAKAROV, A. & DENISOV, E. 2009. Dynamics of Ions of Intact Proteins in the Orbitrap Mass Analyzer. *Journal of the American Society for Mass Spectrometry*, 20, 1486-1495.
- MAKAROV, A., DENISOV, E., KHOLOMEEV, A., BAISCHUN, W., LANGE, O., STRUPAT, K. & HORNING, S. 2006. Performance evaluation of a hybrid linear ion trap/orbitrap mass spectrometer. *Analytical Chemistry*, 78, 2113-2120.
- MAKAROV, A., DENISOV, E. & LANGE, O. 2009. Performance Evaluation of a High-field Orbitrap Mass Analyzer. *Journal of the American Society for Mass Spectrometry*, 20, 1391-1396.
- MAKAROV, A. & SCIGELOVA, M. 2010. Coupling liquid chromatography to Orbitrap mass spectrometry. *Journal of Chromatography A*, 1217, 3938-3945.
- MALZ, F. & JANCKE, H. 2005. Validation of quantitative NMR. *J Pharm Biomed Anal*, 38, 813-823.
- MARCH, R. E. 1997. An introduction to quadrupole ion trap mass spectrometry. *J Mass Spectr*, 32, 351-369.
- MARKOVIC-HOUSLEY, Z., MIGLIERINI, G., SOLDATOVA, L., RIZKALLAH, P. J., MULLER, U. & SCHIRMER, T. 2000. Crystal structure of hyaluronidase, a major allergen of bee venom. *Structure*, 8, 1025-35.
- MATTEUCCI, E. & GIAMPIETRO, O. 2009. Dipeptidyl peptidase-4 (CD26): knowing the function before inhibiting the enzyme. *Curr Med Chem*, 16, 2943-51.
- MATYSIAK, J., SCHMELZER, C. E. H., NEUBERT, R. H. H. & KOKOT, Z. J. 2011. Characterization of honeybee venom by MALDI-TOF and nanoESI-QqTOF mass spectrometry. *J Pharm Biomed Anal*, 54, 273-278.
- MCLAFFERTY, F. 1981. Tandem mass spectrometry. *Science*, 214, 280-287.

- MCNAIR, H. M. & MILLER, J. M. 2011. *Basic gas chromatography*, John Wiley & Sons.
- MECKFESSEL, M. H. & BRANDT, S. 2014. The structure, function, and importance of ceramides in skin and their use as therapeutic agents in skin-care products. *J Am Acad Dermatol*, 71, 177-184.
- MEHTA, A., ZITZMANN, N., RUDD, P. M., BLOCK, T. M. & DWEK, R. A. 1998. α -Glucosidase inhibitors as potential broad based anti-viral agents. *FEBS Letters*, 430, 17-22.
- MENG, Y., YANG, X. X., SHENG, Y. X., ZHANG, J. L. & YU, D. Q. 2012. A novel peptide from *Apis mellifera* and solid-phase synthesis of its analogue. *Chinese Chemical Letters*, 23, 1161-1164.
- MICHALSKI, A., DAMOC, E., HAUSCHILD, J.-P., LANGE, O., WIEGHAUS, A., MAKAROV, A., NAGARAJ, N., COX, J., MANN, M. & HORNING, S. 2011. Mass Spectrometry-based Proteomics Using Q Exactive, a High-performance Benchtop Quadrupole Orbitrap Mass Spectrometer. *Molecular & Cellular Proteomics*, 10.
- MIN, L. J., CUI, T. X., YAHATA, Y., YAMASAKI, K., SHIUCHI, T., LIU, H. W., CHEN, R., LI, J. M., OKUMURA, M., JINNO, T., WU, L., IWAI, M., NAHMIAS, C., HASHIMOTO, K. & HORIUCHI, M. 2004. Regulation of collagen synthesis in mouse skin fibroblasts by distinct angiotensin II receptor subtypes. *Endocrinology*, 145, 253-260.
- MINTA, J. O. & PAMBRUN, L. 1985. *In vitro* induction of cytologic and functional differentiation of the immature human monocytelike cell line U-937 with phorbol myristate acetate. *Am J Pathol*, 119, 111-26.
- MISEKI, K. 1993. *Quadrupole mass spectrometer*. United States patent application 800,069.

- MIURA, Y. 2011. NMR studies on thermal stability of α -helix conformation of melittin in pure ethanol and ethanol–water mixture solvents. *Journal of Peptide Science*, 17, 798-804.
- MIZUKOSHI, K. & TAKAHASHI, K. 2014. Analysis of the skin surface and inner structure around pores on the face. *Skin Res Technol*, 20, 23-29.
- MIZUKOSHI, K., YONEKURA, K., FUTAGAWA, M., NAKAMURA, T., HIRAYAMA, K. & TAKAHASHI, K. 2014. Changes in dermal papilla structures due to aging in the facial cheek region. *Skin Res Technol*, 0, 1-8.
- MOLDOVEANU, S. & DAVID, V. 2015. Solid-phase extraction. *Modern Sample Preparation for Chromatography*. Amsterdam: Elsevier.
- MOLLAY, C., VILAS, U. & KREIL, G. 1982. Cleavage of honeybee prepromelittin by an endoprotease from rat liver microsomes: identification of intact signal peptide. *Proc Natl Acad Sci U S A*, 79, 2260-2263.
- MONHEIT, G., CARRUTHERS, A., BRANDT, F. & RAND, R. 2007. A randomized, double-blind, placebo-controlled study of botulinum toxin type A for the treatment of glabellar lines: determination of optimal dose. *Dermatol Surg*, 33, S51-S59.
- MONINCOVA, L., BUDESINSKY, M., SLANINOVA, J., HOVORKA, O., CVACKA, J., VOBURKA, Z., FUCIK, V., BOROVIKOVÁ, L., BEDNAROVA, L., STRAKA, J. & CEROVSKY, V. 2010. Novel antimicrobial peptides from the venom of the eusocial bee *Halictus sexcinctus* (Hymenoptera: Halictidae) and their analogs. *Amino Acids*, 39, 763-775.
- MONTI, M. C., CASAPULLO, A., SANTOMAURO, C., D'AURIA, M. V., RICCIO, R. & GOMEZ-PALOMA, L. 2006. The Molecular Mechanism of Bee Venom Phospholipase A2 Inactivation by Bolinaquinone. *ChemBioChem*, 7, 971-980.
- MOON, D. O., PARK, S. Y., LEE, K. J., HEO, M. S., KIM, K. C., KIM, M. O., LEE, J. D., CHOI, Y. H. & KIM, G. Y. 2007. Bee venom and melittin reduce

proinflammatory mediators in lipopolysaccharide-stimulated BV2 microglia. *Int Immunopharmacol*, 7, 1092-1101.

MOON, K. M., PARK, Y. H., LEE, J. S., CHAE, Y. B., KIM, M. M., KIM, D. S., KIM, B. W., NAM, S. W. & LEE, J. H. 2012. The effect of secretory factors of adipose-derived stem cells on human keratinocytes. *Int J Mol Sci*, 13, 1239-1257.

MOREAU, S. J. 2013. "It stings a bit but it cleans well": venoms of Hymenoptera and their antimicrobial potential. *J Insect Physiol*, 59, 186-204.

MOURELLE, D., BRIGATTE, P., BRINGANTI, L. D. B., DE SOUZA, B. M., ARCURI, H. A., GOMES, P. C., BAPTISTA-SAIDEMBERG, N. B., RUGGIERO NETO, J. & PALMA, M. S. 2014. Hyperalgesic and edematogenic effects of Secapin-2, a peptide isolated from Africanized honeybee (*Apis mellifera*) venom. *Peptides*, 59, 42-52.

NATURE 2006. Insights into social insects from the genome of the honeybee *Apis mellifera*. *Nature*, 443, 931-949.

NEWTON, K. A., CLENCH, M. R., DESHMUKH, R., JEYASEELAN, K. & STRONG, P. N. 2007. Mass fingerprinting of toxic fractions from the venom of the Indian red scorpion, *Mesobuthus tamulus*: biotope-specific variation in the expression of venom peptides. *Rapid Commun Mass Spectrom*, 21, 3467-76.

NIKOLETOPOULOU, V., MARKAKI, M., PALIKARAS, K. & TAVERNARAKIS, N. 2013. Crosstalk between apoptosis, necrosis and autophagy. *Biochim Biophys Acta*, 1833, 3448-59.

OGAWA, T., TSUBOTA, Y., HASHIMOTO, J., KARIYA, Y. & MIYAZAKI, K. 2007. The short arm of laminin gamma2 chain of laminin-5 (laminin-332) binds syndecan-1 and regulates cellular adhesion and migration by suppressing phosphorylation of integrin beta4 chain. *Mol Biol Cell*, 18, 1621-1633.

OKADA, M., KITAHARA, M., KISHIMOTO, S., MATSUDA, T., HIRANO, T. & KISHIMOTO, T. 1988. IL-6/BSF-2 functions as a killer helper factor in the *in vitro* induction of cytotoxic T cells. *J Immunol*, 141, 1543-1549.

OLSEN, J. V., SCHWARTZ, J. C., GRIEP-RAMING, J., NIELSEN, M. L., DAMOC, E., DENISOV, E., LANGE, O., REMES, P., TAYLOR, D., SPLENDORE, M., WOUTERS, E. R., SENKO, M., MAKAROV, A., MANN, M. & HORNING, S. 2009. A Dual Pressure Linear Ion Trap Orbitrap Instrument with Very High Sequencing Speed. *Molecular & Cellular Proteomics*, 8, 2759-2769.

ORFANOS, C. E., ZOUBOULIS, C. C., ALMOND-ROESLER, B. & GEILEN, C. C. 1997. Current use and future potential role of retinoids in dermatology. *Drugs*, 53, 358-88.

ORSOLIC, N. 2012. Bee venom in cancer therapy. *Cancer and Metastasis Reviews*, 31, 173-194.

OTTE, A., MANDEL, K., REINSTROM, G. & HASS, R. 2011. Abolished adherence alters signaling pathways in phorbol ester-induced human U937 cells. *Cell Communication and Signaling : CCS*, 9, 20-20.

OWEN, D. R. 2008. *Cosmetic compositions containing short bioactive peptides*. United States patent application 10/839,525.

OWEN, D. R., DR. 2002. *Short bioactive peptides and methods for their use*. EU patent application 09159563.7.

OWEN, M. D. & BRIDGES, A. R. 1982. Catecholamines in honey bee (*Apis mellifera* L.) and various vespid (Hymenoptera) venoms. *Toxicon*, 20, 1075-1084.

PADAVATTAN, S., SCHIRMER, T., SCHMIDT, M., AKDIS, C., VALENTA, R., MITTERMANN, I., SOLDATOVA, L., SLATER, J., MUELLER, U. & MARKOVIC-HOUSLEY, Z. 2007. Identification of a B-cell epitope of hyaluronidase, a major bee venom allergen, from its crystal structure in complex with a specific Fab. *J Mol Biol*, 368, 742-752.

PARK, H. J., LEE, S. H., SON, D. J., OH, K. W., KIM, K. H., SONG, H. S., KIM, G. J., OH, G. T., YOON, D. Y. & HONG, J. T. 2004. Antiarthritic effect of bee venom: inhibition of inflammation mediator generation by suppression of NF-kappaB through interaction with the p50 subunit. *Arthritis Rheum*, 50, 3504-3515.

- PARK, H. J., SON, D. J., LEE, C. W., CHOI, M. S., LEE, U. S., SONG, H. S., LEE, J. M. & HONG, J. T. 2007. Melittin inhibits inflammatory target gene expression and mediator generation via interaction with IkappaB kinase. *Biochem Pharmacol*, 73, 237-247.
- PARK, I. H., UM, J. Y., CHO, J. S., LEE, S. H. & LEE, H. M. 2014. Histamine promotes the release of interleukin-6 via the H1R/p38 and NF-kappaB pathways in nasal fibroblasts. *Allergy Asthma Immunol Res*, 6, 567-572.
- PARK, M. H., KIM, J. H., JEON, J. W., PARK, J. K., LEE, B. J., SUH, G. H. & CHO, C. W. 2015. Preformulation studies of bee venom for the preparation of bee venom-loaded PLGA particles. *Molecules*, 20, 15072-15083.
- PASSMORE, J. S., LUKEY, P. T. & RESS, S. R. 2001. The human macrophage cell line U937 as an *in vitro* model for selective evaluation of mycobacterial antigen-specific cytotoxic T-cell function. *Immunology*, 102, 146-156.
- PEDARZANI, P., D'HOEDT, D., DOORTY, K. B., WADSWORTH, J. D., JOSEPH, J. S., JEYASEELAN, K., KINI, R. M., GADRE, S. V., SAPATNEKAR, S. M., STOCKER, M. & STRONG, P. N. 2002. Tamapin, a venom peptide from the Indian red scorpion (*Mesobuthus tamulus*) that targets small conductance Ca²⁺-activated K⁺ channels and afterhyperpolarization currents in central neurons. *J Biol Chem*, 277, 46101-9.
- PEIREN, N., DE GRAAF, D. C., VANROBAEYS, F., DANNEELS, E. L., DEVREESE, B., VAN BEEUMEN, J. & JACOBS, F. J. 2008. Proteomic analysis of the honey bee worker venom gland focusing on the mechanisms of protection against tissue damage. *Toxicon*, 52, 72-83.
- PICKETT, J. A., WILLIAMS, I. & MARTIN, A. P. 1982. (Z)-11-eicosen-1-ol, an important new pheromonal component from the sting of the honey bee, *Apis mellifera* L. (Hymenoptera, Apidae.). *J Chem Ecol*, 8, 163-175.

- RALLIS, E. & KOUMANTAKI-MATHIOUDAKI, E. 2007. Treatment of *Mycobacterium marinum* cutaneous infections. *Expert Opinion on Pharmacotherapy*, 8, 2965-2978.
- RAMADHANI, D., TSUKADA, T., FUJIWARA, K., HORIGUCHI, K., KIKUCHI, M. & YASHIRO, T. 2012. Laminin isoforms and laminin-producing cells in rat anterior pituitary. *Acta Histochem Cytochem*, 45, 309-315.
- RAMOS-E-SILVA, M. & CARNEIRO, S. C. D. S. 2001. Cosmetics for the elderly. *Clinics in Dermatology*, 19, 413-423.
- RAMPERSAD, S. N. 2012. Multiple applications of Alamar Blue® as an indicator of metabolic function and cellular health in cell viability bioassays. *Sensors (Basel)*, 12, 12347-12360.
- RAWLINGS, A. V. 2014. Molecular basis for stratum corneum maturation and moisturization. *Br J Dermatol*, 171 (Suppl. 3), 19-28.
- REED, M. J., DAMODARASAMY, M., CHAN, C. K., JOHNSON, M. N., WIGHT, T. N. & VERNON, R. B. 2013. Cleavage of hyaluronan is impaired in aged dermal wounds. *Matrix Biol*, 32, 45-51.
- REGNIER-VIGOUROUX, A., EL AYEB, M., DEFENDINI, M. L., GRANIER, C. & PIERRES, M. 1988. Processing by accessory cells for presentation to murine T cells of apamin, a disulfide-bonded 18 amino acid peptide. *J Immunol*, 140, 1069-1075.
- RHIE, G., SHIN, M. H., SEO, J. Y., CHOI, W. W., CHO, K. H., KIM, K. H., PARK, K. C., EUN, H. C. & CHUNG, J. H. 2001. Aging- and photoaging-dependent changes of enzymic and nonenzymic antioxidants in the epidermis and dermis of human skin *in vivo*. *J Invest Dermatol*, 117, 1212-1217.
- RHO, Y. H., WOO, J.-H., CHOI, S. J., LEE, Y. H., JI, J. D. & SONG, G. G. 2009. A new onset of systemic lupus erythematosus developed after bee venom therapy. *Korean J Intern Med*, 24, 283-285.

- RISS, T. L., MORAVEC, R. A. & NILES, A. L. 2011. Cytotoxicity testing: measuring viable cells, dead cells, and detecting mechanism of cell death. *In: STODDART, M. J. (ed.) Mammalian Cell Viability: Methods and Protocols*. New York: Humana Press.
- ROSATI, S., ROSE, R. J., THOMPSON, N. J., VAN DUIJN, E., DAMOC, E., DENISOV, E., MAKAROV, A. & HECK, A. J. 2012. Exploring an orbitrap analyzer for the characterization of intact antibodies by native mass spectrometry. *Angew Chem Int Ed Engl*, 51, 12992-12996.
- RUDIHOFF, D. 1998. The effect of dryness on the skin. *Clinics in Dermatology*, 16, 99-107.
- SADICK, N. S., KARCHER, C. & PALMISANO, L. 2009. Cosmetic dermatology of the aging face. *Clinics in Dermatology*, 27, S3-S12.
- SCHMIDT, J. O., MORGAN, E. D., OLDHAM, N. J., DO NASCIMENTO, R. R. & DANI, F. R. 1997. (Z)-11-Eicosen-1-ol, a major component of *Apis cerana* Venom. *J Chem Ecol*, 23, 1929-1939.
- SCHUBERTH, J. 2000. ANALYTICAL TECHNIQUES | Mass Spectrometry. *In: SIEGEL, J. A. (ed.) Encyclopedia of Forensic Sciences*. Oxford: Elsevier.
- SCIANI, J. M., MARQUES-PORTO, R., LOURENCO JUNIOR, A., ORSI, R. D. O., FERREIRA JUNIOR, R. S., BARRAVIERA, B. & PIMENTA, D. C. 2010. Identification of a novel melittin isoform from Africanized *Apis mellifera* venom. *Peptides*, 31, 1473-1479.
- SCIGELOVA, M., HORNSHAW, M., GIANNAKOPOULOS, A. & MAKAROV, A. 2011. Fourier Transform Mass Spectrometry. *Molecular & Cellular Proteomics*, 10.
- SCIGELOVA, M. & MAKAROV, A. 2006. Orbitrap mass analyzer--overview and applications in proteomics. *Proteomics*, 6 Suppl 2, 16-21.

- SCOTT, D. L., OTWINOWSKI, Z., GELB, M. H. & SIGLER, P. B. 1990. Crystal structure of bee-venom phospholipase A₂ in a complex with a transition-state analogue. *Science*, 250, 1563-1566.
- SEPPALA, U., FRANCESE, S., TURILLAZZI, S., MONETI, G., CLENCH, M. & BARBER, D. 2012. *In situ* imaging of honeybee (*Apis mellifera*) venom components from aqueous and aluminum hydroxide-adsorbed venom immunotherapy preparations. *J Allergy Clin Immunol*, 129, 1314-1320.
- SHARMA, A., DIECKE, S., ZHANG, W. Y., LAN, F., HE, C., MORDWINKIN, N. M., CHUA, K. F. & WU, J. C. 2013. The role of SIRT6 protein in aging and reprogramming of human induced pluripotent stem cells. *J Biol Chem*, 288, 18439-18447.
- SHIPOLINI, R. A., CALLEWAERT, G. L., COTTRELL, R. C. & VERNON, C. A. 1971. The primary sequence of phospholipase-A₂ from bee venom. *FEBS Lett*, 17, 39-40.
- SHKENDEROV, S. & KOBUROVA, K. 1982. Adolapin--a newly isolated analgetic and anti-inflammatory polypeptide from bee venom. *Toxicon*, 20, 317-321.
- SINGH, B. & MAIBACH, H. 2013. Climate and skin function: an overview. *Skin Res Technol*, 19, 207-212.
- SON, D. J., LEE, J. W., LEE, Y. H., SONG, H. S., LEE, C. K. & HONG, J. T. 2007. Therapeutic application of anti-arthritis, pain-releasing, and anti-cancer effects of bee venom and its constituent compounds. *Pharmacol Ther*, 115, 246-270.
- SOSA, L. D. V., ALFARO, E., SANTIAGO, J., NARVÁEZ, D., ROSADO, M. C., RODRÍGUEZ, A., GÓMEZ, A. M., SCHREITER, E. R. & PASTRANA-RÍOS, B. 2011. The structure, molecular dynamics, and energetics of centrin–melittin complex. *Proteins: Structure, Function, and Bioinformatics*, 79, 3132-3143.
- SRIVASTAVA, R. M., SRIVASTAVA, S., SINGH, M., BAJPAI, V. K. & GHOSH, J. K. 2012. Consequences of alteration in leucine zipper sequence of melittin in its neutralization of lipopolysaccharide-induced proinflammatory response in

macrophage cells and interaction with lipopolysaccharide. *J Biol Chem*, 287, 1980-1995.

STAFF, J. C. E. 1978. Chemistry of cosmetics. *Journal of Chemical Education*, 55, 802.

STEPHENS, N. A., KIEFT, R., MACLEOD, A. & HAJDUK, S. L. 2012. Trypanosome resistance to human innate immunity: targeting Achilles' heel. *Trends in Parasitology*, 28, 539-545.

STIEFEL, C. & SCHWACK, W. 2014. Photoprotection in changing times - UV filter efficacy and safety, sensitization processes and regulatory aspects. *Int J Cosmet Sci*, 37, 2-30.

STOECKLIN, R., FAVREAU, P., THAI, R., PFLUGFELDER, J., BULET, P. & MEBS, D. 2010. Structural identification by mass spectrometry of a novel antimicrobial peptide from the venom of the solitary bee *Osmia rufa* (Hymenoptera: Megachilidae). *Toxicon*, 55, 20-27.

STREHLOW, K., ROTTER, S., WASSMANN, S., ADAM, O., GROHE, C., LAUFS, K., BOHM, M. & NICKENIG, G. 2003. Modulation of antioxidant enzyme expression and function by estrogen. *Circ Res*, 93, 170-7.

STUHLMEIER, K. M. 2007. *Apis mellifera* venom and melittin block neither NF-kappa B-p50-DNA interactions nor the activation of NF-kappa B, instead they activate the transcription of proinflammatory genes and the release of reactive oxygen intermediates. *J Immunol*, 179, 655-64.

SUCHANEK, G. & KREIL, G. 1977. Translation of melittin messenger RNA *in vitro* yields a product terminating with glutaminyglycine rather than with glutaminamide. *Proc Natl Acad Sci U S A*, 74, 975-978.

SUCHANEK, G., KREIL, G. & HERMODSON, M. A. 1978. Amino acid sequence of honeybee prepromelittin synthesized *in vitro*. *Proc Natl Acad Sci U S A*, 75, 701-704.

- SUNDSTROM, C. & NILSSON, K. 1976. Establishment and characterization of a human histiocytic lymphoma cell line (U-937). *Int J Cancer*, 17, 565 - 577.
- TAKAGAKI, K., NAKAMURA, T., IZUMI, J., SAITOH, H., ENDO, M., KOJIMA, K., KATO, I. & MAJIMA, M. 1994. Characterization of hydrolysis and transglycosylation by testicular hyaluronidase using ion-spray mass spectrometry. *Biochemistry*, 33, 6503-6507.
- TAKASAO, N., TSUJI-NAITO, K., ISHIKURA, S., TAMURA, A. & AKAGAWA, M. 2012. Cinnamon extract promotes type I collagen biosynthesis via activation of IGF-I signaling in human dermal fibroblasts. *J Agric Food Chem*, 60, 1193-1200.
- TAYLOR, S., TATE, T., SYMS, R. & DOREY, H. 2000. *Quadrupole mass spectrometers*. United States patent application 08/939,725.
- TERWILLIGER, T. C. & EISENBERG, D. 1982. The structure of melittin. I. Structure determination and partial refinement. *J Biol Chem*, 257, 6010-6015.
- TERWILLIGER, T. C., WEISSMAN, L. & EISENBERG, D. 1982. The structure of melittin in the form I crystals and its implication for melittin's lytic and surface activities. *Biophys J*, 37, 353-61.
- TETI, A. 1992. Regulation of cellular functions by extracellular matrix. *J Am Soc Nephrol*, 2, S83-S87.
- THRIPPLETON, M. J. & KEELER, J. 2003. Elimination of Zero-Quantum Interference in Two-Dimensional NMR Spectra. *Angewandte Chemie*, 115, 4068-4071.
- TIGANESCU, A., TAHRANI, A. A., MORGAN, S. A., OTRANTO, M., DESMOULIERE, A., ABRAHAMS, L., HASSAN-SMITH, Z., WALKER, E. A., RABBITT, E. H., COOPER, M. S., AMREIN, K., LAVERY, G. G. & STEWART, P. M. 2013. 11beta-Hydroxysteroid dehydrogenase blockade prevents age-induced skin structure and function defects. *J Clin Invest*, 123, 3051-3060.

- TIGANESCU, A., WALKER, E. A., HARDY, R. S., MAYES, A. E. & STEWART, P. M. 2011. Localization, age- and site-dependent expression, and regulation of 11beta-hydroxysteroid dehydrogenase type 1 in skin. *J Invest Dermatol*, 131, 30-36.
- TOSATO, G. & PIKE, S. E. 1988. Interferon-beta 2/interleukin 6 is a co-stimulant for human T lymphocytes. *J Immunol*, 141, 1556-1562.
- TULLO, C. 2013. Consumer Protection: The Cosmetic Products Enforcement Regulations 2013. In: KINGDOM, P. O. T. U. (ed.) 20131478. United Kingdom: The Stationery Office Limited.
- TUSIIMIRE, J., WALLACE, J., DUFTON, M., PARKINSON, J., CLEMENTS, C. J., YOUNG, L., PARK, J. K., JEON, J. W. & WATSON, D. G. 2015. An LC-MS method for the assay of melittin in cosmetic formulations containing bee venom. *Anal Bioanal Chem*, 407, 3627-3635.
- TUSIIMIRE, J., WALLACE, J., WOODS, N., DUFTON, M. J., PARKINSON, J. A., ABBOTT, G., CLEMENTS, C. J., YOUNG, L., PARK, J. K., JEON, J. W., FERRO, V. A. & WATSON, D. G. 2016. Effect of Bee Venom and Its Fractions on the Release of Pro-Inflammatory Cytokines in PMA-Differentiated U937 Cells Co-Stimulated with LPS. *Vaccines (Basel)*, 4, 11.
- VAN DER VELDEN, V. H. (1998). Glucocorticoids: mechanisms of action and anti-inflammatory potential in asthma. *Mediators of Inflammation*, 7, 229–237.
- VAN SNICK, J., VINK, A., UYTENHOVE, C., HOUSSIAU, F. & COULIE, P. 1988. B and T cell responses induced by interleukin-6. *Curr Top Microbiol Immunol*, 141, 181-184.
- VAN VAERENBERGH, M., CARDOEN, D., FORMESYN, E. M., BRUNAIN, M., VAN DRIESSE, G., BLANK, S., SPILLNER, E., VERLEYEN, P., WENSELEERS, T., SCHOOF, L., DEVREESE, B. & DE GRAAF, D. C. 2013. Extending the honey bee venom with the antimicrobial peptide apidaecin and a protein resembling wasp antigen 5. *Insect Mol Biol*, 22, 199-210.

VERHOECKX, K. C., BIJLSMA, S., DE GROENE, E. M., WITKAMP, R. F., VAN DER GREEF, J. & RODENBURG, R. J. 2004. A combination of proteomics, principal component analysis and transcriptomics is a powerful tool for the identification of biomarkers for macrophage maturation in the U937 cell line. *Proteomics*, 4, 1014-28.

VICK, J. A., MEHLMAN, B., BROOKS, R., PHILLIPS, S. J. & SHIPMAN, W. 1972. Effect of the bee venom and melittin on plasma cortisol in the unanesthetized monkey. *Toxicon*, 10, 581-586.

VICK, J. A. & SHIPMAN, W. H. 1972. Effects of whole bee venom and its fractions (apamin and melittin) on plasma cortisol levels in the dog. *Toxicon*, 10, 377-380.

VLASAK, R. & KREIL, G. 1984. Nucleotide sequence of cloned cDNAs coding for preprosecapin, a major product of queen-bee venom glands. *Eur J Biochem*, 145, 279-282.

VLASAK, R., UNGER-ULLMANN, C., KREIL, G. & FRISCHAUF, A. M. 1983. Nucleotide sequence of cloned cDNA coding for honeybee prepromelittin. *Eur J Biochem*, 135, 123-126.

WANG, F. & POLAVARAPU, P. L. 2003. Conformational analysis of melittin in solution phase: Vibrational circular dichroism study. *Biopolymers*, 70, 614-619.

WATSON, D. G. 2012. *Pharmaceutical Analysis: a Textbook for Pharmacy Students and Pharmaceutical Chemists*, London, Elsevier Health Sciences.

WHO/IUIS. 2014. *Allergen Nomenclature* [Online]. www.allergen.org: Allergen Nomenclature Sub-Committee. Available: www.allergen.org [Accessed 02 December 2014].

WILM, M. 2011. Principles of electrospray ionization. *Mol Cell Proteomics*, 10, M111 009407.

WLASCHEK, M., TANTCHEVA-POOR, I., NADERI, L., MA, W., SCHNEIDER, L. A., RAZI-WOLF, Z., SCHULLER, J. & SCHARFFETTER-KOCHANNEK, K.

2001. Solar UV irradiation and dermal photoaging. *J Photochem Photobiol B*, 63, 41-51.
- WOJCIK, R., LI, Y., MACCOSS, M. J. & DOVICHI, N. J. 2012. Capillary electrophoresis with Orbitrap-Velos mass spectrometry detection. *Talanta*, 88, 324-329.
- WOLFLE, U., SEELINGER, G., BAUER, G., MEINKE, M. C., LADEMANN, J. & SCHEMPP, C. M. 2014. Reactive molecule species and antioxidative mechanisms in normal skin and skin aging. *Skin Pharmacol Physiol*, 27, 316-332.
- YANG, Y., ZHANG, W., MENG, L., YU, H., LU, N., FU, G. & ZHENG, Y. 2015. Alpha-melanocyte stimulating hormone inhibits monocytes adhesion to vascular endothelium. *Exp Biol Med (Maywood)*, 240, 1537-42.
- YOON, J. H., KIM, J., LEE, H., KIM, S. Y., JANG, H. H., RYU, S. H., KIM, B. J. & LEE, T. G. 2012. Laminin peptide YIGSR induces collagen synthesis in HS27 human dermal fibroblasts. *Biochem Biophys Res Commun*, 428, 416-421.
- YOUN, U. J., NAM, K.-W., KIM, H.-S., CHOI, G., JEONG, W. S., LEE, M. Y. & CHAE, S. 2011. 3-Deoxysappanchalcone Inhibits Tumor Necrosis Factor- α -Induced Matrix Metalloproteinase-9 Expression in Human Keratinocytes through Activated Protein-1 Inhibition and Nuclear Factor-Kappa B DNA Binding Activity. *Biol. Pharm. Bull.*, 34, 890-893.
- YOUNG, C. S. & DOLAN, J. W. 2003. Success with evaporative light-scattering detection. *LC-GC North America*, 21, 120-128.
- YOUNG, C. S. & DOLAN, J. W. 2004. Success with evaporative light-scattering detection. *LC•GC Europe*, 17, 192-199.
- ZHANG, J., LIU, H. & KATTA, V. 2010. Structural characterization of intact antibodies by high-resolution LTQ Orbitrap mass spectrometry. *Journal of Mass Spectrometry*, 45, 112-120.

ZHANG, L., HARRIS, S., M. & FALLA, T., J. 2008. *Protective skin care peptides*. United States patent application 12/290,236. Dec 06, 2011.

ZHANG, R., WATSON, D. G., WANG, L., WESTROP, G. D., COOMBS, G. H. & ZHANG, T. 2014. Evaluation of mobile phase characteristics on three zwitterionic columns in hydrophilic interaction liquid chromatography mode for liquid chromatography-high resolution mass spectrometry based untargeted metabolite profiling of *Leishmania* parasites. *J Chromatogr A*, 1362, 168-179.

ZHANG, T., CREEK, D. J., BARRETT, M. P., BLACKBURN, G. & WATSON, D. G. 2012. Evaluation of coupling reversed phase, aqueous normal phase, and hydrophilic interaction liquid chromatography with Orbitrap mass spectrometry for metabolomic studies of human urine. *Anal Chem*, 84, 1994-2001.

ZHOU, J., ZHAO, J., ZHANG, S., SHEN, J., QI, Y., XUE, X., LI, Y., WU, L., ZHANG, J., CHEN, F. & CHEN, L. 2010. Quantification of melittin and apamin in bee venom lyophilized powder from *Apis mellifera* by liquid chromatography-diode array detector-tandem mass spectrometry. *Anal Biochem*, 404, 171-178.

ZOUBOULIS, C. C. & MAKRANTONAKI, E. 2011. Clinical aspects and molecular diagnostics of skin aging. *Clin Dermatol*, 29, 3-14.

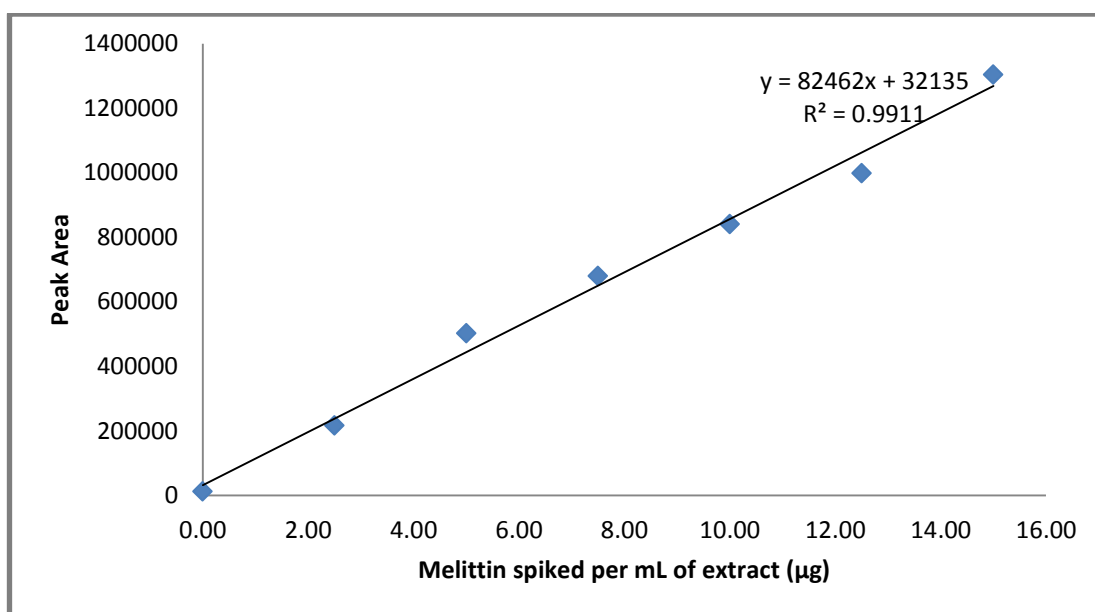
Appendices for Chapters 7 and 8

Appendices and Supplementary Information

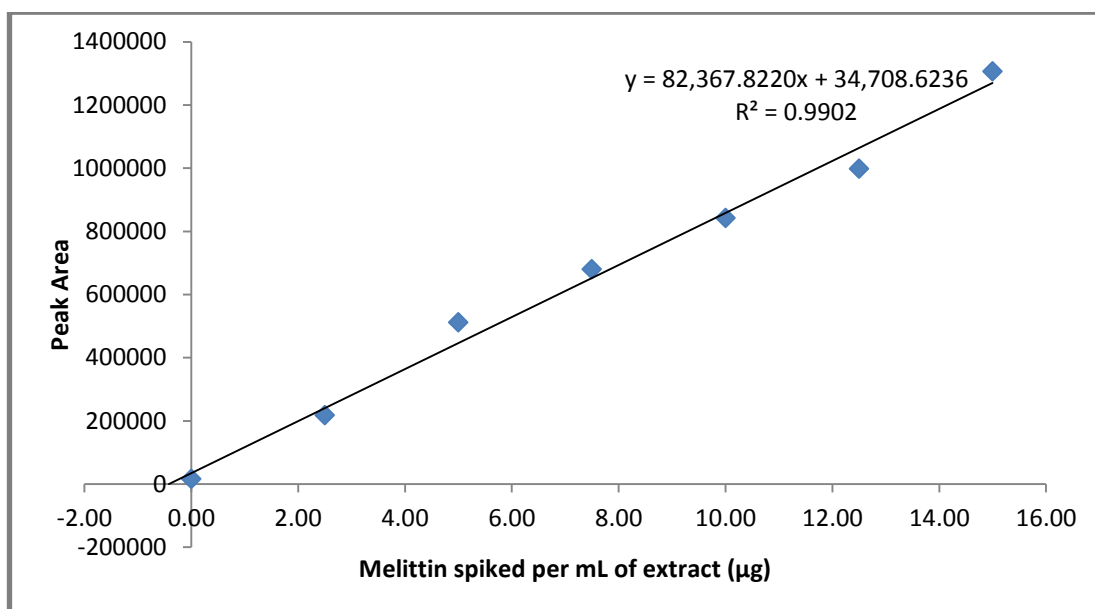
Appendix I: Supplementary data for Chapter 7

Standard Addition Calibration curves for sample A (PBV)

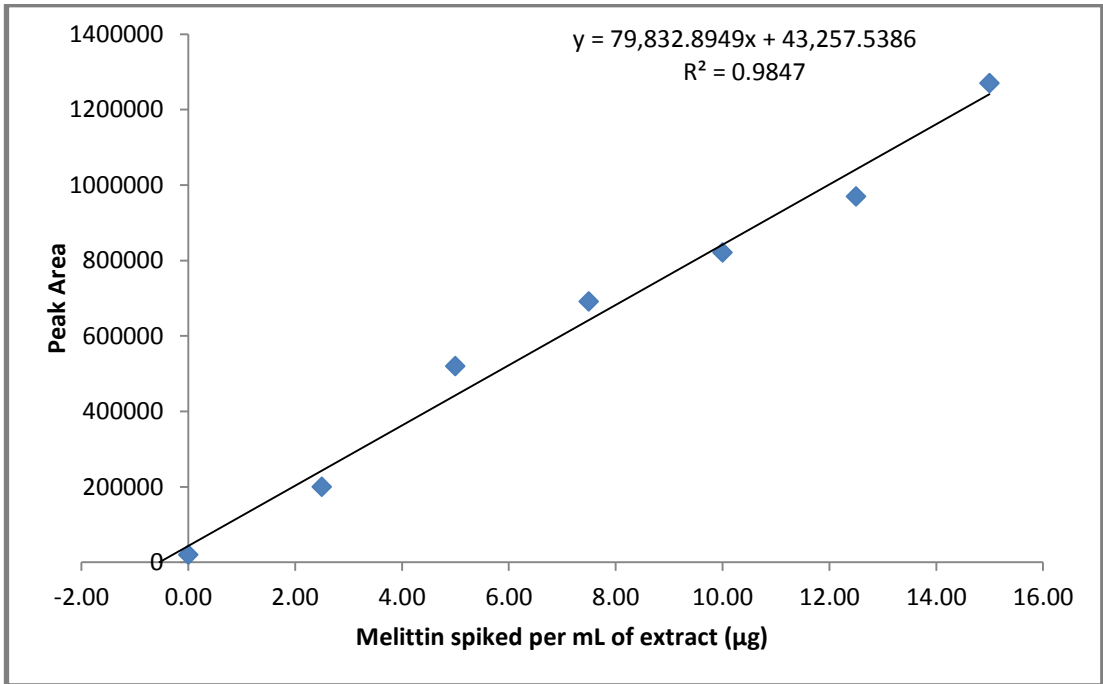
Duplicate I



Duplicate II

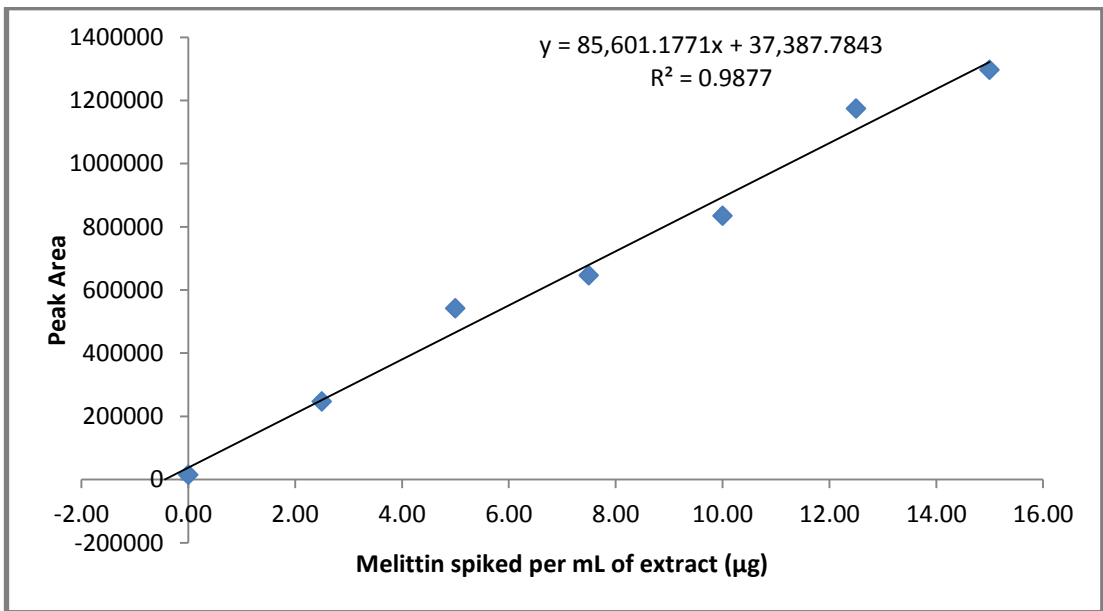


Duplicate III

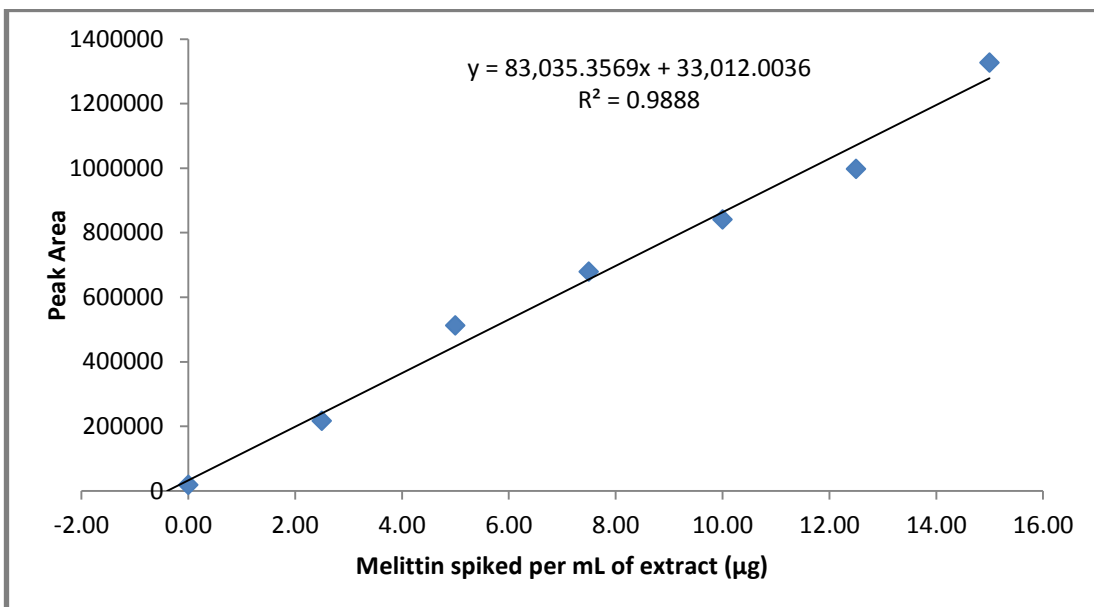


Calibration curves for sample B (BVE)

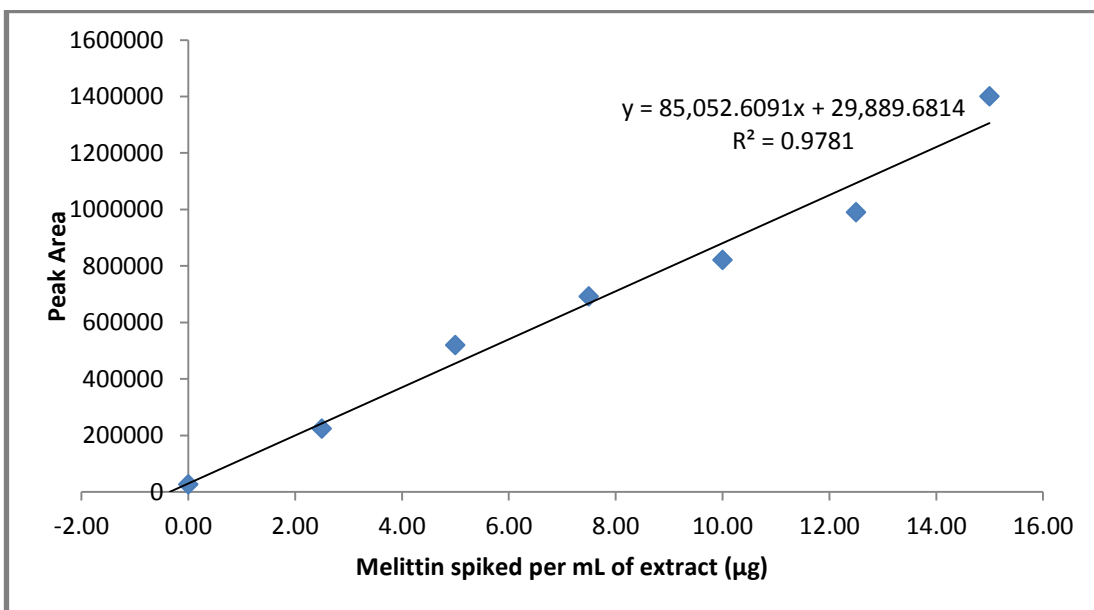
Duplicate I



Duplicate II

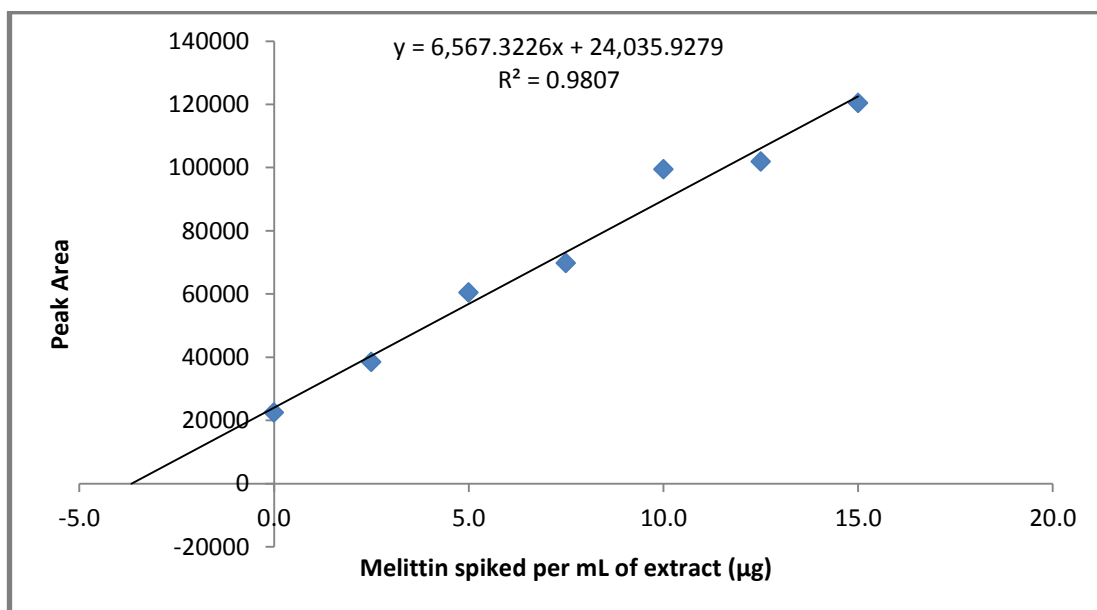


Duplicate III

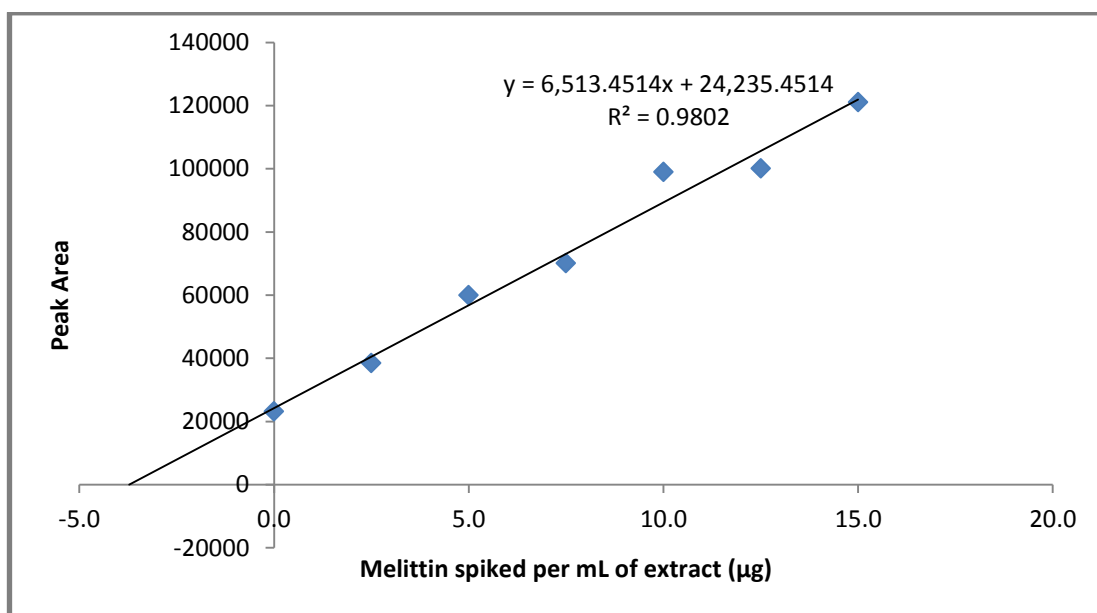


Calibration curves for sample C (MDR1)

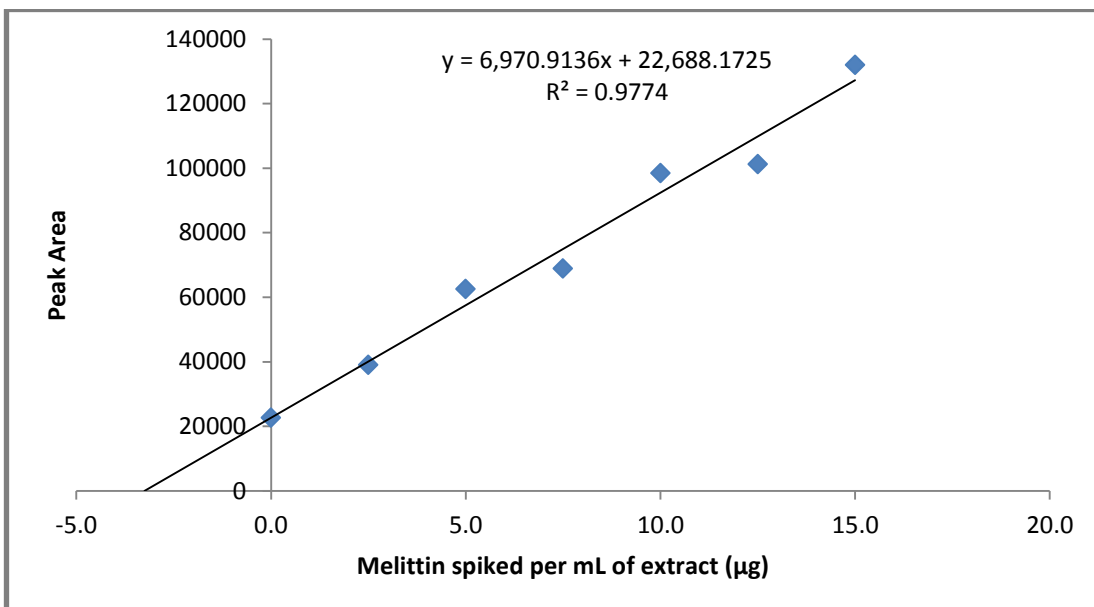
Duplicate I



Duplicate II

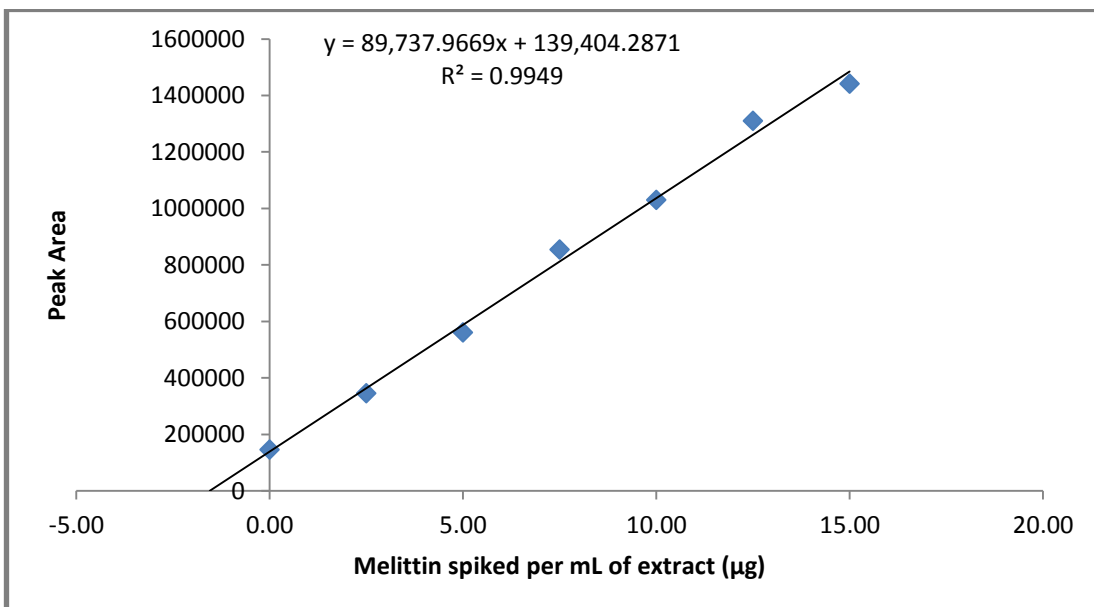


Duplicate III

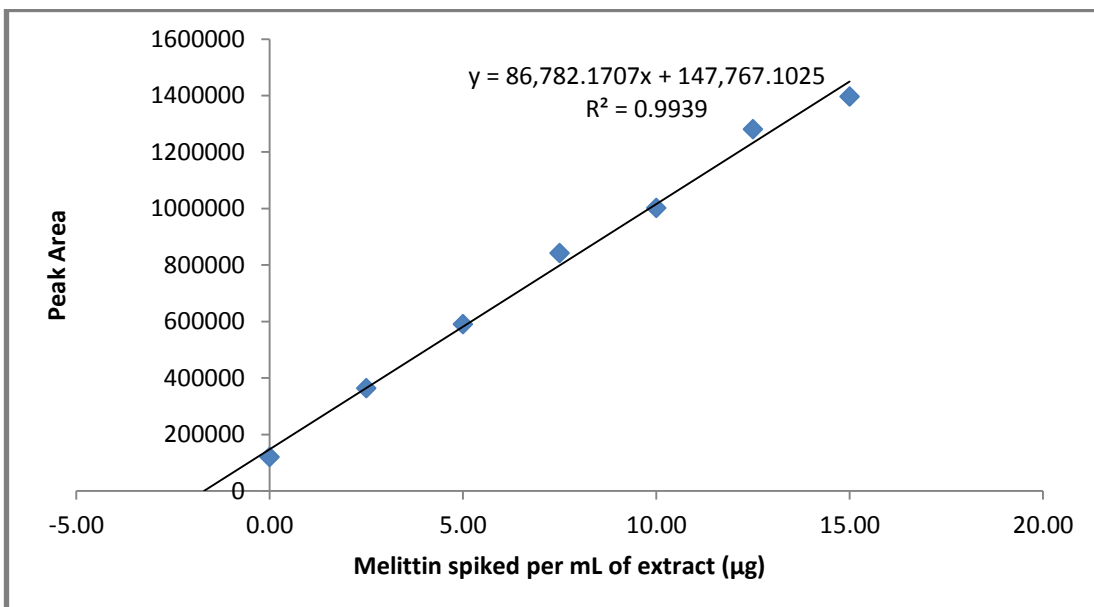


Calibration curves for sample D (NBC)

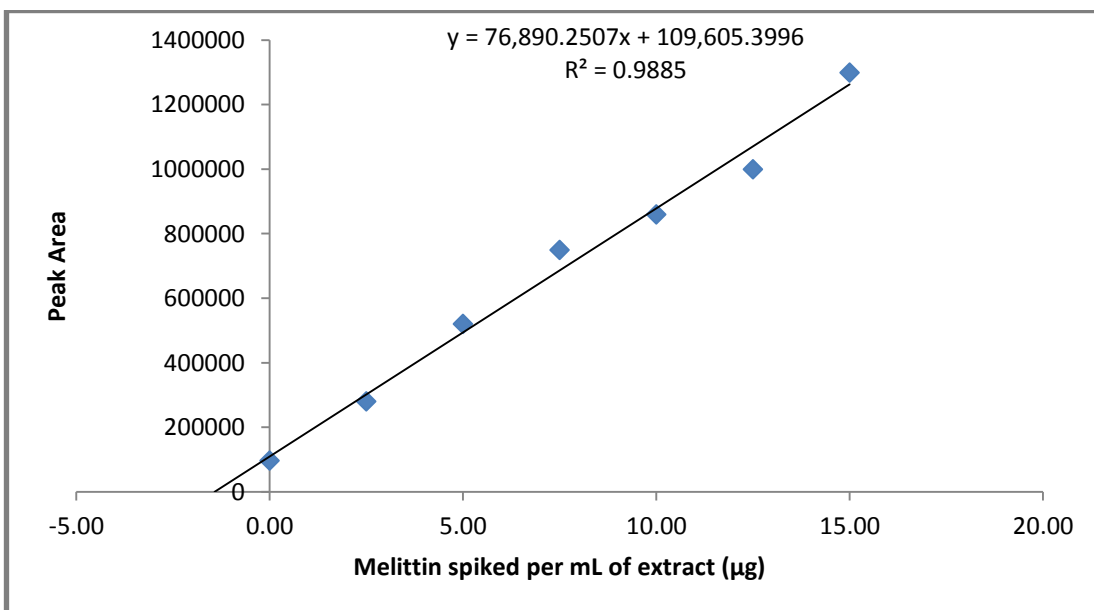
Duplicate I



Duplicate II

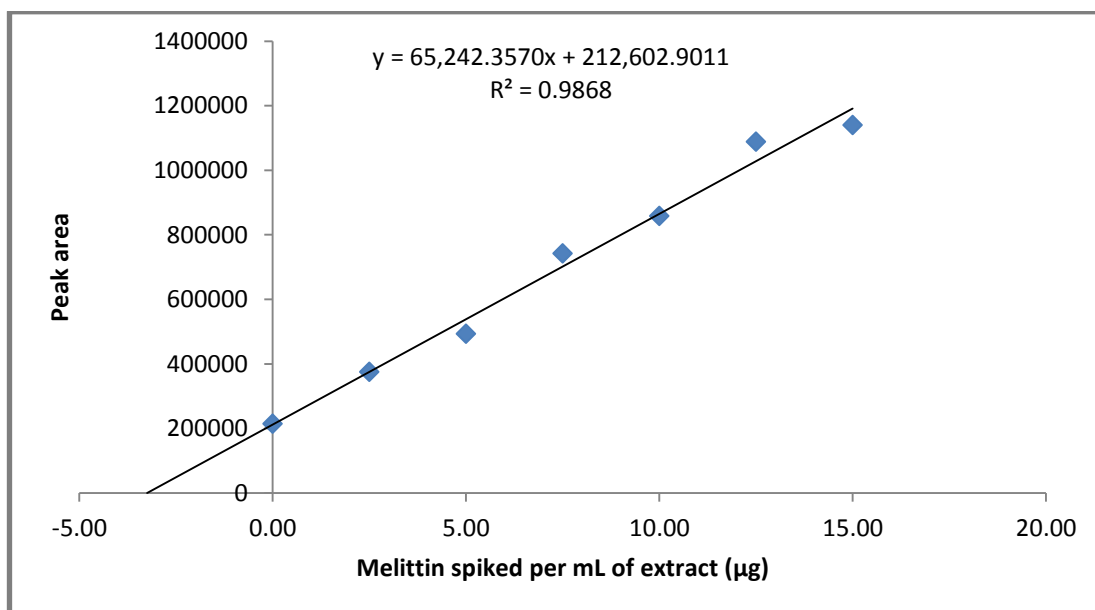


Duplicate III

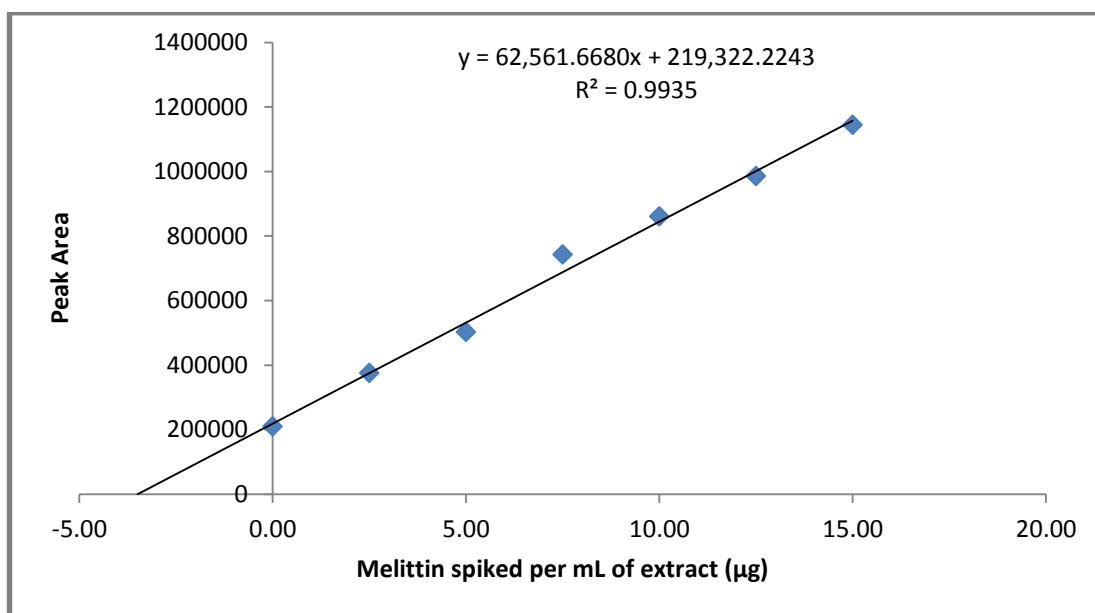


Calibration curves for sample E (MDM)

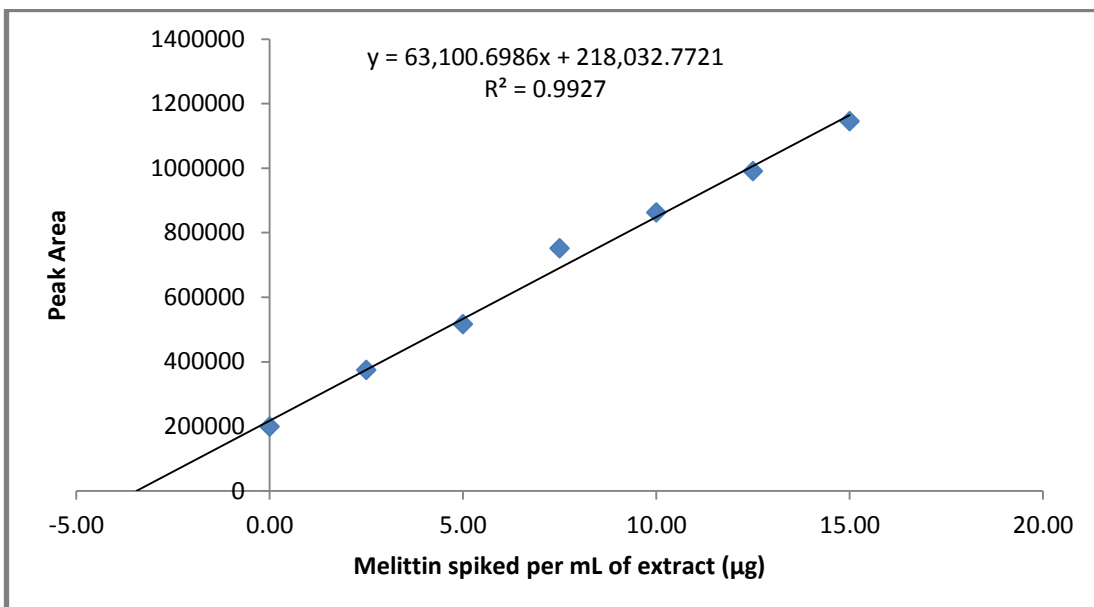
Duplicate I



Duplicate II

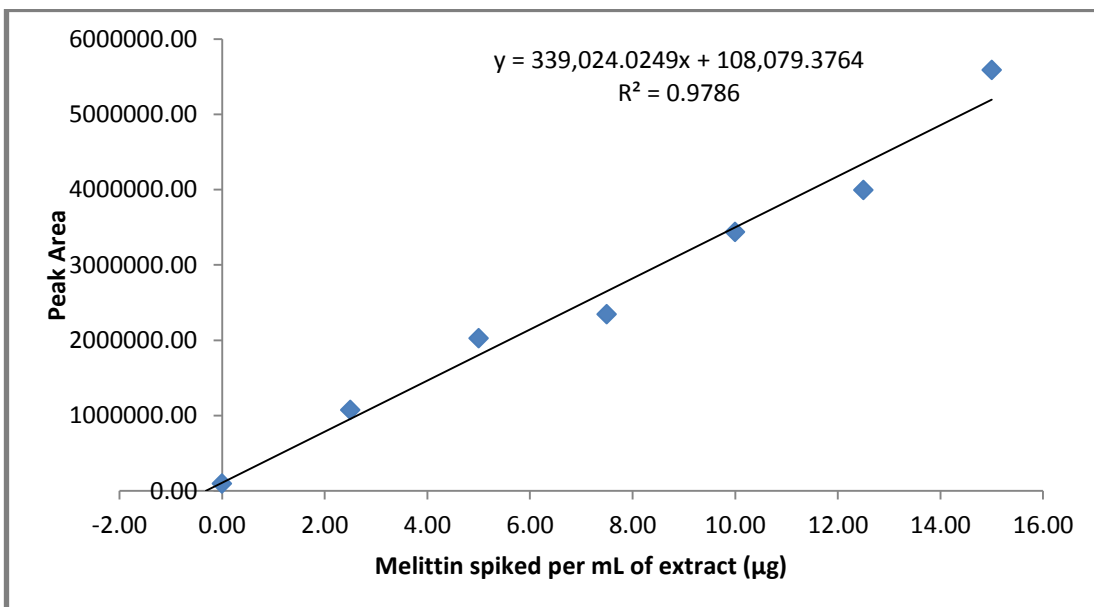


Duplicate III

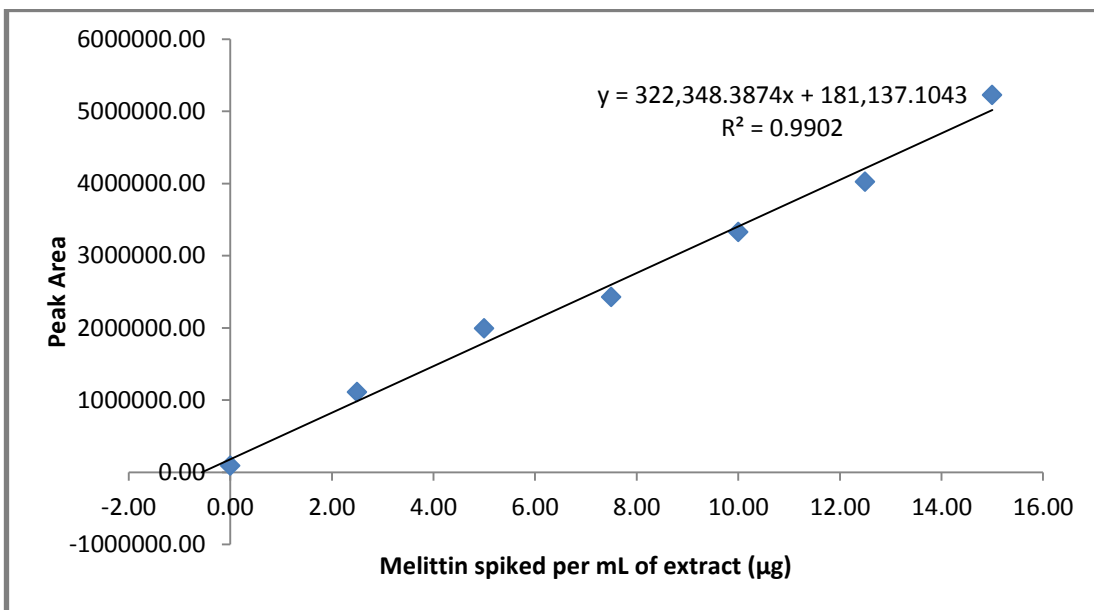


Calibration curves for sample F (MDR2)

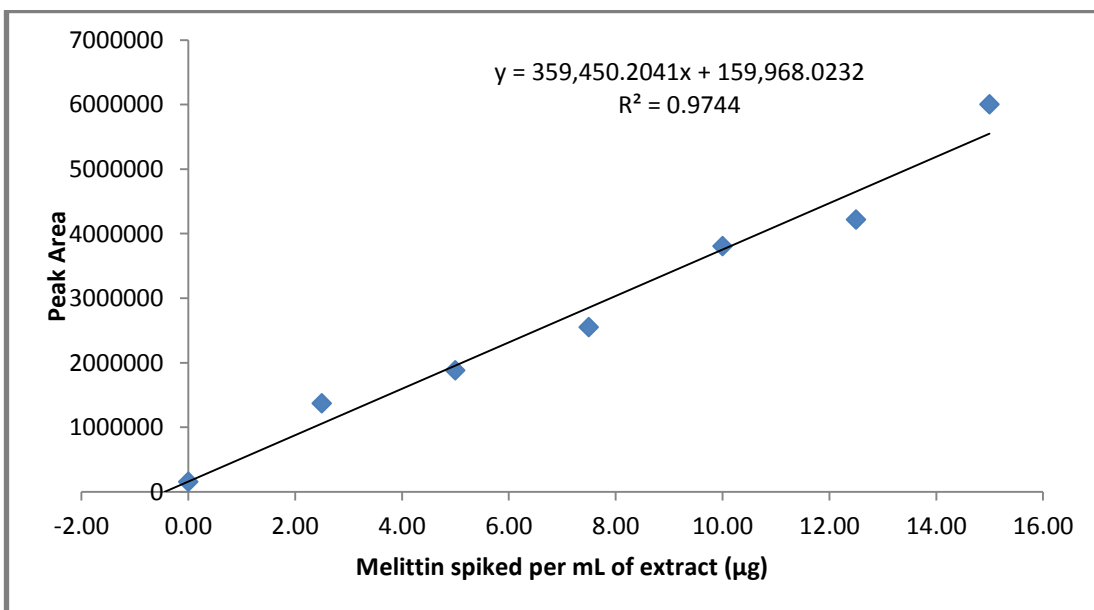
Duplicate I



Duplicate II



Duplicate III



Appendix II: Supplementary data for Chapter 8

Supplementary Figures

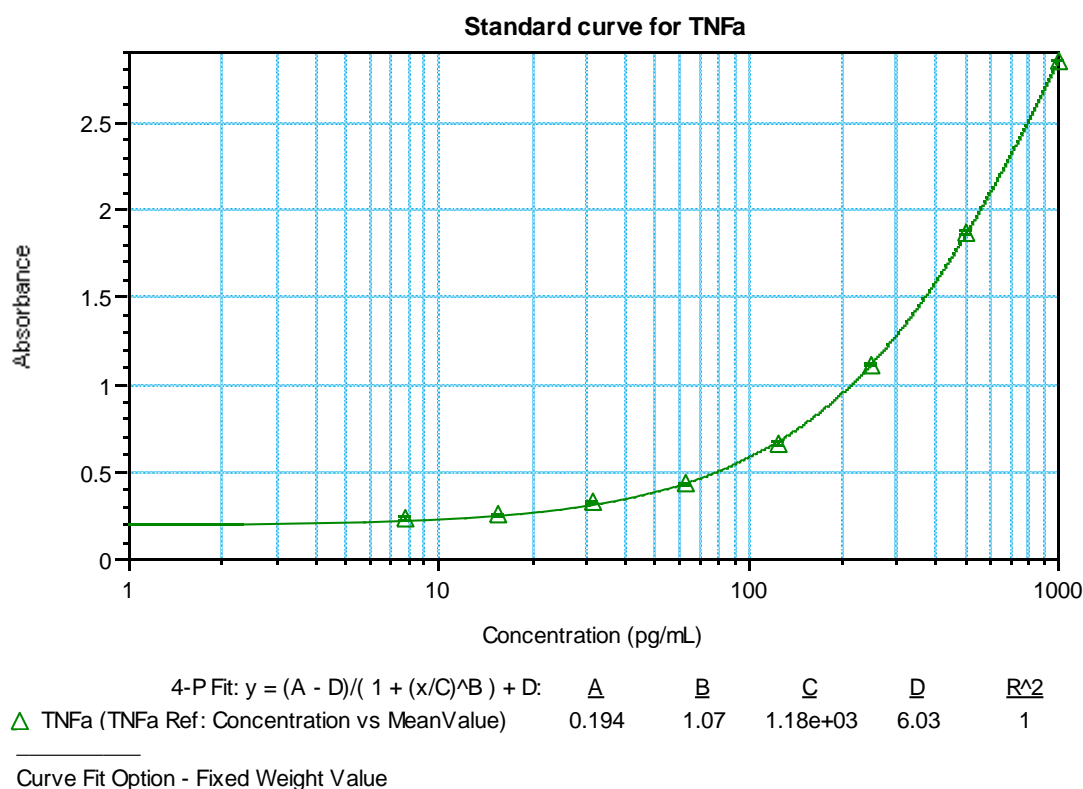


Figure B1: A representative 4-parameter logistic plot of TNF- α standard samples showing the calibration equation and the values of the constants a, b, c, and d with a perfect fit R^2 value of 1.0. Error bars represent standard deviation of absorbance values for duplicate standard concentrations (n=1).

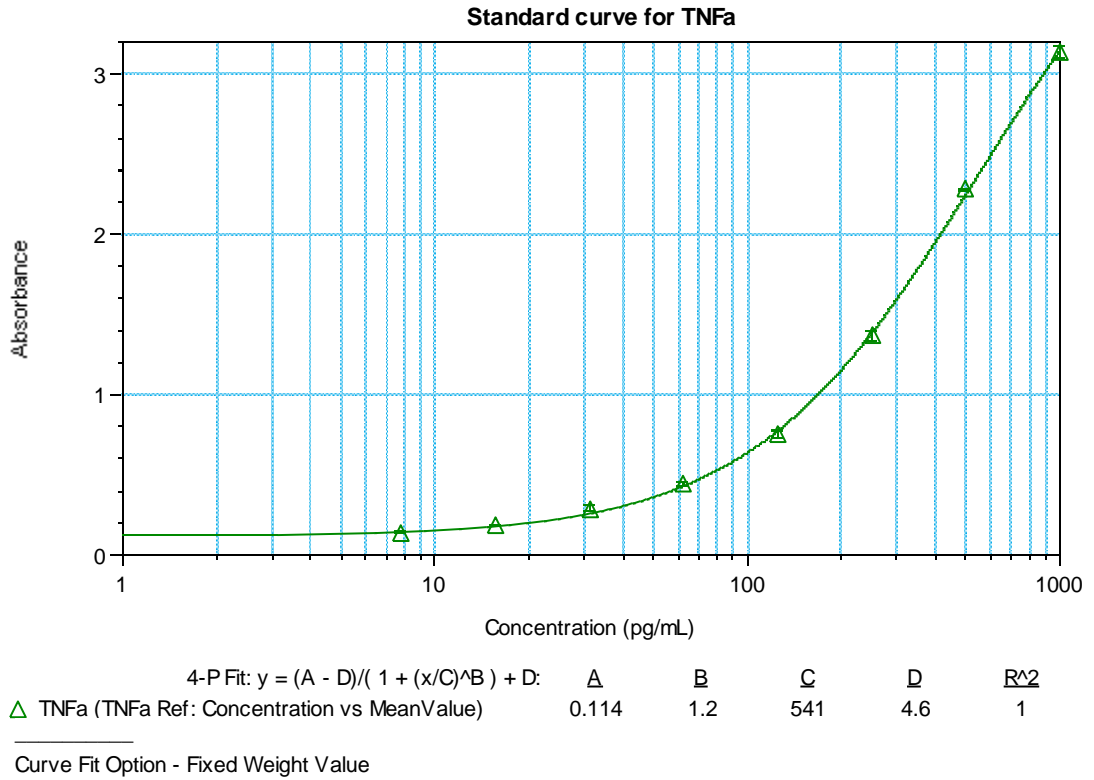


Figure B2: A representative 4-parameter logistic plot of TNF- α standard samples showing the calibration equation and the values of the constants a, b, c, and d with a perfect fit R^2 value of 1.0. Error bars represent standard deviation of absorbance values for duplicate standard concentrations (n=2).

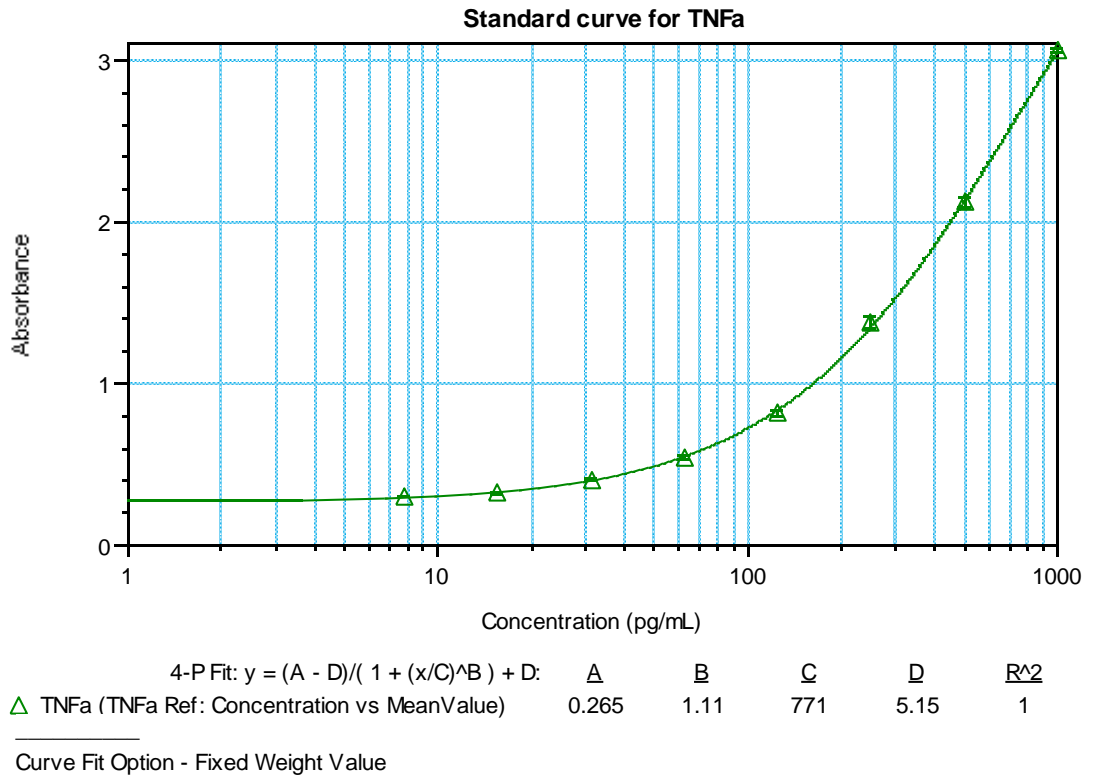


Figure B3: A representative 4-parameter logistic plot of TNF- α standard samples showing the calibration equation and the values of the constants a, b, c, and d with a perfect fit R^2 value of 1.0. Error bars represent standard deviation of absorbance values for duplicate standard concentrations (n=3).

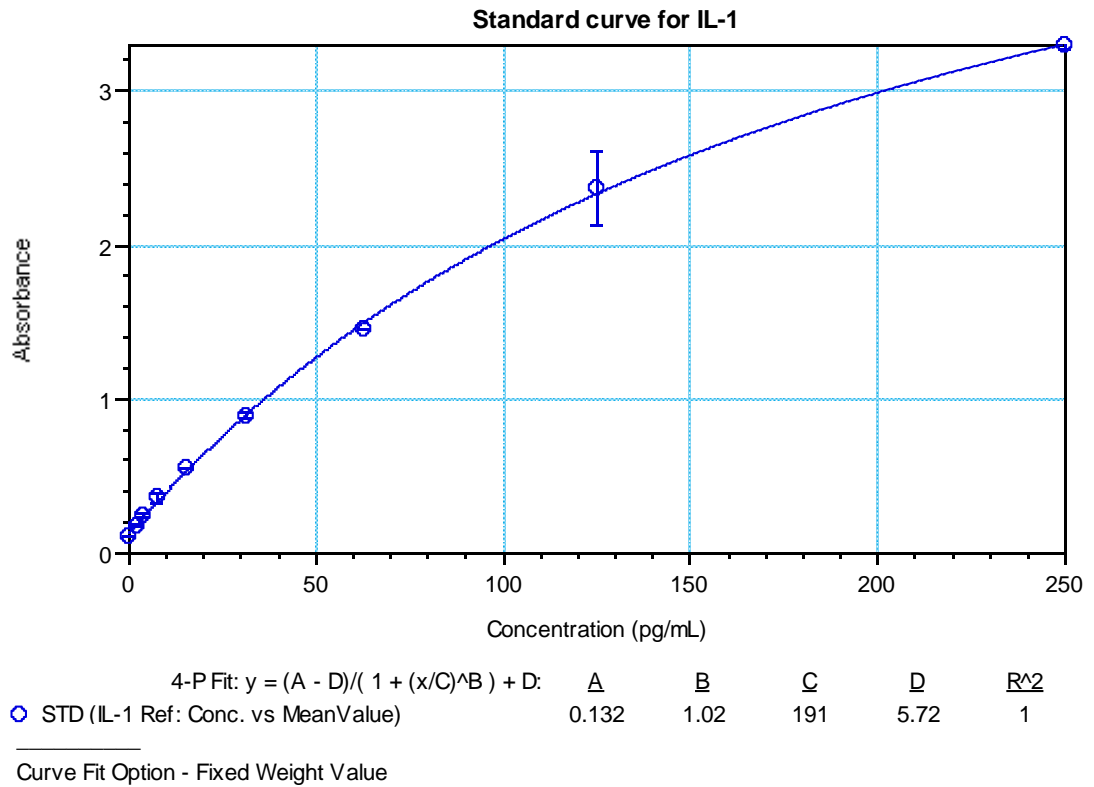


Figure B4: A sample 4-parameter logistic plot of the IL-1 β /IL-1F2 standard samples showing the calibration equation and the values of the constants a, b, c, and d with a perfect fit R^2 value of 1.0. Error bars represent standard deviation of absorbance values for duplicate standard concentrations (n=1).

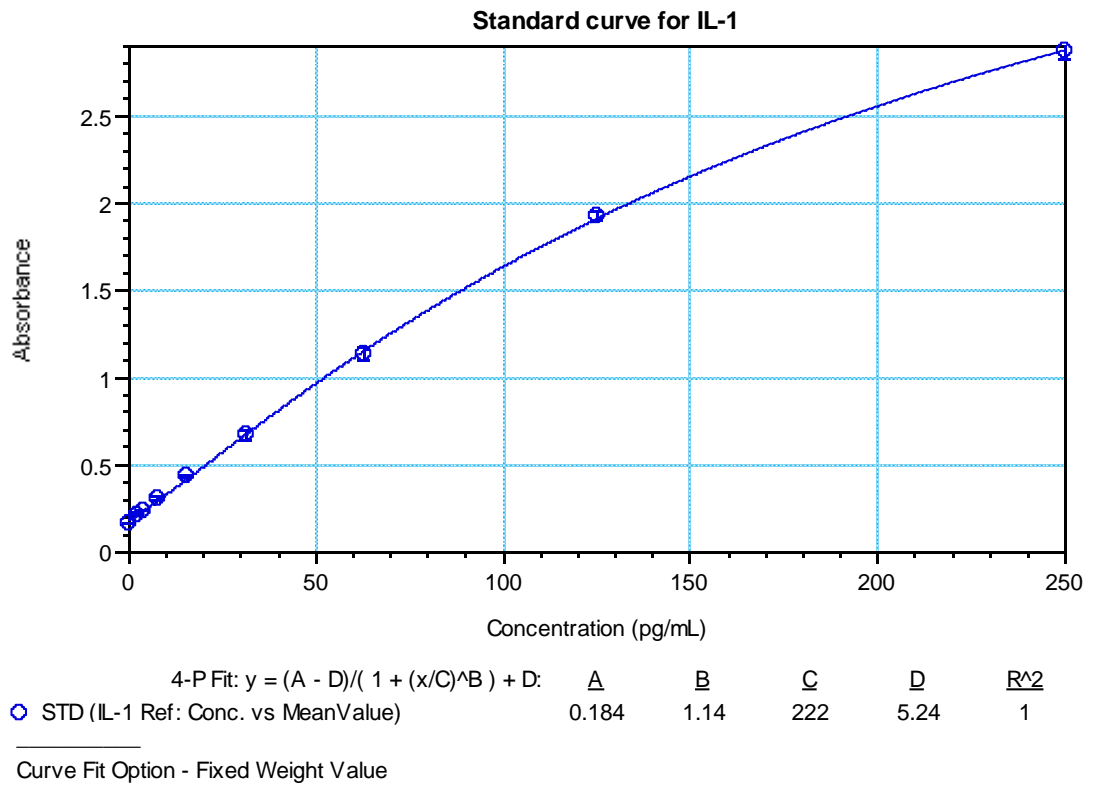


Figure B5: A sample 4-parameter logistic plot of the IL-1 β /IL-1F2 standard samples showing the calibration equation and the values of the constants a, b, c, and d with a perfect fit R² values of 1.0. Error bars represent standard deviation of absorbance values for duplicate standard concentrations (n=2).

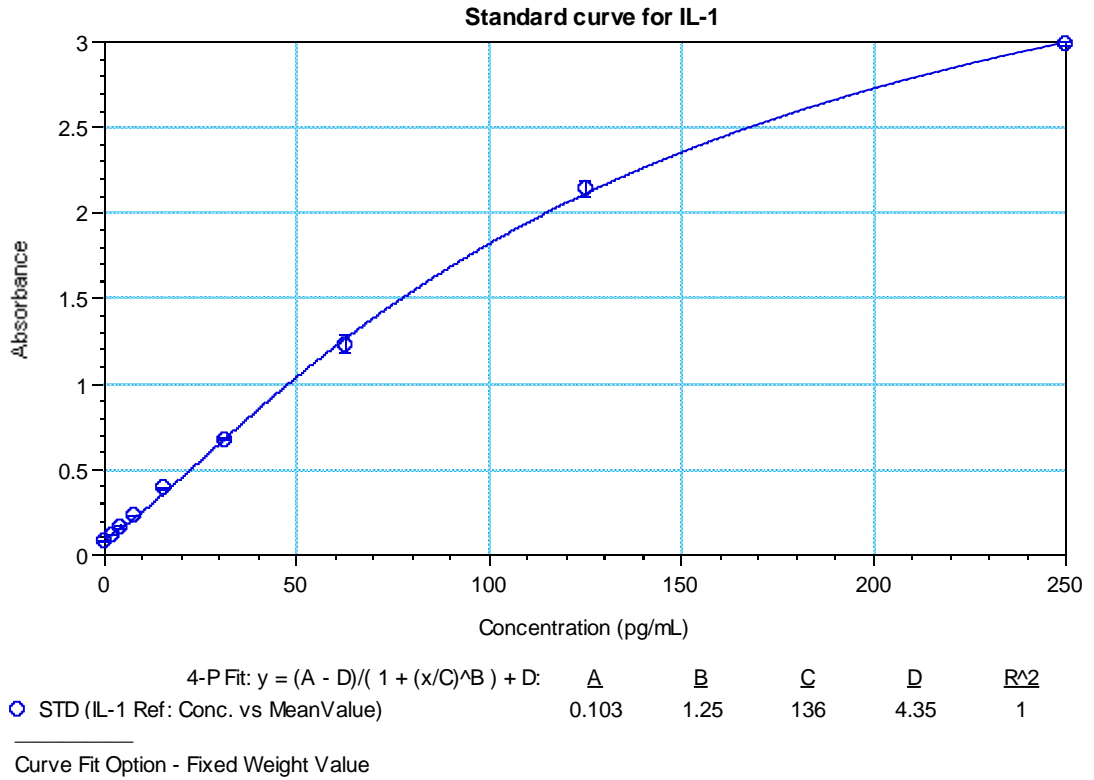


Figure B6: A sample 4-parameter logistic plot of the IL-1 β /IL-1F2 standard samples showing the calibration equation and the values of the constants a, b, c, and d with a perfect fit R^2 value of 1.0. Error bars represent standard deviation of absorbance values for duplicate standard concentrations (n=3).

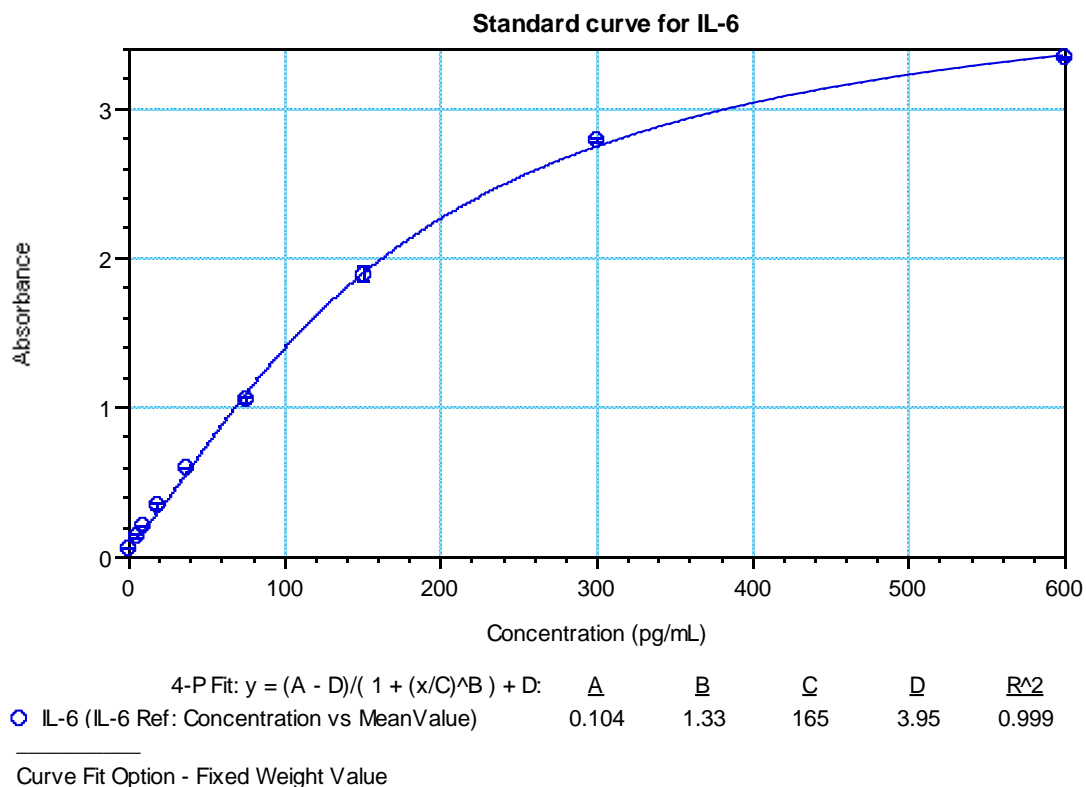


Figure B7: A sample 4-parameter logistic plot of the IL-6 standard samples showing the calibration equation and the values of the constants a, b, c, and d with a perfect fit R^2 value of 1.0. Error bars represent standard deviation of absorbance values for duplicate standard concentrations ($n=1$).

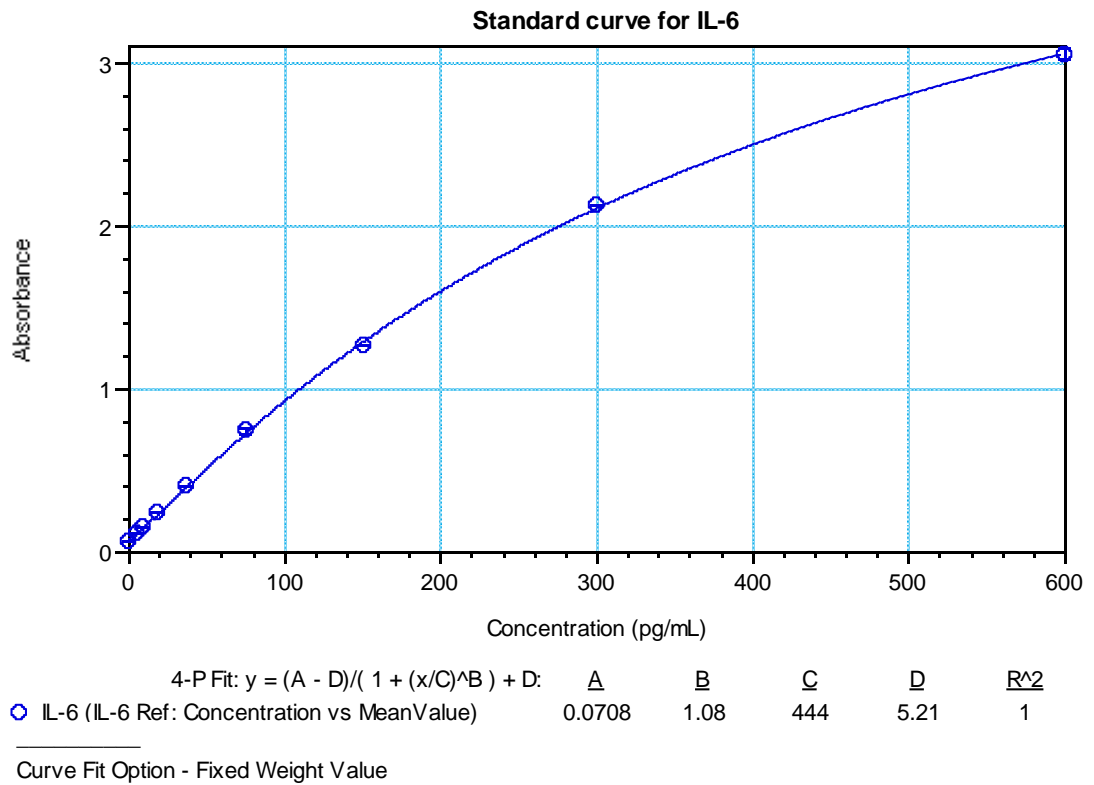


Figure B8: A sample 4-parameter logistic plot of the IL-6 standard samples showing the calibration equation and the values of the constants a, b, c, and d with a perfect fit R^2 value of 1.0. Error bars represent standard deviation of absorbance values for duplicate standard concentrations (n=2).

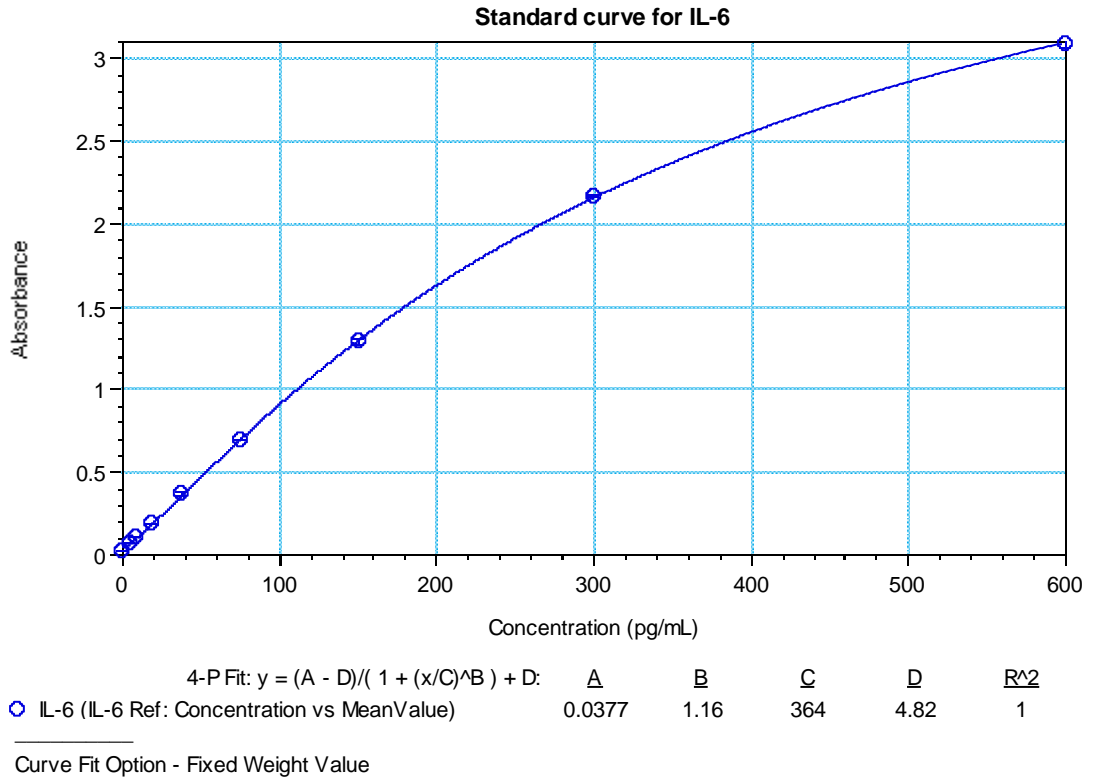


Figure B9: A sample 4-parameter logistic plot of the IL-6 standard samples showing the calibration equation and the values of the constants a, b, c, and d with a perfect fit R^2 value of 1.0. Error bars represent standard deviation of absorbance values for duplicate standard concentrations.

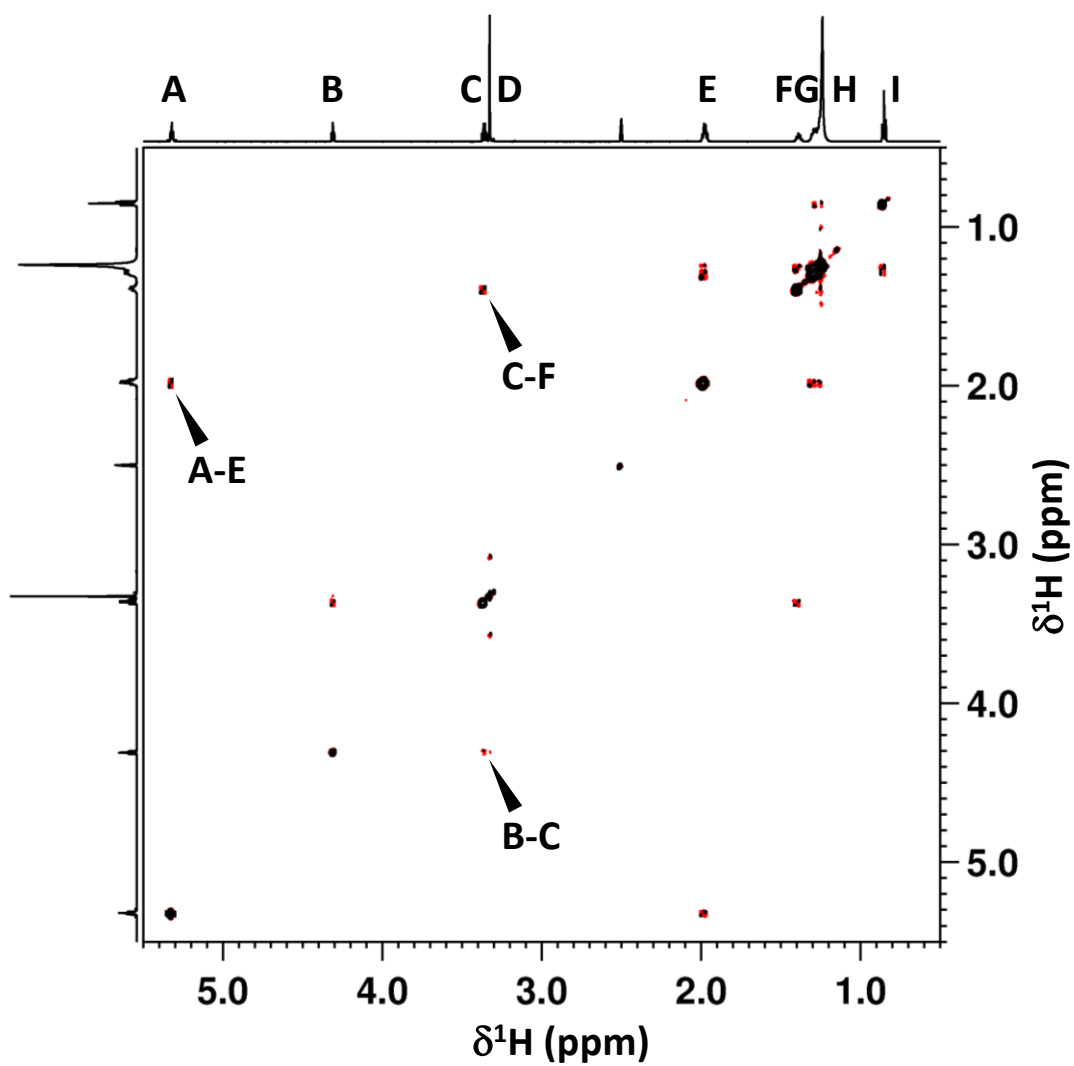


Figure B10: 600 MHz 2D [^1H , ^1H] DQFCOSY NMR spectrum of the BV F4 component molecule with 1D ^1H NMR spectra shown representing horizontal and vertical projections with signal designations shown as A-I. Selected cross-peaks are highlighted. Full cross-peak assignments are summarized in **Table 8.6**.

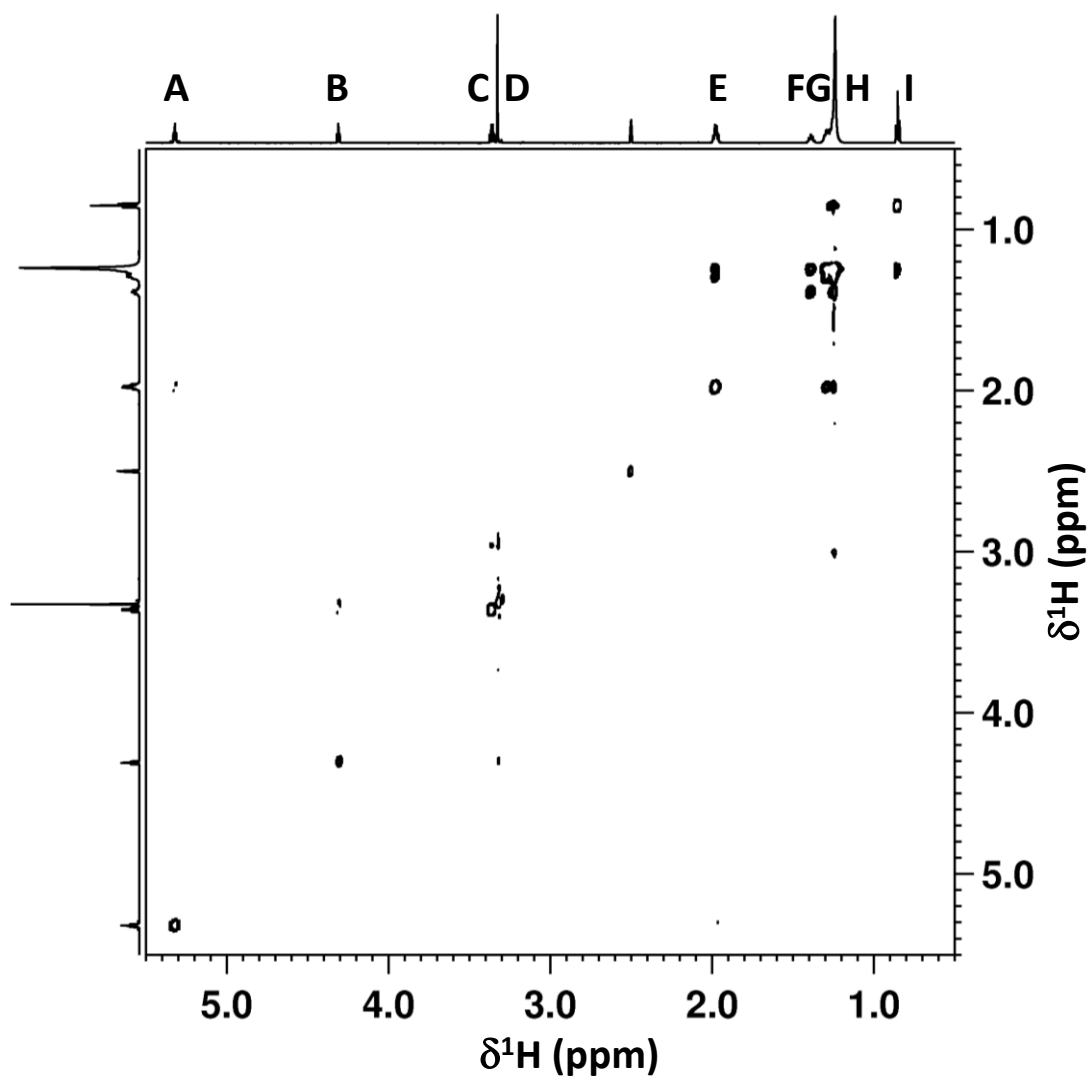


Figure B11: 600 MHz 2D [^1H , ^1H] TOCSY NMR spectrum of the BV F-4 component molecule with 1D ^1H NMR spectra shown representing horizontal and vertical projections with signal designations shown as **A-I**. Full cross-peak assignments are summarized in **Table 8.6**.

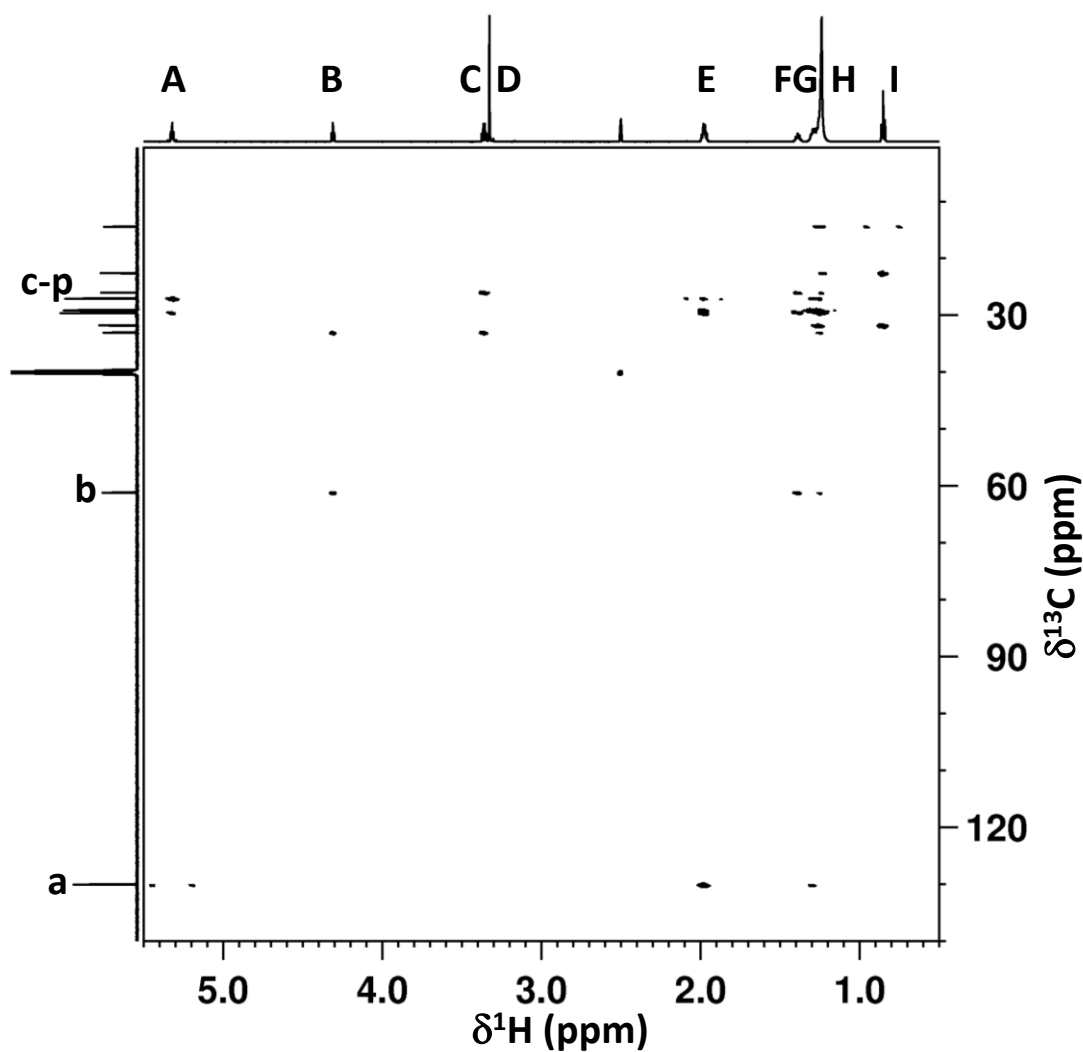


Figure B12: 600 MHz 2D [^1H , ^{13}C] HMBC NMR spectrum of the BV F-4 component molecule with 1D ^1H NMR spectrum shown representing the horizontal projection and 1D $^{13}\text{C}\{-^1\text{H}\}$ NMR spectrum shown representing the vertical projection with signal designations shown as **A-I** and **a-p** respectively. Full cross-peak assignments are summarized in **Table 8.7**.

Supplementary Tables

Table B1: Effect of bee venom and its fractions on TNF- α production in differentiated U937 cells in the presence or absence of LPS co-stimulation (n=3).

<i>Samples</i>	<i>TNF-α concentration (pg/mL)</i>									
Samples	Sample-LPS					Sample+LPS				
	n=1	n=2	n=3	Mean	SD	n=1	n=2	n=3	Mean	SD
F-1	6.1	6.8	3.8	5.6	1.6	68.2	126.8	70.9	88.6	33.1
F-2	5.7	7.2	4.4	5.8	1.4	74.1	162.0	90.8	109.0	46.7
F-3	7.6	8.9	5.2	7.2	1.9	69.5	161.5	84.2	105.1	49.4
F-4	8.0	9.7	8.0	8.6	1.0	88.1	160.1	143.1	130.4	37.6
BV	8.2	7.8	5.0	7.0	1.7	56.0	79.0	81.0	72.0	13.9

TNF- α Controls

<i>Control</i>	<i>TNF-α concentration (pg/mL)</i>				
<i>Replicate No.</i>	<i>n=1</i>	<i>n=2</i>	<i>n=3</i>	<i>Mean</i>	<i>SD</i>
Media	7.3	7.1	4.4	6.2	1.6
LPS	66.2	114.9	73.0	84.7	26.4

Table B2: Effect of bee venom and its fractions on IL-1 β /IL-1F2 production in differentiated U937 cells in the presence or absence of LPS co-stimulation (n=3).

<i>Samples</i>	<i>IL-1β (pg/mL)</i>									
	<i>Sample-LPS</i>					<i>Sample+LPS</i>				
	<i>n=1</i>	<i>n=2</i>	<i>n=3</i>	<i>Mean</i>	<i>SD</i>	<i>n=1</i>	<i>n=2</i>	<i>n=3</i>	<i>Mean</i>	<i>SD</i>
F-1	1.2	1.7	0.5	1.1	0.6	34.4	293.1	86.9	138.1	136.7
F-2	1.2	2.2	0.8	1.4	0.7	53.4	703.1	174.3	310.2	345.6
F-3	1.1	1.8	1.3	1.4	0.4	78.3	279.8	108.3	155.5	108.7
F-4	0.8	3.6	3.4	2.6	1.5	27.1	137.7	71.7	78.8	55.6
BV	<2.0	2.8	2.4	2.6	0.3	24.7	83.3	45.9	51.3	29.7

IL-1 β Controls

<i>Control</i>	<i>IL-1β concentration (pg/mL)</i>				
<i>Replicate No.</i>	<i>n=1</i>	<i>n=2</i>	<i>n=3</i>	<i>Mean</i>	<i>SD</i>
Media	<2.0	1.2	2.5	1.8	0.9
LPS	9.1	49.1	22.0	26.8	20.4

Table B3: Effect of bee venom and its fractions on IL-6 production in differentiated U937 cells in the presence and absence of LPS co-stimulation (n=3).

<i>Samples</i>	<i>IL-6 concentration (pg/mL)</i>									
	<i>Sample-LPS</i>					<i>Sample+LPS</i>				
	n=1	n=2	n=3	Mean	SD	n=1	n=2	n=3	Mean	SD
F-1	<4.7	<4.7	<4.7	<4.7	n/a	93.8	199.1	126.6	139.8	53.9
F-2	<4.7	<4.7	<4.7	<4.7	n/a	113.1	235.6	160.6	169.8	61.8
F-3	<4.7	<4.7	<4.7	<4.7	n/a	112.1	159.0	152.1	141.1	25.3
F-4	<4.7	<4.7	<4.7	<4.7	n/a	32.3	63.7	71.4	55.8	20.7
BV	<4.7	<4.7	<4.7	<4.7	n/a	98.5	198.6	183.9	160.3	54.0

IL-6 Controls

<i>Control</i>	<i>IL-6 concentration (pg/mL)</i>				
<i>Replicate No.</i>	<i>n=1</i>	<i>n=2</i>	<i>n=3</i>	<i>Mean</i>	<i>SD</i>
Media	<4.7	<4.7	<4.7	<4.7	n/a
LPS	58.5	185.5	145.8	129.9	65.0